DIRECT SYNTHESIS GAS CONVERSION TO ALCOHOLS AND HYDROCARBONS USING A CATALYTIC MEMBRANE REACTOR

REUBEN MFON UMOH

A thesis submitted in partial fulfilment of the
requirements of
The Robert Gordon University
for the degree of Doctor of Philosophy

June 2009

ABSTRACT

In this work, inorganic membranes with highly dispersed metallic catalysts on macroporous titania-washcoated alumina supports were produced, characterized and tested in a catalytic membrane reactor. The reactor, operated as a contactor in the forced pore-flow-through mode, was used for the conversion of synthesis gas (H_2 + CO) into mixed alcohols and hydrocarbons via the Fischer-Tropsch synthesis. Carbon monoxide conversions of 78% and 90% at near atmospheric pressure (300kPa) and 493K were recorded over cobalt and bimetallic Co-Mn membranes respectively. The membranes also allowed for the conversion of carbon dioxide, thus eliminating the need for a CO_2 separation interphase between synthesis gas production and Fischer-Tropsch synthesis.

Catalytic tests conducted with the membrane reactor with different operating conditions (of temperature, pressure and feed flow rate) on cobalt-based membranes gave very high selectivity to specific products, mostly higher alcohols (C_2 – C_8) and paraffins within the gasoline range, thereby making superfluous any further upgrading of products to fuel grade other than simple dehydration. Manganese-promoted cobalt membranes were found not only to give better Fischer-Tropsch activity, but also to promote isomerization of paraffins, which is good for boosting the octane number of the products, with the presence of higher alcohols improving the energy density.

The membrane reactor concept also enhanced the ability of cobalt to catalyze synthesis gas conversions, giving an activation energy E_a of 59.5 kJ/mol.K compared with 86.9 – 170 kJ/mol.K recorded in other reactors. Efficient heat transfer was observed because of the open channel morphology of the porous membranes.

A simplified mechanism for both alcohol and hydrocarbon production based on hydroxycarbene formation was proposed to explain both the stoichiometric reactions formulated and the observed product distribution pattern.

DEDICATION

This work is dedicated to my dear parents – to my father Mfon, who would have loved to witness the actualization of this dream but had to answer the ultimate call rather early; and to my mother Mba, for the courage to make all this possible.

ACKNOWLEDGEMENTS

This work would not be possible but for the assistance received from many people some of whose names may not be mentioned here, but to whom I remain eternally grateful.

My sincere appreciation goes to my supervisor, Professor Edward Gobina for his unwavering belief in me. His untiring guidance, encouragement, and great sense of professionalism and friendship were the tools needed to complete this work.

My nation Nigeria made me proud by providing full funding for this programme through the Petroleum Technology Development Fund (PTDF). I would like to thank the staff of PTDF and *UNIVATION* for all their assistance. I also wish to express my gratitude to the Principal of the Petroleum Training Institute in Nigeria, for releasing me to undertake this programme, and to and my colleagues especially those in PPD, for bearing increased workload while I was away on study leave.

I am also grateful to Willie Reid, management and staff of *Gas 2 Limited*, for all their support. The assistance received from Chen, Barry, Ali, Vitor and other colleagues at the Centre for Process Integration and Membrane Technology; and from the technical staff of the School of Engineering notably Bill, Milton, Stan and Steve is hereby acknowledged.

I would like to thank Iain Tough and Emily Hunter for assisting with the SEM and EDXA, John Wood for putting me through with GC techniques for liquid analysis, and all other friends who shared my fears, felt my pains, and assisted in the bid to make this programme such a success.

I am very grateful to my dear wife Nsan, for her support and for taking care of the home, and to my children Ememabasi, Andikan and Ediomi for enduring my rather difficult schedules.

Finally, all thanks to God Almighty for making dreams come true, and for putting the Fountain of Love, Aberdeen here to assist people like me with Prayers and The Word.

TABLE OF CONTENTS

LIST OF FIGURES

CHAPTER 4

LIST OF TABLES

NOMENCLATURE

A	Pre-exponential factor in Arrhenius equation	[units depend on order of reaction]
B_o	morphological parameter defined by equation 4.7	[mol.m/m^2.s.Pa^2]
C_i	Concentration of species i	[mol/m^3]
D_i^e	Effective Knudsen diffusion coefficient	[m^2/s]
D_{ij}^e	Effective molecular binary diffusion coefficient	[m^2/s]
d_p	Pore diameter	[m]
E_a	Activation energy	[kJ/mol.K]
F_i	Molar flow rate of species i	[mol/min]
F_{io}	Molar flow rate of species i in the feed	[mol/min]
F_T	Normalized total flux defined by equation 4.5	[mol.m/m^2.s.Pa]
J_i	Permeability of species i through the membrane	[m^2/Pa.s]
k	Reaction rate constant	[unit depends on the order of reaction]
K_i	Adsorption equilibrium constant i=1,2,3,…	”
K_m	Permeance	[mol/Pa.s.m^2]
Kn	Knudsen number	[–]
K_o	morphological parameter defined by equation 4.6	[mol.m/m^2.s.Pa]
k_p, k_t	Rate of propagation and termination of reaction	[mol/m^2.s.Pa]
M_i	Molecular weight of component i	[kg]
N_i	Molar flux of species i through a membrane	[mol/m^2.s]
n	Number of carbon atoms in the molecule	[–]
P	Total pressure	[kPa]
P_i	Partial pressure of gas i	[kPa]
$\overline{P}$	Mean or average pressure	[kPa]
R	Universal gas constant (a dimensional constant)	[J/mol.K]

r_A	Rate of formation of A	[mol/g-cat.h]
$-r_i$	Rate of disappearance of reactant i	[mol/g-cat.h]
T	Temperature	[^oC or K]
W_n	Weight fraction of hydrocarbon containing n carbon atoms	[–]
x_A, x_B	Concentrations of components A, B in the feed	[mol/m^3]
Y_i	Yield of product i	[mol/g-cat]
y_A, y_B	Concentrations of components A, B in the permeate	[mol/m^3]

Greek alphabets

α	Chain growth probability	[–]
$\alpha_{A/B}$	Selectivity factor	[%]
δ_M	Membrane thickness	[m]
ε	Porosity	[%]
λ_i	Mean free path of molecule	[m]
η_i	Dynamic viscosity of component i	[Pa.s]
τ	Tortuosity	[–]
μ	Kinematic viscosity	[m^2/s]

ABBREVIATIONS

ASAP	Analysis of surface area and porosimetry
ASF	Anderson-Schulz-Flory
BET	Brunauer-Emmett-Teller
BTL	Biomass-to-liquids
CFBR	Circulating fluidized bed reactor
CMR	Catalytic membrane reactor

CTL	Coal-to-liquids
CVD	Chemical vapour deposition
EDXA	Energy dispersive x-ray analysis
EPMA	Electron probe micro-analysis
FFBR	Fixed fluidized bed reactor
FTS	Fischer-Tropsch synthesis
GC	Gas Chromatograph
GHSV	Gas hourly space velocity [h^{-1}]
G-L-S	Gas-liquid-solid
GMS	Generalized Maxwell-Stefan equation
GTL	Gas-to-liquids
HAS	Higher alcohols synthesis
HLM	Hybrid liquid membrane
HTFT	High temperature Fischer-Tropsch
IMR	Inert membrane reactor
IUPAC	International Union of Pure and Applied Chemistry
LTFT	Low temperature Fischer-Tropsch
MF	Microfiltration
MTBE	Methyl *tertiary*-butyl ether
MTFBR	Multitubular fixed bed reactor
NF	Nanofiltration
PBMR	Packed bed membrane reactor
PFT	Pore-flow-through
SAS	*Sasol* advanced *synthol*
SBCR	Slurry bubble column reactor

SEM	Scanning electron microscopy
SLM	Supported liquid membrane
SMDS	Shell middle distillate synthesis
SMSI	Strong metal-support interaction
TWR	Tube-wall reactor
UF	Ultrafiltration
WGS	Water gas shift reaction

CHAPTER 1: Introduction

Synthesis gas conversion to mixed alcohols and hydrocarbons has been effected in this work by the Fischer-Tropsch synthesis (FTS) route in a catalytic membrane reactor. A catalytic membrane reactor is a multifunctional device which provides improved performance over conventional reactors by combining in the same unit a catalyst, providing conversion; and a membrane that controls transfers to and from the catalyst. This combination has a synergic effect, and the results should be superior to those provided by the catalytic reactor and separation equipment working separately. In such an integrated process, the membrane is used as an active participant in chemical transformation for increasing the reaction rate, selectivity and yield. The most successful systems (up to now) are those employing polymeric membranes, but their use is limited to low temperature applications [Smid *et al*., 1996].

Inorganic membranes currently in use are metallic, ceramic, zeolitic or carbon, and they provide good thermal and chemical stability, compared with the polymeric materials, which make them suitable for many chemical reactions. Dense membranes have been largely and successfully investigated in membrane reactors, for reactions consuming or generating H_2 or O_2 [Bredesen *et al*., 2004]. They are usually permselective, and gas transport occurs via the solution diffusion mechanism. Porous membranes have been extensively used in catalytic reactors [Julbe & Ayral, 2007]. They are less or non permselective, offer a higher permeability, and transport mechanism can be related to the ratio between the pore sizes and the mean free path length of the gas molecule.

Inorganic membranes are used mainly for conducting hydrogenation or dehydrogenation reactions and synthesis of oxyorganic compounds [Li, 2007]. However, potentials exist

for the application of inorganic membranes in many areas, especially those involving multiphase reactions as shown in Table 1.1.

Table 1.1: Some examples of the application of inorganic membranes for catalytic reactions [Adapted from Westermann & Melin, 2009]

Reaction	Membrane	Active catalyst
1-Butene isomerization	Anodized alumina	None
CO oxidation	Porous silicon	Pd
VOC decomposition	Porous ceramic, γ-alumina	Pt
Methanol photocatalytic oxidation	α-alumina	TiO_2
Methanol selective dehydrogenation	α-alumina	γ-Al_2O_3
Methane oxidative coupling	Asymmetric α-alumina	Sm_2O_3
Propane selective epoxidation	Microporous glass	Cs-Ag, Re-Ag, Ag_2O
Methanol autothermal reforming	Cu-matrix	Cu/ZnO
Fischer-Tropsch synthesis	Composite porous metal	Co
Isobutene dimerization	Porous ceramic	Zeolite layer

1.1 Applications of Catalytic membrane reactors

The most common applications in the combination of a membrane and a chemical reactor with potentials for use in synthesis gas conversion processes are described schematically in Figure 1.1. A membrane reactor can function as an extractor, a distributor or a contactor [Menendez, 2008].

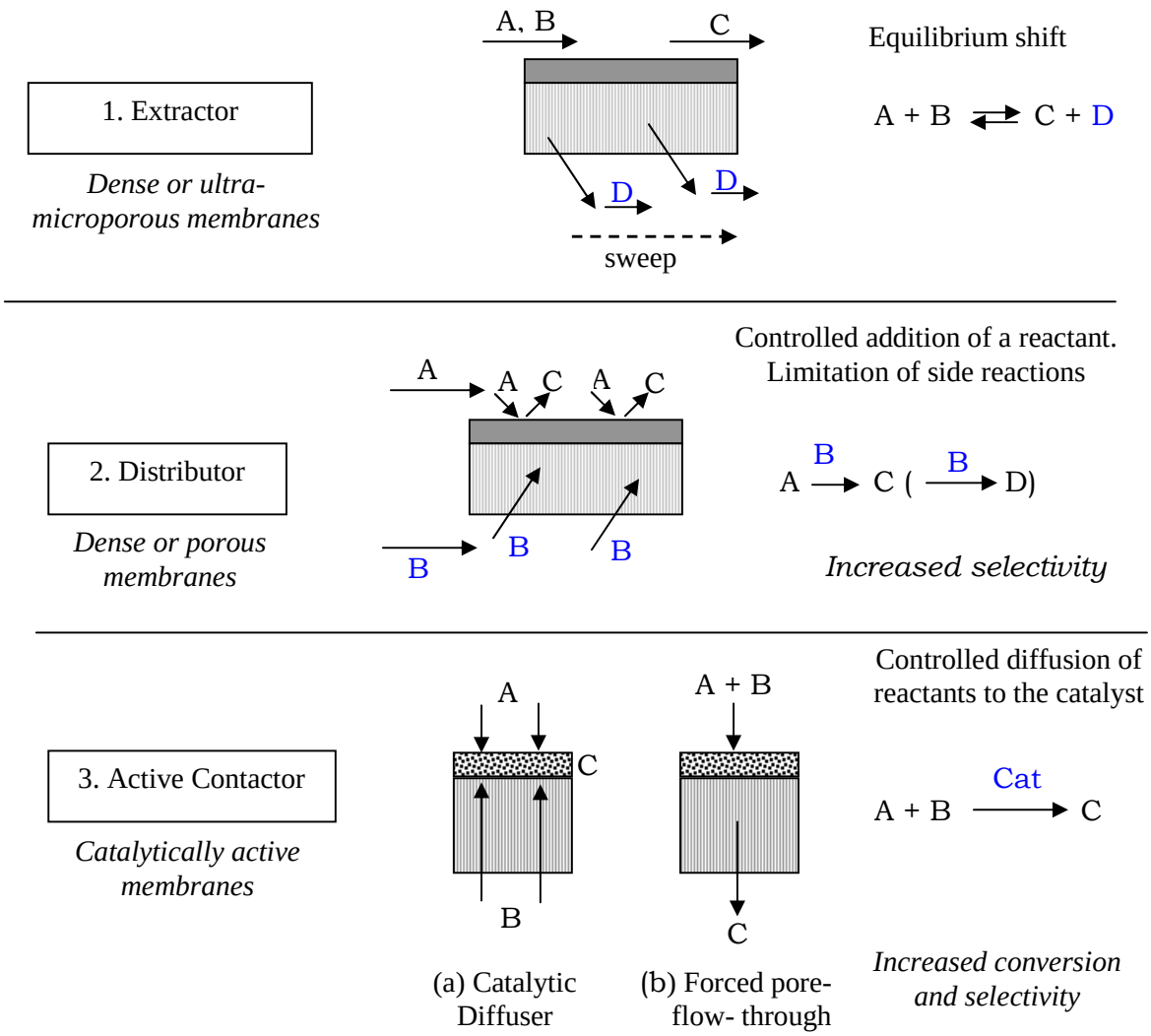

Figure 1.1: Membrane functions in a membrane reactor [Adapted from Julbe *et al.*, 2001]

1.1.1 Extractor membrane reactor

Dense membranes are used to effect the removal of the products and thus increase conversion by shifting the reaction equilibrium. Major areas of application of the extractor include:

a) Selective Product removal.

In some processes, thermodynamic equilibrium can limit the level of conversion achievable in conventional reactors and the removal of a product as it is being formed can help to improve the conversion. An example is the use of palladium membranes for the selective removal of hydrogen in natural gas reforming and hydrocarbon

dehydrogenation reactions [Wieland *et al*., 2001; Dittmeyer *et al*., 2001, Menendez, 2008].

Both fixed bed and fluidized bed membrane reactors are being employed for steam methane reforming, sometimes combined with autothermal reforming, with the aim of producing hydrogen using membrane reactors [Uemiya *et al*., 1991; Adris *et al*., 1991. A major advantage of the fluidized bed membrane reactor for large scale operations is the good isothermal conditions it provides [Adris & Grace, 1997].

In Fischer-Tropsch synthesis, a hydrophilic membrane extractor could be used for in-situ water removal to reduce water-promoted catalyst deactivation, boost reactor productivity, and displace the water gas shift (WGS) equilibrium to enhance the conversion of CO_2 to hydrocarbons [Rohde *et al*., 2008].

b) Reactant purification.

The membrane used in this case is selective to one reactant, and thus allows it to be separated in the same device used for the chemical reaction. The use of ceramic ionic transport membranes selective to oxygen, used for catalytic partial oxidation of natural gas to generate synthesis gas, is the major area of application [Chen, 2005; Foy & McGovern, 2005]. This research is now in the pilot plant level but if it becomes successful in large scale, significant reductions in capital cost will be achieved, because the expensive oxygen separation plant required for many processes would be avoided [Menendez, 2008].

1.1.2 Distributor membrane reactor

Dense or porous membranes are used as distributors to control the addition of reactants to the reaction mixture. The main aim here is to limit side reactions and increase selectivity

of the desired product. They are particularly useful for partial oxidation and coupling of reactions [Westermann & Melin, 2009]. Some of the major functions include:

i) ***Catalytic activity***

Where the membrane has catalytic activity, premixing of reactants can be avoided by designing the reaction in such way that the reactants contact each other in the membrane, avoiding premixing. This kind of catalytically active membranes has been tested in partial oxidation of methane to achieve a H_2/CO ratio of 2:1 required for FT synthesis [Olsen, 2003]. The configuration provides a suitable distribution and better usage of the catalytic material.

ii) ***Distribution of the reactant along the reactor***

This offers controlled addition of the a reactant and can improve selectivity to the desired product, offer better temperature control and afford better safety by avoiding the premixing of reactants that is needed in conventional reactors. Since reactants are not premixed it is possible to feed the reactant systematically in molar ratios that would be within acceptable explosion limits. [Guillou *et al*., 2008]

iii) ***Product removal in non-equilibrium limited reactions***

The removal of a product in some cases is not aimed at shifting the equilibrium, but at increased reaction rate or a lower catalyst deactivation rate. This is the case in Fischer-Tropsch synthesis (FTS) reactors where in situ removal of water is aimed at lowering the rate of catalyst deactivation [Rohde *et al*., 2008]. In other cases a useful intermediate product can be removed from the reaction environment to avoid further reaction to other undesired compounds.

1.1.3 Active contactor membrane reactor

This is applicable where the controlled diffusion of reactants is required to intensify the contact between reactants and the catalyst. The active contactor membrane acts as a

barrier and does not need to be permselective but catalytically active. The operational modes of interest include the forced-through or forced pore-flow-through (PFT), catalytic diffuser, and the multiphase contactor.

i) Forced pore-flow-through (PFT) catalytic membrane reactors

This is the concept employed in this work and involves using a non permselective porous catalytic membrane applied in dead-end mode, and forcing a mixed stream of reactants to flow through the membrane in order to provide a reaction space time with short controlled residence time and high catalytic activity. Pore diffusion can be eliminated if the mixed reactants are "pumped" through an asymmetric ceramic membrane of suitable pore size or just a ceramic support coated with catalytically active metals.

ii) ***Catalytic diffuser***

Contactor membrane reactors could also be arranged in such a way that enables reactants to be brought into intimate contact from different sides of the membrane. In this case, it controls the diffusion of reactants to the catalyst interface and acts as a catalytic diffuser. Examples include the aqueous-organic contactor, and the unselective interfacial contactor [Westermann & Melin, 2009].

iii) ***Multiphase contactor***

This concept is used in packed-bed and fluidized bed membrane reactors to allow a continuous flow of reactant and products. Catalytically active membranes can be applied to three-phase reactions (liquid, gas and solid catalyst) and have advantages over conventional particle catalysts.

Catalytically active components are deposited in the thin fine-porous membrane layer of an asymmetrical ceramic membrane. One reactant is dissolved in the liquid and diffuses through the porous structure of the membrane to the active inner surface; the

other reactant is fed through the support to the catalytic layer from the other side of the membrane; thereby, an effective contact between the two reactants and the solid catalyst is established. Under these conditions catalytically active membranes can typically be applied in hydrogenation or oxidation processes.

1.2 The need for Membranes in synthesis gas conversion processes

An important aspect of catalyst development for synthesis gas (syngas) conversion is the need to control selectivity and this necessitates the control of contact between catalyst and reactants because such syntheses usually are complicated exothermal three-phase processes. Appendix A1 highlights some of the processes involved in syngas conversion, while Appendix A2 summarizes syngas conversion process conditions, and provides information on products from the different syngas conversion processes.

The reacting molecules of the gas phase have to dissolve in the phase of liquid products before contacting the surface of the solid catalyst particles. Also, the products must evaporate to the gas phase in order to 'quit' the catalyst bed. The mass-transport within the flooded catalyst particle is several orders of magnitude slower than that in the case of a two phase process, due to lower diffusivities in the liquid phase [Hilmen *et al*., 2005]. These and some other specific features make the following requirements which are common for all syngas conversion reactors quite crucial [Khassin *et al*., 2005]:

(1) Isothermal catalyst bed (temperature drop, at less than 10 K);

(2) High concentration of the catalytically active substance in the reactor volume;

(3) High gas-liquid interface surface area (at least 20 cm^2 / cm^3);

(4) Small effective size of catalyst grains (preferably, less than 50 nm but large enough to avoid sintering);

(5) Low pressure drop.

The design of slurry bed reactors seem to satisfy demands (1) and (3) – (5) described above. However, the catalyst concentration in the reactor volume is rather low due to the conflict between the loading of a particular matter in the slurry and its effective dynamic viscosity, which promotes coalescence of gas bubbles and a decrease in gas hold-up in the slurry. The interphase mass-transfer in the bubble slurry reactors strongly diminishes when the catalyst loading is above 20-25 wt %. [Beenackers & van Swaaij, 1993]. This results in a low space-time yield of hydrocarbons in FTS with the dimensions of industrial apparatuses becoming very huge. For instance, the *Sasol* slurry phase distillate (SPD) reactor operating at 20 bar with productivity of 2500 barrels per day is 22 m in height and 5 m in diameter [Jager, 1995]. The fixed catalyst bed is much denser, but the conflict between the reasonable hydraulic resistance (large catalyst grains needed) and low diffusion constraints (small catalyst grains needed) results in even worse process performance. “Egg-shell” catalysts with a low concentration of the active component with respect to the entire particle volume have been used to resolve this, but mass transfer restrictions through the fixed bed of egg-shell catalysts still remains an issue which could lead to large pressure drops.

The present work suggests that the solution to this problem is by using the heat-conductive forced pore-flow-through (PFT) active contactor membranes. In this application the membrane is porous and intrinsically active, having had a catalyst deposited within the pores. The membrane geometry allows for a degree of control of the contact time. It is operated in the cross-flow mode, in which all of the reactant is forced to flow through the membrane by feeding it to one side of a membrane reactor with a closed exit as illustrated schematically in Figure 1.2. This configuration gives a uniform contact time, which can be tailored to a particular reaction by the choice of membrane thickness and/or reactant flow rate. The pore size of the membrane controls the diffusion regime.

Also, the membrane geometry can be used to place a catalyst in the membrane optimally, or to control the partial pressure of the reactants in the phase in contact with the catalyst.

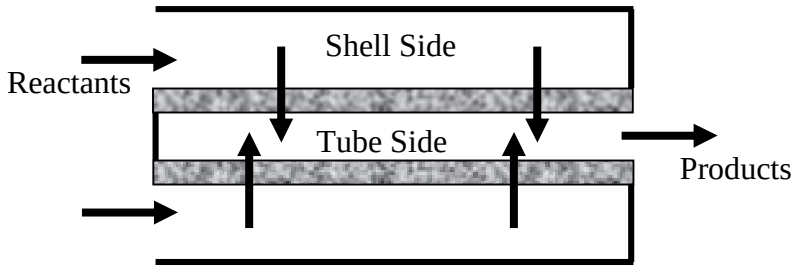

Figure1.2: Schematic of a catalytic membrane reactor operated in the forced pore-flow-through mode

In this work, aqueous impregnation was used to deposit the catalyst particles in the pores of a macroporous support (6000nm). This ensured crystallization of the appropriate grain size of catalyst particles, and facilitated the formation of a non permselective membrane while maintaining viscous flow through the membrane. Figure 1.3(b) shows a catalyst impregnated into the pores of a porous membrane either as individual particles or as a layer.

In classical reactions, conversion is often limited by the diffusion of reactants into the pores of catalyst support as well as by intraparticle diffusion. With a catalyst dispersed in the pore of the membrane, a combination of the open pore path and transmembrane pressure helps to provide easier access of the reactants to the catalyst, reduce contact time, reduce tortousity effects and increase the effectiveness of the catalyst. The benefits include higher reaction rates, improved selectivity, and better product quality.

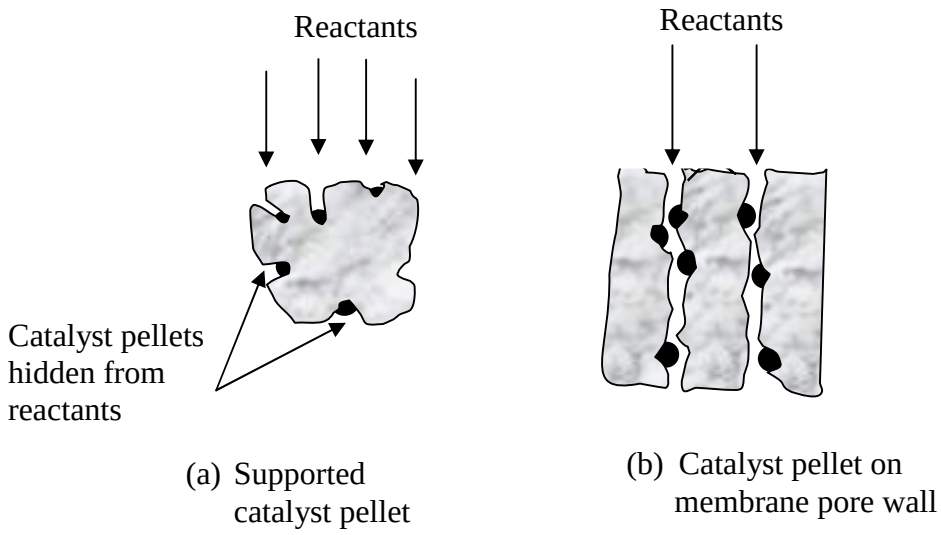

Figure 1.3: Comparison of reactants/catalyst contact in: (a) classical bed reactor and (b) active membrane contactor

The elimination of mass transfer resistance in a forced pore-flow-through contactor catalytic membrane reactor is best appreciated when a comparison is made of what obtains in most conventional catalytic reactors, where the slowest step is the rate determining step for the reaction. Depending on the chosen process parameters, mass transfer can become the rate determining step. For three-phase heterogeneously catalyzed reactions like those encountered in most syngas conversion processes, the limitation to mass transfer is caused by both bulk and intraparticle diffusion and the overall reaction can be broken down into the following steps:

1. Mass transfer of the gaseous reactant from the free gas phase into the gas-liquid interface;
2. Mass transfer by diffusion of the dissolved gaseous reactants in the bulk of the liquid;
3. Diffusion of liquid reactants through the liquid –solid interface to the catalyst;

4. Diffusion of dissolved reactants within the pores of the catalyst to the active sites – pore diffusion;
5. Adsorption of the dissolved reactants at the catalytic active surface – chemisorption;
6. Chemical reaction at the catalyst surface;
7. Desorption of the products;
8. Diffusion of the products out of the pores to the external surface of the catalyst particle;
9. Diffusion of the products through the external liquid interface into the bulk of the liquid.

Figure 1.4 is a schematic illustration of the steps outlined above.

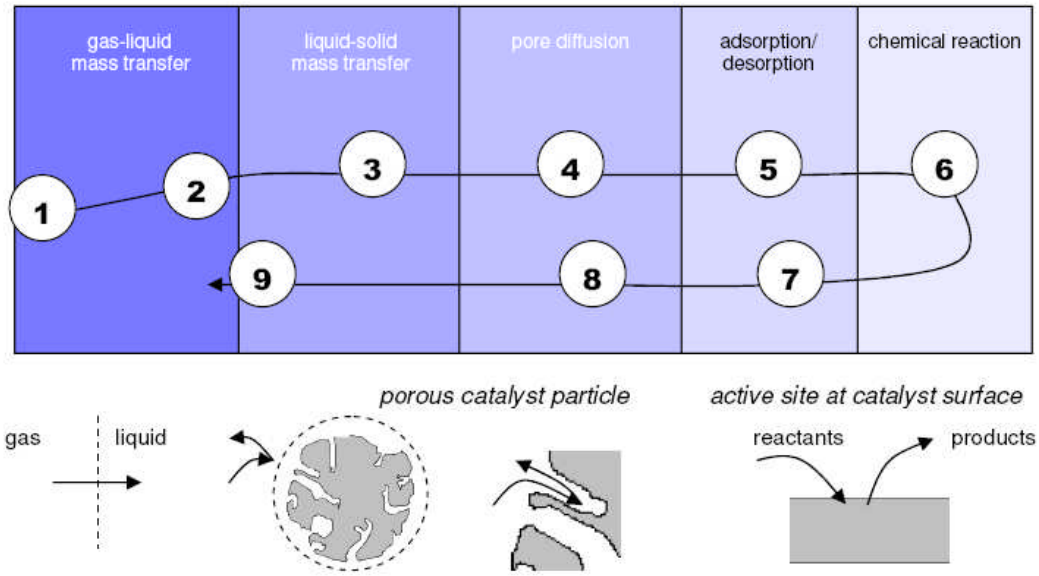

Figure 1.4: Steps in heterogeneously catalyzed, three-phase reaction on a porous catalyst

In a catalytic membrane reactor operated in the forced PFT mode, steps (1) – (4), (8) and (9) are completely eliminated.

1.3 Membrane Fabrication

Many synthesis techniques are available for the fabrication of active catalytic membranes. These include chemical vapour deposition (CVD), precipitation, electroless plating, wet impregnation, sol-gel process, etc.

1.3.1 Chemical vapour deposition

Chemical reactions transform gaseous molecules, called precursors, into a solid material, in the form of a thin membrane film on the surface of a support. This is mostly used for preparing dense composite and highly permselective membranes.

1.3.2 Precipitation

Metallic catalysts could be precipitated or co-precipitated onto a porous support from a solution of their precursors using appropriate chemical reagents. For proper bonding onto the substrate, the membrane support may require pre-treatment using a nucleating agent.

1.3.3 Electroless plating

This is a chemical reduction process which depends upon the catalytic reduction of metal ions in an aqueous solution (containing a chemical reducing agent) and the subsequent deposition of the metal without the use of electrical energy. It provides uniform metallic membrane coating on porous supports.

1.3.4 Aqueous impregnation

A porous support is dipped in a solution of the appropriate salt and the resulting membrane is calcined and the metallic oxide reduced to give the required metal catalyst. This technique reduces clustering of metallic particles in the pores because of high

dispersion in solution. However, multi-step impregnation is not well adapted for controlling the composition of a multi-component membrane material.

1.3.5 Sol-gel process

The sol-gel process is used to disperse a metal precursor in the membrane itself during the synthesis, or to directly synthesize inherently catalytic membranes (single or mixed oxides). It is very attractive for multilayer depositions which can lead to a controlled structure, composition and activity for the membrane.

1.4 Membrane Characterization

Information on some important membrane properties are obtained using a number of characterization methods, some of which are discussed below.

1.4.1 Gas Permeation Tests

These tests provide useful information on the gas transport characteristics of components (both reactants and products) through the membrane. An understanding of flow mechanisms through the membrane is essential to ensure that there is no permselective separation of any of the components of the feed gas mixture as it permeates through the membrane. For macroporous and mesoporous membranes, transport by Knudsen diffusion can be neglected if the Knudsen number (Kn) is significantly smaller than 1; where Knudsen number is the ratio between the mean free path of the molecule (λ_i) and the pore diameter (d_p).

1.4.2 Analysis of surface area and porosimetry (ASAP)

Full gas adsorption/desorption isotherms are provided from tests conducted using nitrogen gas which is dosed very precisely for both adsorption and desorption processes to generate highly accurate isotherm data for the sample material. In addition to the isotherm data, this technique is used for obtaining a full porosimetry testing method through the provision of pore size distribution, pore area distribution and pore volume data. These are reported together with the Brunauer-Emmett-Teller (BET) surface area of the sample. Typically pore sizes in the range 0.55 nm to 350 nm are measured by this technique, although this may be extended to larger pore sizes depending on the nature of the sample. The test is, therefore, ideal for the characterisation of microporous and mesoporous materials and may be combined further with mercury porosimetry to cover the complete range of micro pores through to macro pores at approximately 600μm.

1.4.3 Scanning electron microscopy (SEM)

SEM is used to obtain images of the membranes and membrane supports showing the morphology and topology and also such features as the geometry of the pores, the pore size, any asymmetry in the structure, and also catalyst particles deposited within the pores.

1.4.4 Energy dispersive x-ray analysis (EDXA)

When combined with other electron spectroscopic techniques EDXA provides qualitative and quantitative information about the composition of catalysts support on the membrane. Elemental maps from EDXA provide valuable information on two-dimensional elemental distributions in supported catalysts and are especially useful for characterizing bimetallic or multiphase catalysts [Liu, 2004].

1.4.5 Electron probe microanalysis (EPMA)

Electron Probe Microanalysis (EPMA) is an elemental analysis technique which uses a focused beam of high energy electrons to non-destructively ionize a solid specimen surface (including thin films and particles) for inducing emission of characteristic x-rays. The element concentrations can be determined from the intensity of the detected wave dispersive x-ray.

1.5 Aim and objectives of this work

The main aim of this work is to produce composite membranes made from metallic catalysts deposited in asymmetric macroporous ceramic supports for the conversion of synthesis gas to mixed alcohols and hydrocarbons. It is interesting to note that none of the work documented in literature has explored the possibility of using such a non permselective macroporous membrane impregnated with FT catalysts that will apart from tackling mass transfer restrictions and showing good heat conductivity, ensure selectivity to the required band of products, show good mechanical strength and thermal stability, and also allow for joint permeation of the reactants. This arrangement, according to Coronas & Santamaria [1999], has the advantage of improved gas-solid contact as well as higher conversions and selectivity to the desired products. Wetermann and Melin [2009] agreed that operated as an integral flow-through catalytic membrane reactor, this reaction system can reach complete conversion in minimum time or space, taking advantage of the high catalytic efficiency, or can reach maximum selectivity for a given reaction due to the narrow contact time distribution.

On a tubular macroporous ceramic support, synthesis of small metal crystallites (could be less than 50nm) of the catalyst at high local surface densities is enhanced because of increased rate per surface catalyst atom (turn over rate). This promotes high volumetric

productivity, decreases reactor volume requirements and significantly improves process economics. The physico-chemical properties of the ceramic support also determine the spectrum of products formed. Most FT syntheses are carried out on silica and alumina-supported catalysts. These materials have been reported to suffer deterioration in alkaline environments [Adesina, 1996; Timken & Kyung, 2005]. The alumina support used for this investigation was washcoated with titania which delivered relatively high hydrogenation activities due to strong metal-support interaction, and therefore promoted the formation of alcohols over high molecular weight hydrocarbons. Using tubular membranes, it is possible to work with a high gas pressure inside the membrane while the reactor is itself operated at atmospheric pressure [Reif & Dittmeyer, 2003]. This leads to a simplified process design, and overall, to a safer and cheaper process.

Allowing for the presence of carbon dioxide in the feed not only reversed the water-gas shift activity but also eliminated the need for a gas purification interphase between syngas production and conversion.

The objectives of this research therefore included:

- production of a hybrid membrane for the conversion of synthesis gas to alcohols and hydrocarbons which could be used as fuels, as octane rating enhancers or as precursors for the production of chemicals,
- carrying out Fischer-Tropsch synthesis using non permselective active contactor catalytic membranes operated in the forced pore-flow-through (PFT) mode,
- designing of a catalytic membrane reactor for testing the effects of operating variables on the kinetics of the process,
- studying the effects of membrane properties and process parameters on the conversion of reactants and the product distribution pattern,

- postulation of a possible reaction pathway for the process based on the kinetic data generated.

Mass-transfer limitations are known to affect the performance of many three-phase catalytic processes such as the Fischer-Tropsch synthesis. Numerous studies have been carried out, aimed at reducing the mass- and heat- transfer problems. This becomes even more challenging because of the need to reduce both the internal diffusion resistance of high molecular weight materials formed and the gas-liquid mass transfer restrictions, as well as provide fast heat-transfer within the catalyst bed while retaining its homogeneity and a low pressure drop [Khassin *et al*., 2003]. Bartholomew and Farrauto [2006] reported that the majority of FTS kinetic studies up to about 1990 did not address pore diffusion, heat/mass transfer, and deactivation effects which are quite significant in FTS. This novel concept applied in this work eliminates pore diffusion by forcing the feed mixture through the active contactor membrane and the porous asymmetric support at flow rates that ensure that short contact times are achieved. Total elimination of pore diffusion also leads to the absence of concentration gradients in the pores of the catalytic layer. Thus products are removed from the reaction zone as soon as they are formed which forestalls secondary and consecutive reactions and partly explains the observed selectivity of the products to only mixed alcohols and gasoline.

One of the on-going efforts to develop lower-cost synthesis gas generation technologies is the use of ceramic membrane reactors. This is based on the use of ionic or oxygen transport membranes which will couple air separation and partial oxidation in one unit operation, thereby eliminating the need for a conventional oxygen separation plant [Olsen & Gobina, 2004]. Although still at a fundamental level, work in this area is being aggressively pursued by two industrial consortia. One consortium led by Air Products, is being co-funded by the U.S. Department of Energy, and includes such participants as

ARCO, Babcock and Wilcox, Chevron, Norsk Hydro, etc. The second consortium based entirely on industrial funding, involves Amoco, BP, Praxair, Statoil, Phillips Petroleum and Sasol.

At the Centre for Process Integration and Membrane Technology of the Robert Gordon University, Aberdeen, membranes have been successfully used in the production of synthesis gas [Olsen, 2003; Olsen & Gobina, 2004]. This work is currently being tested for commercialization in a spin-off company, *Gas2 Limited*. Since syngas production is only the first step in synthetic fuels technology, it is reasonable to adapt a similar technology (using catalytic membrane reactors), for the entire process. This innovation will greatly reduce ulterior design problems and move us a step forward in the quest for the fabrication of an integrated but modular plant for the conversion of natural gas into value-added liquid fuels, even at production platforms or flow stations. The liquid products could then be transported through conventional oil pipelines, thereby helping to monetize stranded gas.

It had been estimated that the GTL process may ultimately play an important role in the transportation fuel supply chain if the price of crude exceeds US$20/bbl [Dry, 2004]. The surge in the price of oil to $147/bbl in July 2008 should be enough to signpost the urgent need to fully explore this age-old technology.

1.6 Relevant Publications from this work

1. British Patent Application Number 0718398.1. *Process for the Production of alcohols using a catalytic membrane reactor*. The Robert Gordon University, Aberdeen. September, 2007.

2. Umoh, R. M., Gobina, E. N. and Reid, W., *Higher Alcohols Production to tackle gas flaring in the Niger Delta*. Prepared for presentation at the 1st Postgraduate Researchers' Conference, Dundee, 29 - 30 September 2008.

1.7 References

Adesina, A. A. (1996). Hydrocarbon synthesis via Fischer-Tropsch reaction: travails and triumphs. *Applied Catalysis A: General* 138, p.351.

Adris, A. M., Grace, J. R. (1997). Characteristics of fluidized-bed membrane reactors: Scale-up and practical issues. *Industrial and Engineering Chemistry Research*, 36, pp.4549-4556.

Adris, A. M., Elnashaie, S., Hughes, R. (1991). A fluidized-bed membrane reactor for the steam reforming of methane. *Canadian Journal of Chemical Engineering*, 69, p.1061.

Bartholomew, C. H., Farrauto, R. J. (2006). *Fundamentals of Industrial Catalytic Processes*, 2nd Ed. New York: John Wiley and Sons.

Beenackers, A. A. C. M., van Swaaij, W. P. M. (1993). Mass transfer in gas-liquid slurry reactors. *Chemical Engineering Science* 48 (18), pp.3109-3139.

Bredesen, R., Jordal, K., Bolland, O. (2004). High temperature membranes in power generation with CO_2 capture. *Chemical Engineering and Processing* 43 (9), pp.1129-58.

Chen, C. (2005). *Ceramic membrane reactor systems for converting natural gas to hydrogen and synthesis gas (ITM Syngas)*. FY 2005 Progress Report IV.A.11, DOE Hydrogen Program. pp.124-126. http://www.hydrogen.energy.gov/pdfs/progress05/iv_a_11_chen.pdf [Accessed 5 November, 2008].

Coronas, J., Santamaría, J. (1999). Catalytic reactors based on porous ceramic membranes *Catalysis Today* 51, (3-4), pp.377-389.

Dittmeyer, R., Hollein, V., Daub, K. (2001). Membrane reactors for hydrogenation and dehydrogenation processes based on supported palladium. *Journal of Molecular Catalysis A: Chemical* 173, (1-2), pp.135-184.

Dry, M. E., 2004. Present and future applications of the Fischer-Tropsch process. *Applied Catalysis A: General*, 276 (1-2), pp.1-3.

Foy, K., McGovern, J. (2005). *Comparison of ion transport membranes*. In Conference Proceedings of 4th Annual Conference on Carbon Capture and Sequestration DOE/NETL, 2-5 May.

Guillou, L., Paul, S., Le Courtois, V. (2008). Investigation of H2 staging effects on CO conversion and product distribution for Fischer-Tropsch synthesis in a structured microchannel reactor. *Chemical Engineering Journal*, 136, pp.66-76.

Hilmen, A. -M., Bergene, E., Lindvag, O. A., Schanke, D., Eri, S., Holmen, A. (2005). Fischer-Tropsch synthesis on monolithic catalysts with oil circulation. *Catalysis Today* 105, pp.357-361.

Jager, B., Espinoza, R. (1995). Advances in low temperature Fischer-Tropsch synthesis. *Catalysis Today* 23, pp.17-28.

Julbe, A., Ayral, A. (2007). Catalytic membrane reactors involving inorganic membranes – a short overview. http://water-environment.vin.bg.ac.yu/proceedings/3%20Strana%2030-3%20B5%20Julbe-Belgrade%202007.doc. [Accessed: 23 November, 2008].

Julbe, A., Farruseng, D., Guizard, C. (2001). Porous ceramic membranes for catalytic reactors – overview and new ideas, *Journal of Membrane Science*, 181, p.4.

Khassin, A. A., Sipatrov, V. A., Chermashentseva, G. K., Yurieva, T. M., Parmon, V. N. (2005). Fischer-Tropsch synthesis using plug through contactor membranes based on permeable composite monoliths: Selectivity control by porous structure parameters and membrane geometry. *Topics in Catalysis*, 32 (1-2), pp.39-46.

Khassin, A. A., Yurieva, T. M., Sipatrov, A. G., Kirillov, V. A., Chermashentseva, G. K., Parmon, V. N. (2003). Fischer-Tropsch synthesis using a porous catalyst packing: experimental evidence of an efficient use of permeable composite monoliths as a novel type of the Fischer-Tropsch synthesis catalyst. *Catalysis Today*, 79-80, pp.465-473.

Li, K. (2007). Ceramic Membranes for Separation and Reaction. West Sussex: John Wiley, pp.16-17.

Liu, J. (2004). Advanced electron microscopy characterization of nanostructured heterogeneous catalysts. *Microscopy and Microanalysis*, 10, pp.55-76.

Menendez, M. (2008). Inorganic membrane reactors. [Accessed: 7 November 2008] http://topics.scirus.com/Inorganic_Membrane_Reactor.html

Olsen, S., Gobina, E. (2004). GTL synthesis gas generation membrane for monetizing stranded gas. *Membrane Technology*, June, p.5-10.

Olsen, S., (2003). Catalytic membrane reactors for synthesis gas production via partial oxidation, PhD thesis, Robert Gordon University-Aberdeen.

Reif, M., Dittmeyer, R. (2003). Porous catalytically active ceramic membranes for gas-liquid reactions: a comparison between catalytic diffuser and forced flow through concept. *Catalysis Today* 82, pp.3-14.

Rohde, M. P., Schaub, G., Khajavi, S., Jansen, J. C., Kapteijn, F. (2008). Fischer–Tropsch synthesis with in situ H_2O removal – Directions of membrane development. *Microporous and Mesoporous Materials*, 115 (1-2), pp.123-136.

Smid, J., Avci, C. G., Gunay, V., Terpstra, R. A., van Ejik, J. P. G. M. (1996). Preparation and characterization of microporous ceramic hollow fibre membranes. *Journal of Membrane Science*, 112, p.85.

Timken, H., Kyung, C. (2005). *Homogeneous modified-alumina Fischer-Tropsch catalysts support*. World Patent # WO/2005/060448.

Uemiya, S., Sato, N., Ando, H., Matsuda, T., Kikuchi, E. (1990). Steam reforming of methane in a hydrogen-permeable membrane reactor. *Applied Catalysis*, 67 (1), pp.223-230.

Westermann, T., Melin, T. (2009). Flow-through catalytic membrane reactors –principles and applications, *Chemical Engineering and Processing*, 48 (1), pp.17-28.

Wieland, S., Melin, T., Lamm, A. (2001). Membrane reactors for hydrogen production. *Chemie Ingenieur Technik-CIT*, 73 (6), p.768.

Chapter 2 – Literature Review

CHAPTER 2: Literature Review

2.1 Membrane Technology

Traditionally, the term membrane is associated with the concept of a layer of material which is capable imposing certain restrictions on the permeation flux of some substances. Thus in selective permeation membranes, only certain molecules meet the permeation requirements, and the membrane acts as a barrier for the rest. Interestingly, only a few membrane systems conform strictly to this definition. For instance, in flow-through membranes, permeation of the entire reactant stream through the membrane takes place, and in some catalytic membranes, the reactants converge on the membrane rather than permeating across it.

In the IUPAC definition, a membrane reactor is a device that combines a membrane-based separation process with a chemical reaction step in one unit [Dittmeyer *et al*., 2001]. Membrane technology therefore finds application in two broad areas namely; separation and chemical or biological reactions, and sometimes combine the two unit operations in one equipment.

2.1.1 Membrane Separation Processes

Membrane processes have been employed for a wide range of separations and reactions [Li, 2007]. The driving force for separation could be difference in pressure, concentration or electric field across the membrane. They can therefore be differentiated according to the driving force, molecular size or type of operation. For membrane contactors, separation is primarily based on phase equilibria. Membrane separations involve the separation of a feed (stream) into components using a semi-permeable barrier through

which the components move with different velocities. Some components are allowed passage by the membrane into a permeate stream, whereas others are retained by it and accumulate in the retentate stream, and a so-called sweep stream can be used to remove the permeate as shown in Figure 2.1.

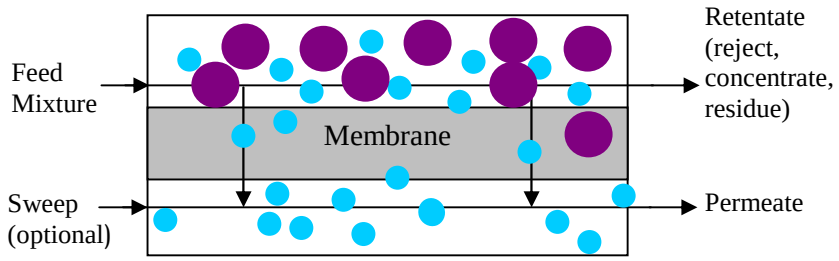

Figure: 2.1: Membrane separation process

Industrial processes that utilize membrane separation include reverse osmosis and nano filtration, dialysis, electrodialysis, microfiltration, ultrafiltration, pervaporation, thermopervaporation, gas separation, electro-osmosis, electrophoresis, and membrane distillation [Scott & Hughes, 1996]. Supported liquid membranes (SLM) are also used for example, in the recovery of zinc and nickel and other metals from waste water and process streams [Ho *et al*., 2001].

A liquid membrane system, hybrid liquid membrane (HLM), was developed for the separation of solutes (metal ions, acids, etc.) by Kishik and Eyal [1996]. It utilizes a solution of an extracting reagent (carrier solution), flowing between membranes. Membrane contactors represent a technology where porous membranes are used as ‘packing materials’ for interphase mass transfer. Therefore, all traditional gas stripping and absorption, distillation, liquid-liquid extraction, as well as emulsification, crystallization and phase transfer catalysis can be carried out in membrane contactors [Li, 2007].

2.1.2 Types of membranes

Membranes can be classified as organic or inorganic. Inorganic membranes for reactors can be inert or catalytically active; they can be either dense or porous, made from metals, carbon, glass or ceramics. They can be uniform in composition, composite (i.e. made from different materials), homogeneous or asymmetric porous structures. Membranes can also be supported on such materials as porous glass, sintered metal, granular carbon or ceramics like alumina. Different membrane shapes can be used: flat discs, tubes (dead-end or not), hollow fibres, or monolithic multi-channel elements (for ceramic membranes), and also foils, spirals or helix for metallic membranes [Julbe *et al*., 2001].

In porous ceramic membranes, their traditional applications and separation mechanisms correspond to the pore size of the membranes as shown in Table 2.1.

Table 2.1: Category of ceramic membranes [Adapted from Li, 2007]

Type	Pore size (nm)	Mechanism	Applications
Macroporous	>50	• Viscous flow • Molecular sieving	Ultrafiltration (UF), Microfiltration (MF)
Mesoporous	2-50	• Knudsen diffusion	UF, Nanofiltration (NF), Gas separation
Microporous	<2	• Pore diffusion	Gas Separation
Dense	–	• Surface flow • Solution diffusion	Gas Separation, Reaction

They generally have a macroporous support which provides the mechanical strength, one or two mesoporous intermediate layers to bridge the pore size differences between the support layer and top layer where separation actually occurs. Figure 2.2 gives a representation of such an asymmetric composite membrane.

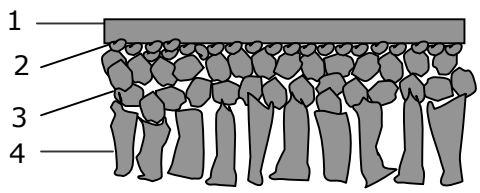

1. Modified separation layer (dense or <2nm)
2. Separation layer (3-100nm)
3. Intermediate layer(s) (100-1500nm)
4. Porous support (1-15µm)

1+2+3+4 nanofiltration or gas separation membranes
2+3+4 ultrafiltration membranes
3+4 microfiltration membranes

Figure 2.2: Schematic representation of an asymmetric composite membrane [Li, 2007]

2.1.3 Membrane Transport Mechanisms and Separation Performance

In dense membranes, solution diffusion generally takes place, although surface reactions are also important. In porous ceramic membranes, permeation behaviour may be dominated by viscous flow, Knudsen diffusion, surface diffusion, capillary condensation, and molecular sieving. These mechanisms are as a result of the interaction between the membrane and the permeating molecules, which also determine the selectivity and permeability of the membranes. The pore size and pore size distribution of the membrane, operating temperature and pressure, and the nature of the membrane material and permeating molecules control the extent of interaction with and mass transfer across the membrane [Shelekhin *et al.*, 1995]. Figure 2.3 shows some major gas transport mechanisms through membranes.

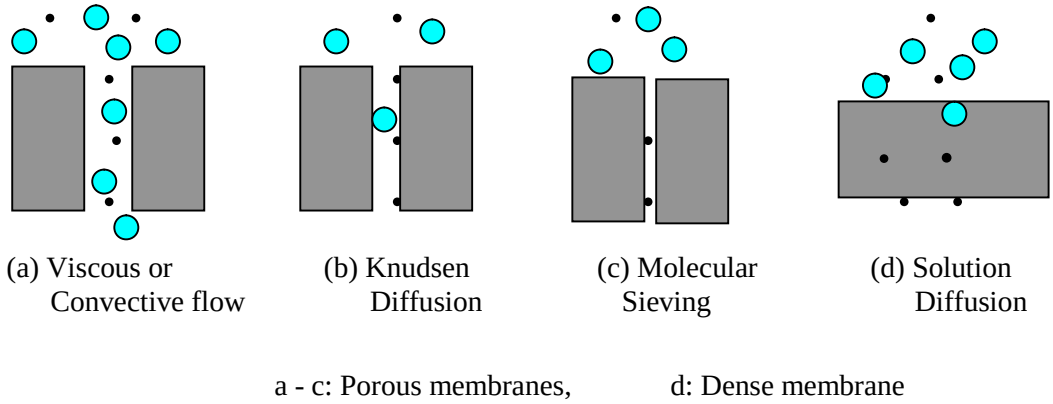

Figure 2.3: Mechanisms for gas separation using membranes [Adapted from Ho & Sirkar, 1992]

The performance of a membrane is measured by its permeance for a given species or ratio of permeance for the species to be separated. Permeance $\boldsymbol{K_M}$ can be compared to a mass transfer coefficient. For a membrane with thickness δ_M (m) and driving force Δc (mol/m^3, kg/m^3) or Δp (Pa), transport rate N_i per m^2 area (or "**flux**") can be defined as:

$$N_i = \frac{J_i}{\delta_M} \times (driving\ force) = \boldsymbol{K_{M,\,i}} \times (driving\ force) \qquad (2.1)$$

where J_i is the **permeability**, and $\boldsymbol{K_{M,\,i}}$ is the permeance for species i.

The selectivity of the membrane towards mixtures is usually expressed in terms of the separation factor α. For a mixture consisting of components A and B the **selectivity factor** $\boldsymbol{\alpha}_{A/B}$ is given by:

$$\boldsymbol{\alpha}_{A/B} = \frac{y_A / y_B}{x_A / x_B} \qquad (2.2)$$

where y_A and y_B are concentrations of components A and B in the permeate and x_A and x_B are the concentrations of the components in the feed [Mulder, 2000].

Gas permeation in macroporous and mesoporous membranes can occur by molecular diffusion, Knudsen flow and convective (viscous or Poisseuille) flow mechanisms. As

stated earlier, when the Knudsen number (Kn) is significantly smaller than 1 (as in liquids), Knudsen diffusion can be neglected.

$$Kn = \frac{\lambda_i}{d_p} \tag{2.3}$$

where $\boldsymbol{\lambda_i}$ is the mean free path of the molecule and d_p is the pore diameter of the membrane. The mean free path could be expressed as [Bernauer, 2006]:

$$\lambda_i = \frac{16\eta_i}{5\pi\bar{p}}\left[\frac{\pi RT}{2M_i}\right]^{1/2} \tag{2.4}$$

where $\bar{p}$ is the mean gas pressure, η_i the dynamic viscosity and M_i the molecular weight. It is therefore assumed that permeation through such membranes can be described by the dusty-gas model to compute concentration fields in the membrane. Dusty gas model provides the constitutive flux equations in the following implicit form [Zhu & Kee, 2003; Bernauer, 2006]:

$$\frac{N_i}{D_i^e} + \sum \frac{P_j N_i - P_i N_j}{P D_{ij}^e} = -\frac{1}{RT}\nabla P_i - \frac{B_o P_i}{D_i^e \mu}\frac{1}{RT}\nabla P \tag{2.5}$$

$$\sum_k \frac{N_k}{D_k^e} = -\left[1 + \frac{B_o}{\mu}\sum_k \frac{P_k}{D_k^e}\right]\frac{\nabla P}{RT} \tag{2.6}$$

where N_i is the flux density of species i through the support, $P_{i\text{-}k}$ are partial pressures of the species, P is the total pressure, μ is the mixture viscosity, B_0 is a morphological parameter, D_{ij} is the effective molecular binary diffusion coefficient and D_i^e is the effective Knudsen diffusion coefficient of species i which is given by

$$D_i^e = \frac{4}{3}K_o\sqrt{\frac{8RT}{\pi M_i}} \tag{2.7}$$

The morphological parameters B_0 and K_0 are given by [Papavassiliou *et al*., 1997]

$$K_o = \varepsilon d_p / 4\tau \qquad B_o = \varepsilon d_p^2 / 32\tau \tag{2.8}$$

where ε, and τ are the porosity and tortuosity respectively, of the porous membrane.

By eliminating the total pressure gradient from equation (2.5) using equation (2.6), the relation between the gradient of partial pressure of i-th compound and the fluxes could be obtained as:

$$\frac{N_i}{D_i^e} + \sum_{j \neq i} \frac{P_j N_i - P_i N_j}{P D_{ij}^e} = -\frac{1}{RT} \nabla P_i + \frac{B_o P_i}{D_i^e \mu} \frac{\sum_k \frac{N_k}{D_k^e}}{1 + \frac{B_o}{\mu} \sum_k \frac{P_k}{D_k^e}} \tag{2.9}$$

The net flux density N_i through the membrane is the sum of molecular, Knudsen and viscous flux contributions,

$$N_i = N_{dif,i} + N_{Kn,i} + N_{vis,i} \tag{2.10}$$

For a composite membrane, similar sets of equations could be generated for both the membrane and support layers, except in the case of a microporous membrane sublayer where the generalized Maxwell-Stefan (GMS) constitutive relations (based on the momentum transfer between particles in motion) have to be applied for mlticomponent mixtures.

Table 2.2 shows the gas transport mechanism in membranes together with the separation performance and the flux.

Table 2.2: The separation performance of membranes and their flow mechanism

Mechanism	Separation Performance	Flux
Viscous flow	No separation – large pores	High for all gas molecules
Molecular sieving	Excludes large molecules from the pores by virtue of pore size	High for smaller molecules, low for larger ones
Knudsen diffusion	Separation is based on molecular weight. $\lambda_i > d_p$ or total pressure is low	High for lighter molecules
Pore diffusion	Preferential adsorption of molecules on pore surface	Low with high selectivity
Solution diffusion	Gas dissolves into membrane material and diffuses across it.	Low

2.1.4 Membrane Reactors

The overwhelming majority of chemical processes involve both reaction and separation and membrane reactors try to take advantage of the synergistic effects of these operations. Membrane reactors are categorized into two types: packed-bed membrane reactor (PBMR) or inert membrane reactor (IMR) and catalytic membrane reactor (CMR). PBMRs have different zones for reaction and separation and are used to improve the distribution of the reactant throughout the length of the reactor, whereas in catalytic membrane reactors, reaction and separation occur simultaneously.

Some possible configurations of porous membrane reactors are listed in Table 2.3 [Coronas & Santamaria, 1999]. Pore-flow-through (PFT) catalytic membrane reactors seek to utilize the advantage offered by co-feeding the reactants, which basically is the improvement of the gas-solid contact, leading to improvements in conversion and selectivity.

Table 2.3: Possible configurations of Porous Membrane Reactors [Coronas Santamaria, 1999]

Configuration	Advantages sought	Types of membrane
A: Inert membrane reactor (IMR) – permeation of products	Increased reaction yield by equilibrium displacement	(i) Selective. Thin metallic layers (e.g. Pd or Ag-based alloys on ceramic substrates) (ii) Nonselective. Porous membranes: silica, alumina, titania, glass, etc
B: Permeation of products plus reaction coupling	As above, although higher yields could be expected due to the thermal/chemical coupling of reactions	As above
C: IMR – distribution of reactants	Increased selectivity through control of the concentration of selected species along the reactor. Increased reactor safety.	Meso- or microporous membranes
D: Catalytic membrane reactor (CMR) – Mobile and active lattice oxygen	Control of the oxygen distribution in the reactor. In principle, it is possible to avoid the presence of gas phase oxygen	(i) Thin layers of Ag-based alloys on top of porous ceramic membranes. (ii) Thin layers of dense oxide on top of porous ceramic membranes
E: CMR – Segregation of reactants on both sides of the membrane	Confinement of reaction to a finite thickness zone inside the membrane. Reaction slip is avoided. Improved safety	Porous catalytic membranes
F: Inert/catalytic composite membrane	Control of the concentration of a reactant by means of mass transfer resistance in the IMR zone	Composite membranes: inert (diffusion) zone plus catalytically active zone
G: CMR – Segregation of liquid and gaseous reactants	Improved mass transfer in G-L-S reactions	Porous catalytic membranes
H: CMR – Joint permeation of reactants	Improved G-S contact, higher conversions	Porous catalytic membranes

2.1.4.1 Membrane-catalyst arrangement in membrane reactors

One of the major challenges in the application of catalytic membranes is the incorporation of the catalyst within the membrane, which depends on the function desired. Figure 2.4 shows the main membrane/catalyst combinations that are commonly used [Li, 2007].

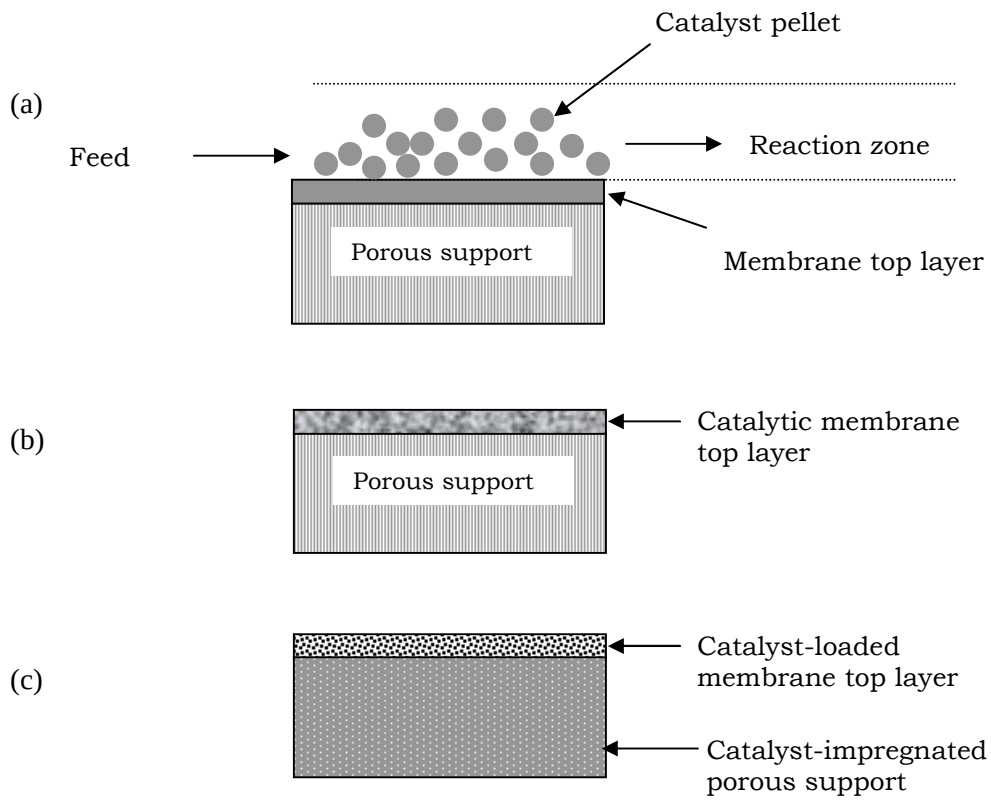

Figure 2.4: Coupling of membrane with catalyst [Li, 2007]

In Figure 2.4 (a) the catalyst is physically separated from an inert membrane (IMR). The reactor is loaded with conventional pellet catalysts, with the membrane forming the inner wall of the tubular reactor without being directly involved in the catalytic reaction. The catalyst pellets are usually packed or fluidized on the membrane or coated in the form of a paste. The latter technique is used in the preparation of monolithic catalytic membranes. They have been used as oxygen distributors in partial oxidation, oxy-dehydrogenation of alkanes, and in the oxidative coupling of methane [Julbe *et al.*, 2001]. The membranes used for this type of application strive to maintain the desired transmembrane flux whilst avoiding back diffusion of the second reactant. The latter function can be achieved in meso- or macro-porous membranes by imposing a pressure gradient.

In (b), the membrane itself is inherently catalytic. The active catalyst is a thin membrane layer deposited on the surface of an inert porous support. A typical example is the dense permselective Pd or Pd alloys membrane used in hydrogenation or dehydrogenation reactions to facilitate H_2 separation [Bobrov *et al*., 2005; Dittmeyer *et al*., 2001]. Such a membrane can also be used solely for hydrogen purification.

Porous inorganic materials with intrinsic catalytic properties such as alumina, titania, zeolites with acid sites, rhenium oxide, LaOCl, RuO_2-TiO_2 and RuO_2-SiO_2, VMgO, or La-based perovskites have been investigated [Julbe & Ayral, 2007]. They are used as active contactors to improve access of the reactants to the catalyst whilst also serving as separators. According to Julbe and Ayral [2007], such a membrane does not need to be permselective but needs to be highly active for the considered reaction, to contain a sufficient quantity of active sites, to have a sufficiently low overall permeability and to operate in a diffusion-controlled regime.

Figure 2.4 (c) shows a catalyst immobilized within the pores of a membrane providing for the catalytic and separation functions to be engineered in a very compact fashion. The catalyst is impregnated into pores of the support, and can also form a monolayer of catalyst particles on the surface of the support.

Among the number of membrane concepts developed for membrane reactor applications, porous infiltrated composite membranes have attractive prospects [Julbe *et al*., 2001]. These porous membranes, in which the membrane material is deposited inside the pores of a robust porous support (Figure 2.5), have a good thermo-chemical resistance, a low sensitivity to the presence of defects, a sufficiently low permeability (barrier effect) and are more easily reproducible than thin supported membrane layers.

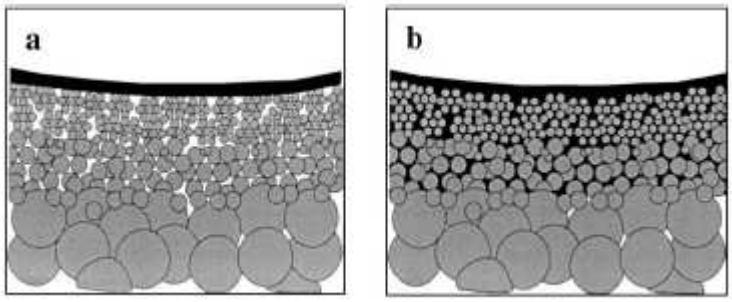

Figure 2.5: Schematic representation of: (a) a thin supported membrane layer on an asymmetric support, and (b) a composite membrane infiltrated in an asymmetric support

The effects of the thickness of the membrane layer could be studied using a simple fast reaction:

$$A + B \longrightarrow C \longrightarrow D$$

Figure 2.6 shows graphically that by adjusting the value of x_1 (making it close to x_2), the reaction can be tailored to maximize the production of C.

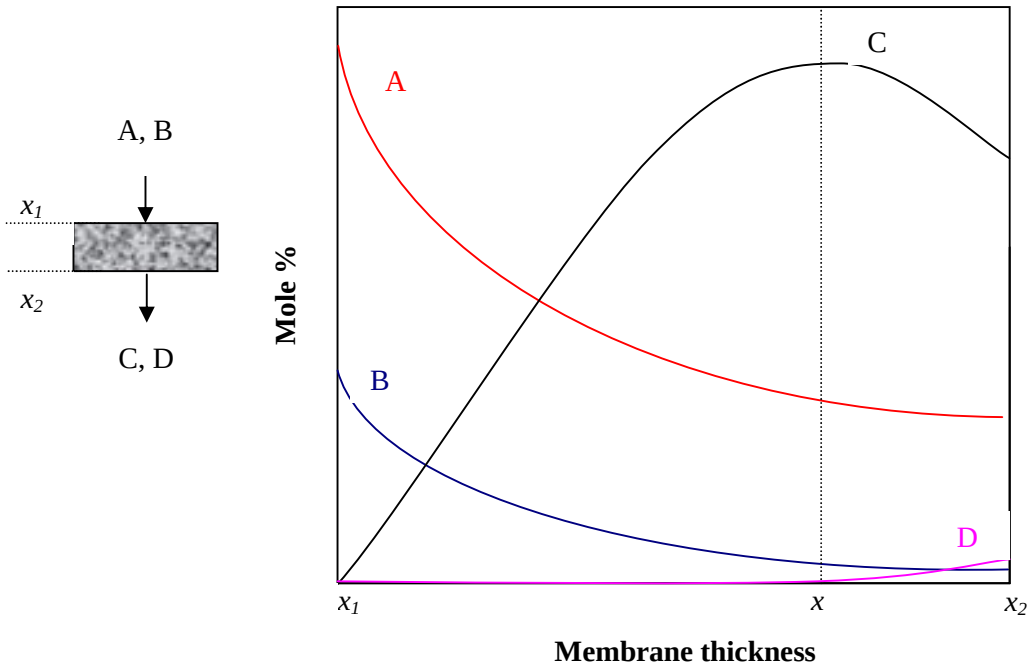

Figure 2.6: Typical concentration profiles within the membrane for a fast reaction

2.1.5 Current Trends in catalytic membranes research

Catalytic membranes are currently being studied in many places, because the vision of process integration and intensification by multifunctional reactors has stimulated a lot of academic and industrial research, which is impressively demonstrated by more than 100 scientific papers on membrane reactors being published every year [Dittmeyer *et al*., 2001]. In a review of the preparation and application of catalytic polymeric membranes, Ozdemir and co-workers [Ozdemir *et al*., 2006] indicated that many reactions have been carried out in polymeric catalytic membrane reactors (PCMR) with gas permeation and even in the liquid phase. Gas phase applications include hydrogenation of linear and cyclic alkenes, dienes and alkynes, reduction of nitrous oxide, decomposition of methyl – tertiary butyl ether (MTBE), and dimerization of isobutene. Liquid phase reactions include catalytic oxidations, acid-catalysed hydrations, hydrogenation of methylacetoacetate and 4-chlorophenol, esterifications and epoxidation of propylene to propylene oxide.

Most applications for membrane reactors involve inorganic membranes. The shape of the separative element induces a specific surface/volume ratio for the reactor, which needs to be maximized, typically above 500 m^2/m^3, for industrial applications [Caro *et al*., 2007]. Apart from the evident need for low cost, resistant and efficient membranes for the process, highly permeable supports are required for all applications involving composite membranes. Catalytic inorganic membranes have found wide usage in oxidation and hydrogenation/dehydrogenation reactions including multiphase reactions [Armor, 1998; Coronas & Santamaria, 1999; Gryaznov, 1999; Centi *et al*., 2003, Julbe & Ayral, 2007]. A comprehensive review of available literature on catalytic membrane reactors and their applications has been undertaken by Koros and Fleming [1993], and Dixon [2003] with

discussions about the opportunities that exist for the commercialization of existing technologies in the future.

2.2 Application of catalytic membrane reactors in Fischer-Tropsch Synthesis

Most of the reactors for the Fischer-Tropsch synthesis (FTS), which are also similar to those used in other syngas conversion processes, suffer from one disadvantage or another, as shown in Table 2.4.

Table 2.4: Comparison of Industrial FTS Reactors

Reactor Type	Major features/ Application	Advantages	Disadvantages
Multitubular Fixed Bed (MTFBR)	Catalysts pellets are packed in tubes and the cooling medium flows around the outside of the tubes, similar to a shell and tube heat exchanger. Tube diameter limited to 25-50mm because of heat transfer limitations within the tubes; catalyst pellet not larger than 0.5mm to avoid reaction rate being limited by intraparticle diffusion. Used for low temperature Fischer-Tropsch reactions – Sasol I (*Arge*) and Shell middle distillate synthesis (SMDS).	• Relatively simple design	• Expensive construction due to large number of tubes, and difficult to scale up. • Radial and axial temperature gradients exist in tubes; problem with heat removal • May give high pressure drop in tubes. • Catalyst replacement is cumbersome.
Circulating Fluidized Bed (CFBR)	Fused Fe catalysts is circulated with syngas through a complex reactor/hopper/standpipe system and heat is removed as steam through coils suspended in the reactor section. The reactor needs a complex support system to cope	• Better heat removal and temperature control. • Less pressure drop problems • Online catalyst	• Physically complex and suspended in a complex structure. • Circulation of large tonnage of catalyst can cause erosion in some regions of the

	with the circulating catalyst loads and temperature differences. Used for high temperature Fischer-Tropsh (HTFT) process in Sasol I & II (Synthol Reactor).	removal/ addition. • Intraparticle mass transfer limitation is absent.	reactor, and may also lead to considerable recycle gas compression with added costs. • Presence of liquid products causes agglomeration of catalyst particles thereby disturbing fluidization. • Requires downstream recovery facilities.
Fixed Fluidized Bed (FFBR)	Basically a vessel with a gas distributor at the bottom and heat exchanger tubes suspend in the catalyst bed. Catalysts inventory and selectivity to low molecular weight compounds (especially olefins) same as for Synthol reactors. Used in Sasol II & III HTFT process as Sasol Advanced Synthol (SAS) reactor.	• Lower construction cost than CFBR. • Higher performance than CFBR. • Improved stability and lower catalyst consumption • Less erosion than in CFBR.	• Presence of heavier hydrocarbons decreases bed fluidization. • Can only be operated above the dew points of hydrocarbons, implying that only light products can be produced.
Slurry Bubble Column (SBCR)	Syngas is bubbled up through a slurry of catalyst suspended in a heavy oil medium or wax, while heat is removed from the column by means of a heat exchanger coil carrying cooling water.	• Near isothermal conditions in the reactor. • Simple design and much lower construction cost. • Good selectivity control.	• Bulk diffusion limitations of reactants from gas phase through the wax to the small solid catalyst pellets. • Catalyst attrition.

		• Low pressure drop. • Ease of addition and removal of catalyst. • Improved catalyst economy and low turn down ratio. • Potential high capacity.	• Problem of separation of catalysts from waxy liquid products. • Back mixing of the gas phase bubbling through slurry decreases conversion per pass and reactor productivity. • Presence of any poisons in the syngas affects all the catalyst in the reactor.

It could therefore be concluded that up till now, no reactor concept is available industrially for syngas conversion processes, which combines optimal features in all relevant aspects [Guettel *et al*., 2008]. An ideal reactor would have the following characteristics:

- fixed bed catalyst
- high catalyst efficiency due to short diffusion distances
- highly efficient gas-liquid mass transfer
- isothermal operation at highest possible temperatures.

Alternative reactor designs developed for FTS include the use of structured catalyst such as catalytic wall reactors, honeycomb monolith or foam shaped catalysts, micro-structured reactors and membrane reactors. Others include spinning basket reactor and Berty reactor. Tube-wall reactors (TWR) or catalytic wall reactors have been used for FTS, where aluminium or stainless steel plates or tubes are coated with a thin film of

supported or unsupported catalysts [Dalai *et al*., 1997; Giornelli *et al*., 2007]. The major issue raised in these systems was the difficulty in coating the metallic substrate, although plasma-assisted chemical vapour deposition (CVD) looks promising. R. M. de Deugd and co-workers mentioned the use of another type of reactor – the gas lift recycle reactors which showed good mixing of temperatures as a result of high recirculation rates [de Deugd *et al*., 2003a]

2.2.1 Monolithic Reactors

The use of honeycomb monolithic reactors seems to have attracted a lot of interest, going by the number of articles that have been published. Hilmen *et al*., [2001] reported an attempt to use monolithic structures to overcome problems associated with particle size of catalysts and transport limitations. They observed that with a monolithic reactor, a short diffusion distance can be maintained without having to reduce the fraction of active material, since the catalyst is located in the thin walls (washcoat) of the monolithic structure. Advantages include low pressure drop, high gas-liquid mass transfer rates in two-phase flow, the possibility of using liquid and gas throughputs and good temperature control by direct cooling of the catalyst with a liquid medium and external heat removal. De Deugd *et al*. [2003b] also designed a monolithic loop reactor for FTS to provide the process needs concerning selectivity, heat removal, pressure drop and catalyst attrition and separation. Their experimental results showed apart from competitive activity and chain growth probability, high olefin to paraffin ratios. In another work, they presented a model of a monolithic loop reactor and concluded that the reactor demonstrated a high productivity and acceptable pressure drop, whilst ensuring high selectivity and low temperature rise in the reactor [de Deugd et al., 2003c]. Using a porous catalyst packing of permeable composite monolithic catalysts in a membrane reactor, Khassin and his

colleagues reported high productivity of hydrocarbons at considerably low pressure and temperature (0.6MPa and 484K), high selectivity towards heavy hydrocarbons, as well as high conductivity and high mechanical strength [Khassin *et al*., 2003]. Other publications on the use of monolithic reactors include Bradford *et al*., 2005; Liu *et al*., 2008; Hilmen *et al*., 2005; Bakhtiari *et al*., 2008; Boger *et al*., 2003; Khassin *et al*., 2005; Kapteijn *et al*., 2005, etc. However, while monolithic reactors seem to have met the requirement for classification as ideal, poor radial heat conductivity of the honeycombs means that these reactors have to be operated adiabatically, with external recirculation of liquid product to prevent temperature runaways [Guettel *et al*., 2008].

2.2.2 Composite Membrane Reactors

Quite a few people in recent times have worked towards the development of catalysts for use in composite membrane reactors. The major concepts considered were distributed feeding to control heat production, in situ water removal using hydrophilic inorganic materials, forced-through flow mode, and encapsulated catalyst to modify product distribution. A summary of their publications with regard to their concepts of membrane application in FTS reactors is presented in Table 2.5 [Rohde *et al*. 2005a]. They also used a membrane reactor to enhance CO_2 hydrogenation during FT conditions [Rohde *et al*., 2005b]. A recent work by Rohde has a mathematical model for an FT membrane reactor with in situ water removal [Rohde *et al*., 2008].

Table 2.5: Concepts of membrane application in FTS reactors [Adapted from Rohde *et al*., 2005a]

Authors	Concept	Reactor	Membrane/ Support	Catalyst/ Operating condition
Leonard et al.	Distributed feeding	PBNMR	γ-Al_2O_3/α-Al_2O_3 ZSM-5/ α-Al_2O_3	Co/Al_2O_3 180°C,10 bar
Espinoza et al.	Selective H_2O removal	PBMR	Mordenite/ZSM-5/ silicalite/ stainless steel	Non-reactive 200-300°C, 20 bar
Rohde et al.	Selective H_2O removal reactant distribution	PBMR	$Si(OH)_xO_y$/γ-Al2O3/ α-Al_2O_3	Fe/Al_2O_3/5K/Cu 225-250°C,10 bar
Khassin et al.	Forced-through flow catalytic membrane	CNMR	Porous catalyst/ copper	Co/Al_2O_3 210°C, 6 bar
Bradford et al.	Forced-through flow catalytic membrane	CNMR	Catalyst/ γ- /α-Al_2O_3	P/Pt-Co/Al_2O 185-214°C, 24 bar
He et al.	Control of product traffic	PBCMR	ZSM-5/catalyst pellet	Co/SiO_2 260°C, 10 bar
Dalai et al.	Temperature control in Tube wall catalytic membrane	CNMR	Stainless steel	Co –Fe 250-275°C, 6.9-10.3 bar

PBNMR: packed-bed non-permselective membrane reactor, PBMR: packed-bed MR, CMR: catalytic MR, CNMR: catalytic non-permselective MR

Figure 2.7 (a) shows a picture of a honeycomb monolith catalyst support for use in a monolithic reactor, while (b) shows tubular ceramic membrane supports which were utilized in the forced pore-flow-through (PFT) catalytic membrane reactor concept used in this research work.

(a)

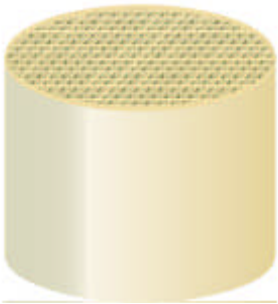

(b)

Figure 2.7: Structured catalyst supports for membrane reactors: (a) honeycomb monolith; (b) tubular ceramic membrane supports

2.3 Catalysts for Fischer-Tropsch reactors

At present, catalysts based on cobalt or iron are mostly used industrially for FTS, depending on the types and quantities of FT products desired, and the choice of either the low temperature (LTFT) or the high temperature (HTFT) process. Generally, cobalt catalysts are used at low temperatures (200-240°C) because of their propensity to produce a significant amount of methane at higher temperatures. Cobalt also gives high yields of high molecular weight linear waxes which could be upgraded to diesel. The high temperature process (300-350°C) utilizes iron catalyst and yields more gasoline and low molecular weight olefins and oxygenates.

The three key properties of FT catalysts are lifetime, activity and product selectivity. Optimizing these properties for desired commercial application has been the focus of FT catalyst research and development since the processes were first discovered. Each one of these properties can be affected by a variety of strategies including;

- Use of promoters (structural and chemical)
- Catalyst preparation and formulation
- Pretreatment and reduction
- Selective poisoning
- Shape selectivity with zeolites.

Pichler and Buffleb [1940] compared catalysts which were active for FT synthesis and observed these common characteristics:

- They are active for hydrogenation reactions.
- They are capable for metal carbonyl formation.
- The FT reaction conditions (temperature, pressure) are not far from those where thermodynamics would allow the metals to be converted into metal carbonyls.

The latter observation led to the suggestion that 'surface carbonyls' play an essential mechanistic role in the formation of FT products as would be discussed in section 2.4 of this work.

Group VIII transition metals have been reported as having measurable CO hydrogenation activity with the product distribution being the distinguishing feature [Adesina, 1996]. Vanice [1975], using alumina (Al_2O_3) as the support, reported that the activities of Group VIII metals declined in the order Ru, Fe, Ni, Co, Rh, Pd, Pt, and Ir. With silica (SiO_2) as the support, the activity declined in the order: Co, Fe, Ru, Ni, Rh, Ir, Pd [Vanice, 1977]. From his work, it is evident that the choice of support which is usually dictated by such factors as basicity, dispersion effect, electronic modification and the level of metal-support interaction, has a significant part to play in the catalytic behaviour of the metals [Jacobs *et al*., 2002, Zhang *et al*., 2003]. Mauldin [1986] stressed that the choice of support for cobalt-based catalysts is critical. The most popular supports for FT catalysts are silica, alumina, titania, magnesia, zirconia and zeolites. They are sometimes referred to as structural or textural promoters [Wender, 1996]. Textural promoters, such as catalyst supports and support modifiers, are used typically to increase the dispersion of the clusters, improve attrition resistance, enhance sulphur tolerance, or electronically modify the active metal site [Jacobs *et al.*, 2002]. Wender [1996] also reported that apart from furnishing a large surface area and preventing recrystallization and sintering of the active catalyst, there is evidence that they often interact chemically with various oxidation states of the catalyst and can even exchange oxygen atoms. The pore size of the support is even believed to affect the reducibility of the catalyst precursor and hence impact on FT reaction rates and selectivities [Khodakov *et al*., 2002; Dalai *et al*., 2005]. Supports such as SiO_2, yield a large cluster size and offer the highest percentage reduction, while

supports like Al_2O_3, which stabilize a smaller cluster size, have significant support interactions which impede reduction. Therefore, SiO_2 (acidic) support has proved to be more preferable to Al_2O_3 (amphoteric) and TiO_2 (basic) in terms of both catalytic activity and selectivity to FTS liquid hydrocarbon products [Doi *et al*., 1987].

Catalytic experiments have revealed that Co species located in the wide-pore silicas are much more active in FTS and they exhibit lower methane selectivities than smaller cobalt particles situated in narrow supports [Duvenhage & Shingle, 2002]. These have been attributed to the higher reducibility of cobalt particles and thus, higher concentrations of active metal sites. It was also observed that the unique porous structure of mesoporous silicas provide a great potential for stabilizing higher cobalt dispersion in the supported catalysts with high cobalt loadings.

Chemical promoters (potassium or other alkali metals) are usually added to FT catalysts, especially iron. Their effects include (a) suppression of hydrogenation ability, (b) increase in CO dissociation, (c) increase in formation of long-chain hydrocarbons, and (d) decrease in the conversion activity of CO [Wender, 1996]. These effects have been studied by Uner [1998]; Wang *et al*. [2008]; and Yang [1982], who all concluded that the addition of potassium or potassium salts to iron FT catalysts enhance activity and selectivity to long chain hydrocarbons.

Chemical promotion can also be effected by the addition of one or more metal(s) which individually possess FT activity. The use of bimetallic catalysts has been shown to lead to better FT catalysis, and has been the subject of numerous researches the world over [Pennline *et al*., 1987; Hutchings *et al*., 1989; Duvenhage & Coville, 2002; Ngwenya *et al*., 2005; Morales *et al*., 2005; Herranz *et al*., 2006; Morales *et al*., 2007].

Iron catalysts for FTS show high activity and selectivity especially when promoted with copper and potassium. Fe is usually precipitated from solution and structural stabilizers such as alumina or silica could be added. The iron catalysts used in high temperature application is prepared by fusing magnetite with K_2O and Al_2O_3 or MgO [Dry, 2002]. The active phase for FTS appears to be the carbide phase and oxides of carbon formed during the reaction are active for the water-gas shift reaction. This makes iron-based catalysts particularly good for the conversion of low-hydrogen syngas such as that from coal. Thus, apart from being the cheapest catalyst for FTS, iron is more flexible towards the H_2/CO feed ratio of the syngas. However, it has a tendency to form elemental carbon which leads to loss in activity. Moreover, large quantities of water produced as a side product inhibit hydrocarbon formation, resulting in low conversions per pass.

Cobalt catalysts are only used in the low temperature processes since excess methane is produced at higher temperatures. Water-gas shift activity is usually low but selectivity to high molecular weight hydrocarbons is high because of olefin re-adsorption. Cobalt is usually dispersed on high area stable metal oxides supports such as alumina, silica and titania in order to minimize the amount and maximize available surface area of metal. The catalysts are also usually promoted with a small amount of Ru, Re or Pt to prevent deactivation by carburization or oxidation. Compared to iron, Co-based catalysts give higher conversions per pass. A comprehensive historical review of cobalt catalyst design was carried out by Bartholomew [2003] who traced the development of cobalt catalyst from the simple cobalt oxide on asbestos to sophisticated, high-activity, highly optimized cobalt catalysts supported on carefully modified alumina, silica, or titania carriers and promoted with noble metals and basic oxides.

Ruthenium catalysts are the most active FT catalysts. A high molecular weight wax is obtained at reaction temperatures as low as 423K. The catalyst is active in its metallic form and no promoters are required to stabilize its activity. However, like nickel, the selectivity changes to mainly methane at elevated temperatures, and their high price excludes their application on industrial scale [Dijk, 2001].

Typical FTS catalyst constituents and user companies are listed in Table 2.6

Table 2.6: Typical FTS catalyst constituents [Samuel, 2003]

Company	**Typical catalyst constituents**			
	Primary	**Reduction Promoter**	**Activity/Selectivity promoter**	**Support**
Conoco	Co	Re, other	N/A	Alumina, other
Gulf (Shell)	Co	Ru	Oxide promoters	Alumina
Exxon	Co	Re/Ru	Oxide promoters	Titania or titania/silica
IFP	Co			
Intevep	Co	–	Oxide and carbide promoters	Silica
Rentech	Fe	N/A	N/A	–
Shell	Co	with or without a noble metal	Zirconia	Silica, silica/alumina
Statoil	Co	Re	Oxide promoters	Alumina
SASOL	(Fe) Co	Pt	–	Alumina
Williams	Co	with or without a noble metal	with or without oxide promoter	Doped alumina

2.4 Fischer-Tropsch synthesis products distribution

The Fischer-Tropsch synthesis is an ideal polymerization (reductive oligomerization) reaction involving consecutive reactions that produce a range of olefins, paraffins and oxygenated products of various chain lengths through diverse reaction routes and pathways. Although there are controversies about the actual mechanistic pathway owing to the large number of surface species formed during FT reaction, there seems to be

general acceptance that chain growth proceeds by a stepwise process. Chain growth selectivity and final product composition is strongly influenced by operating conditions and catalyst composition [Iglesia, 1997]. The product distribution follows Anderson-Schulz-Flory (ASF) distribution, which can be expressed as [Anderson, 1956]:

$$\frac{W_n}{n} = (1-\alpha)^2 \alpha^{n-1} \tag{2.11}$$

where W_n is the weight fraction of hydrocarbon molecules containing n carbon atoms. The chain growth probability α (i.e. the probability that a molecule will continue reacting to form a longer chain) is defined by:

$$\alpha = \frac{k_p}{k_p + k_t} \tag{2.12}$$

where k_p and k_t are the rate of propagation and termination respectively. In general, $\boldsymbol{\alpha}$ which determines the total carbon number distribution of the FT products, is a function of the type of catalyst and the specific process conditions. It is known that the higher the pressure, and the lower the temperature, and the lower the inlet H_2/CO ratio, the higher is $\boldsymbol{\alpha}$ [Steynberg & Dry, 2004]. The chain growth probability also depends on the characteristics of the catalyst (e.g. pellet size, pore size, active site density, promoters etc.). Equation 2.11 is graphically represented in Figure 2.8.

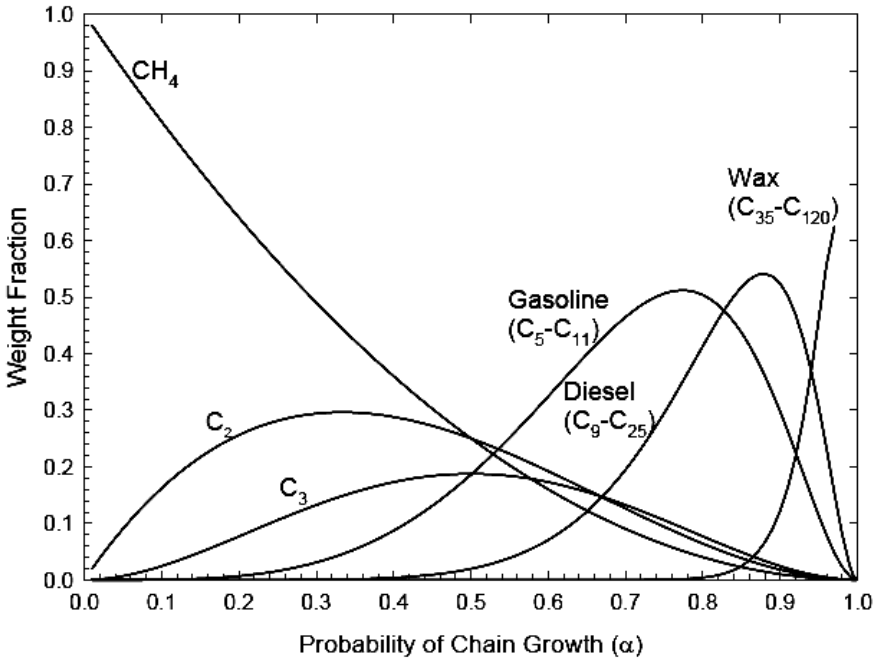

Figure 2.8: Anderson-Schulz-Flory Distribution [Spath & Dayton, 2003]

When written in logarithmic form, equation 2.11 becomes:

$$\log(\frac{W_n}{n}) = n\log\alpha + \frac{(1-\alpha)^2}{\alpha} \qquad (2.13)$$

From a plot of equation 2.13, the value of α can be obtained and typical ranges for Ru, Co and Fe are 0.85-0.95, 0.70-0.80, and 0.50-0.70 respectively [Dry, 1982]. Figure 2.9 illustrates plots of equation 2.13 with different α values (plotted as semi-log chart) for the major FT catalysts [Zhang & Davis, 2000].

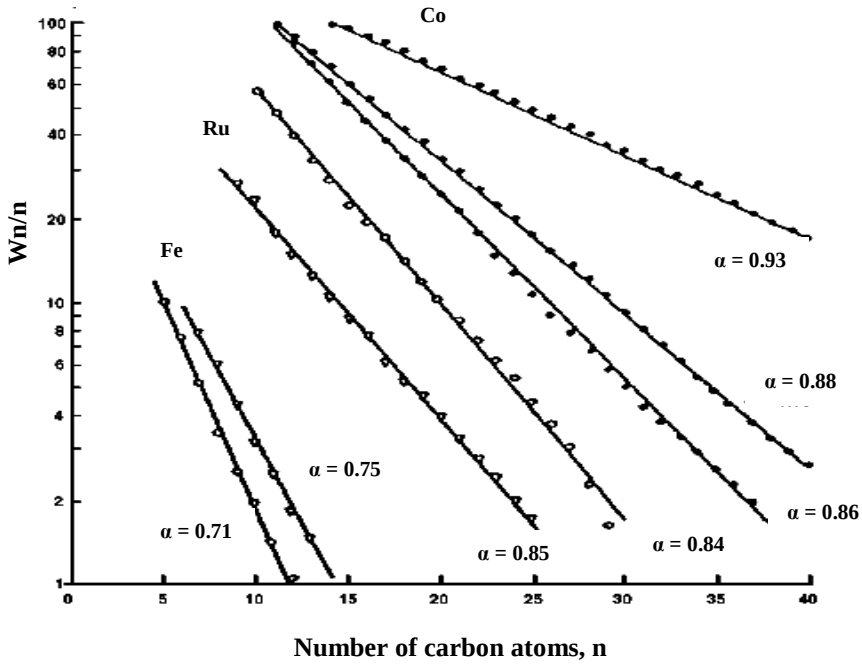

Figure 2.9: Typical carbon number distributions [Zhang & Davis, 2000]

In practice, there is often a deviation from this ideal ASF distribution. For example, C_1 yields are usually higher than predicted while that of C_2 is usually lower [Oukaci, 2002]. Other deviations are possible, especially where secondary reaction such as cracking occur on acidic supports or where olefin products are re-inserted into the growing chain [Kuipers *et al*., 1996]. Cases of multiple product distribution have also been reported, and were explained by the assumption that more than one type of active site for hydrocarbon chain formation was available, each with a slightly different chain growth probability [Madon & Taylor, 1981]. Tailoring of the product distribution is also possible by a limitation of chain growth by pore size [Roper, 1983]

2.5 Fischer – Tropsch reaction mechanisms and kinetic models

The stoichiometric reactions of Fischer-Tropsch synthesis are summarized below:

1. Paraffins $$(2n+1)H_2 + nCO \longrightarrow C_nH_{2n+2} + nH_2O \qquad (2.14)$$

2. Olefins $2nH_2 + nCO \longrightarrow C_nH_{2n} + nH_2O$ (2.15)

3. Water-gas shift $CO + H_2O \rightleftharpoons CO_2 + H_2$ (2.16)

4. Alcohols $2nH_2 + nCO \longrightarrow C_nH_{2n+1}OH + (n-1)H_2O$ (2.17)

5. Boudard $2CO \longrightarrow C + CO_2$ (2.18)

FTS has been recognized as a polymerization reaction which involves such steps as reactant adsorption, chain initiation, chain growth, chain termination, product desorption, readsorption and further reaction [Adesina, 1996]. The vast product spectrum which results from the large number of surface species present during the reaction, has led to the consideration of several mechanistic pathways for FTS. Organometallic model complexes and surface science techniques have been widely used to obtain mechanistic information about this heterogeneous process [Overett *et al*., 2000]. Bartholomew and Farrauto [2006] admitted that it is difficult, if not impossible to propose a most favourable path from available information.

2.5.1 Reaction Mechanisms

Three major mechanisms have been reported, although there seems to be several variants for each mechanism [Dijk, 2001]. The principal schemes are:

1. The carbene or carbide (alkenyl/alkyl) mechanism which involves the dissociative adsorption of CO on the catalyst surface, hydrogenation of adsorbed C ($C_{adsorbed}$) to CH_x species like surface carbide (C), vinyl (CH) or methylene ($=CH_2$) groups, and the insertion of the CH_x species into a metal-carbon bond of an adsorbed alkyl or alkenyl (vinyl) chain as shown in Figure 2.10;

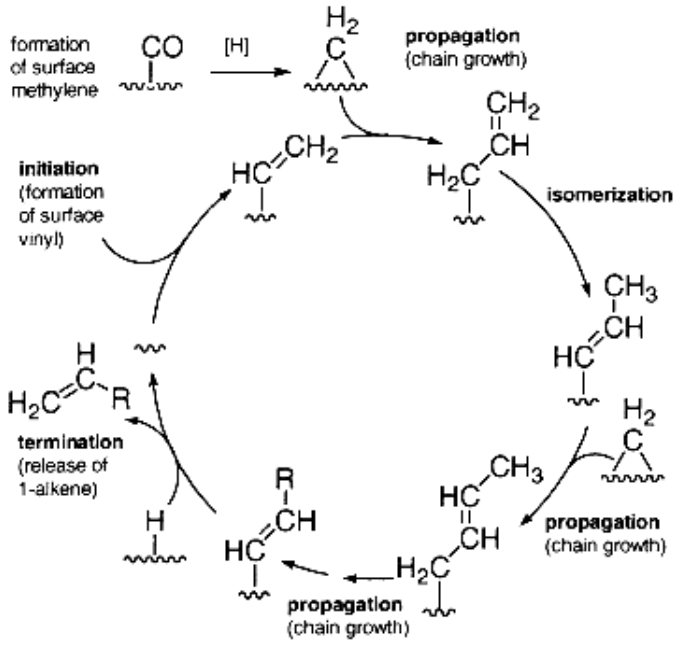

Figure 2.10: The carbene (alkyl or alkenyl) mechanism for FT homologation
[Turner *et al.*, 2002]

2. The hydroxycarbene (enol) mechanism which involves the partial hydrogenation of adsorbed CO to form a hydroxycarbene (enol) species and the condensation of two enolic species with the elimination of water, which readily explains the formation of alcohols as primary products (Figure 2.11);

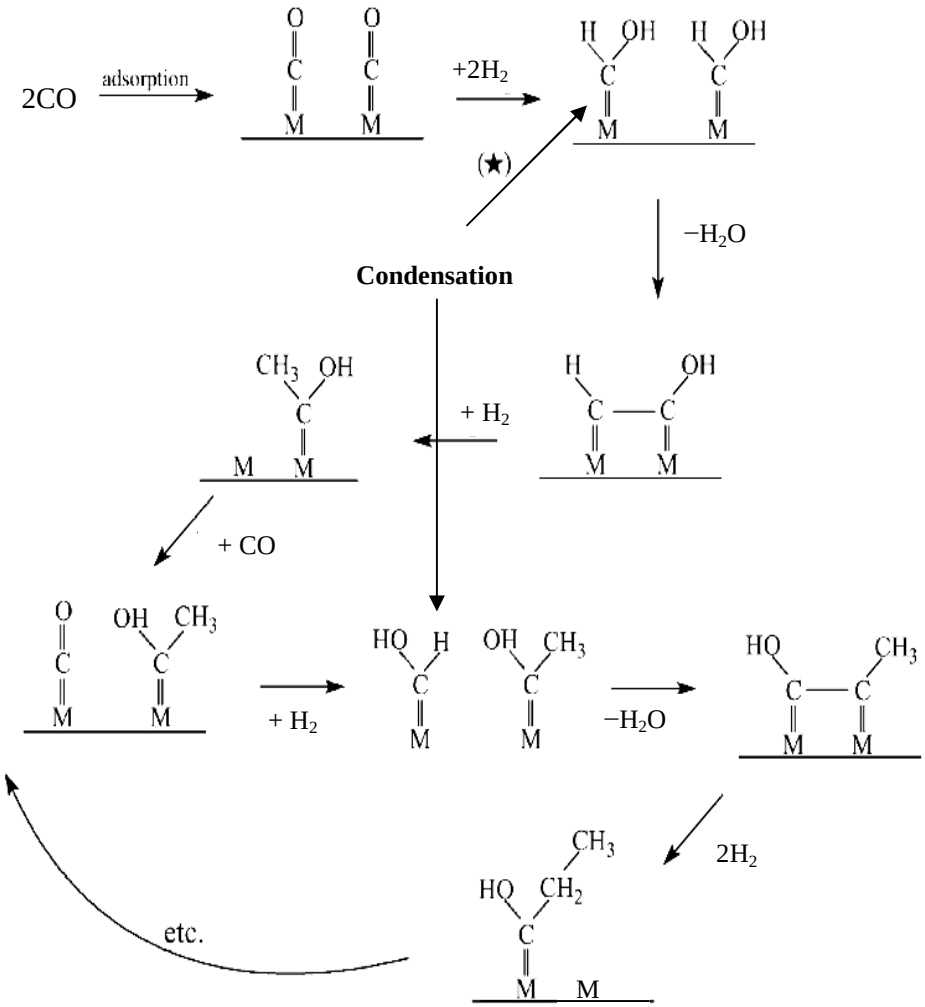

Figure 2.11: Hydroxycarbene (Enol) Mechanism [Ziegler, 2008]

The surface hydroxycarbene can undergo multi-site condensation and subsequent hydrogenation to propagate the chain. Chain termination is believed to occur by cleavage of the alkyl hydroxycarbene to give an aldehyde, or via β-elimination of olefins under regeneration of the hydrocarbene. Subsequent hydrogenation of these products gives alcohols or paraffins respectively.

3. The carbonyl (CO) insertion mechanism which proceeds via the insertion of a carbonyl intermediate ($CO_{adsorbed}$) into the metal-alkyl bond as shown in Figure 2.12.

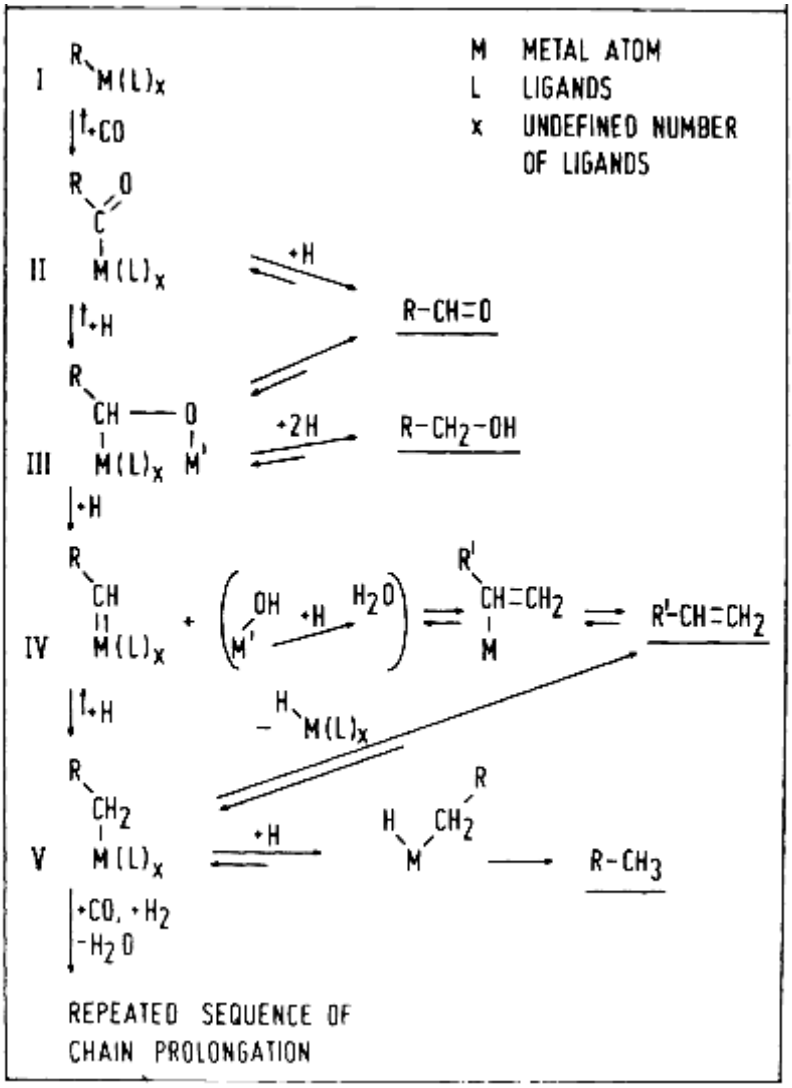

Figure 2.12: CO insertion mechanism for chain growth and product desorption during FTS [Schulz, 1979]

Extensive reviews of these mechanisms and their variants are available in the literature [Anderson, 1984; Hindermann *et al*., 1993; Dry, 1996; Overett *et al*., 2000; Maitlis *et al*., 1999; Davis, 2008].

One of the most encompassing mechanisms to have been postulated is that given by Dry [1996] where it is shown that CO may adsorb associatively or disassociatively on transition metals. The dissociation is equally thought to occur in two ways namely, unassisted and H-assisted. H-assisted CO dissociation leads to the formation of the enolic species (HCO). As shown in Figure 2.13, both CH_2 and CO are active surface intermediates. CO insertion into a growing chain produces oxygenated products while linear α-alkenes are generated from non-oxygenated species. Adesina [1996] and Wender [1996] admitted that the features of this mechanism are adequately supported by experimental data from other workers.

Mechanistic study on Fischer-Tropsch methanol and higher alcohols synthesis reported in literature, shows two types of reaction mechanisms which seem to agree with Dry's mechanism for FTS [Bell, 1981; Xiaoding *et al*., 1987; Xu *et al*., 1997; Teng *et al*., 2005, Teng *et al*., 2006]. The main difference between the two mechanisms is in the chain growth by stepwise insertion of adsorbed CH_2 species or CO species, which is well illustrated in Figure 2.13.

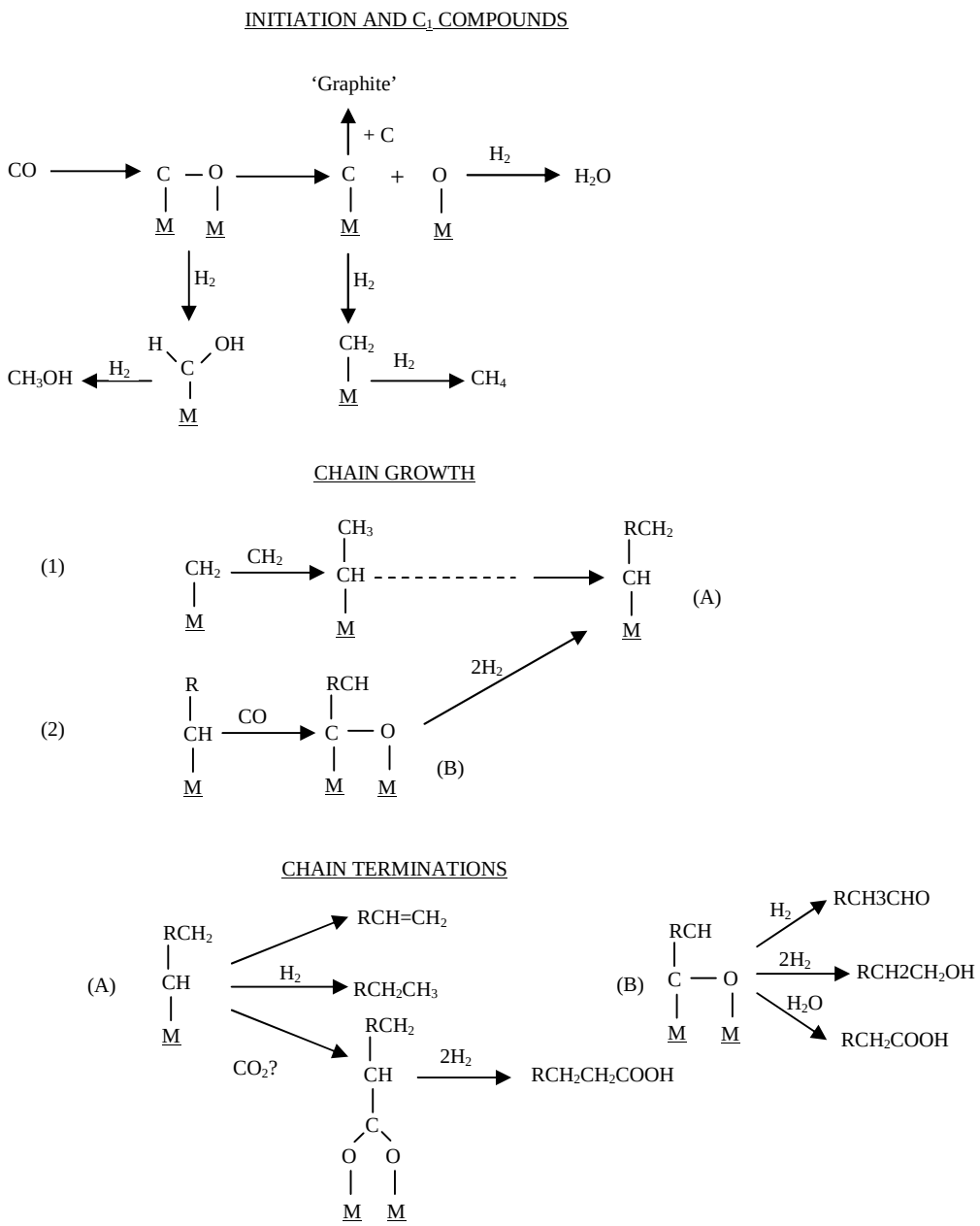

Figure 2.13: Dry's mechanism of FT reaction [Dry, 1996]

For syngas feed containing appreciable amounts of CO_2 such as the one used for the experiments reported in this work, Chaumette e*t al*. [1995] proposed a mechanism based on the formation of adsorbed acyl species HCO and HCOO. This mechanism shows that hydrocarbon formation proceeds via carbene polymerization owing to carbon-oxygen

bond rupture, while methanol and higher alcohols are formed directly by the hydrogenation of adsorbed acyl entities. This mechanism is shown in Figure 2.14.

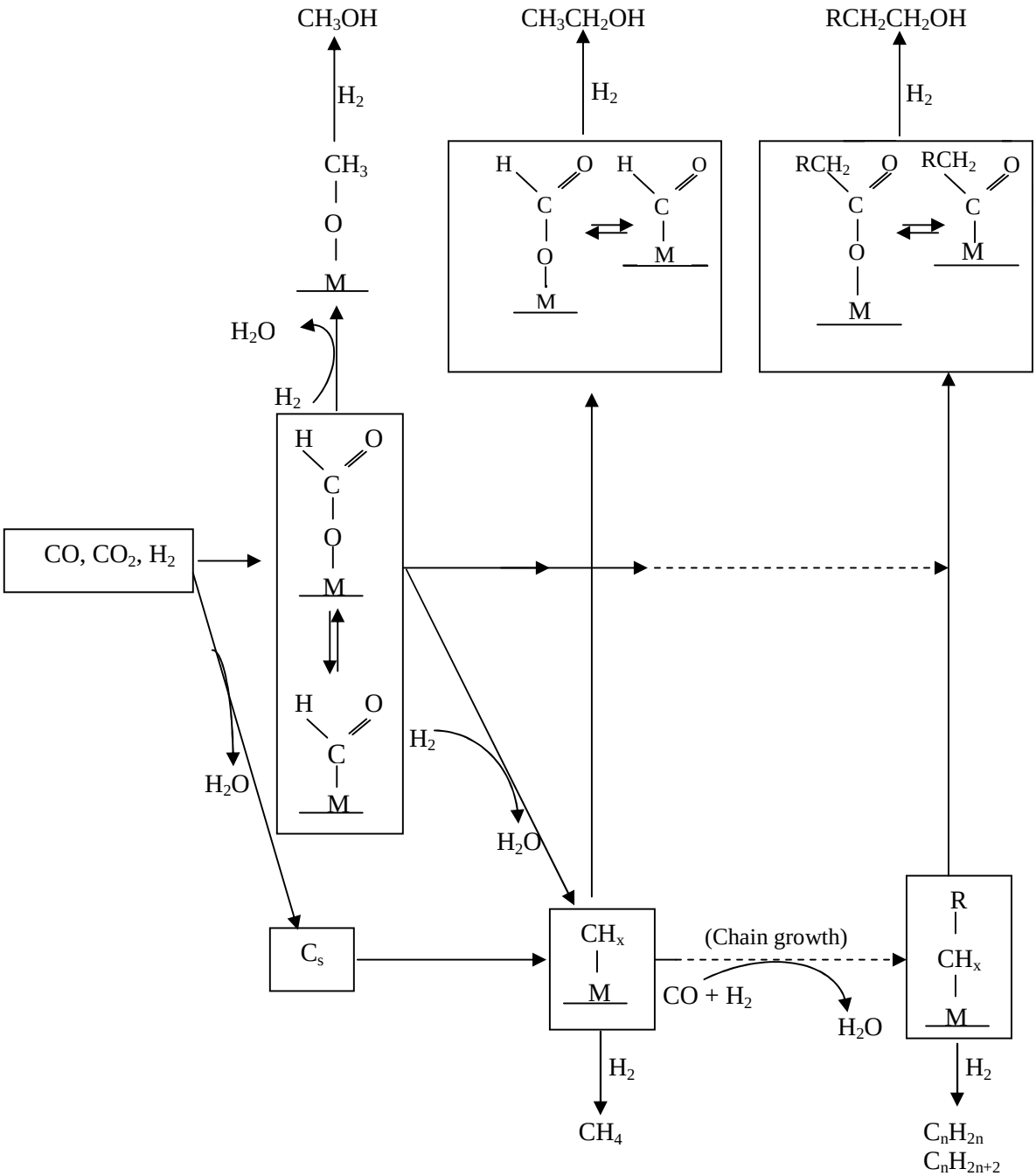

Figure 2.14: Mechanism of alcohol and hydrocarbon formation on FT catalysts

[Adapted from Chaumette *et al*., 1995]

All the mechanisms given in this section seem to ignore the fact that methanol could have been formed as a primary product as shown in Figures 2.13 and 2.14, and that subsequent homologation and carbonylation could have yielded higher alcohols and hydrocarbons respectively.

2.5.2 Kinetic models for Fischer-Tropsch synthesis.

The Langmuir-Hinshelwood models derived from reaction mechanisms are generally found to fit rate data well for a number of catalytic reactions like FTS and higher alcohol synthesis [van Steen & Schulz, 1999; Calverly & Smith, 1992, Yates & Satterfield, 1991; Wojciechowski, 1998; Paul, 2008]. This non-linear model is shown in equation 2.19.

$$r_{C_{2+}} = \frac{A\exp(-E_a / RT).p_{H_2}^m.p_{CO}^n}{(1+K_1 p_{CO} + K_2^{0.5}.p_{H_2} + ...)^2} \tag{2.19}$$

where r_{C2+} is the rate of formation of hydrocarbons or oxygenates with more than one carbon atom, A is the Arrhenius constant, Ea is activation energy, R is the universal gas constant, K_1, K_2,... are adsorption equilibrium constants and p_{H2}, p_{CO}, etc. are partial pressures of the gases.

Huff and Satterfield [1984] proposed a kinetic model for rate of syngas consumption on iron-based FT catalysts given by:

$$-r_{CO+H_2} = \frac{a.p_{H_2}.p_{CO}}{p_{H_2O} + b.p_{H_2}.p_{CO}} \tag{2.20}$$

or in a linearized form

$$\frac{p_{H_2}}{-r_{CO+H_2}} = \frac{b}{a} + \frac{1}{a}.\left[\frac{p_{H_2O}}{p_{H_2}.p_{CO}}\right] \tag{2.21}$$

where a and b are constants.

The parameters according to Maretto & Krishna [1999] are

$$a = 8.8533\times10^{-3}\exp\left[4494.41\left(\frac{1}{493.15}-\frac{1}{T}\right)\right](molkg_{cat}bar^{-2}s^{-1}) \qquad (2.22)$$

$$b = 2.226\exp\left[-8236\left(\frac{1}{493.15}-\frac{1}{T}\right)\right] \qquad (bar^{-1}) \qquad (2.23)$$

Van Steen and Schulz [1999] reported that the model gave a poor fit for iron catalyst operated at low temperatures, probably because Huff and Satterfield [1984] tested their rate expression using fused magnetite operated at rather high temperatures (275°C).

For cobalt-based catalysts, the rate expression proposed by Outi *et al* [1981] is:

$$-r_{CO+H_2} = \frac{c.p_{H_2}.p_{CO}^{1/2}}{\left[1+d.p_{CO}^{1/2}\right]^3} \qquad (2.24)$$

This can be linearized to give

$$\left[\frac{pH_2.p_{CO}^{1/2}}{-r_{CO+H_2}}\right]^{1/3} = \frac{1}{c^{1/3}} + \frac{d}{c^{1/3}}.p_{CO}^{1/2} \qquad (2.25)$$

where b and c are temperature-dependent constants.

There appears to be little information in literature for Fischer-Tropsch oxygenates kinetics based on cobalt because it is generally believed that due to their lack of water-gas shift activity, cobalt catalysts do not produce oxygenated compounds. Even when CO_2 is present in the syngas and strongly influences alcohols formation, it is often believed that it is first converted to carbon monoxide through the reverse water-gas shift reaction [Herranz *et al*., 2006]. As a result, most intrinsic kinetic expressions relating to alcohols production via Fischer-Tropsch synthesis are based on iron catalysis; or in the alternative, kinetics of mixed alcohols synthesis using syngas are used.

In their work, Calverly and Smith [1992] obtained an expression describing the overall rate of higher alcohol formation over a promoted $Cu/ZnO/Cr_2O_3$ catalyst. The assumption was made that the formation of carbon-carbon bonds occurs between any two formyl intermediates, produced from carbon monoxide, carbon dioxide and methanol on different types of active sites:

$$r_{HA} = \left(\frac{p_{CO}(p_{H_2})^{1/2}}{A + Bp_{MeOH}} + Cp_{MeOH}(p_{H_2})^{-3/2} + \frac{p_{CO_2}(p_{H_2})^{1/2}}{D + Ep_{CO_2} / p_{CO}} \right)^2 \qquad (2.26)$$

where A = 7782, B = 1853, C = 0.331, D = 34.15, E = 18640; MeOH – methanol; HA – mixture of higher alcohols without methanol.

Methanol formation rate can be described by:

$$r_{MeOH} = k \frac{p_{CO}}{1 + K_{CO} p_{CO}} p_{H_2}^2 \qquad (2.27)$$

which can be linearized for the case $K_{CO} \times p_{CO} >> 1$, and $n=2$ to give the fit obtained by Kulawska & Skrzypek [2001], described by the power law:

$$r = k_o p_{H_2}^n \qquad (2.28)$$

where k_o is the temperature-dependent rate constant defined as:

$$k_o(T) = Ae^{-E_a/RT} \qquad (2.29)$$

A is the Arrhenius constant, and E_a is the activation energy.

Kulawska & Skrzypek [2001] concluded that the mechanism for alcohol synthesis is different for different catalytic systems, depending on the metal, the support, the promoter and the reaction conditions, making it difficult to determine a universal mechanism for the process. A comprehensive review of the various FTS models for hydrocarbons and alcohols formation over different catalysts and a variety of operating conditions is

available in literature [Yates & Satterfield, 1991; van der Laan *et al*., 1999; Jun, 2004; Li, 2004; Iliuta *et al*., 2008,].

There are two major barriers to using kinetic-based models, especially where heterogeneous catalysts are employed. Firstly, there is the need for high quality experimental data to determine the many parameters required for accurate predictions - assuming that a suitable model can be found for the system of equations; and even with data suitable for estimating model parameters, the resulting model is only truly representative of the catalyst used in the experiments over the range of operating conditions explored. Using the model outside the range of operating conditions introduces increased uncertainty the more removed the estimate is from the experimental conditions used to develop the model. Secondly, catalyst performance is very sensitive to many factors that can arise during their production such as preparation techniques, support characteristics (surface area, morphology) and even handling.

The kinetic experiments in this work were designed to tests the effects of changes in operating variables on the intrinsic kinetics of cobalt-based catalysts in a membrane reactor operated as a contactor in the forced PFT mode. There is no claim of universality for all such systems, except if the CMR is operated within the limits of conditions specified. Efforts were however made to ensure that data generated were as accurate as possible, while great care was taken to keep the membranes from contamination

2.6 References

Adesina, A. A. (1996). Hydrocarbon synthesis via Fischer-Tropsch reaction: travails and triumphs. *Applied Catalysis A: General*, 138, pp.345-367.

Anderson, R. B. (1984). *The Fischer-Tropsch synthesis*. New York: Academic Press.

Anderson, R. B. (1956). *Catalyst for the Fischer-Tropsch synthesis*, vol.4. New York: Van Nostrand Reinhold.

Armor, J. N. (1998). Applications of catalytic inorganic membrane reactors to refinery products. *Journal of Membrane Science*, 147. pp.217-233.

Bakhtiari, M., Khorashsh, F., Zamanian, A., Nakhaeipour, A., Irani, M. (2008). Preparation, evaluation and characterization of monolithic catalysts for Fischer-Tropsch synthesis. *Petroleum & Coal*, 50 (3), pp.56-61.

Bartholomew, C. H., Farrauto, R. J. (2006). *Fundamentals of Industrial Catalytic Processes*, 2nd Ed. New York: John Wiley and Sons.

Bartholomew, C. H. (2003). *History of cobalt catalyst design for FTS.* Prepared for presentation at the national spring meeting of the American Institute of Chemical Engineers, New Orleans, March 30 – April 3.

Bell, A. T. (1981). Catalytic Synthesis of Hydrocarbons over Group VIII Metals. A Discussion of the Reaction Mechanism. *Catalysis Reviews* – Science and Engineering, 23 (1 & 2), pp.203 – 232

Bernauer, B. (2006). Phenomenological models of transport and separation in membranes. Lecture L08, XXIII EMS Summer School on Membranes, Prague, September 3-6, 2006.

Bobrov, V. S., Digurov, N. G., Skudin, V. V. (2005). Propane dehydrogenation using catalytic membrane. *Journal of Membrane Science* 253, pp.233-242

Boger, T., Roy, S., Heibel, A. K., Borchers, O. (2003). A monolith loop reactor as an attractive alternative to slurry reactors. *Catalysis Today*, 79-80, pp.441-451.

Bradford, M. C. J., Te, M., Pollack, A. (2005). Monolithic loop membrane reactor for Fischer-Tropsch synthesis. *Applied Catalysis A: General* 283, pp.271-274.

Caro, J., Caspary, K. J., Hamel, C., Hoting, B., Kölsch, P., Langanke, Nassauer, B; Schiestel, T., Schmidt, A., Schomäcker, R., Seidel-Morgenstern, A., Tsotsas, E., Voigt, L., Wang, H., Warsitz, R., Werth, S., Wolf, A. (2007). Catalytic Membrane Reactors for Partial Oxidation Using Perovskite Hollow Fiber Membranes and for Partial Hydrogenation using a Catalytic Membrane Contactor, *Industrial Engineering Chemistry Research*, 46 (8), pp.2286 -2294.

Calverley, E. M., Smith, K. J. (1992). Kinetic model for alcohol synthesis over a promoted Cu/ZnO/Cr2O3 catalyst. *Industrial Engineering Chemistry Research* 31, pp.792-803.

Centi, G., Dittmeyer, R., Perathoner, S., Reif, M. (2003). Tubular inorganic catalytic membrane reactors: advantages and performance in multiphase hydrogenation reactions. *Catalysis Today*, 79-80, pp.139-149.

Chaumette, P., Courty, Ph., Kiennemann, A., Ernst, B. (1995). Higher alcohol and paraffin synthesis on cobalt based catalysts: comparison of mechanistic aspects. *Topics in Catalysis 2*, pp.117-126

Coronas, J., Santamaria, J. (1999). Catalytic reactors based on porous ceramic membranes. *Catalysis Today*, 51, p.382

Dalai, A. K., Das, T. K., Chaudhari, K. V., Jacobs, G., Davis, B. H. (2005). Fischer–Tropsch synthesis: Water effects on Co supported on narrow and wide-pore silica. *Applied Catalysis A: General*, 289 (2), pp.135-142.

Dalai, A. K., Bakshi, N. N., Esmail, M. N. (1997). Conversion of syngas to hydrocarbons in a tube-wall reactor using Co-Fe plasma sprayed catalyst: experimental and modelling studies. *Fuel Processing Technology*, 51, pp.219-238

Davis, B. H. (2008). Fischer-Tropsch synthesis: Reaction mechanism for iron catalysts. *Catalysis Today*, doi:1016/j.cattod.2008.03.005

de Aquino, A., Cobo, A. J. G. (2001). Synthesis of higher alcohols with cobalt and copper based model catalysts: effects of the alkaline metals. *Catalysis Today* 65, p.209

de Deugd R. M., Kapteijn, F., Moulijn, J. A. (2003a). Trends in Fischer- Tropsch reactor technology – opportunities for structured reactors. *Topics in Catalysis*, 26 (1-4), pp.29-39.

de Deugd R. M., Kapteijn, F., Moulijn, J. A. (2003b). Using monolithic catalysts for highly selective Fischer-Tropsch synthesis. *Catalysis Today*, 79-80, pp.495-501.

de Deugd R. M., Chougule, R. B., Kruetzer, M. T., Meeuse, F, M., Grievink, J., Kapteijn, F., Moulijn, J. A. (2003c). Is a monolithic loop reactor a viable option for Fischer-Tropsch synthesis? *Chemical Engineering Science*, 58, pp.583-591.

Dijk, H. A. J. van (2001). The Fischer-Tropsch synthesis: A mechanistic study using transient isotopic tracing. PhD Thesis – Technische Universiteit Eindhoven.

Dittmeyer, R., Hollein, V., Daub, K. (2001). Membrane reactors for hydrogenation and dehydrogenation processes based on supported palladium. *Journal of Molecular Catalysis A: Chemical* 173 (2001), pp.135-184.

Dixon, A. G. (2003) Recent Research in Catalytic Inorganic Membrane Reactors, *International Journal of Chemical Reactor Engineering*, 1, R6.

Doi, Y., Miyake, H., Soga, K. (1987). Electronic effects on CO hydrogenation over Ru-metal oxide catalysts. *Journal of the Chemical Society: Chemical communications*, 5, pp.347-348.

Dry, M. E. (2002). The Fischer-Tropsch process: 1950 – 2000, *Catalysis Today* 71, pp.227-241.

Dry, M. E. (1996). Practical and theoritical aspects of the catalytic Fischer-Tropsch process. *Applied Catalysis A: General*, 138, pp. 319-344.

Dry, M. E. (1982). Sasol's Fischer-Tropsch experience. *Hydrocarbon Processing*, pp. 121-124.

Duvenhage, D, J., Coville, N. J. (2002). Fe:Co/TiO_2 bimetallic catalysts for the Fischer-Tropsch reaction part 2. The effect of calcination and reduction temperature. *Applied Catalysis A: General 233*, pp.63-75.

Duvenhage, D. J., Shingles, T. (2002). Synthol reactor development. *Catalysis Today* 71, pp.301-305.

Gryaznov, V. (1999). Membrane Catalysis. *Catalysis Today*, 51, pp.391-395.

Guettel, R., Kunz, U., Turek, T. (2008). Reactors for Fischer-Tropsch synthesis. *Chemical Engineering Technology*, 31 (5), pp.746-754.

Herranz, T., Rojas, S., Perez-Alonso, F. J., Ojeda, M., Terreros, P., Fierro, J. L. G. (2006). Hydrogenation of carbon oxides over promoted Fe-Mn catalysts prepared by the microemulsion methodology. *Applied Catalysis A: General*, 311, pp.66-75.

Hilmen, A. -M., Bergene, E., Lindvag, O. A., Schanke, D., Eri, S., Holmen, A. (2005). Fischer-Tropsch synthesis on monolithic catalysts with oil circulation. *Catalysis Today* 105, pp.357-361.

Hilmen, A. -M., Bergene, E., Lindvag, O. A., Schanke, D., Eri, S., Holmen, A. (2001). Fischer-Tropsch synthesis on monolithic catalysts of different materials. *Catalysis Today* 69, pp.227-232.

Hindermann, J. P., Hutchings, G. J., Kiennemann, A. (1993). Mechanistic aspects of the formation of hydrocarbon and alcohols from CO hydrogenation. *Catalysis Reviews – Science and Engineering*, 35 (1), pp.1-127.

Ho, W. S. W., Wang, B., Neumuller, T. E., Roller, J. (2001). Supported liquid membranes for removal and recovery of metals from waste waters and process streams. *Environmental Progress*, 20 (2), pp.117-121.

Ho, W. S. Winston, Sirkar, K. K (Eds). (1992). *Membrane Handbook*. New York: Chapman & Hall.

Huff, G. A. Jr., Satterfield, C. N. (1984). Intrinsic kinetics of the Fischer-Tropsch synthesis on a reduced fused-magnetite catalyst. *Industrial & Engineering Chemistry Process Design and Development*, 23 (4), pp.696-705.

Hutchings, G. J., van der Riet, M., Hunter, R. (1989). CO hydrogenation using cobalt/manganese oxide catalysts. Comments on the mechanism of carbon-carbon bond formation, *Journal of the Chemical Society, Faraday Transactions 1*, 85 (9), pp.2875-2890.

Iglesia, E. (1997). Design, synthesis, and use of cobalt-based Fischer-Tropsch synthesis catalysts. *Applied Catalysis A: General*, 161, pp.59-78.

Iliuta, I., Larachi, F., Anfray, J., Dromard, N., Schweich, D. (2008). Comparative simulations of cobalt-and iron-based Fischer-Tropsch synthesis slurry bubble column reactors. *Industrial and Engineering Chemistry Research*, 47, pp.3861-3869.

Jacobs G., Das T.K., Zhang Y., Li, J., Racoillet, G., Davis B.H. (2002). Fischer-Tropsch synthesis: support, loading, and promoter effects on the reducibility of cobalt catalysts. *Applied Catalysis A: General*, 233(1), pp. 263-281.

Jager, B., Van Berge, P., Steynberg, A. P. (2001). Developments in Fischer-Tropsch technology and its application. *Studies in Surface Science and Catalysis*, 136, pp. 63-68

Julbe, A., Ayral, A. (2007). Catalytic membrane reactors involving inorganic membranes – A short overview. http://water-environment.vin.bg.ac.yu/proceedings/3%20Strana%2030-43%20B5%20Julbe-Belgrade%202007.doc. [Accessed: 23 December, 2008].

Julbe, A., Farruseng, D., Guizard, C. (2001). Porous ceramic membranes for catalytic reactors – overview and new ideas, *Journal of Membrane Science*, 181, pp.3-20.

Jun, Y. (2004). A review of kinetics for Fischer-Tropsch synthesis. http://www.chemistrymag.org/cji/2004/064027re.htm. [Accessed: 23 December, 2008].

Kapteijn, F., de Deugd, R. M., Moulijn, J. A. (2005). Fischer-Tropsch synthesis using monolithic catalysts. *Catalysis Today*, 105, pp.350-356.

Khassin, A. A., Sipatrov, A. G., Yurieva, T. M., Chermashentseva, G. K., Rudina, N. A., Parmon, V. N. (2005). Performance of Catalytic membrane reactor for the Fischer-Tropsch synthesis. *Catalysis Today*, 105, pp.362-366.

Khassin A. A., Yurieva, T. M., Sipatrov, A. G., Chermashentseva, G. K., Parmon, V. N. (2003). Fischer-Tropsch synthesis using a porous catalyst packing : experimental evidence of an efficient use of permeable composite monoliths as a novel type of Fischer-Tropsch synthesis catalyst. *Catalysis Today*, 79-80, pp.465-470.

Khodakov, A. Y., Griboval-Constant, A., Bechara, F., Zholobenko, V.L. (2002). Pore size effects in Fischer-Tropsch synthesis over cobalt-supported mesoporous silicas, *Journal of Catalysis* 206 (2), pp.230-241.

Kishik, V. S., Eyal, A. M. (1996). Hybrid liquid membrane systems in separation technologies. *Journal of Membrane Science*, 111 (2), pp.259-272.

Koros, W. J., Fleming, G. K. (1993). Membrane-based gas separations. *Journal of Membrane Science***,** 83, p. 1

Kuipers, E. W., Schepper, C., Wilson, J. H., Vinkenburg, I. H., Oosterbeek, H. (1996). Non-ASF Product Distributions Due to Secondary Reactions during Fischer–Tropsch Synthesis**.** *Journal of Catalysis*, 158 (1), pp.288-300.

Kulawska, M., Skrzypek, J. (2001). Kinetics of the synthesis of higher aliphatic alcohols from syngas over a modified methanol synthesis catalyst. *Chemical Engineering and Processing* 40, pp.33-40.

Li, Y. –W. (2004). *Clean diesel production from coal based syngas via Fischer-Tropsch synthesis: Technology status and demands in China*. Presented at the 21st Annual International Pittsburg Coal conference held at Osaka, Japan, September 13-17.

Li, K. (2007). *Ceramic membranes for separation and reaction*. Chichester: John Wiley.

Liu, W. Hu, J., Wang, Y. (2008). Fischer–Tropsch synthesis on ceramic monolith-structured catalysts. *Catalysis Today*, doi:10.1016/j.cattod.2008.10.015

Madon, R. J., Taylor, W. F. (1981). Fischer-Tropsch synthesis on a precipitated iron catalyst. *Journal of Catalysis*, 69 (1), pp.32-43

Maitlis, P. M., Quyom, R., Long, H. C., Turner, M. L. (1999). Towards a chemical understanding of the Fischer-Tropsch reaction: alkene formation. *Applied Catalysis A: General*, 186, pp. 363-374.

Maretto, C., Krishna, R. (1999). Modelling a bubble column slurry reactor for Fischer-Tropsch synthesis. *Catalysis Today*, 52, pp.276-289.

Mauldin, C. H. (1986). Cobalt catalysts for the conversion of methanol to hydrocarbons and for Fischer-Tropsch synthesis. U. S. Patent number 4568663.

Morales, F., de Smit, E., de Groot, F. M. F., Visser, T., Weckhuysen, B. M. (2007). Effects of manganese oxide promoter on the CO and H_2 adsorption properties of titania-supported cobalt Fischer-Tropsch catalysts. *Journal of Catalysis*, 246, pp.91-99.

Morales, F., de Groot, F. M. F., Gijzeman, O. L. J., Mens, A., Stephan, O., Weckhuysen, B. M. (2005). Mn promotion in Co/TiO_2 Fischer-Tropsch catalysts as investigated by XPS and STEM-EELS. *Journal of Catalysis*, 230, pp.301-308.

Mulder, M. (2000). *Basic Principles of Membrane Technology*. Dordrecht: Kluwer Academic Publishers.

Ngwenya, T., Glasser, D., Hilderbrandt, D., Coville, N., Mukoma, P. (2005). Fischer-Tropsch results and their analysis for reactor synthesis. *Industrial Engineering Chemistry Research*, 44, pp.5987-5994.

Oukaci, R. (2002). *The Fischer-Tropsch Synthesis*. 2nd Annual Global GTL summit Executive Briefing in London, May 28-30.

Outi, A., Rautavuoma, I., van der Baan, H. S. (1981). Kinetics and mechanism of the Fischer tropsch hydrocarbon synthesis on a cobalt on alumina catalyst. *Applied Catalysis*, 1 (5), pp.247-272.

Overett, M. J., Hill, R. O., Moss, J. R. (2000). Organometallic chemistry and surface science: mechanistic models for the Fischer-Tropsch synthesis. *Co-ordination Chemistry Reviews*, 206-207, pp.581-605.

Ozdemir, S. S., Buonomenna, M. G., Drioli, E. (2006). Catalytic polymeric membranes: Preparation and application. *Applied Catalysis A: General*, 307, pp.167-183.

Paul, U. P. (2008). Microkinetic model of Fischer-Tropsch synthesis on iron catalysts. PhD Thesis, Brigham Young University.

Pennline, H. W., Zarochak, M. F., Stencel, J. M., Deehl, J. R. (1987). Activation and promotion studies in a mixed slurry reactor with an iron-manganese Fischer-Tropsch catalyst, *Industrial Engineering Chemistry Research*, 26, pp.595-601.

Pichler, H., Buffleb, H. (1940). *Die Synthesis von Paraffin an Rutheniumkatalysatoren bei Drucken bis zu 1000 Atm* (Synthesis of paraffins on Ru-catalysts at pressures up to 1000 atm), *Brennstoff-Chemie*, 21, p. 257

Rhode, M. P., Schaub, G., Khajavi, S., Jansen, J. C., Kapteijn, F. (2008). Fischer- Tropsch synthesis with in situ H_2O removal –Directions of membrane development. *Microporous and Mesoporous Materials*, 115, pp.123-136.

Rhode, M. P., Unruh, D., Schaub, G. (2005a). Membrane applications in Fischer-Tropsch synthesis reactors – overview of concepts. *Catalysis Today*, 106, pp.143-148.

Rhode, M. P., Unruh, D., Schaub, G. (2005b). Membrane application in Fischer-Tropsch synthesis to enhance CO_2 hydrogenation. *Industrial Engineering Chemistry Research*, 44, pp.9653-9658.

Roper, M. (1983). Fischer-Tropsch synthesis, in: Keim, W. (Ed.), *Catalysis in C_1 Chemistry*. Dordrecht: D. Reidel Publishing Company.

Samuel, P. (2003). GTL – Challenges and opportunities in catalysis. *Bulletin of the Catalysis Society of India*, 2 ,pp.82-99.

Schulz, H. (1979). Trends in research and development of coal conversion to liquid fuels and basic chemicals in Europe. *Pure and Applied Chemistry*, 51, pp.2225-2241.

Scott, K., Hughes, R. (Eds.)(1996). *Industrial Membrane Separation Technology*.1st Edition Glasgow: Blackie Academic and Professional, Chapman and Hall.

Shelekhin, A. B., Dixon, A. G., Ma, Y. H. (1995). Theory of gas-diffusion and permeation in inorganic molecular sieve membranes. *AIChE Journal*, 41 (1), pp. 58-67.

Spath, P. L., Dayton, D. C. (2003). Preliminary screening – technical and economic assessment of synthesis gas to fuels and chemicals with emphasis on the potential for biomass-derived syngas. NREL/TP-510-34929. National Energy Renewable Laboratory Technical Report, December 2003, Colorado, USA.

Steynberg, A., Dry, M. (2004). *Fischer-Tropsch Technology*, Vol. 152, Amsterdam: Elsevier B. V.
Teng, B., Chang, J., Zhang, C., Cao, D., Yang, J., Liu, Y., Guo, X., Xiang, H., Li, Y. (2006). A comprehensive kinetics model of Fischer-Tropsch synthesis over an industrial Fe-Mn catalyst. *Applied Catalysis A: General*, 301, pp.39-50.

Teng, B., Zhang, C. Yang, J., Cao, D., Chang, J., Xiang, H., Li, Y. (2005). Oxygenate kinetics in Fischer-Tropsch synthesis over an industrial Fe-Mn catalyst. *Fuel*, 84, pp.791-800.

Turner, M. L., Marsih, N., Mann, B. E., Quyoum, R., Long, H. C., Maitlis, P. M. (2002). Investigations by ^{13}C NMR spectroscopy of ethene-initiated catalytic CO hydrogenation. *Journal of the American Chemical Society*, 124 (35), pp.10456-10472.

Uner, D. O. (1998). A sensible mechanism of alkali promotion in Fischer-Tropsch synthesis: Adsorbate mobilities. *Industrial & Engineering Chemistry Research* 37 (6), pp. 2239-2245.

Van der Laan, G. P., Beenackers, A. A. C. M. (1999). Kinetics and selectivity of the Fischer-Tropsh synthesis: A literature review. *Catalysis Reviews – Science and Engineering*, 41 (3&4), pp.255-318.

Van Steen, E., Schulz, H. (1999). Polymerization kinetics of the Fischer-Tropsch CO hydrogenation using iron and cobalt based catalysts. *Applied Catalysis A: General* 186, pp.309-320.

Vannice, M. A. (1977). The catalytic synthesis of hydrocarbons from H_2/CO mixtures over the Group VIII metals: V. The catalytic behaviour of silica-supported metals, *Journal of Catalysis*, 50 (2), pp.228-236.

Vannice, M. A. (1975). The catalytic synthesis of hydrocarbons from H_2/CO mixtures over the Group VIII metals: II. The kinetics of the methanation reaction over supported metals. *Journal of Catalysis*, 37 (3), pp.462-473.

Wang, Z., Dong, T., Kan, T., Li, Q. (2008). Effect of potassium addition on co-precipitated iron catalysts for Fischer-Tropsch synthesis using bio-oil-syngas. *Chinese Journal of Chemical Physics*, 21, pp.141-150.

Wender, I. (1996). Reactions of synthesis gas. *Fuel Processing Technology*, 48, pp.189-297.

Wojciechowski, B. W. (1988). The Kinetics of the Fischer-Tropsch Synthesis. *Catalysis Reviews – Science and Engineering*, 30 (4) pp.629 - 702

Xiaoding, X., Doesburg, E. B. M., Scholten, J. J. F. (1987). Synthesis of higher alcohols from syngas - recently patented catalysts and tentative ideas on the mechanism. *Catalysis Today*, 2 (1), pp.125-170.

Xu, L., Bao, S., Houpt, D. J., Lambert, S. H., Davis, B. H. (1997). Role of CO_2 in the initiation of chain growth and alcohol formation during the Fischer-Tropsch synthesis. *Catalysis Today*, 36 (3), pp.347-355.

Yang, C. H., Chen, Y.W., Goodwin, J. G. Jr., Wender, I. (1982). The influence of support on K promotion of Ru for the Fischer-Tropsch synthesis. [Accessed: 21 November, 2008]. www.anl.gov/PCS/acsfuel/preprint%20archive/Files/27_3-4_KANSAS%20CITY_09-82_0151.pdf

Yates, I., Satterfield, C. N. (1991). Intrinsic kinetics of the Fischer-Tropsch synthesis on a cobalt catalyst. *Energy & Fuels*, 5 (11), pp.168-173.

Zhang, Y., Davis, B. H. (2000). *Indirect liquefaction – where do we stand?* In Spivey, J. J. (Editor), Catalysis, Volume 15, Cambridge: The Royal Society of Chemistry, pp.149.

Zhang, J., Chen, J., Ren, J., Li, Y., Sun, Y. (2003). Support effect of Co/Al_2O_3 catalysts for Fischer-Tropsch synthesis, *Fuel*, 82 (5), pp.581-586.

Zhu, H., Kee, R. J. (2003). A general mathematical model for analyzing the performance of fuel-cell membrane-electrode assembly. *Jornal of Power Sources*, 117, pp.61-74.

Ziegler, J. L. T. (2008). *Modelling of the Fischer-Tropsch synthesis catalyzed on a Fe (1,0,0) surface*. Symposium on Computational Catalysis, 235th ACS National Meeting, April 6 – 10, 2008, New Orleans, Louisiana.

Chapter 3 – Experimental Design

CHAPTER 3: Experimental Design

3.1 Introduction

In this work, catalytic membranes consisting of $Co/TiO_2/Al_2O_3$ (labelled BCo1 and BCo2), $Co\text{-}Cu/TiO_2/Al_2O_3$ (BCo3), $Co\text{-}Cu\text{-}K/TiO_2/Al_2O_3$ (BCo4), $Co\text{-}Mn/TiO_2/Al_2O_3$ (BCo5), $Fe\text{-}Mn\text{-}Cu\text{-}K/TiO_2/Al_2O_3$ (BFe1), were produced and tested. All catalytic membranes produced were supported on titania-washcoated alumina and their composition is shown in Table 3.1.

Table 3.1: Composition of membranes

S/No.	Membrane Code	Active catalyst/promoter
1	BCo1	Cobalt
2	BCo2	Higher loading of cobalt
3	BCo3	Cobalt-copper
4.	BCo4	Cobalt-copper-potassium
5.	BCo5	Cobalt-manganese
6.	BFe1	Iron-copper-manganese-potassium

Figure 3.1 (a) gives a pictorial view of the two supports used, with (b) showing the cross-section and geometrical configuration. The supports could be easily distinguished by the colour of the glazed ends. Both types of ceramic supports were supplied by *Ceramiques Techniques et Industrielles* (CTI SA) of France.

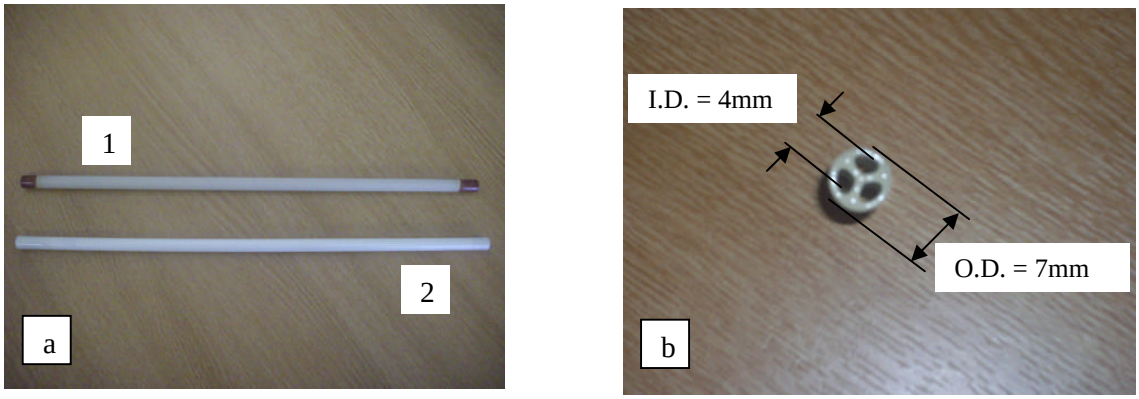

Figure 3.1: Ceramic α-alumina supports used for membrane production.
(a) Supports 1 & 2; (b) Cross section of support

The active metal of the catalytic membrane was impregnated on the α-alumina tubular supports washcoated with titania. The support with an average pore size of 6 microns (based on supplier's information) was chosen for this work to enhance the forced pore flow-through (PFT) concept used in these contactor membranes.

3.2 Experimental set-up for catalytic tests

The pore-flow-through catalytic membrane reactor was used for all the catalytic tests of membranes produced. The reactor itself consisted of a stainless steel tube (25mm O.D., 17mm I.D., 390mm length) grooved at the ends to accommodate graphite seals and fitted screw ends. A pictorial view of the reactor assembly is shown in Figure 3.2.

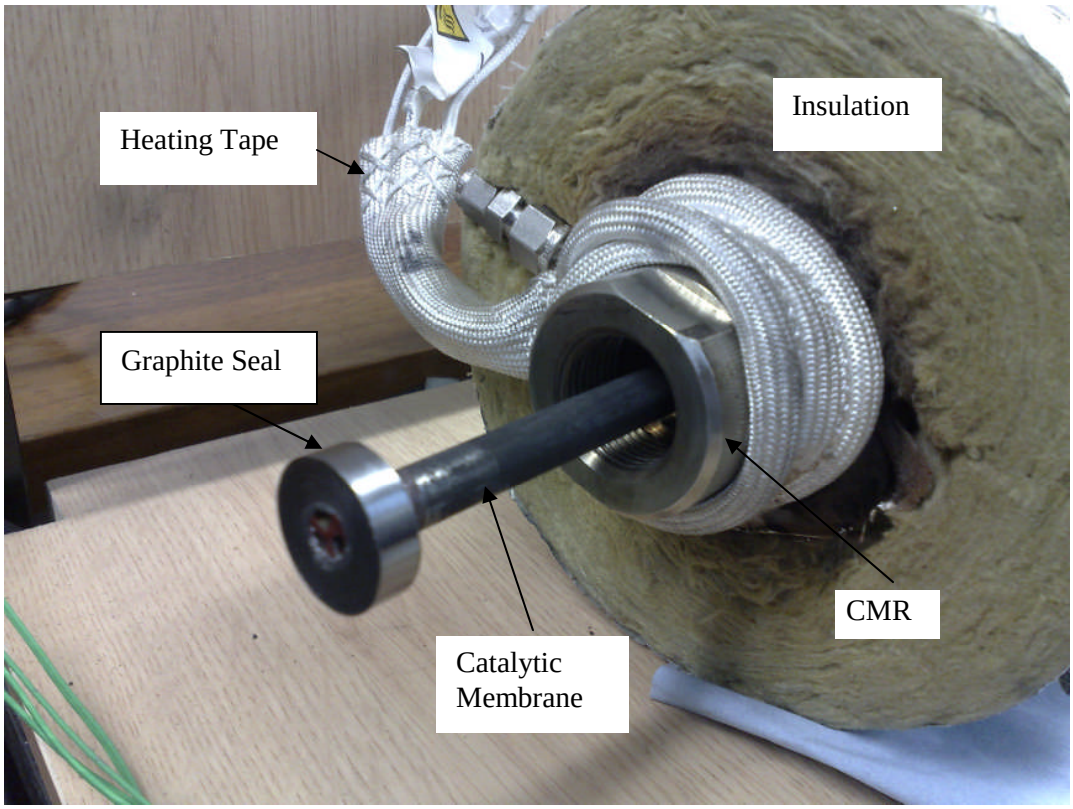

Figure 3.2: Pictorial view of a catalytic membrane reactor assembly

The graphite seals were used to secure the catalytic membrane at both ends of the reactor, and to ensure an airtight seal as the screwed ends of the reactor compressed it against both the membrane and the walls of the reactor. The syngas was introduced into the reactor as shown in Figure 3.3 and flowed through the annular space between the catalytic membrane and the inner wall of the reactor (shell side). The reacting mixture was forced through the pores of the membrane thereby contacting the active catalyst dispersed on the surface and within the pores of the membrane as it permeated into the tube side of the membrane, maintained at the desired reaction temperature and pressure.

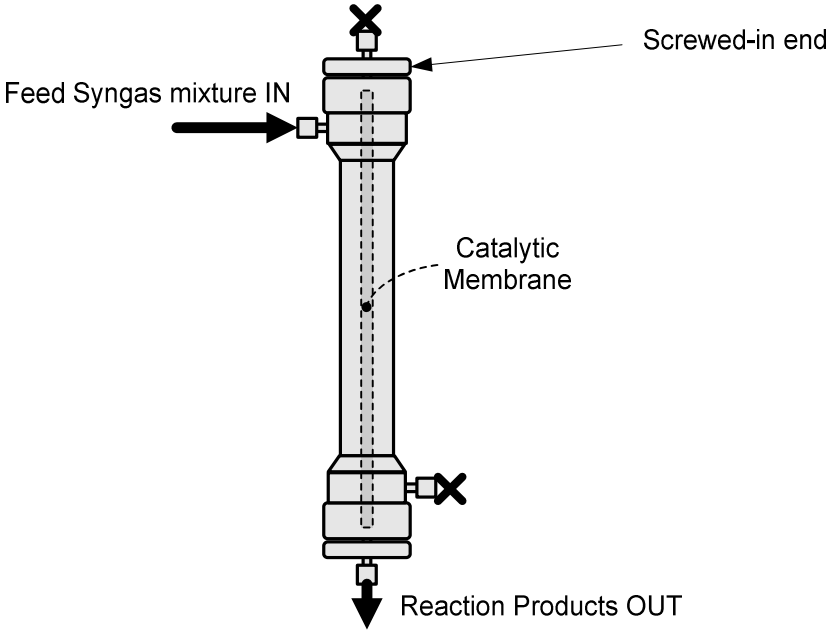

Figure 3.3: Catalytic membrane reactor (CMR) in the forced PFT mode

The temperature of the reactor was monitored by means of four k-type thermocouples stuck to the side and touching the outer surface of the reactor at different locations, and also through the top of the reactor into the mid portion of the membrane. The full experimental set-up for catalytic tests is shown in the process flow diagram in Figure 3.4.

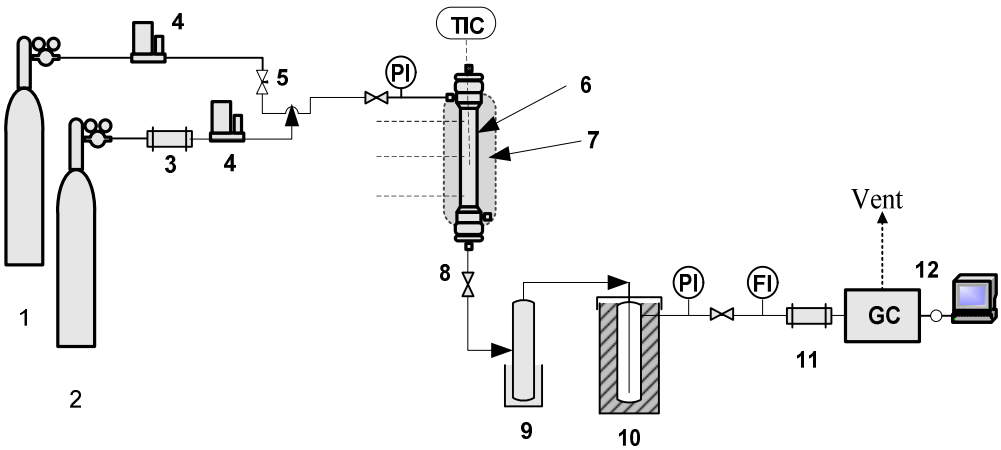

1 – H_2 gas cylinder	**2 – Synthesis gas mixture cylinder**	**3 – Carbonyl trap**
4 – Mass flow controllers	**5 – Needle valve**	**6 – CMR**
7 – Heating Tape & Insulation	**8 – Back pressure regulator valve**	**9 – Hot trap**
10 – Cold trap	**11 – Dehydrator**	
12 – Gas Chromatograph + Workstation		
PI – Pressure gauge	**FI – Flow meter**	**TIC – Thermocouple/Temperature controller**

Figure 3.4: Flow diagram of the catalytic membrane reactor rig

The experiments were performed under different operating conditions but the feed gas was maintained at a H_2:CO ratio of 2.0 (H_2 = 60%, CO = 30%, CO_2 = 10%).in line with stoichiometric requirements for FTS and HAS as shown in Appendix A2.

Flow rates of the feed gases were measured and controlled using mass flow controllers (*Brooks Instruments Model 8744, #5).* The synthesis gas mixture (as supplied by BOC) was passed through a carbonyl trap of activated carbon to remove all iron carbonyl impurities likely to form from the reaction of CO with the steel containers under pressure [Inouye & DeVan, 1978]. It was then metered using the mass flow controllers into the tube side of the reactor which was heated with a heating tape (*Barnstead/Electrothermal*

HT 95508) covered with fibre glass insulation and connected to a power regulator (*MC 227)*. The pressure in the reactor was controlled by a back pressure regulator valve located downstream of the reactor assembly. Catalytic tests were carried out for between 5-8 hours after the catalytic membrane had been activated by hydrogen reduction for 2 hours. Heavy products were collected in the hot trap maintained at 100°C, while liquid products were condensed in the cold trap kept at 0°C. Uncondensed gases were passed through a dehydrator to a TCD gas chromatograph (*Varian CP-3800)* for on-line separation and quantification. Condensed liquid collected in the cold trap was analyzed using two chromatographs: a *Varian 3900* micro-GC fitted with FID; and *Varian CP-3800* gas chromatograph/*Varian Quadrupole MS 1200* mass spectrometer (GC/MS) fitted with a *Varian Factor 4* capillary column.

3.3 Choice of Support

Pore size is known to greatly influence the property and catalytic performance of supported catalysts [Qui *et al*., 2001]. Apart from determining the particle size and hence the reducibility of the active metal, the pore size of the support also affects the level of dispersion of the active material. Permeation tests were carried out on different pore sizes of supports impregnated with equal amounts of dissolved salt precursors of the active metal, to determine the most suitable support for the membranes.

It was important to choose supports with pores that facilitate the crystallization of cobalt particle sizes small enough to be easily reduced but large enough to avoid sintering and leaching. Also, the flow through the membrane had to be maintained in the viscous or convective regime to avoid separation of the feed gas mixture within the membrane thickness, in order to maintain the same syngas ratio throughout (i.e. both during and after

the reaction). This, together with constant temperature is considered essential factors for selectivity [de Deugd *et al*., 2003]. The latter case is also expedient for situations where the once-through conversion of syngas was low and would therefore necessitate a recycling of unreacted syngas, especially when the reactor was operated in a differential mode for the purpose of generating kinetic data.

The titania washcoat was desirable because it is known to enhance intimate interaction with the metal and also assist in stabilizing the particles of the active catalyst metal whilst avoiding unwanted broad particle size distribution of the active component [Toebes *et al*., 2001]. Titania possesses high surface density of reactive hydroxyls (relative to Al_2O_3 or SiO_2) which allows for the formation of a close-packed monolayer of the supported metals [Wachs *et al*., 1993; Burch & Hayes, 1997]. This is believed to increase cobalt-promoter interface considered useful to accommodate chemisorbed CO that is carbon-bound to a cobalt atom and oxygen bound to a promoter ion, resulting in improved metal-promoter interaction. This mode of CO adsorption is important in the catalytic synthesis of oxygenates from syngas mixtures [Kiennemann *et al*., 1987].

3.4 Choice of Promoter

The choice of Mn promoter for the catalytic membrane was based on the need to improve overall activity as well as improve selectivity towards C_2 oxygenates. One of the reported mechanisms for Mn promotion is that it enhances CO dissociation by forming tilt-adsorbed CO species that is C-bonded to Co and O-bonded to Mn, resulting in weakening of the C-O bond, and thereby increasing activity [Ichikawa & Fukushima, 1985]. Mn is also thought to weaken the adsorption strength of CO, leading to less carbon coverage,

and allowing for increased surface concentration of H_2 species necessary for increased activity [Egbebi, 2008].

Alkali promoters were also used to enhance CO dissociation rates by suppressing hydrogenation activity of Co (and other group VIII metals), promote oxygenate formation and shift the product distribution towards higher molecular weights [Uner, 1998]. It is however only effective if the hydrogenation suppression decreases the formation of methane more than it does other products since alkali promotion is known to cause a reduction in the overall reaction rate.

3.5 Catalytic membrane preparation

All catalytic membranes were prepared by the aqueous impregnation method. For bimetallic and mixed metallic catalytic membranes, co-impregnation was adopted. This is because wet impregnation and low concentration of the metal in solution improves metal dispersion by producing a more uniform metal profile distribution along the membrane [Galarraga, 1998]. A determined weight of precursor salt based on the target metal composition was dissolved in distilled water maintained at 80°C.

The support was dried in the oven at 110°C for 1 h and quickly transferred to the impregnation cylinder where it was allowed to sit in the salt solution for 2 h. It was then carefully withdrawn and dried in air for 1 hr before being transferred into the oven and maintained at 65°C for 2 h. It was then finally left to dry overnight in the oven at 110°C.

Subsequent multi-impregnation steps followed similar procedures before the salt-impregnated support was calcined in the furnace according to the typical temperature profile such as is shown in Figure 3.5. Calcinations in air were required to transform the salt to the oxide of the metal that can easily be reduced by hydrogen to the metal itself.

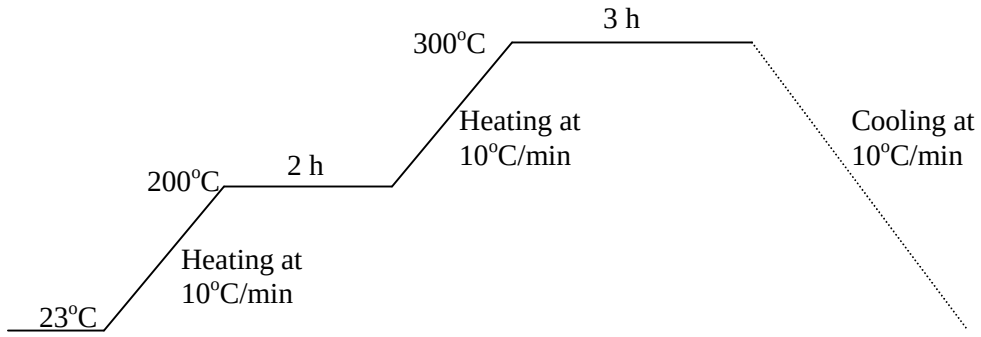

Figure 3.5: Typical calcination profile in catalyst preparation

It is important to know the decomposition temperature of the salt in order to determine the final calcination temperature. Table 3.2 shows the decomposition temperature of some of the salts used in this work [van Berge *et al*., 2001; Nissinen *et al.*, 2005, Elmasry *et al.*, 1998; Ryu *et al*., 2003].

The final step in catalytic membrane production is the reduction of the metallic oxide produced in the calcination step to the required metal. The effectiveness of this reduction is very important to ensure that active metal needed for catalysis is produced. Reducibility of a metallic oxide has been observed to depend on the degree of dispersion, the nature of the support, the reduction temperature, and the influence of promoters [Storsaeter *et al*., 2005; Zhang *et al*., 2006]. Reduction in the reactor was effected with a determined flow of H_2 for 6-8 h at 300°C. The flow rate of reducing hydrogen and the duration of the reduction process depends on the loading of the catalyst precursor on the support.

Table 3.2: Decomposition temperatures of precursor salts.

Precursor Salt	Decomposition temperature (^{o}C)
Cobalt nitrate	120 *
Copper nitrate	182 -312
Manganese nitrate	160
Iron nitrate	250
Potassium nitrate	≈ 400

* [van Berge *et al*, 2001]

All precursor salts and chemical reagents used in this work were of reagent grade (98% and above) as supplied by *Sigma-Aldrich* and *Fisher Scientific* respectively, while all gases were supplied certified by the British Gas Company BOC, in high pressure bottles fitted with the appropriate pressure gauges and flow regulators

3.6 Catalytic Membrane Characterization

Catalytic membranes were characterized by means of gas permeation, scanning electron microscopy (SEM), and energy dispersive X-ray analysis (EDXA) respectively.

3.6.1 Gas Permeation Tests

The flow of gas through the membrane could be used for quantitative determination of the pore size of the membrane. The supports used for this work were reported by the manufacturers to have an average pore size of 6000nm. The pore size of the membrane obtained by the preparation procedure described in section 3.5 had to be ascertained, in order to determine the flow regime of gases as they pass through the membrane. This was done through gas permeation tests conducted using the catalytic membrane reactor, with

the same procedure carried out using an inert gas (argon), hydrogen and carbon dioxide. The gas cylinder was connected to the permeation cell and the regulator valve was opened. The valve on the annular reactor was adjusted to give the same reading on the digital pressure gauge as the one on the regulator of the gas cylinder. Once the digital pressure gauge was calibrated, the regulator valve was re-adjusted to give various readings between 1 and 5 bars. With each new pressure reading, the corresponding flow rate was measured using the digital flow meter. The data obtained for several runs together with geometrical dimensions of the membrane was used to calculate the permeance of the gases as well as the mean pore radius of the membranes. Figure 3.6 shows a schematic diagram of the experimental set-up for the permeation tests, and the results are presented in Figure 4.2.

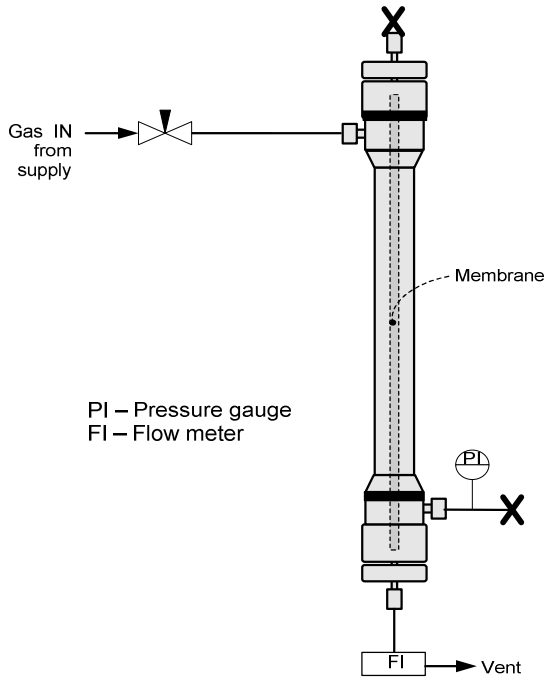

Figure 3.6: Experimental set-up for the gas permeation tests.

3.6.2 Scanning Electron Microscopy (SEM)

The scanning electron microscope (SEM) is used as a high resolution surface imaging instrument capable of providing topographical and morphological information required for investigating membrane structure.

A finely focused beam of electrons is generated from the heating of a tungsten filament housed in an electron gun at the top of the microscope column. This beam of electrons are accelerated toward the specimen by means of an applied accelerating voltage between the filament assembly and an anode plate, and made to scan across the specimen under inspection in a raster fashion. The scanning action is synchronized with the display monitor where an image is generated line by line. As the electron beam traverses the sample, a number of different interactions occur resulting in a variety of signals being emitted from the surface, such as secondary electrons, backscattered electrons, and characteristic x-rays. As shown in Figure 3.7, the SEM was fitted with two imaging detectors – a secondary electron detector and a backscattered electron detector.

A Leo 430 scanning electron microscope operated in the secondary electrons (low energy electrons of less than 50eV) imaging mode was used to analyse various samples of the ceramic α-alumina supported catalytic membranes with magnification up to 300,000 times and a resolution of 3-4nm. The samples were fixed on aluminium SEM stubs by means of adhesive conducting graphite pads. The working distance was adjusted using the stage positioning motors to ensure that the electron beam was concentrated more precisely on the sample surface, and the appropriate magnification was chosen.

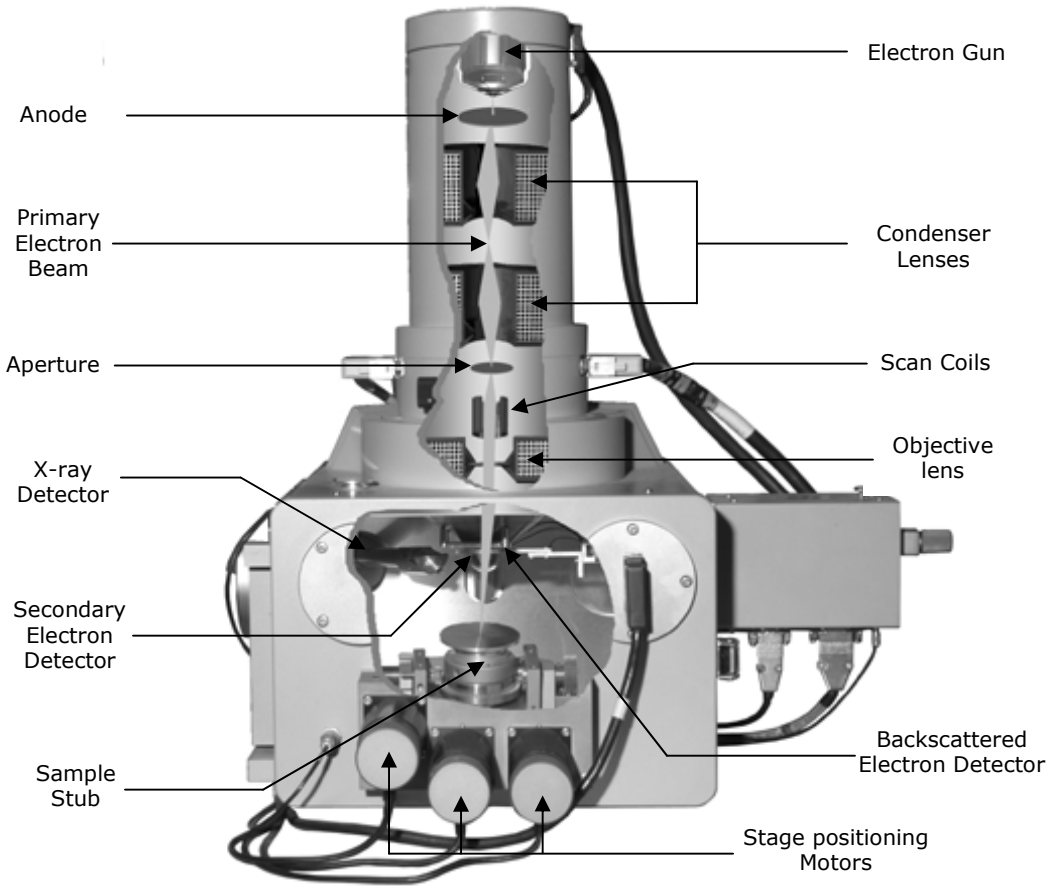

Figure 3.7: Scanning Electron Microscope

The focus was then adjusted to find the point of maximum contrast and the final image was composed on the screen with the brightness and contrast adjusted until all areas of the surface could be clearly seen. A typical SEM micrograph of the ceramic support 2 used in this work is shown in Figure 3.8, clearly indicating a magnification of 5000 times, working distance of 19mm, and the secondary electron detector imaging (SE1) mode.

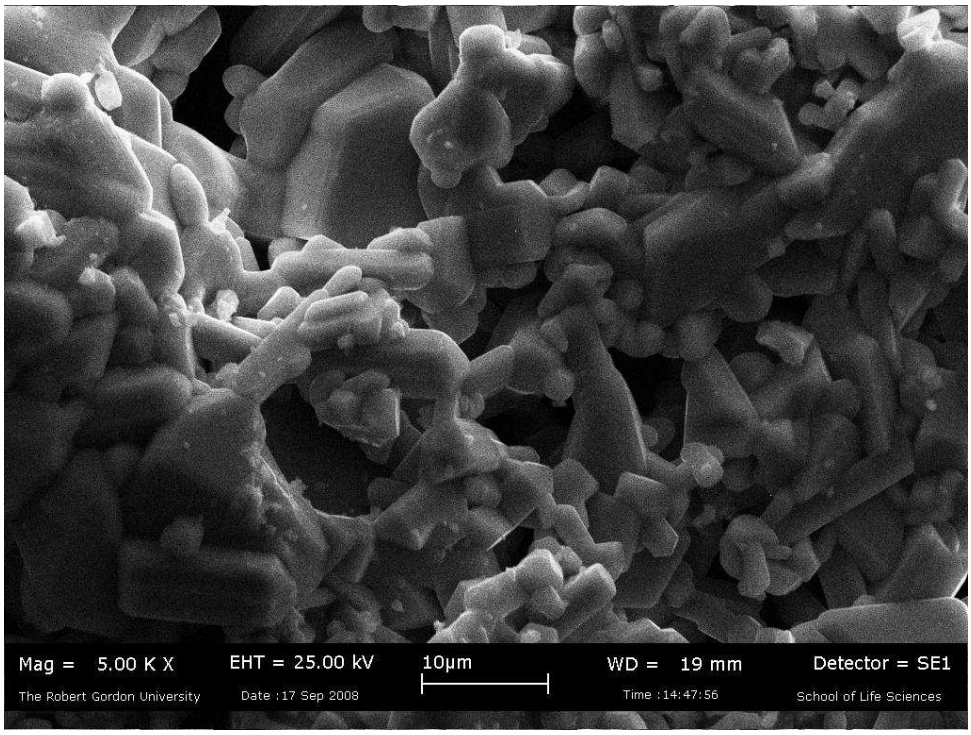

Figure 3.8: SEM micrograph showing the external surface of support 2

3.6.3 Energy Dispersive X-ray Analysis (EDXA)

Energy dispersive X-ray analysis (EDXA) is a very powerful analytical tool. As a beam of electrons from the scanning electron microscope is directed at the sample under analysis, they are scattered elastically and inelastically. The inelastic scattering results in the release of excited characteristic x-rays which are detected by the EDXA instrument. This allows a full quantitative elemental analysis to be performed. The elemental composition can be obtained across the surface of the sample during a scan or at various depths at a single location [Braun, 1987].

The energy dispersive spectrometer employed a solid-state lithium drifted [Si(Li)] crystal detector operated at the temperature of liquid nitrogen, which converted the energy of an x-ray photon into an electrical signal of proportional magnitude. This signal was then sent to the computer for sorting.

The *exL II* x-ray analyser used for the elemental analysis of supports and membranes was fitted with the *INCAmics* microscope image capture unit, *INCAx-stream* microanalytical processor and the INCA Energy System Display as shown in Figure 3.9.

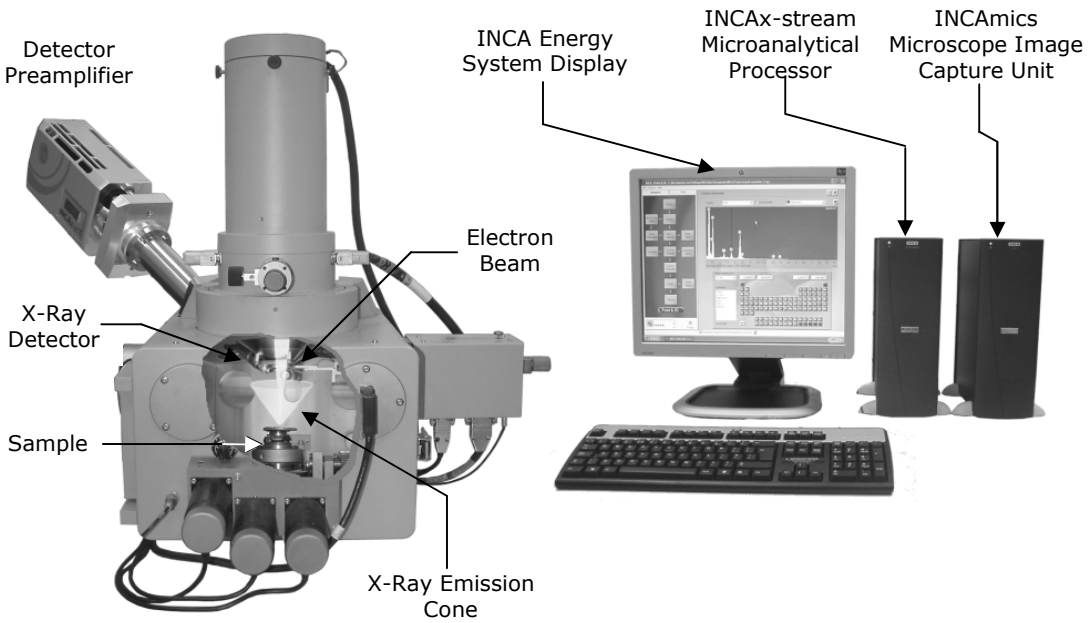

Figure 3.9: SEM- EDXA Assembly

The efficiency of the x-ray analysis lies in proper sample-detector orientation. The sample was mounted flat in the sample chamber and the detector was placed in such a way as to match the angle of x-ray take-off. This means that a critical working distance of about 24mm was required for efficient collection of x-rays

A typical x-ray analysis of a cobalt-based catalytic membrane is shown in Table 3.3, whilst its x-ray spectrum is shown in Figure 3.10.

Table 3.3: EDXA elemental analysis for a cobalt based catalytic membrane

Element	Weight %	Atomic %
O	35.69	63.79
Al	0.37	0.39
Ti	42.80	25.56
Co	21.13	10.26
Totals	100.00	

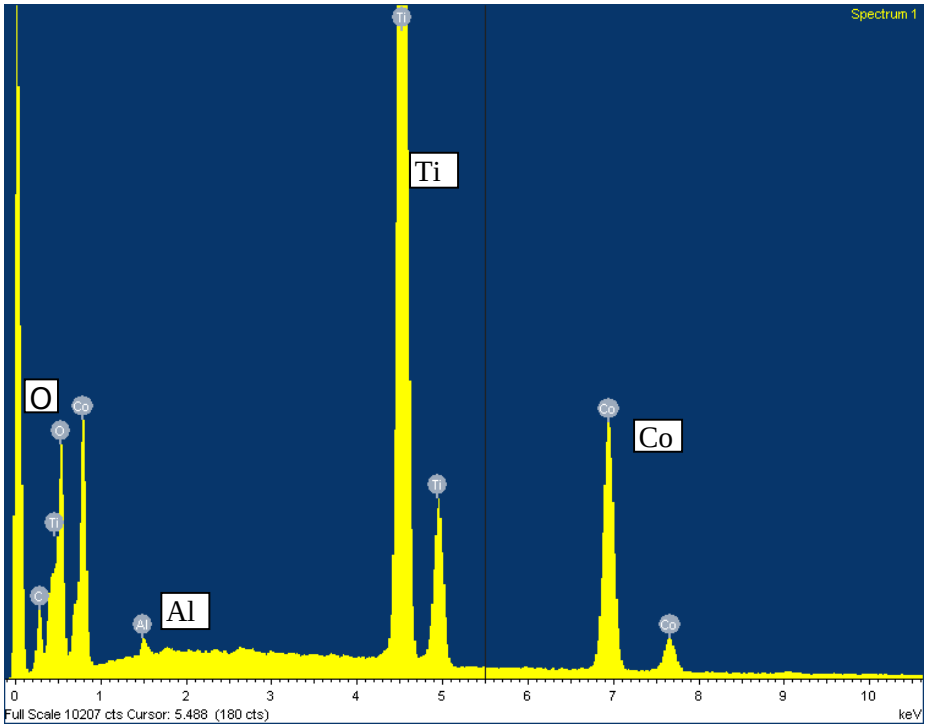

Figure 3.10: EDXA spectrum of a cobalt-based catalytic membrane supported on TiO_2/Al_2O_3.

3.7 Products Analysis

Products were collected in four groups namely; residual gas, water plus oxygenates, light oils (C_{5+}), and wax. These except the wax, were analysed using the gas chromatograph (GC) with different columns and detectors.

3.7.1 Gas Detection and analysis

A gas chromatograph (*Varian CP-3800)* was used for the detection, separation and quantification of gaseous effluents from the reactor after condensation of waxy and liquid products in the traps.

Gas chromatography is the separation technology whereby components in a mixture sample are injected into the head of a column, vaporized and caused to separate by adsorption and partitioning. The injected sample is transported through the column by the flow of an inert gas (mobile phase) called the carrier gas. Commonly used gases include nitrogen, helium, argon and carbon dioxide.

The column itself is either a *packed column* with finely divided, inert, solid material coated with the liquid stationary phase, or a *capillary column* coated with the stationary phase. Three types of capillary columns are in use [Langford *et al*., 2005]. These are the wall-coated open tubular (WCOT) column where the liquid stationary phase is on the inside wall of the column; the support –coated open tubular (SCOT) column, with the liquid phase coated on solid support attached to inside wall of the column; and the porous layer open tubular (PLOT) column with solid stationary phase on the inside wall of the column. Open tubular capillary columns offer higher resolution, shorter analysis time, and greater sensitivity than packed columns, but have lower capacity for the sample [Langford *et al*., 2005].

As the vaporized sample passes through the column, each component in the sample is adsorbed or partitioned to the stationary phase according to its characteristic concentration ratio. Concentration equilibration occurring repeatedly between the mobile and stationary phases causes a difference in the rate of movement for each component

within the column, resulting in the components eluting separately and at different times from the column.

The basic structure of the gas chromatograph used for gas analysis is shown in Figure 3.11. The GC was fitted with two packed columns arranged in series – a 13x molecular sieve *5A MS*, 2m long, 2mm i.d., which separated hydrogen, methane and carbon monoxide; and *Porapak Qs 50-80* for the separation of carbon dioxide and methane.

The column was operated isothermally at 150°C. Argon with a thermal conductivity of 0.016W/mK was chosen as the carrier gas (as against hydrogen or helium which have been known to be the best carrier gases to use in conjunction with a thermal conductivity detector (TCD) [Mendham *et al*., 2000]. This was because hydrogen was among the components to be quantified, and also because the thermal conductivity of hydrogen (0.168W/mK) is very close to that of helium (0.142W/mK). Multiple point calibration of the GC was routinely done using standard mixed gas bottles supplied by BOC containing certified compositions of all the gases to be analyzed

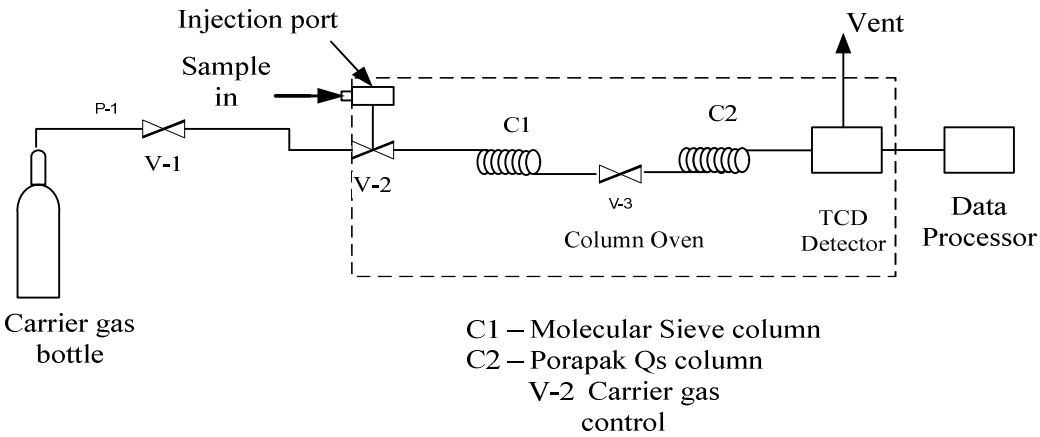

Figure 3.11: Basic structure of the *Varian CP-3800* GC

The output from the GC was monitored by the TCD detector. This type of detector could sense and measure the small amounts of the separated gas components present in the carrier gas stream leaving the column, using a differential technique based on the difference in thermal conductivity between the carrier gas and the carrier gas/gas sample mixture. The output from the detector was then fed to a computer which produced a trace called chromatogram.

Details of the methods used for gas analysis are shown in Appendix C1, and a sample of the chromatogram for gas analysis is shown in Appendix C2

3.7.2 Analysis and Detection of Liquid products

Liquid products showed two distinct phases – the oily phase made up principally of hydrocarbons, and the aqueous phase which contained dissolved alcohols. A pictorial view of a liquid sample collected from a typical catalytic test is shown in Figure 3.12, which clearly indicates the two phases.

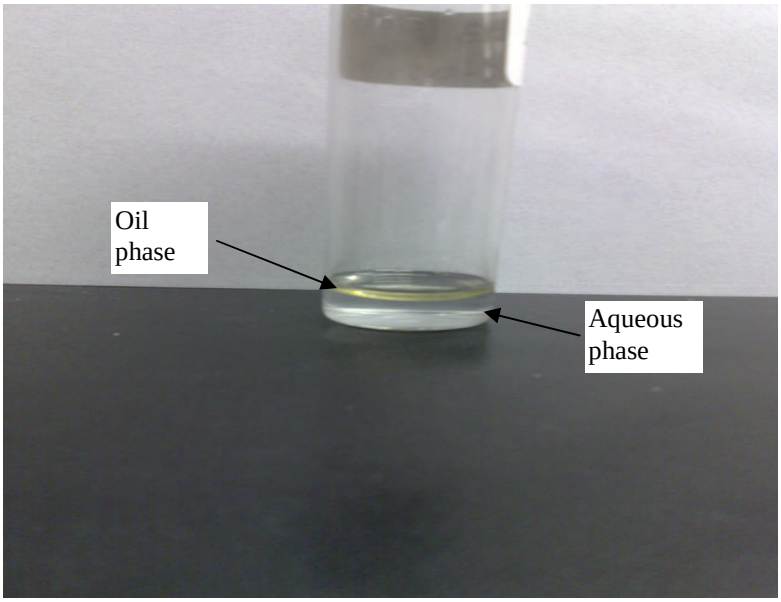

Figure 3.12: A typical condensed liquid sample from a catalytic test run with a cobalt-based membrane

The aqueous and hydrocarbon phases were separated and analyzed initially using the GC/MS for qualitative information on the constituents. After calibration of the *Varian 3900* Micro GC, it was used for quantification of the components by split manual injection (injector type 1177) at a split ratio of 80 with temperature programme and a flame ionization detector (FID).

The FID is particularly useful for the analysis of a broad range of organic molecules. It involves mixing the exit gas stream from the column with hydrogen which is burned in air to produce a flame with sufficient energy to ionize solute molecules having low ionization potentials. The ions produced are collected and the resulting ion current amplified and measured. The flame ionization detector is very sensitive, stable, with a fast linear response over a wide concentration range [Mendham *et al*., 2000]. Its major drawback is that the sample is destroyed during analysis. A pictorial view of the *Varian 3900* micro GC fitted with FID used for liquid analysis, together with the data processing unit is shown in Figure 3.13.

Figure 3.13: A pictorial view of the *Varian 3900* micro GC for liquid analysis

Mass spectrometry when used in conjunction with GC provides a powerful tool for identifying the components of complex mixtures. The procedure requires computer control of the instrument and for data storage/analysis. As shown in Figure 3.14, compounds eluting from the column are bombarded by electrons causing fragmentation and production of charged species. These charged species are separated by the mass spectrometer on the basis of their mass-to-charge ratio. Ions passing through the mass spectrometer are detected by an electron multiplier tube.

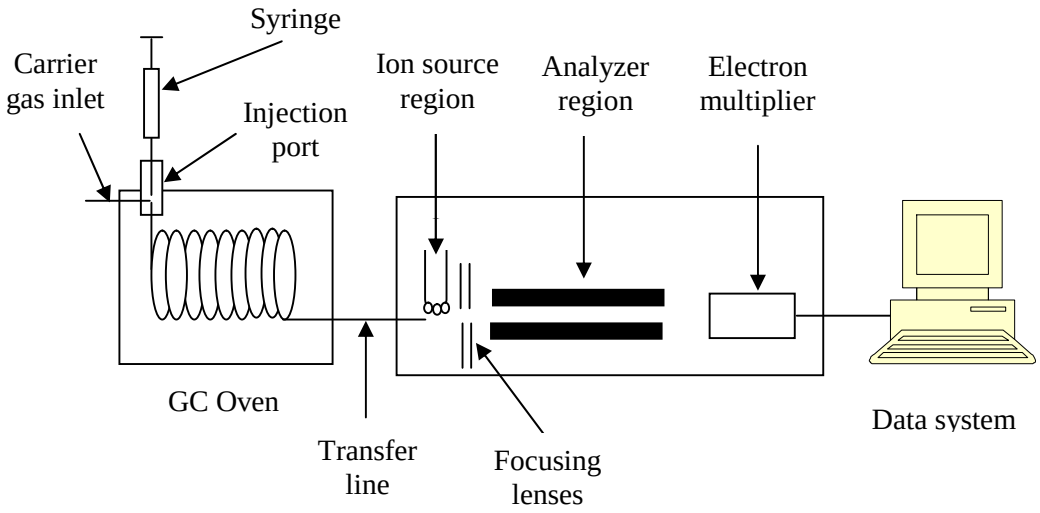

Figure 3.14: Schematic diagram of the capillary *Varian 3800 GC/ Varian Quadrupole MS 1200* mass spectrophotometer

Injection of 0.2µl samples into the *Varian CP 3900* micro GC fitted with FID was performed using a *Hamilton* gas-tight microlitre syringe through a septum. Both WCOT fused silica *CP-Wax 57 CB* (25m × 0.25mm × 0.39mm) column and *Zebron – ZB-Wax plus* (l = 30m; i.d. = 0.25mm; film thickness = 0.25µm) column, which was more resistant to water were used. On the GC/MS, the same split ratio and temperature programme were used except that the *Varian Factor 4* capillary column, VF-1ms (l = 15m; i.d. = 0.25mm, film thickness = 0.25 µm) was used. Injection of samples into the GC/MS was done

automatically using an auto-sampler. Details of the method (BENHAS) used for liquid detection and analysis is shown as Appendix C3. In all cases involving the analysis of liquid products, helium was used as the carrier gas, and the MS system required a vacuum. A typical chromatogram from the *Varian 3900* micro GC with FID detector is shown in Appendix C4.

3.8 References

Braun, R. D. (1987). *Introduction to Instrumental Analysis*. Singapore: McGraw-Hill, Inc.

Burch, R., Hayes, M. J. (1997). The Preparation and Characterisation of Fe-Promoted Al_2O_3-Supported Rh Catalysts for the Selective Production of Ethanol from Syngas. *Journal of Catalysis*, 165 (2), pp.249-261

De Deugd, R. M., Chougule, R. B., Kreutzer, M. T., Meeuse, F. M., Grievink, J., Kapteijn, F., Moulijn, J. A. (2003). Is a monolithic loop reactor a viable option for Fischer-Tropsch synthesis? *Chemical Engineering Science*, 58, pp.583-591.

Egbebi, A. A. (2008). Catalytic synthesis of ethanol from biomass-derived syngas. PhD Thesis, Louisiana State University and Agricultural and Mechanical College.

Elmasry, M. A. A., Gaber, A., Khater, E. M. H. (1998). Thermal decomposition of Ni(II) and Fe(III) nitrates and their mixture. *Journal of Thermal Analysis* 52, pp.489-495

Galarraga, C. E. (1998). Heterogeneous catalyst for the synthesis of middle distillate hydrocarbons. M.Eng. Sc. Thesis, University of Western Ontario.

Ichikawa, M., Fukushima, T. (1985). Infrared studies of metal additive effects on carbon monoxide chemisorption modes on silicon dioxide-supported rhodium-manganese, -titaniun and iron catalysts. *Journal of Physical Chemistry*, 89 (9), pp.1564-1567.

Inouye, H., DeVan J. H. (1978). Formation of iron carbonyl between a ½ % Mo steel and high-pressure gases containing carbon monoxide.
http://www.ornl.gov/info/reports/1978/3445605151411.pdf [Accessed: 6 May, 2009].

Kiennemann, A., Breault, R., Hindermann, J. P., Laurin, M. (1987). Ethanol promotion by the addition of cerium to rhodium-silica catalysts. *Journal of the Chemical Society – Faraday Transactions I*, 83 (7), pp.2119-2128.

Langford, A., Dean, J., Reed, R., Holmes, D., Weyers, J., Jones, A. (2005). *Practical Skills in Forensic Science*. Harlow: Pearson/Prentice Hall.

Mendham, J., Denney R. C., Barnes J. D., Thomas, M. J. K. (2000). *Vogel's Textbook of Quantitative Chemical Analysis (6th Edition).* New York: John Wiley.

Nissinen, T., Leskela, M., Gasik, M., Lamminen, J. (2005). Decomposition of mixed Mn and Co nitrates supported on carbon. *Thermochimica Acta*, 427, pp.155-161.

Qui, X., Tsubaki, N., Fujimoto, K. (2001). Hydroformylation of 1-Hexene over Co/SiO_2 catalysts: Influence of pore size on support. *Journal of Chemical Engineering of Japan*, 34 (11), pp.1366-1372.

Ryu, S. K., Woon, K. L., Soo, J. P. (2003). Thermal decomposition of hydrated copper nitrate $[Cu(NO_3)_2.3H_2O]$ on activated carbon fibers. *Journal of Carbon Science* 5, (4), pp.180-185.

Storsaeter, S., Totdal, B., Walmsley, J. C., Tanem, B. S., Holmen, A. (2005). Characterization of alumina-, silica-, and titania-supported cobalt Fischer-Tropsch catalysts. *Journal of Catalysis*, 236, pp.139-152.

Toebes, M. L., van Dillen, J. A., de Jong, K. (2001). Synthesis of supported palladium catalysts. *Journal of Molecular Catalysis A: Chemical* 173, pp.75-98.

Uner, D. O. (1998). A sensible mechanism of alkali promotion in Fischer-Tropsch synthesis: Adsorbate mobilities. *Industrial and Engineering Chemistry Research*, 37, pp.2239-2245.

Van Berge, P. J., van de Loosdrecht, J., Visagie, J. (2001). Cobalt Catalysis. World Patent number WO/2001/039882.

Wachs, I. E., Deo, G., Vuurman, M. A., Hu, H., Kim, D. S., Jehng, J. (1993). Molecular design of supported metal oxide catalysts: An initial step to theoretical models. *Journal of Molecular Catalysis*, 82 (2-3), pp. 443-455

Zhang, C., Yang, Y., Teng, B., Li, T., Zheng, H., Xiang, H., Li, H. (2006). Study of an iron-manganese Fischer-Tropsch synthesis catalyst promoted with copper. *Journal of Catalysis*, 237, pp.405-415.

Chapter 4 – Results and Discussion

CHAPTER 4: **Results and Discussion**

4.1 Catalytic Membrane Preparation

An important aspect of membrane catalyst preparation involves the loading of the catalyst precursor into the membrane, followed by calcination to transform it into the oxide, and activation or reduction of the oxide by hydrogen to give the active metal.

All results presented in this chapter were averaged over three experimental points with an

4.1.1 Catalyst loading

The wet or aqueous impregnation method used for the production of membrane showed some interesting features with respect to the amount of precursor salt that could be retained in the membrane after impregnation and subsequent drying, and also the effect of increasing the solute concentration. These are shown in Figure 4.1.

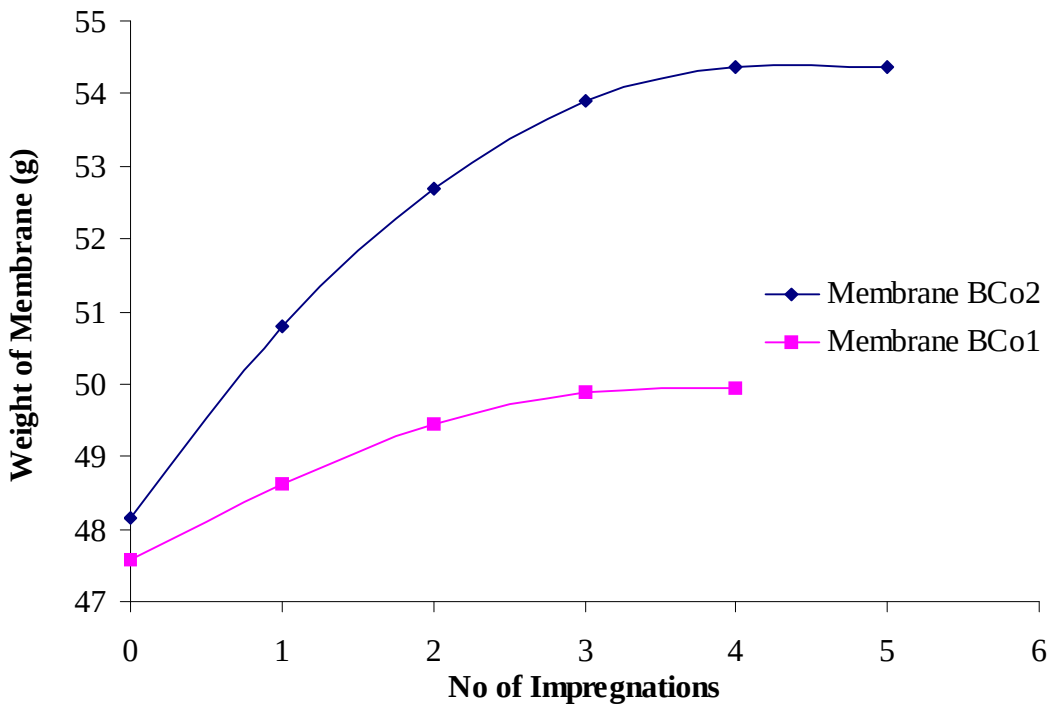

Figure 4.1: Variation in catalyst loading with the number of impregnations

Membrane BCo2 was obtained by impregnating the support with a solution having higher cobalt nitrate concentration, and showed a massive improvement in loading. However, the apparent saturation of the support with the precursor salt after three successive impregnations due to mass transfer limitation was observed in both cases.

4.2 Catalytic Membrane Characterization

Gas permeation tests were used to establish flow characteristics of gases through the membrane. The supports and the catalytic membranes produced were subsequently characterized using surface imaging techniques such as SEM for morphological and structural analysis and EDXA for elemental bulk surface composition.

All experimental data reported in this chapter were the average values from three similar sets of experiments, with an error margin of less than 2%.

4.2.1 Gas permeation tests

Gas permeation tests reveal that flow through the membranes could be characterized mostly by viscous or convective regime at ambient temperature as shown in Figure 4.2.

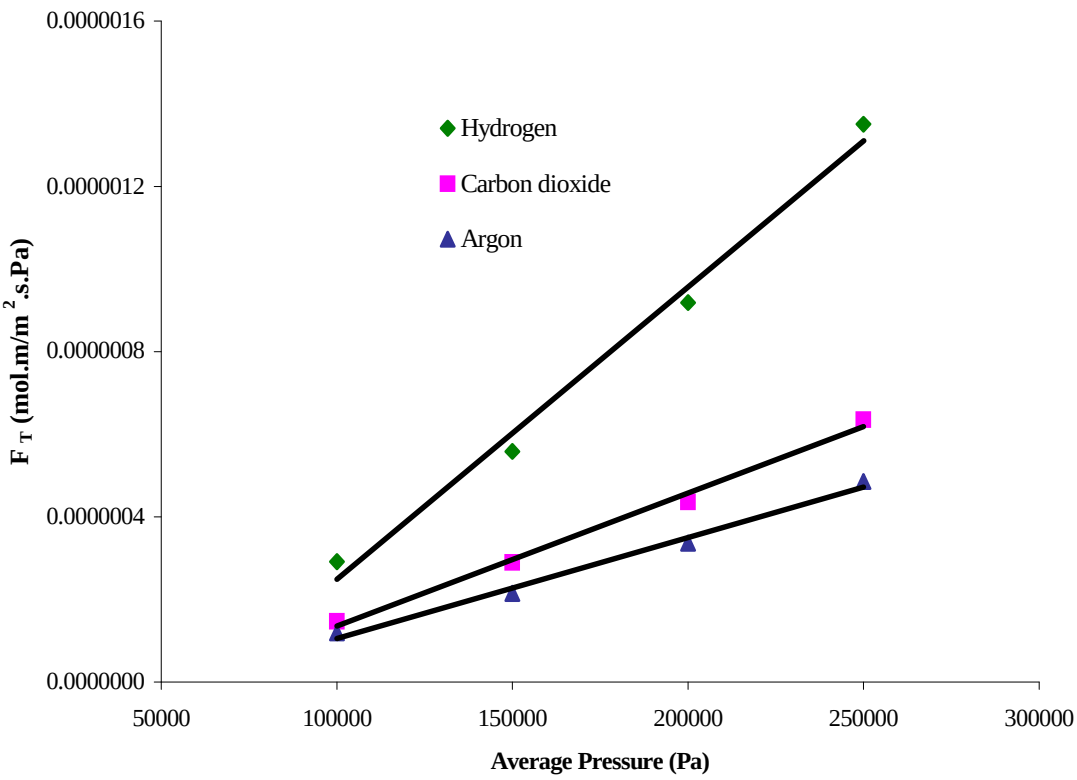

Figure 4.2: Characteristics of Gas flow through the membrane at 300K

The mass transport of a single gas in porous media is usually well described by the laws of Fick and Darcy, and the net flux is a contribution of Knudsen diffusion and of viscous flow [Uchytil *et al.*, 2000]. According to Roque-Malherbe [2007], the increase of permeability with pressure is a sign that viscous gaseous flow might be responsible for mass transfer, since Knudsen diffusion does not show such dependency on pressure. Therefore, the total gas permeation rate through a porous membrane can be written in a general non mechanistic flux equation in terms of Knudsen flow and viscous flow. For gas transport through a long capillary pore (tube) of a membrane with a radius of r_p by Knudsen and viscous flow, their molar flux can be expressed in terms of the following equations [Li, 2008]

$$N_{Knud} = \tfrac{2}{3}\sqrt{\frac{8}{\pi MRT}}\left(r_P\right)\frac{\Delta P}{\delta_M} \tag{4.1}$$

$$N_{vis} = \frac{r_P^2}{8\mu RT}\,\overline{p}\,\frac{\Delta P}{\delta_M} \tag{4.2}$$

Hence the overall mathematical equation approximating gas flux through the membrane could be written as:

$$N_{Total} = \tfrac{2}{3}\sqrt{\frac{8}{\pi MRT}}\left(r_P\right)\frac{\Delta P}{\delta_M} + \frac{r_P^2}{8\mu RT}\,\overline{p}\,\frac{\Delta P}{\delta_M} \tag{4.3}$$

where N_{Knud} and N_{vis} are the gas molar flux under Knudsen and viscous flows respectively, in molm^{-2}s^{-1}, R is the gas constant (8.3174m^{3}Pa.mol^{-1}K^{-1}), M is the molecular weight in g/mol, ΔP is the pressure differential across the membrane, in Pa, δ_M is the effective thickness of the membrane, μ is the viscosity of gas, in Pas and $\overline{p}$ is the average pressure across the membrane, in Pa.

Dividing equation 4.3 by $\Delta P / \delta_M$ gives the normalized total flux:

$$F_T = K_o + B_o\,\overline{p} \tag{4.4}$$

where $F_T = N_{Total}\dfrac{\delta_M}{\Delta P}$ $\left(\dfrac{mol.m}{m^2.s.Pa}\right)$ (4.5)

where K_o and B_o are parameters that characterize the structure of the porous matrix and are defined by equations 4.6 and 4.7 respectively

$$K_o = \frac{8r_p}{3\left(2\pi MRT\right)^{1/2}} \qquad \left(\frac{mol.m}{m^2.s.Pa}\right) \tag{4.6}$$

$$B_o = \frac{r_p^2}{8\mu RT} \qquad \left(\frac{mol.m}{m^2.s.Pa^2}\right) \tag{4.7}$$

If the plot of equation 4.6 has the form, $F_T = K_o$, the permeation is characterized by Knudsen flow; if it has the form $F_T = B_o \bar{P}$, then the flow is in the viscous regime. A plot of the type shown in equation 4.6 indicates a combined Knudsen and viscous flow condition.

Figure 4.2 seems to suggest that there is a small contribution of Knudsen flow to the total flux. In the viscous flow regime, gas flux through a porous membrane is inversely proportional to the viscosity of the gas, but under Knudsen flow conditions, it is inversely proportional to the square root of the molecular weight of the gas [Silva *et al*., 2008]. A consideration of the pattern of the ratios of fluxes of the gases to the inverse of both the ratio of viscosities and the square root of the ratio of molecular weights will therefore help to determine the actual flow characteristics through the membrane.

For Knudsen flow:

$$\frac{F_1}{F_2} = \sqrt{\frac{M_2}{M_1}} \tag{4.8}$$

where M is the molecular weight, and for viscous flow;

$$\frac{F_1}{F_2} = \frac{\mu_2}{\mu_1} \tag{4.9}$$

where $\boldsymbol{\mu}$ is the viscosity.

Table 4.1 gives the fluxes and flow ratios obtained for hydrogen and carbon dioxide in the gas permeation tests.

Table 4.1: Ratios of fluxes for hydrogen and carbon dioxide at 300K.

ΔP (bar)	F_{H2} (ml/min)	F_{CO2} (ml/min)	F_{H2}/F_{CO2}
1	45	22.65	1.99
2	115	59.65	1.93
3	213	101	2.11
4	334	157	2.13

The viscosity of carbon dioxide, μ_{CO2} = 1.5127×10^{-5} kg/m.s (at 300K) and that of hydrogen, μ_{H2} = 8.8871×10^{-6} kg/m.s [http://www.1mnoeng.com, 2009]. The ratio of the viscosities of CO_2 to H_2 = 1.7, while the ratio of the square root of molecular weights = 4.67. Thus, it could be safely concluded that under the conditions of the experiments reported in this thesis, viscous flow characteristics were maintained by the membranes. The small deviation from ideal viscous flow seen in Figure 4.2 could have arisen as a result of the presence of micropores within the macroporous membrane matrix. During catalytic test conditions it is important to maintain viscous flow through the membrane in order to ensure that no separation of the synthesis gas mixture occurs as this would alter the H2:CO ratio required for the conversion.

Having established that the prevalent flow characteristics through the membrane is the viscous regime, the pore size of the membrane could be estimated from the slope of the graph using equation 4.4. For carbon dioxide, B_o = 3.2223 ×10^{-12} mol/m^2.s.Pa and μ_{CO2}= 1.5127×10^{-5} kg/m.s at 300K. Solving equation 4.7 for CO_2 gives r_p = 9.8209×10^{-7}m. This means that the estimated particle diameter is 0.98 microns. Using the slope obtained from Figure 4.2 for hydrogen, B_o = 7.0781 ×10^{-12} mol/m^2.s.Pa. The viscosity of hydrogen at 300K is 8.8871×10^{-6} kg/m.s. Equation 4.7 yields a value for r_p = 1.1204 ×10^{-6}m.

The calculated values of r_p range from 0.98 microns to 1.12 microns or pore diameter d_p of 1.96 – 2.24 microns, and fits perfectly with measured pore diameter of about 2 microns obtained from SEM. This indicates that the pore size of the support had been reduced from its original value of 6 microns to about 2 microns in the membrane as a result of catalyst impregnation.

4.2.1 SEM

SEM images show the outer (shell side) surfaces (O.S.), inner (tube side) surfaces (I.S.) and thein some cases, cross sectional surfaces (X.S.) of the supports used and the membranes produced. Figure 4.3 shows the SEM micrographs of the two supports used, which though similar in composition and pore size, were produced from different batches, with different types of glazing at the end of the ceramic tubes, as shown in Figure 3.1.

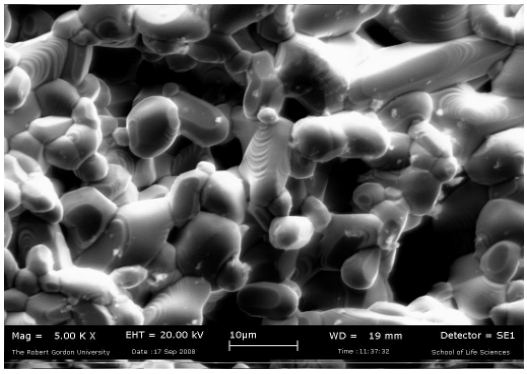

(a)

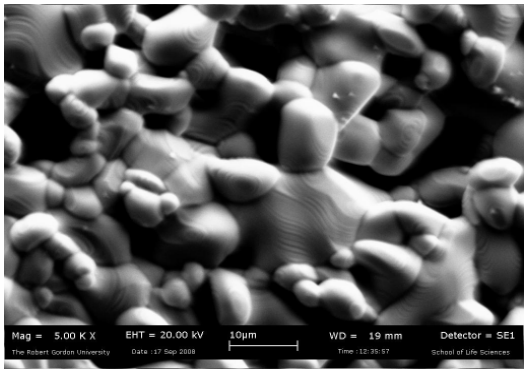

(b)

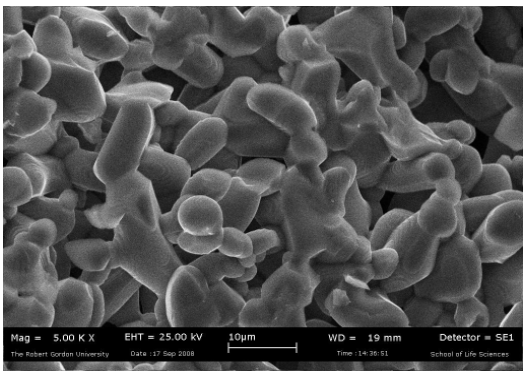

(c)

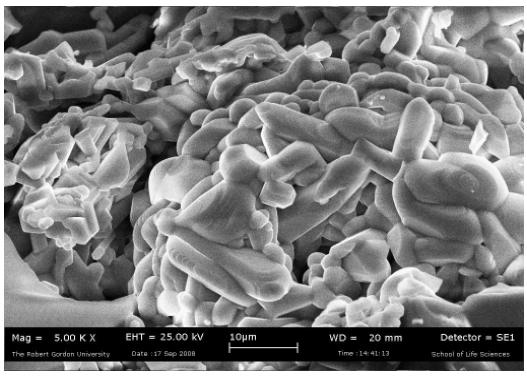

(d)

Figure 4.3: SEM micrograph of membrane supports. (a): O.S. of support 1; (b): I.S. of support 1; (c): X.S. of support 1; and (d): X.S. of support 2.

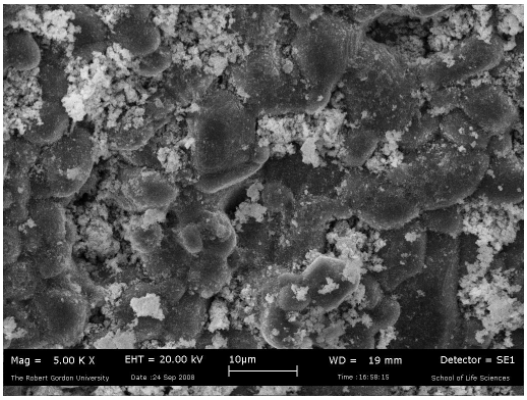

(a)

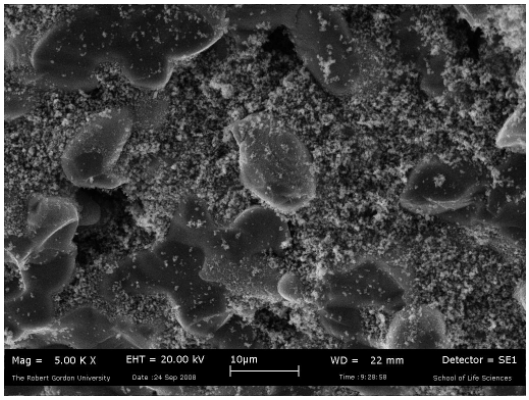

(b)

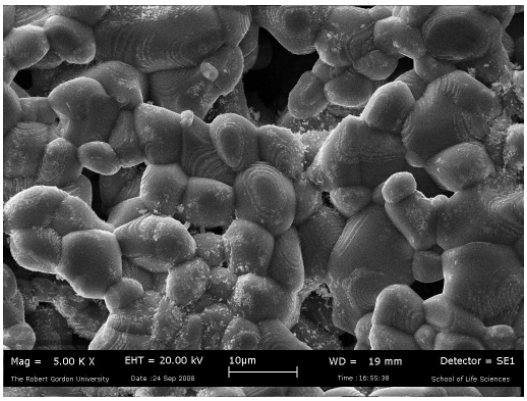

(c)

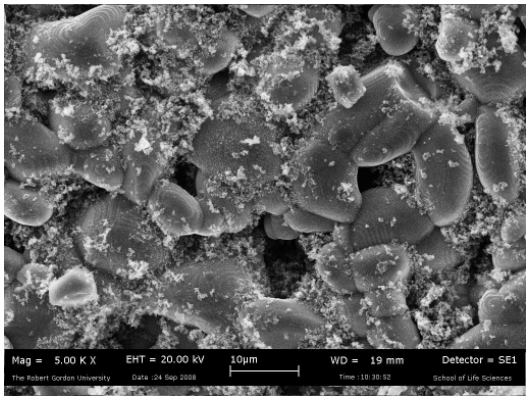

(d)

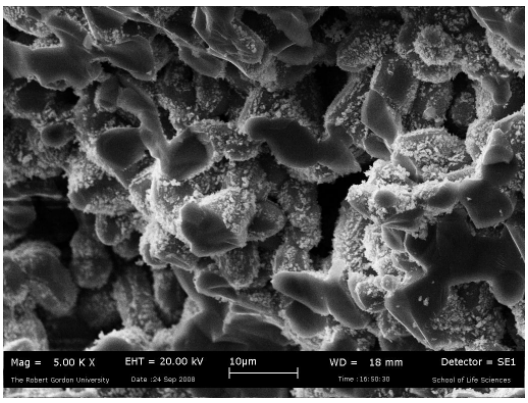

(e)

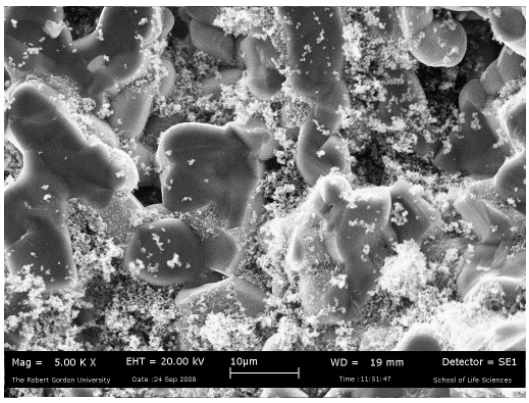

(f)

Figure 4.4: SEM micrographs of membrane BCo1 (Cobalt). (a): O.S. before catalytic tests; (b): O.S. after tests; (c): I.S. before catalytic tests; (d): I.S. after tests; (e): X.S. before catalytic tests; (f): X. S. after tests

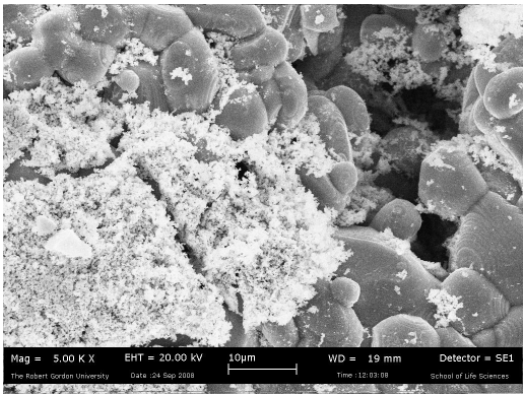

(a)

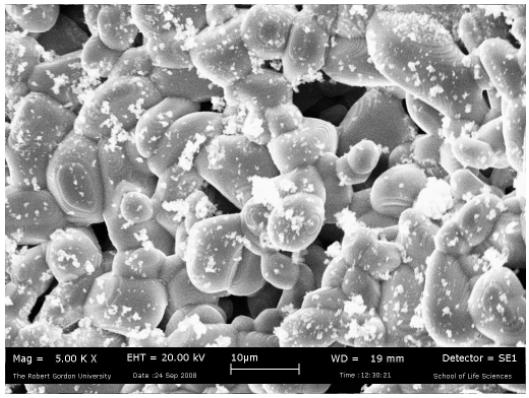

(b)

Figure 4.5: SEM micrographs of Membrane BCo2 (cobalt) showing the increase in catalyst cluster as a result of increase in precursor concentration. (a): O.S., (b): I.S.

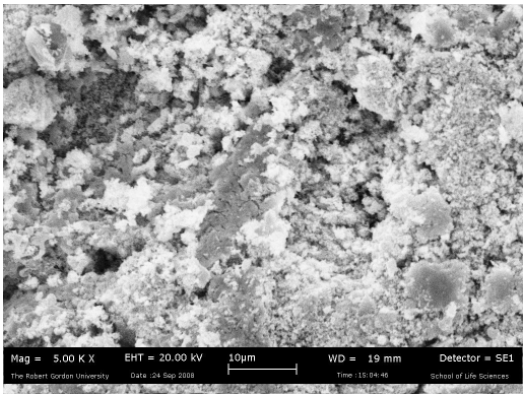

(a)

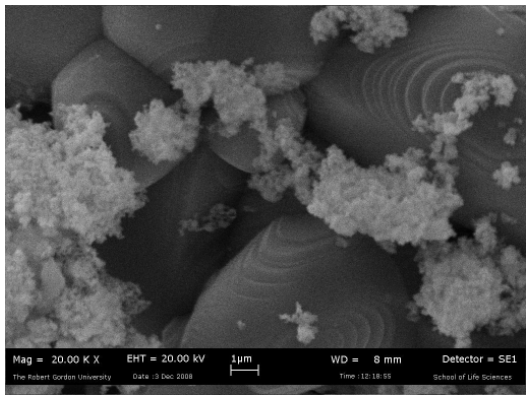

(b)

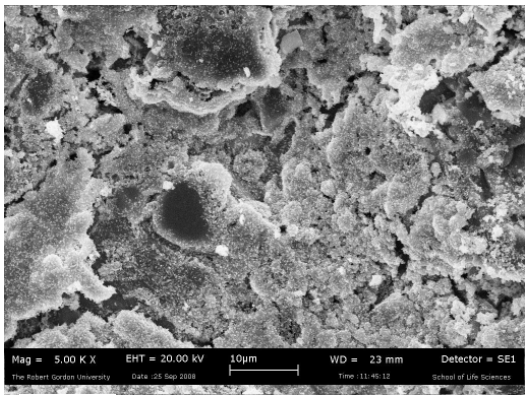

(c)

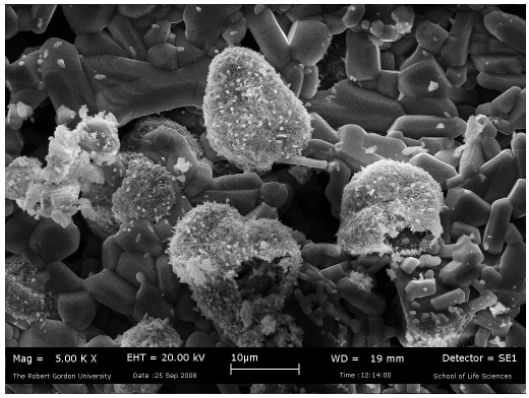

(d)

Figure 4.6: SEM micrographs of membranes BCo3 (Co-Cu) (a): O.S., (b): I.S. and BCo4 (Co-Cu-K) (c): O.S., (d): I.S.

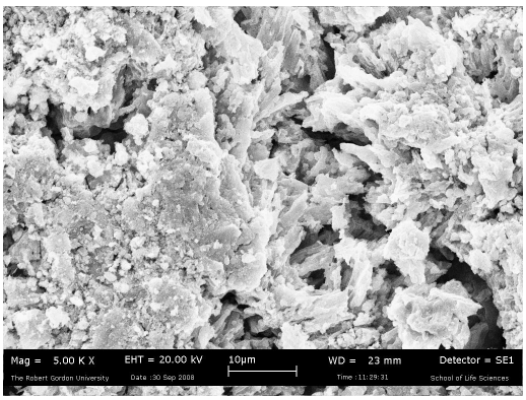

(a)

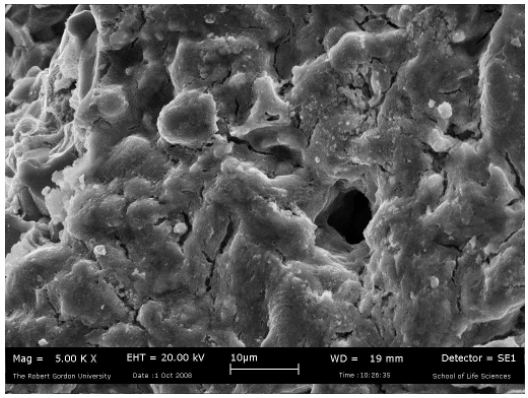

(d)

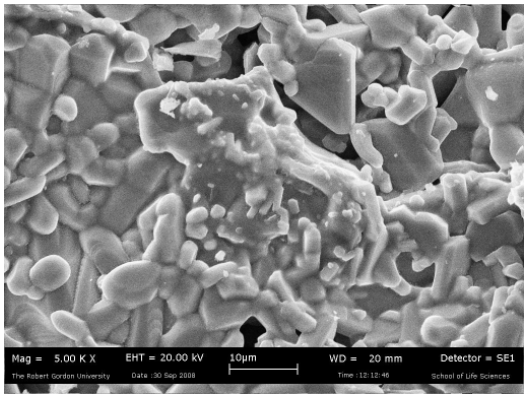

(b)

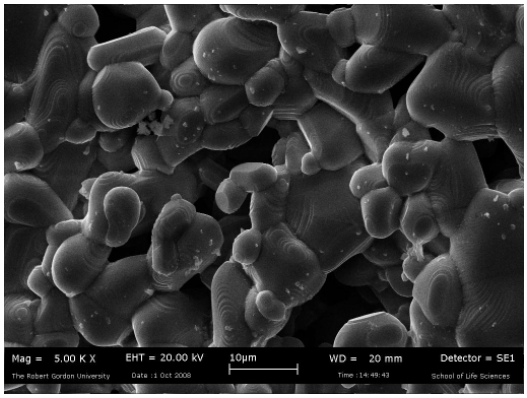

(e)

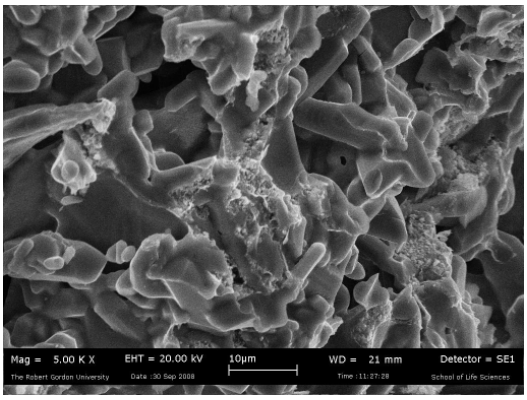

(c)

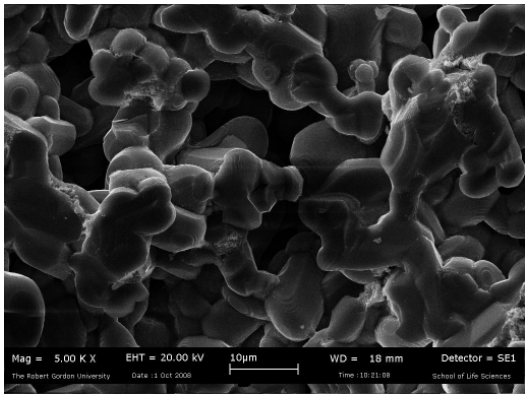

(f)

Figure 4.7: SEM micrographs of membrane BCo5 (Co-Mn) (a): O.S., (b): I.S., (c): X. S., before catalytic tests, and (d): O.S., (e): I.S., (f): X.S., after tests

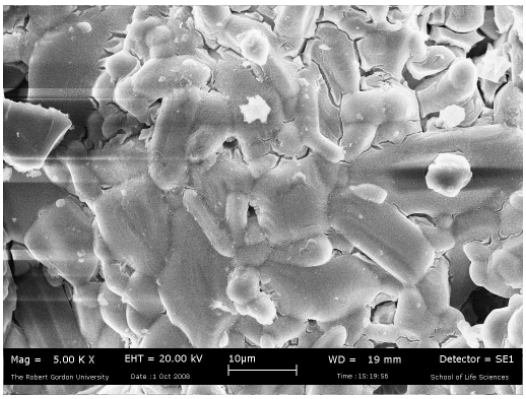

(a)

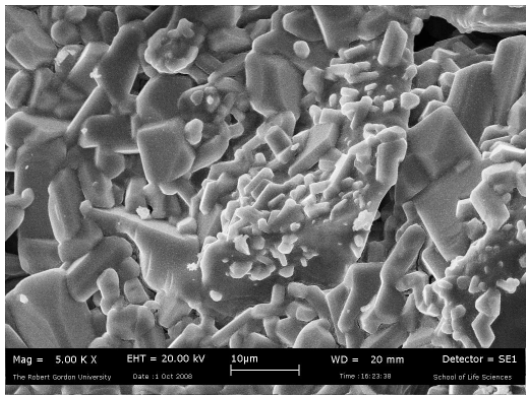

(b)

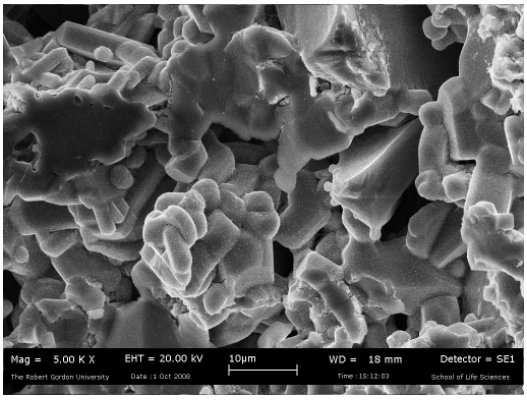

(c)

Figure 4.8: SEM micrographs of membrane BFe1 (Fe-Mn). (a): O.S., (b): I.S., and (c): X.S.

The SEM micrographs shown in Figure 4.3 indicate the morphology of the support matrix with fully rounded edges of the titania-washcoated α-alumina prior to impregnation with the metal catalyst precursor. The structure of the asymmetric oxide support shows well-defined pores which increase from the shell side (O.S.) to the tube side (I.S.).

Figure 4.4 (a), (c) and (f) indicate a highly dispersed arrangement of cobalt catalyst within the membrane after calcinations for eight hours at 573K, and subsequent reduction with flowing hydrogen. In figure 4.4 (d) however, there appears to be complete dissociation of the bulky aggregates seen in figure 4.4 (a) into finer and better dispersed catalyst particles after the catalytic conversions of syngas. This could have resulted from subjecting the

membrane to reaction temperatures of up to 673K for longer periods of time, and seem to suggest that the higher the calcination temperature and/or the longer the duration, the better the cobalt dispersion. An increase in the concentration of catalyst precursor in the impregnating sol resulted in an increase in catalyst loading in the membrane as shown in Figure 4.5, with the formation of larger but equally well-dispersed cobalt particles.

Figure 4.6 (a) and (b) are the micrographs for cobalt-copper catalysts supported on titania-washcoated α-alumina. They showed the formation of larger particles when compared to (c) and (d) in which potassium was added. The catalyst also appear to be more homogeneously distributed on the outer surface of the membrane arising from the smaller pore size as well as the growth of catalyst crystallites on the surface. The interaction of the support with the catalyst also appears to be very strong as demonstrated in Figure 4.6 (d), where the catalyst particles tend to form clusters around support constituent parts. Thus the presence of potassium seems to promote catalyst-support interaction which has been known to have a pronounced effect on the reactivity of the catalyst [Adesina, 1996].

The micrographs of cobalt-manganese catalyst shown in Figure 4.7 indicate a very high loading of catalysts which seemed to agglomerate into a layer on the outer surface of the membrane. After catalytic conversion tests however, they tended to form an amorphous crust with visible cracks on it. This could have been the result of the formation of a mixed oxidic phase of the cobalt-manganese catalyst species owing to a strong Co-Mn interaction that tended to prevent crystallization of the active phase. Morales *et. al.*, [2007] observed a similar loss in crystallinity from X-ray diffraction (XRD) patterns and attributed it to the interaction between Co_3O_4 and manganese to form a $Co_{3-x}MnO_4$ type solid solution. This loss in metallic behaviour resulted in higher cobalt-time yield and

decreased methane production [Cano et al., 2004]. XPS results from the work of Morales and co-workers showed that after calcinations the catalyst contained mainly a Co_3O_4 phase, and that only a fair fraction was reduced to metallic Co after reduction in H_2 flow for 4 hours [Morales *et al*. 2005]. Figures 4.7 (e) and (f) also seem to suggest that there was decoration of the cobalt catalyst particles on the outer surface of the membrane by manganese. The high Mn/Co ratios shown in Table 4.2 seem to support both high dispersion of Mn and Co over the TiO_2 support, and the surface decoration. This electronic promotional effect by manganese could have actually increased the activity, selectivity and stability of the membrane although it has also been reported that under certain conditions some metal ions can diffuse into the TiO_2 lattice forming very stable compounds [Voβ *et al*., 2002]. This means that the possibility of the formation of the spinel cobalt titanate phase is not by any means ruled out. The presence of these oxides in close association with metallic cobalt may have led to the non dissociative adsorption of CO, resulting in the production of alcohols from cobalt catalysts [Blanchard *et al*., 1989].

A similar effect to that displayed by the cobalt-manganese membrane was observed for the iron-based membrane in Figure 4.8. The outer surface appeared to display a decorating effect by manganese without any visible crystallization, although the inner surface showed crystallization of large catalyst particles of up to two microns in diameter. This is not surprising because the membrane was produced from an equimolar concentration of iron and manganese with copper and potassium constituting less than 5% of the membrane.

4.2.3 EDXA

Elemental compositions of the supports and membranes were obtained using the energy dispersive x-ray analyzer and the results are shown in Table 4.2.

TABLE 4.2: EDXA RESULTS - ELEMENTAL COMPOSITION

Weight %	Outer Surface (O.S)				Inner Surface (I.S)				Cross Section (X.S.)
	1	2	3	Average	1	2	3	Average	
Sample 1: SUPPORT 1									
O	65.13	66.01	69.71	66.95	62.74	61.81	62.51	62.35	
Al	0.88	0.79	0.93	0.87	0.4	0.52	0.54	0.49	
Si	0.26	0.27	0.26	0.26					
Ti	33.74	32.93	29.09	31.92	36.86	37.67	36.95	37.16	
Sample 2: SUPPORT 2									
O	75.95	72.37		74.16	67.6	66.23	66.36	66.73	
Br	12.18	15.06		13.62	11.85	11.2	11.39	11.48	
Si	0.55	0.37		0.46					
Ti	11.32	12.2		11.76	20.55	22.57	21.22	21.45	
Sample 3: Membrane BCo1 (before catalytic tests)									
O	13.94	28.19	26.25	22.79	40.05	41.04	37.64	39.58	75.14
Al	0.23	1.38	0.39	0.67	0.23	0.31	0.25	0.26	0.16
Ti	44.13	19.4	42.64	35.39	47.64	46.36	52.36	48.79	20.92
Co	40.78	50.22	30.72	40.57	8.15	8.43	5.79	7.46	3.78
C					3.94	3.85	3.95	3.91	
Sample 4: Membrane BCo1 (after catalytic tests)									
O	52.85	53.04	52.8	52.90	43.69	44.85	48.83	45.79	46.2
Al	0.49	0.65	0.59	0.58	0.27	0.36	0.37	0.33	
Ti	43.87	42.23	43.63	43.24	53.93	53.41	49.19	52.18	50.46
Co	2.80	4.08	2.79	3.22	2.10	1.38	1.62	1.70	3.35
Si	0.16		0.18	0.17					
Sample 5: Membrane BCo2 (after catalytic tests)									
O	27.86	24.63	29.89	27.46	55.98	55.04	54.55	55.19	51.41
Al	0.44	0.32	0.53	0.43	0.28	0.4	0.32	0.33	
Ti	37.3	35.13	38.95	37.13	41.99	42.72	43.58	42.76	35.67
Co	34.4	39.92	30.63	34.98	0.68	1.84	1.55	1.36	12.91
Sample 6: Membrane BCo3 (after catalytic tests)									
O	3.12	3.2	2.85	3.06	44.61	44.94	53.15	47.57	19.95
Al					0.32	0.39	0.37	0.36	0.14
Ti	1.29	1.32	0.97	1.19	53.05	52.35	44.54	49.98	55.65
Co	54.4	54.14	55.04	54.53	0.56	0.62	0.56	0.58	6.41
Cu	41.19	41.34	41.13	41.22	1.48	1.71	1.38	1.52	17.84
Sample 7: Membrane BCo4 (before catalytic tests)									
O	32.99	33.34	33.32	33.22	47.73	47.68	47.52	47.64	55.54
Al	1.97	3.74	2.82	2.84	3.66	3.85	3.31	3.61	0.41
K	1.68	1.69	1.78	1.72	0.62	0.8	0.84	0.75	
Ti	7.45	8.94	6.64	7.68	30.33	29.43	30.56	30.11	40.78
Co	30.85	24.72	27.03	27.53	4.29	4.54	4.55	4.46	1.35
Cu	24.77	27.57	28.11	26.82	13.05	13.38	12.91	13.11	0.94
Sample 8: Membrane BCo4 (after catalytic tests)									
O	21.14	19.75	22.98	21.29	43.27	41.94	43.98	43.06	43.39
Al	3.72	4.64	3.91	4.09		3.75	3.36	3.56	1.9
K	1.99	1.83	1.77	1.86	0.25	0.3	0.32	0.29	0.5

Ti	14.56	14.79	18.07	15.81	36.5	38.99	40.15	38.55	34.79
Co	32.94	32.52	28.38	31.28	2.87	4.42	3.61	3.63	11.35
Cu	25.65	26.46	24.88	25.66	5.95	10.42	8.45	8.27	8.07
Sample 9: Membrane BCo5 (before catalytic tests)									
O	30.92	29.37	31.52	30.60	49.39	50.35	50.52	50.09	
Al	0.59	1.06	0.39	0.68	3.32	3.17	4.32	3.60	
Ti	24.66	24.9	24.57	24.71	40.8	40.28	37.71	39.60	
Mn	22.17	21.61	20.79	21.52	2.57	2.73	2.78	2.69	
Co	41.42	42.81	42.51	42.25	3.84	3.81	3.85	3.83	
Sample 10: BCo5 (after catalytic tests)									
O	46.23	47.97	47.99	47.40	51.92	52.09	52.65	52.22	
Al	0.40	0.42	0.40	0.41	0.29	0.3	0.34	0.31	
Ti	27.78	27.02	30.51	28.44	45.35	40.21	44.6	43.39	
Mn	10.21	9.84	8.43	9.49	1.05	1.09	1.03	1.06	
Co	15.38	14.75	12.66	14.26	1.40	1.31	1.38	1.36	
Sample 11: BFe1 (before catalytic tests)									
O	50.05	50.73	49.81	50.20	56.5	55.57		56.04	
Al	6.66	5.68	5.05	5.80	5.71	7.82		6.77	
K	0.95	1.13	1.08	1.05	0.39			0.39	
Ti	34.1	30.88	33.06	32.68	34.12	33.2		33.66	
Mn	0.59	0.95	0.89	0.81	0.96	1.16		1.06	
Fe	4.9	7.85	7.24	6.66	1.43	1.80		1.62	
Cu	2.52	2.79	2.69	2.67	0.19			0.19	
Si	0.23		0.17	0.20					

The analysis reveals that the titania washcoat on support 1 was quite high (about 32%) compared to that on support 2 ($\approx$12%). Therefore membranes made from support 1 exhibited more of the catalyst-support interaction as would be expected, and showed greater capacity for alcohols over hydrocarbon formation. It is also important to note that although the quantity of titania used for support 2 was smaller, the surface coverage of the α-alumina backbone is actually better.

After impregnation with the catalysts, and subsequent calcination and reduction processes, the weight of atomic oxygen on the outer surfaces of the supports dropped by about 80%. However, during reaction, the catalysts appeared to have been oxidized, thereby raising the percentage of elemental oxygen. Oxidation of the active phase of the catalyst results in loss of activity and could have been effected by adsorbed oxygen species present

during the reaction or by atmospheric oxygen. This led to a very dramatic drop in the weight of active cobalt in membrane BCo1, after being used cumulatively for over 400 hours of reaction.

A comparison of the weight of cobalt left in membrane BCo2 after a longer period of use than that in membrane BCo1 shows that although the increase in precursor concentration led to the formation of larger catalyst clusters, and possibly lowered the rate of reduction to the active state, the rate of deactivation was much lower. However, membrane BCo2 showed reduced activity for alcohols formation, and better selectivity to hydrocarbons.

Copper addition has been known to decrease reduction temperature of supported cobalt catalysts [Leite *et al*., 2006]. This was the intention in membrane BCo3 but its concentration was rather too high resulting in a competition for the active catalyst position as against the promoter effect required. When the membrane was used in the same way as the other cobalt-based membranes, there was no conversion of syngas at all. Introduction of potassium in membrane BCo4 activated the copper, although the effect of cobalt observed with the cobalt-based membranes was not very evident. This is because the copper oxide has a tendency to concentrate at the surface of the particles, thus enriching the surface with copper, at the expense of cobalt [Dulov *et al*., 1987]. These cobalt-copper membranes also exhibited unusual decrease in the weight percent of oxygen after catalytic tests, suggesting that the calcination and reduction procedures used for the cobalt membranes were not adequate to fully transform the copper-promoted membranes into their catalytically active state for syngas conversion. It thus appears that alcohol formation by active cobalt was effected via the Fischer-Tropsch route and not through the methanol or higher alcohols synthesis (HAS) route.

Membrane BCo5 clearly shows that manganese was used as a promoter and its role was very visible in the catalytic conversion tests, with very high conversions and an equally high selectivity to higher hydrocarbons. The extent of deactivation by oxidation of the active metals was very low as shown in the table, even after over 200 hours of catalytic reaction.

Membrane BFe1 was based on iron and led principally to the production of hydrocarbon wax.

4.2 Catalytic Conversion Tests

Catalytic conversion of carbon dioxide rich-synthesis gas was performed in a contactor membrane reactor operated in the forced pore-flow-through mode using membranes BCo1 ($Co/TiO_2/Al_2O_3$), BCo2 (similar to BCo1 but with increased Co loading), BCo3 ($Co\text{-}Cu/\ TiO_2/Al_2O_3$), BCo4 ($Co\text{-}Cu\text{-}K/\ TiO_2/Al_2O_3$), BCo5 ($Co\text{-}Mn/TiO_2/Al_2O_3$) and BFe1 ($Fe\text{-}Mn\text{-}Cu\text{-}K/TiO_2/Al_2O_3$) at temperatures of 180°C to 350°C and pressures ranging from 100kPa to 500kPa. Residence time was also controlled by varying the gas hourly space velocity (GHSV) of the feed gas mixture.

The effects of changes in these parameters on the conversion of reactants yield of products, and selectivity to linear alcohols or straight chain hydrocarbons were also studied.

Some of the terms used in measuring the performance of these membranes, and which would often be referred to in this section, are defined below:

Conversion of component i, X_i is the amount of component i that has reacted in the reactor to form products,

$$X_i = \frac{\text{concentration of component i in the feed - concentration of component i in the products}}{\text{concentration of component i in the feed}}$$

(4.10)

Selectivity S, is defined as the molar concentration of reactants converted that has reacted to produce a particular product. Therefore selectivity of component i,

$$S_i = \frac{\text{Moles of component i produced}}{\text{Moles of CO in inlet - moles of CO in outlet}} \quad (4.11)$$

and $S_j = 1 - \sum_{i=1}^{n} S_i$ (4.12)

where S_j is the selectivity of any other species produced during the reaction, and both S_i and S_j are calculated based on the concentration of CO in the feed alone. It is known that some CO might be formed from the reverse water-gas shift reaction, but the thermodynamics of the reaction is not favoured by the prevailing reaction conditions.

Yield of a particular product Y_i, is the fractional conversion of the reactants to that product. In other words, yield is the ratio of the moles of a particular product formed to the theoretical moles of that product that could be formed from the moles of the reactant consumed.

$$Y_i = \frac{\text{molar concentration of a particular product}}{\text{molar concentration of CO/CO}_2\text{ in the feed}} \times \left(\frac{\text{number of carbon atoms in the product}}{\text{number of carbon atoms in the feed}} \right)$$

(4.13)

Usage Ratio (UR) of hydrogen to carbon monoxide is the rate at which hydrogen is consumed relative to the rate at which carbon monoxide is being consumed.

If UR equals 2, the water-gas shift reaction does not occur [Clark & Walker, 2000]. If all the water formed in the FT reaction is consumed in the water-gas shift reaction, then the overall UR would be 0.5. Therefore, the exit H2/CO ratio in the FTS can be lower or

higher than the initial syngas ratio at the inlet of the reactor, depending on whether the initial syngas ratio is higher or lower than the usage ratio [Govender *et al*., 2006].

Synthesis rate r, normalized to the total catalyst content for an ideal differential reactor is defined as:

$$r_A = \left(\frac{X}{W/F_{A0}} \right) \left[\frac{mole}{g_{cat}.h} \right] \tag{4.14}$$

where W is the weight of the catalyst (g) and F_{A0} is the feed flow rate (moles/hour).

The extent of the water-gas shift reaction **WGS extent** can be calculated as:

Mole% CO_2 / mole% (CO_2 + H_2O)

4.3.1 Cobalt –Titania/alumina Membranes

Two of the prepared membranes consisted only of cobalt and the titania-washcoated alumina support. Membrane BCo1 contained 1.14g of cobalt whilst membrane BCo2 had 3.265g of cobalt. Catalytic performance of these membranes was measured in terms of the conversion of the reactants, yield of products, selectivities, and usage ratios. The results showed that the performance was affected by both the catalyst loading and the operating parameters. The operating parameters measured were temperature, partial and total pressure, and the gas hourly space velocity (GHSV). The effect of GHSV could be explained by the fact that FTS is a polymerization reaction that yields a wide spectrum of products. The type of product obtained from the consecutive reactions involved depends therefore on how long a reacting species spends within the reactor.

4.3.1.1 Performance of cobalt-titania membranes

Figure 4.9 shows the conversion CO, CO_2 and H_2 in membrane BCO1 at a total pressure of 200KPa, temperature of 220°C and a feed flow rate of $1624h^{-1}$.

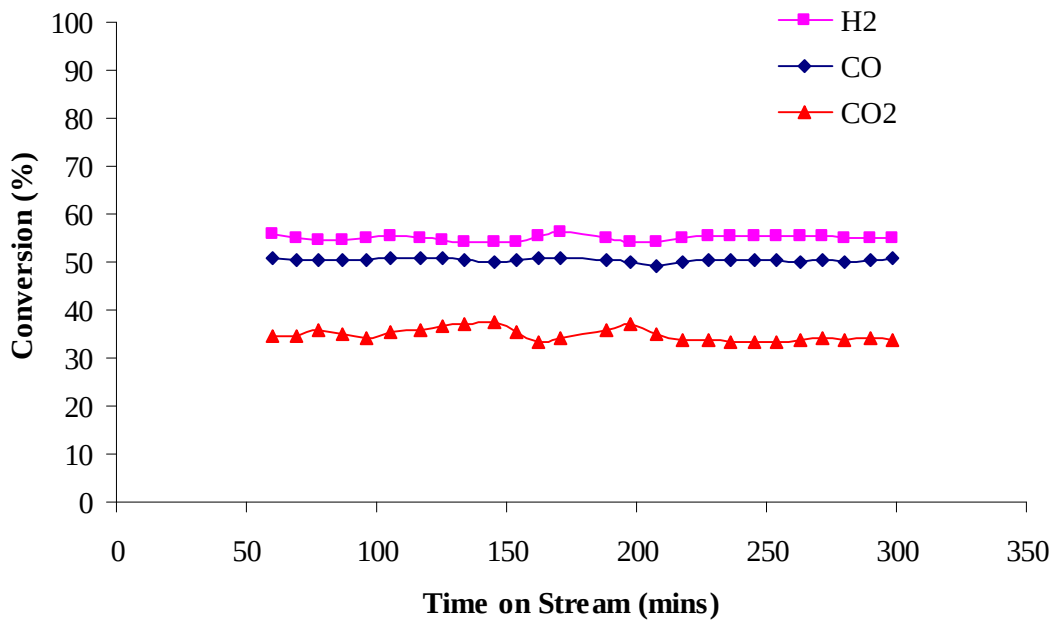

Figure 4.9: Syngas conversion on Membrane BCo1 (T = 210°C, P = 200kPa)

The relative stability of the conversion over the time on stream demonstrates another advantage of using a membrane reactor operated in the forced pore-flow-through mode. Most researchers observed that equilibrium was only attained for FTS in other types of reactors after up to 10 hours of operation [Zennaro *et al*., 2000], but van de Loosdrecht *et al*. [1997] showed that their cobalt catalysts derived from different precursors and supported on alumina demonstrated similar stability in the 7h tests in a micro-flow quartz reactor, albeit at very low conversions.

On membrane BCo2 under similar conditions, the average conversion increased by 74%, 36% and 28% for CO_2, CO and H_2 respectively, as shown in figure 4.10.

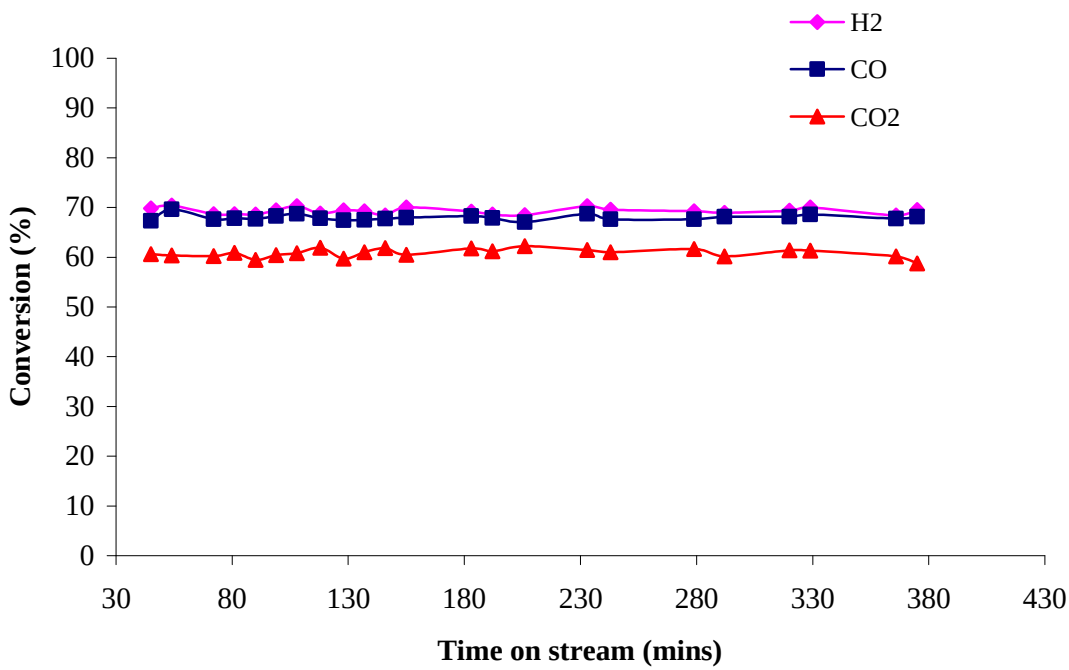

Figure 4.10: Syngas conversion on Membrane BCo2 (T = 210°C, P = 200kPa)

This means that an increase in catalyst loading availed the reactants of more active sites and thereby increased conversion accordingly. Again, the conversion remained relatively stable over the entire duration of the experiment, although there seemed to be a slight decrease after six hours.

The productivities of membranes BCo1 and BCo2 with respect to liquid production were observed to be 140mg/gcat.h and 61mg/gcat.h respectively, while the selectivity to methane was 16% and 26% respectively. This is in agreement with the findings of Davis [2003] who observed that when an iron catalyst is operated at lower conversion levels, the catalyst provides a higher CO conversion per unit weight of catalyst, and that a higher fraction of CO converted goes to desirable products rather than producing excess H_2 and CO_2. The usage ratio for membrane BCo1 was 2, which confirmed the absence of the water-gas shift reaction but for Membrane BCo2, UR was found to be 2.3. This means

that either excess hydrogen was produced which would be unlikely in this case because of the presence of CO_2 in the feed, or more CO was being converted to methane. Figure 4.11 shows that selectivity to methane increases with increase in conversion.

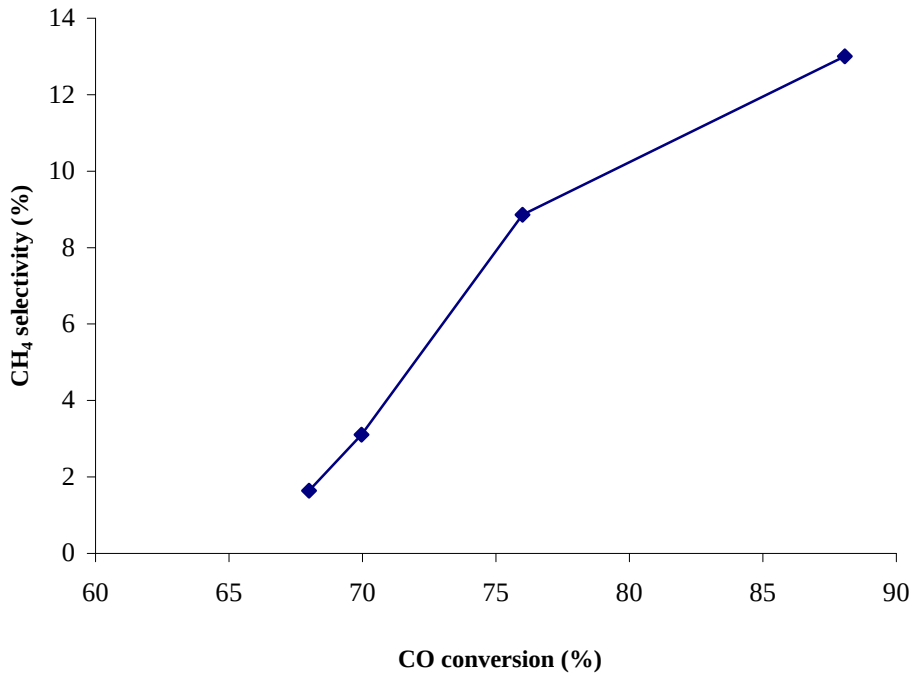

Figure 4.11: Variation of methane selectivity with CO conversion on Membrane BCo2 (P=200kPa, GHSV=1642h^{-1})

Raje *et al*. [1997] agreed that the CO conversion per pass of a low temperature Fischer-Tropsch reactor must be limited, since at high CO conversion the methane selectivity increases.

4.3.1.2 Effect of Temperature on Membrane Performance

The kinetics of the Fischer-Tropsch synthesis is strongly influenced by reaction temperature [Farias *et al*., 2007]. The phase behaviour of the reaction media, thermo-physical properties of the mixture (reactants and products), and the actual rates of the

various reactions that occur on the catalyst surface are all affected by the reaction temperature.

Effect on conversion and methane selectivity

Figure 4.12 demonstrates the effect of temperature on the conversion of hydrogen, carbon monoxide and carbon dioxide, and methane selectivity for membranes BCo1 and BCo2 over the temperature range studied.

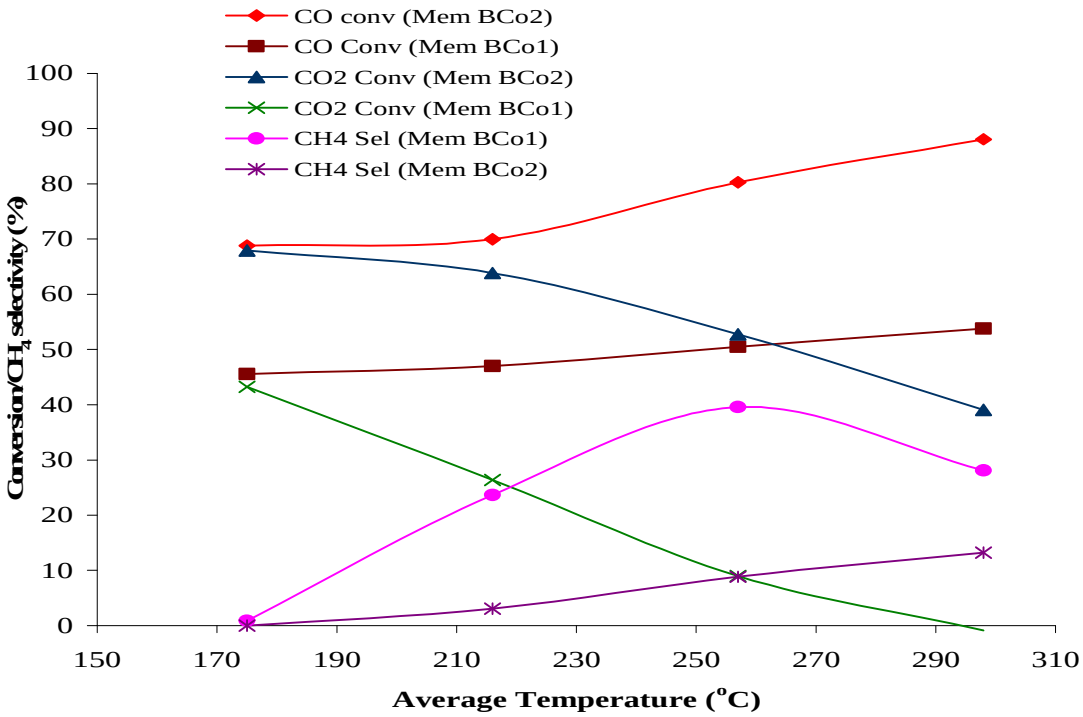

Figure 4.12: The effects of reaction temperature on conversion and methane selectivity (P = 200kPa, GHSV=1642h^{-1})

The conversion of CO showed a linear increase with increase in temperature for membrane BCo1, whereas for membrane BCo2, the linear increase was observed above 215°C. In the case of CO_2, the conversion decreased sharply with increase in temperature, up to about 300°C where CO_2 was being formed instead of being consumed. However, it could be observed that the conversion of CO_2 and CO were almost similar at about 180°C,

in agreement with Sakurai & Haruta [1995] who noticed that more CO_2 can actually be hydrogenated at low temperatures than CO on supported gold catalyst to produce methanol. Visconti *et al*., [2007] showed that cobalt-based catalysts display a steady rise in CO conversion with increasing temperature. Heranz *et al*., [2006] also reported an exponential increase for carbon monoxide hydrogenation with temperature on Fe-Mn catalysts. High methane selectivity observed with this membrane is usually associated with lower activity [Zenarro *et al*., 2000]. It is also generally admitted that the reaction rate and the production of light products are favoured by an increase in the temperature of the reaction [Roper, 1983; Bechara *et al*., 2001]. Studies had revealed that high methane selectivity over cobalt catalysts is generally attributed to the presence of unreduced cobalt oxides [Jalama *et al*., 2007]. Reuel and Bartholomew [1984] reported that cobalt oxides catalyze the water-gas shift reaction (WGS) which increases the local H_2/CO ratio near the Co metal sites, hence favouring the hydrogenation of adsorbed species leading to higher methane selectivity. On the contrary, Khodakov *et al*. [2002] reported an inverse relationship between methane selectivity and the Co reduction extent for a series of cobalt catalysts supported on mesoporous silicas with different pore sizes, arguing that higher methane selectivity could be attributed to the presence of unreduced species or small particles, rather than to the WGS reaction.

In this study, CO_2 was consumed in almost all the runs suggesting that the WGS reaction was not significant and because the macroporous structure of the support would not favour the crystallization of small cobalt particles, high methane selectivity could only have resulted from the presence of unreduced cobalt oxides.

The observed decrease in the conversion of CO_2 whilst methane selectivity was increasing seemed to contradict the view that CO_2 hydrogenation leads mostly to methane

formation [Akin *et al*., 2002; Visconti *et al*., 2009]. Instead, there seems to be competitive adsorption of both CO and CO_2 on Co active sites, the conversion following different reaction pathways, with the latter producing mostly alcohols [Zhang *et al*., 2002, Kusama *et al*., 2000]. It would thus appear that CO_2 did not only enter the reaction mechanism network at the termination stage as is sometimes reported [Dry, 1996]. Visconti *et al*. [2009] concluded that in the presence of CO, CO_2 has no effect on the reaction, i.e. it acts an inert gas, ascribing it to the competitive adsorption of CO on the catalyst free sites, in particular CO coordination over cobalt sites which hinders CO_2 molecular adsorption and inhibits its activity. This however, does not seem to explain the conversion of both CO and CO_2 recorded in this work.

A pathway that would account for chain initiation by both CO and CO_2 could be proposed based on non dissociative adsorption of CO and hydrogen assisted dissociation of the formyl species (or formate when CO_2 is present) to yield the enolic species responsible for the formation of alcohols, and the alkenyl species responsible for the formation of parrafins as shown in Figure 4.13. This mechanism shows some features of both the carbene and the hydroxycarbene mechanisms and accounts for the formation of hydrocarbons and alcohols.

INITIATION

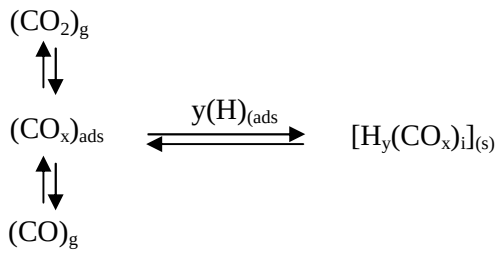

PROPAGATION AND TERMINATIONS

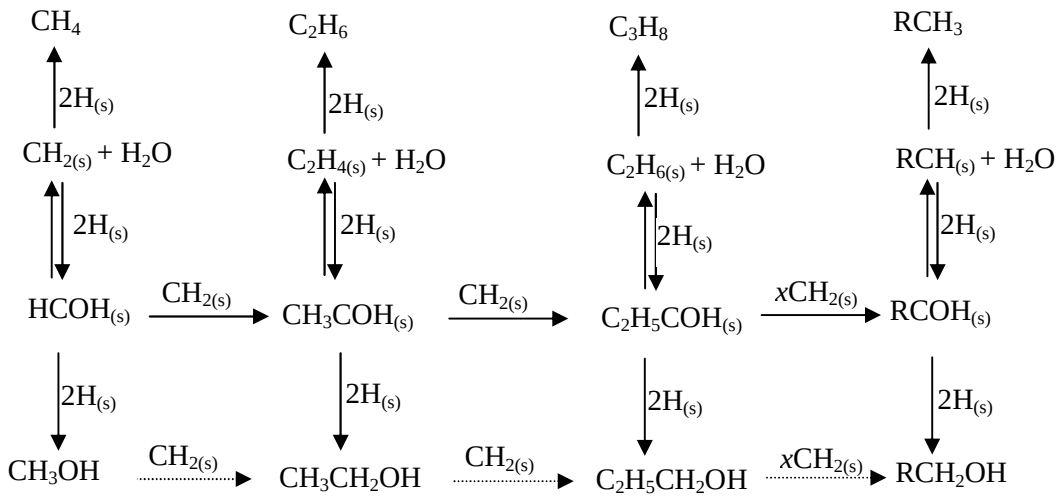

Figure 4.13: Proposed pathway for FTS showing chain initiation by both CO and CO_2

Surface species are shown with the subscript (s) and the possibility of alcohols homologation is shown with broken arrows.

The proposed mechanism appears to be in excellent agreement with the observation made by Blanchard *et al.* [1989], Calverly & Smith, 1992; Zhang *et al.* [2002], Subramani & Gangwal [2008], and supported by evidence in a recent work by Davis [2009] using iron catalysts.

Strong metal-support interaction (SMSI) as was exhibited by the cobalt-titania membrane catalyst is also known to increase the selectivity of liquid products, whilst depressing the yield of methane [Kim, 1993; Borodko & Somorjai, 1999].

In the absence of the water-gas shift and CO_2-forming reactions (because of the large amount of CO_2 in the reactant stream), the stoichiometry of this synthesis is thought to be based on the following reactions:

$$n\mathrm{CO} + (2n+1)\,\mathrm{H_2} \longrightarrow \mathrm{C_nH_{2n+2}} + n\mathrm{H_2O} \qquad (4.15)$$

$$n\mathrm{CO} + 2n\mathrm{H_2} \longrightarrow \mathrm{C_nH_{2n+1}OH} + (n-1)\mathrm{H_2O} \qquad (4.16)$$

$$\mathrm{CO} + 3\mathrm{H_2} \longrightarrow \mathrm{CH_4} + \mathrm{H_2O} \qquad (4.17)$$

$$n\mathrm{CO_2} + 3n\mathrm{H_2} \longrightarrow \mathrm{C_nH_{2n+1}OH} + (2n-1)\mathrm{H_2O} \qquad (4.18)$$

This would make the overall reaction scheme based on carbon balance to look like:

$$(2n+1)\mathrm{CO} + n\mathrm{CO_2} + (7n+4)\mathrm{H_2} \longrightarrow \mathrm{C_nH_{2n+2}} + 2\mathrm{C_nH_{2n+1}OH} + \mathrm{CH_4} + (3n-1)\mathrm{H_2O} \qquad (4.19)$$

Equation 4.15 would perhaps give an insight into our explanation for the reason why the prevalence of alcohols over hydrocarbons is observed, because for every mole of paraffin (other than methane) produced; two moles of alcohols are formed. It would also suggest that the stoichiometric requirement for hydrogen was not met in the syngas mixture of 6:3:1 (H_2:CO:CO_2) that was used. Both the proposed mechanism and the stoichiometric reactions indicate that for every mole of (CH_2) formed, one mole of water is produced and account for the observed large quantity of water observed in the condensed products. For example, at n =1, equation 4.15 gives,

$$\mathrm{CO} + \tfrac{1}{2}\mathrm{CO_2} + 5\tfrac{1}{2}\mathrm{H_2} \longrightarrow \mathrm{CH_4} + \mathrm{CH_3OH} + \mathrm{H_2O}$$

Effect of reaction temperature on alcohols distribution

Alcohols distribution pattern was also affected by changes in reaction temperature as shown in Figure 4.14.

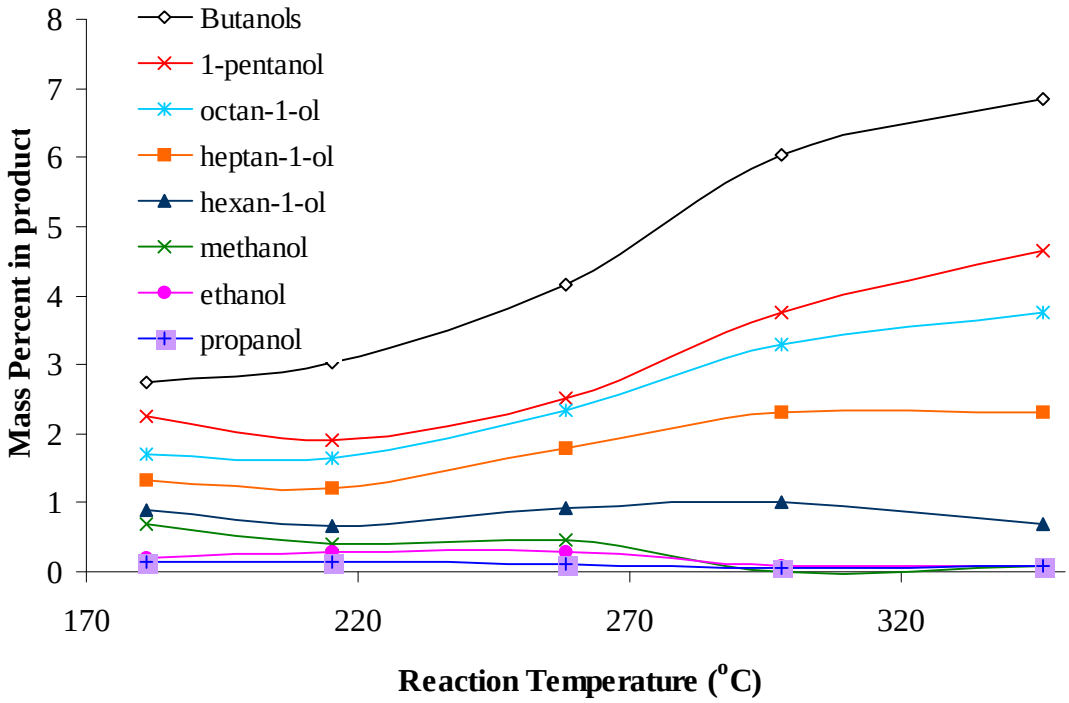

Figure 4.14: Effect of temperature on selectivity to alcohols on Membrane BCo1 (Pressure=200kPa, GHSV=1642h^{-1})

The general trend in the formation of mixed alcohols as a function of reaction temperature was observed to be in perfect agreement with those reported in the literature for different catalyst systems [Park *et al*., 1997; Qin *et al*., 2004; Mahdavi *et al*., 2005; Li *et al*., 2007; Tien-Thao *et al*., 2007a].

As temperatures increases, the selectivity to lower molecular weight alcohols tends to decrease, indicating a possible increase in homologation reactions to form higher alcohols [Matsuzaki *et al*., 1997]. Koizumi *et al*., [2004] observed in their work that methanol space time yield (STY) and selectivity increased with increasing temperature at 5.1MPa

up to a temperature of 320°C and then dropped to a constant value. However, Figure 4.14 shows a steady decline up to 270°C when it finally dropped to a constant value. Nunan *et al*., [1989] performed a ^{13}C-NMR study of the $C_2 - C_4$ alcohol products and showed that lower alcohols were incorporated into the synthesis to form higher alcohols, which resulted in the observed decrease in selectivity of lower molecular weight alcohols with increase in higher alcohols formation. This is in agreement with the earlier observed drop in methane activity at temperatures above 260°C.

Both n-butanol and iso-butanol were produced and together formed the most dominant products. This observation is typical of high temperature higher alcohols synthesis using zinc chromite-type catalysts [Herman, 2000]. Most alcohol synthesis processes report the formation of more methanol, which makes them not too suitable as octane enhancers until methanol distillation is effected [Subramani & Gangwal, 2008]. Therefore this process is superior because of low methanol concentration in the product mixture, which requires only dehydration to make it useful in internal combustion engines either as stand-alone fuels or as octane number boosters. More information relating to alcohols synthesis in general and homologation of lower alcohols is available in Appendix B.

Effect of reaction temperature on hydrocarbon/alcohol selectivity

The effect of temperature on the ratio of condensed alcohols to hydrocarbons is shown in Figure 4.15.

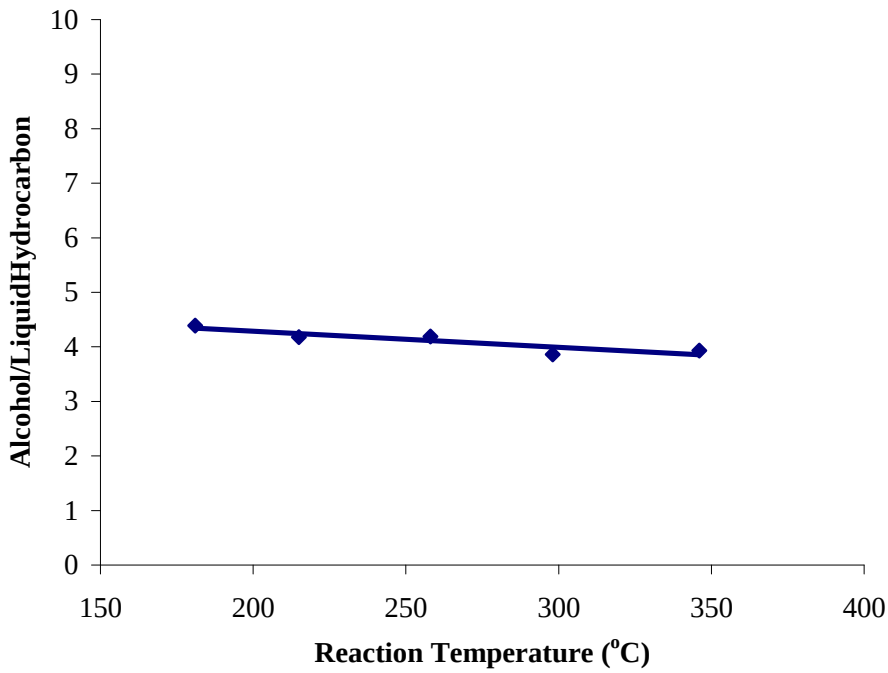

Figure 4.15: Effect of temperature on alcohol/liquid hydrocarbon ratio on membrane BCo1 (Pressure=200kPa

It could be seen that as temperature increased, alcohol selectivity in the condensed products decreased, a trend similar to that reported by Jiang *et al*., [2001] over Zn-Cr-K catalyst. Fang *et al*. [2009] also reported that the selectivity of alcohols in their work reached a high level at lower temperatures than 300°C. However, Chu *et al*. [1995] observed that with cobalt-promoted $CuLa_2Zr_2O_7$ catalysts, both alcohol and hydrocarbon yields increased with the reaction temperature, but with better alcohol selectivity. They concluded that the selectivity to hydrocarbons decreased with rising reaction temperature. Initially, cobalt-based FTS catalysts were used for the production of higher hydrocarbons, but not for the formation of oxygenates [Anderson, 1984]. It was reported that highly dispersed cobalt supported on silica with noble metals, such as, Ir, Ru, Rh and Pt was also active in the formation of C_2 oxygenates during CO hydrogenation [Hamada *et al*., 1984; Matsuzaki *et al*., 1996]. In this work however, alcohols were the dominant product from the hydrogenation of CO and CO_2 over membrane BCo1, produced only from

alumina/titania-supported cobalt, an observation which could be attributed to a number of factors, which include:

- the SMSI effect of the titania washcoat,
- high dispersion of the catalyst in the membrane arising from the large pore size of the support and the catalyst impregnation technique employed,
- the presence of both metallic and oxidic cobalt within the membrane because of low reduction temperatures,
- the presence of CO_2 in the feed which largely favours methanol formation, and
- the mechanism of the reaction within the membrane as proposed above.

Figure 4.16 shows total alcohols to total condensed hydrocarbons. It is observed that mixed alcohols formed over 80% of all organic products obtained over the temperature range studied.

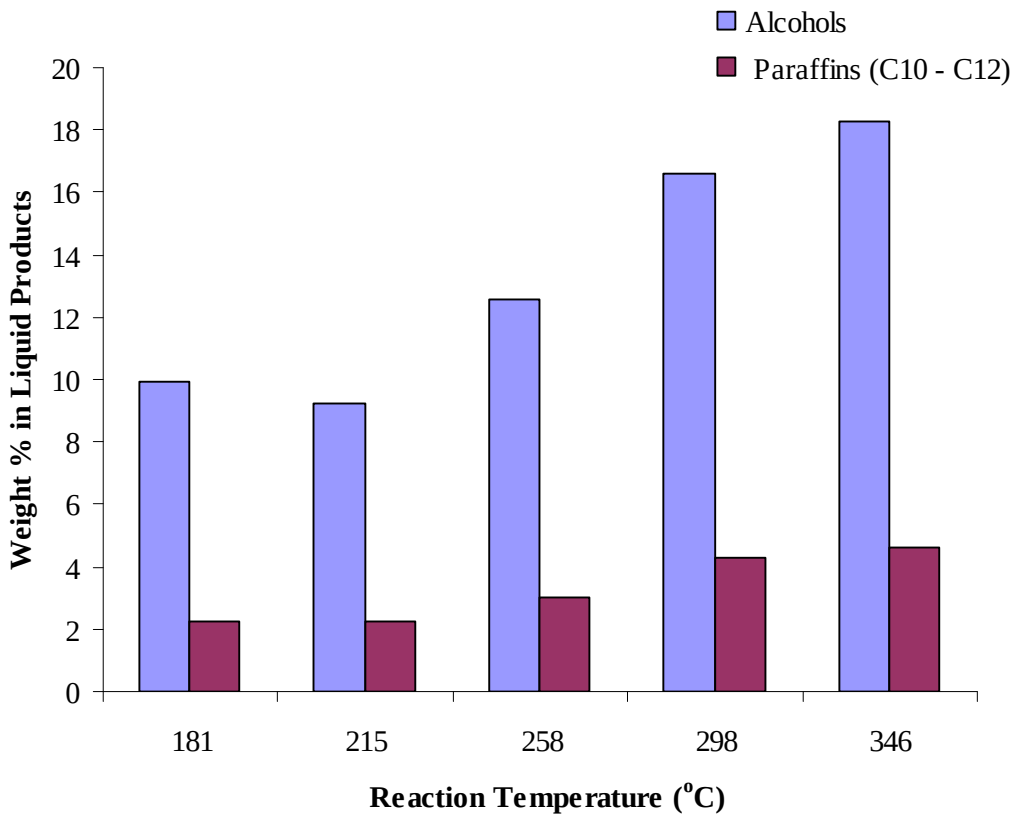

Figure 4.16: Effects of temperature on mixed alcohols/hydrocarbon production on membrane BCo1 (P=200kPa, GHSV=1642h^{-1})

Minahan *et al*. [2004] noted that reaction rates are not dramatically increased by increased temperatures, rather the product distribution between methanol/higher alcohols and hydrocarbons is shifted; pointing out that increasing temperature to 440°C cuts the total alcohol selectivity and the methanol rate in half and almost triples hydrocarbon rate.

Effect of reaction temperature on space-time yield

The effect of temperature on space-time yield of alcohols is illustrated in Figure 4.17.

The space-time yield of alcohols mirrors that of CO conversion; that is, the higher the conversion the lower the alcohols production. As the temperature increases with subsequent increase in conversion, more paraffins are produced relative to alcohols. This

was particularly so for membrane BCo2 where CO conversions rose to as high as 88% at 300°C and 200kPa, and the ratio of alcohols to hydrocarbons dropped dramatically to about 0.1.

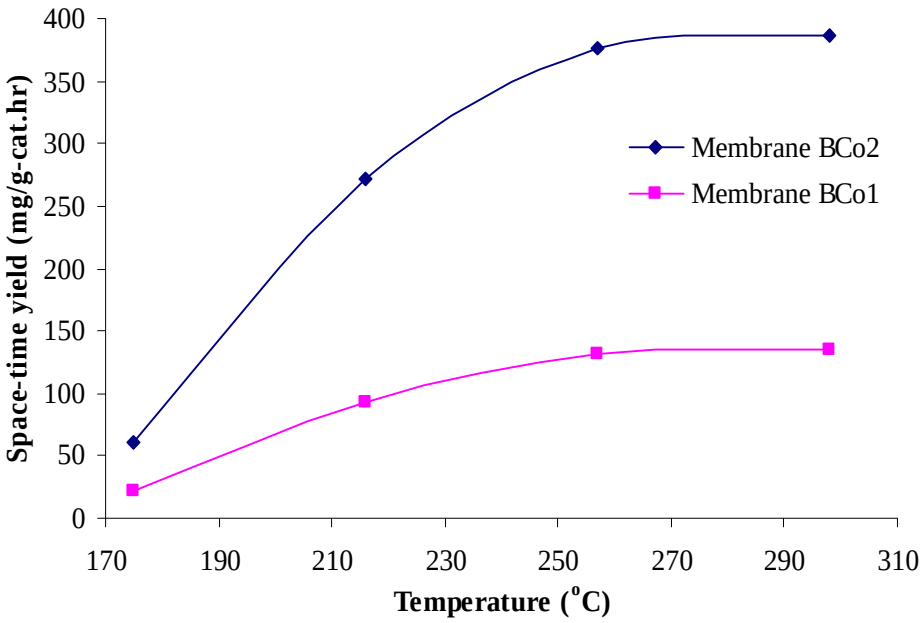

Figure 4.17: Effect of temperature on space-time yield of alcohols (P = 200kPa, GHSV=1642h^{-1})

It was observed that the space-time yields of total liquid products for both membranes BCo1 and BCo2 as well as the composition of the products varied with increase in temperature. Increasing catalyst loading by a factor of 2.86 gave a corresponding increase by a factor of 2.88 in the space-time yield at 300°C, except that selectivities of the products shifted in favour of hydrocarbons. It could therefore be concluded that low catalyst loading (membrane BCo1) favoured the production of alcohols while higher catalyst loadings enhanced the formation of paraffins; an observation which might be

caused by the level of dispersion of the catalyst, as confirmed by the SEM micrographs for the two membranes.

4.3.1.3 Non Anderson-Schulz-Flory (ASF) distribution of products

Typical non-ASF behaviour for the distribution of products from the cobalt-based membranes used in this work is shown in Figure 4.18. This suggests that different processes such as CO and CH_2 insertion, hydrogenation (as indicated in the reaction mechanism), alcohol homologation, and even hydroformylation could have been involved in the synthesis.

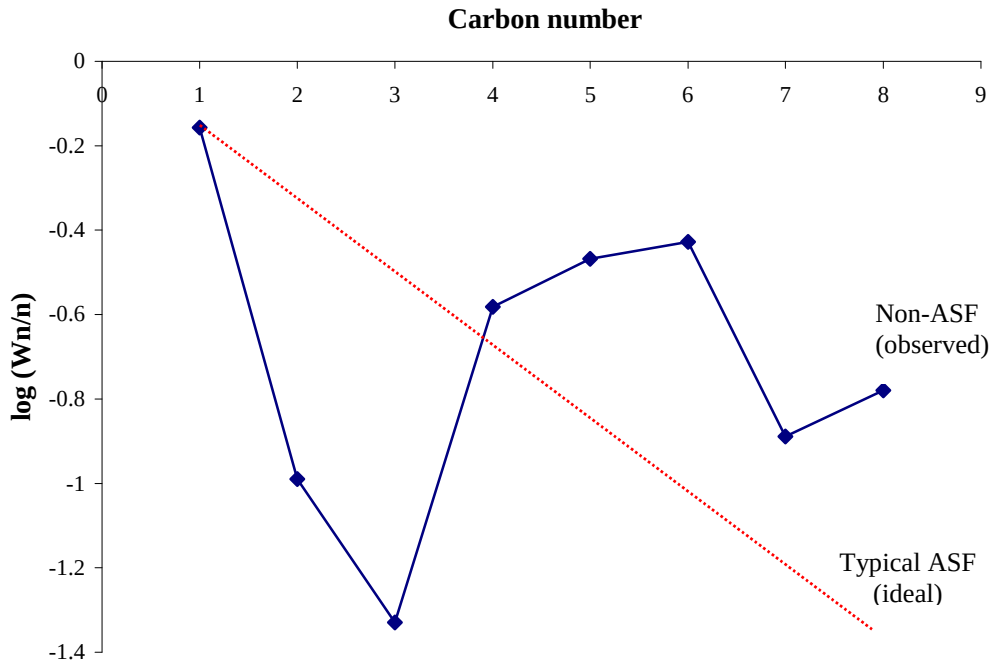

Figure 4.18: Non-ASF Distribution of Alcohols on membrane BCo1 (P=200kPa, T=210°C, GHSV=1642h^{-1})

Neither the alcohol nor hydrocarbon products condensed in the cold trap followed the Anderson-Schulz-Flory (ASF) distribution, which may be indicative of the interplay of chain-length-dependent reinsertion and hydrogenolysis as reported by Kuipers *et al*.

[1996] for Co/SiO_2 catalysts. In a Fischer-Tropsch reaction over a Co/Nb_2O_5 catalyst in a fixed bed reactor, the hydrocarbon product distributions that were experimentally determined were reported by Ahon *et al*. [2006] to exhibit an unusual behaviour. Snel [1988] also observed deviations from an Anderson-Schulz-Flory distribution for the product of the Fischer-Tropsch synthesis. The catalyst was a complex-derived iron-calcium catalyst promoted with caesium sulphate and therefore, neither carrier acidity nor shape selectivity could explain the deviations. ASF and non-ASF chain length distributions were obtained for thin washcoats in $CoRe/Al_2O_3$ monolithic catalysts tested in the Fischer-Tropsch synthesis in a temperature window (180-225 °C) under synthesis gas compositions ranging from stoichiometrically excess carbon monoxide to excess hydrogen (H_2/CO = 1-3) [Kapteijn *et al*., 2005].

Cu-based higher alcohols synthesis catalysts show non-ASF distribution of products because the reaction is believed to proceed by a combination of hydrogenation and carbon-carbon bond formation via aldol condensation [Epling *et al*., 1997].

A similar non-ASF product distribution pattern for alcohols was observed in a recent work by Dong *et al*., [2009] for syngas conversion to higher alcohols over nanotube-supported Co-Cu catalyst.

4.3.1.4 Effect of syngas feed rate on membrane performance.

The effect of variation of syngas flow rate on conversion, space-time yield and selectivity of membrane BCo1 to liquid products, alcohols, $C_{10} - C_{12}$ hydrocarbons and methane is shown in Table 4.3. The data was obtained on membrane BCo1 at a pressure of 200KPa and temperature of 210°C.

Table 4.3: The effect of GHSV on membrane performance

GHSV (h^{-1})	CO conversion (%)	CO_2 conversion (%)	STY (mg/gcat.h)	Selectivity (%)			
				$S_{Liquids}$	S_{Alc}	S_{HC}	S_{CH4}
912	29.07	12.30	180.12	76.76	11.1	3.18	23.24
1642	50.44	34.78	253.33	84.0	11.5	2.21	16.0
2280	73.95	68.98	152.05	97.11	16.6	4.39	2.89
2736	41.57	38.49	145.60	97.02	29.0	6.64	2.98
3192	21.34	14.45	112.30	97.98	22.6	5.50	2.02

Increase in the rate of syngas feed (GHSV) resulted in a decreased contact time, but it was observed that the conversion of both CO and CO_2 increased for low gas flow rates until it reached a maximum of 73.95% and 68.98% for both gases respectively at an equivalent feed flow rate of 250ml/min after which the conversion decreased with increasing feed rate. The latter observation is in agreement with the findings of Mahdavi *et al*. [2005]. Tien-Thao *et al*. [2007a] also reported a gradual decline in CO conversion with increased space velocity, but noted that although hydrocarbon productivity decreased, alcohols production reached a maximum of about 140mg/g-cat/h at GHSV = 12,000–15,000h^{-1} in a continuous flow fixed-bed micro-reactor using nano-sized $LaCO_{0.7}Cu_{0.3}O_3$ perovskite catalysts. In this work however, the productivity of the membrane or space-time yield of total products was a maximum at 1642h^{-1}, conversion at 2280h^{-1} but the selectivity to alcohols reached a maximum at a higher flow rate. The large pore size of the membranes placed a limitation on the feed flow rate that could be used for any meaningful conversion to take place. However, by increasing the total pressure of the system, the contact time could be controlled using the appropriate flow velocity.

Figure 4.19 is a representation of the information shown in Table 4.3 in such a way that makes it easy to deduce the optimal flow conditions for the process, with the initial

increase in conversion arising from the distribution of residence times within the membrane, while Figure 4.20 gives the selectivity of the different alcohols as a function of the contact time. The initial drop in selectivity of all products at low space velocities could be caused by the strong adsorption of alcohols on the catalyst surface to take part in side reactions, which converts such intermediates into olefins by dehydration [Campos-Martin *et al*., 1996; Tien-Thao *et al*., 2007b]. Incidentally, the cobalt carbonyl complexes or formate species present on the catalyst surface which are very active for hydroformylation of olefins at these reaction conditions [Ugo, 1983] coupled with the high hydrogen partial pressures (necessary for hydrogenation reactions) explains the complete absence of olefins in the products. The formation of higher alcohols is favoured at very high space velocities although the conversion decreased remarkably.

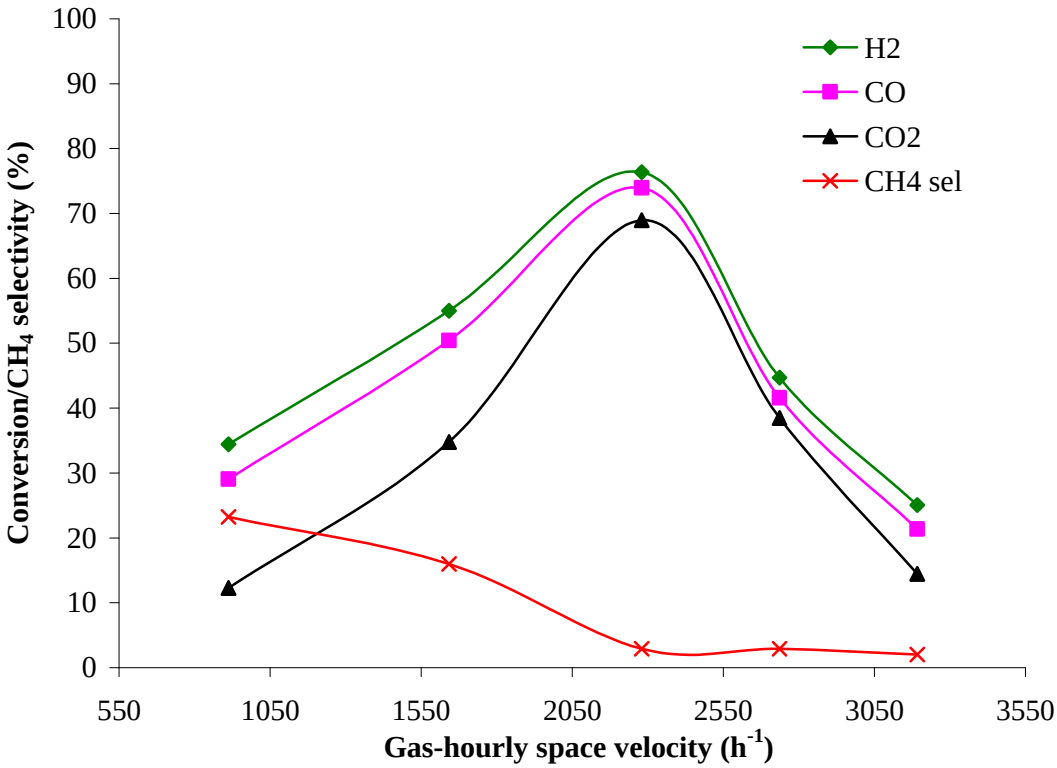

Figure 4.19: Variation of conversion with respect to contact time (GHSV) for membrane BCo1. (T=220°C, P=200kPa)

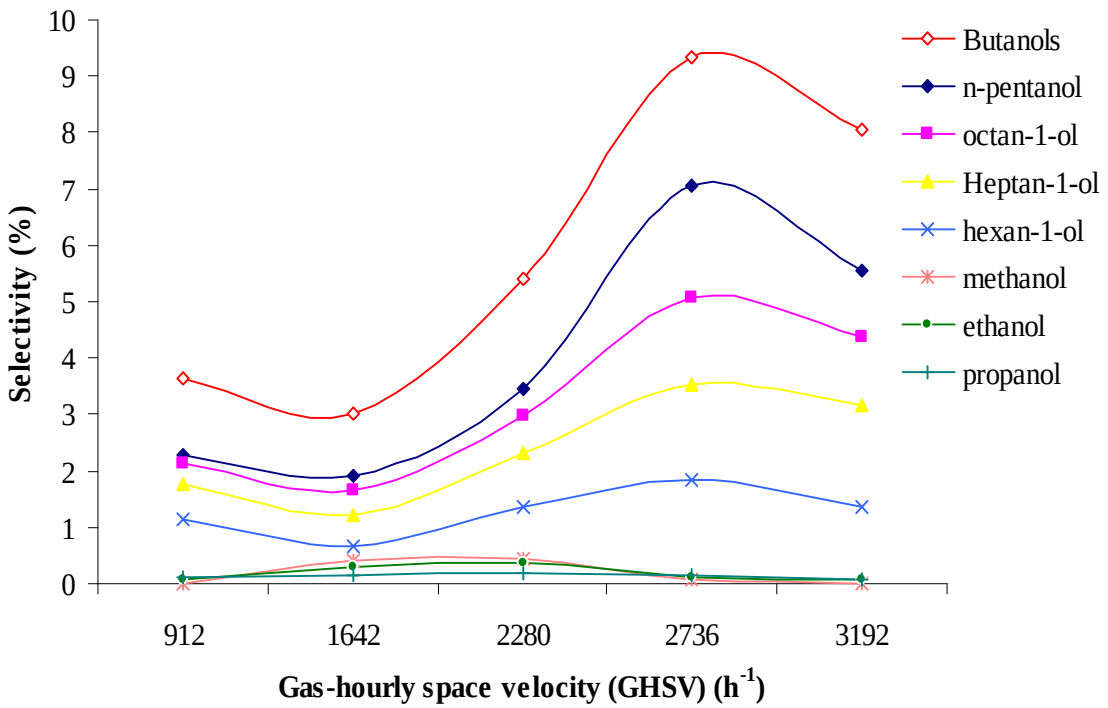

Figure 4.20: Effect of Syngas flow rate on alcohols selectivity for membrane BCo1 [T=220°C, P=200kPa].

By increasing flow rate of feed gas, selectivity to methane dropped to 3% and remained unchanged. A similar effect was observed for the alcohols to hydrocarbon ratio, which rises initially but remains constant at 4.2 for all contact times studied as shown in Figure 4.21. This conformed to observations made for higher alcohols synthesis by Mahdavi *et al*. [2005], over alumina-supported copper-cobalt-based catalysts.

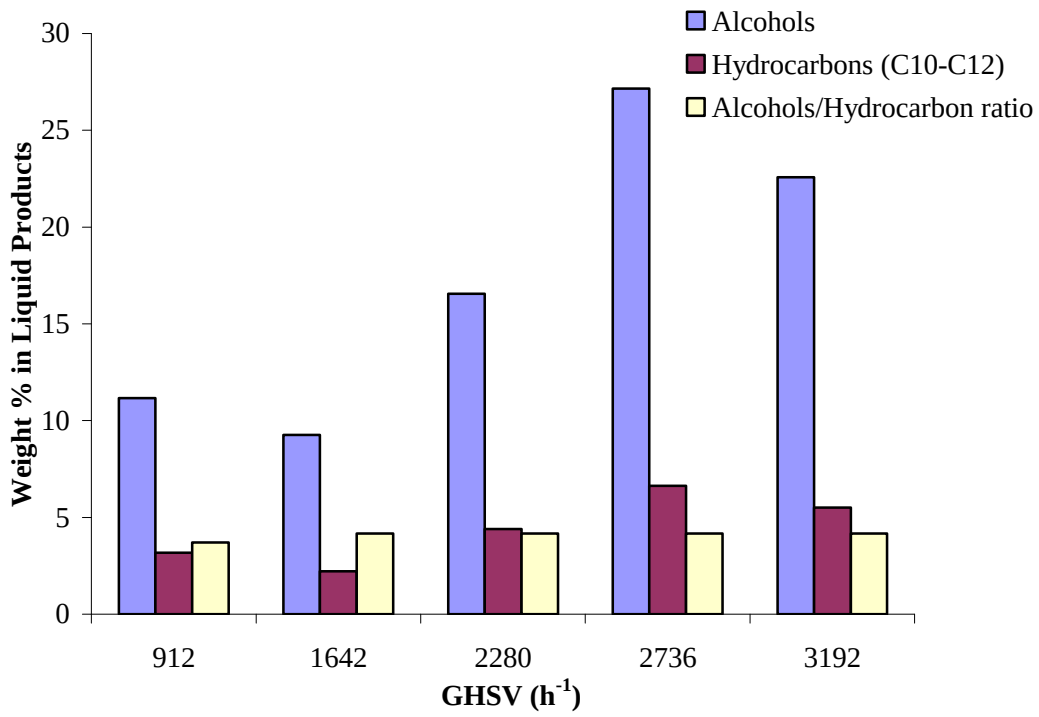

Figure 4.21: Effect of space velocity (contact time) on alcohol/liquid hydrocarbon production for membrane BCo1. (T=210°C, P=200kPa)

4.3.1.5 Effect of Pressure on membrane performance

Apart from the previously described reaction parameters, pressure remains an important factor in the hydrogenation of carbon oxides. The most important influence of the reaction pressure is the correlation with the partial pressures of the reacting species at the catalytically active centres. An increase in pressure will raise the concentration of the reactants at these active sites. These effects of total pressure on conversion of CO, CO_2 and H_2 and the selectivity to methane and alcohols, and also its effect on productivity and alcohol/hydrocarbon ratio are discussed in this section.

Effect of total pressure on conversion

For both cobalt-based membranes, the conversion of all reactants at 220°C passed through a maximum with increase in pressure as shown in Figure 4.22.

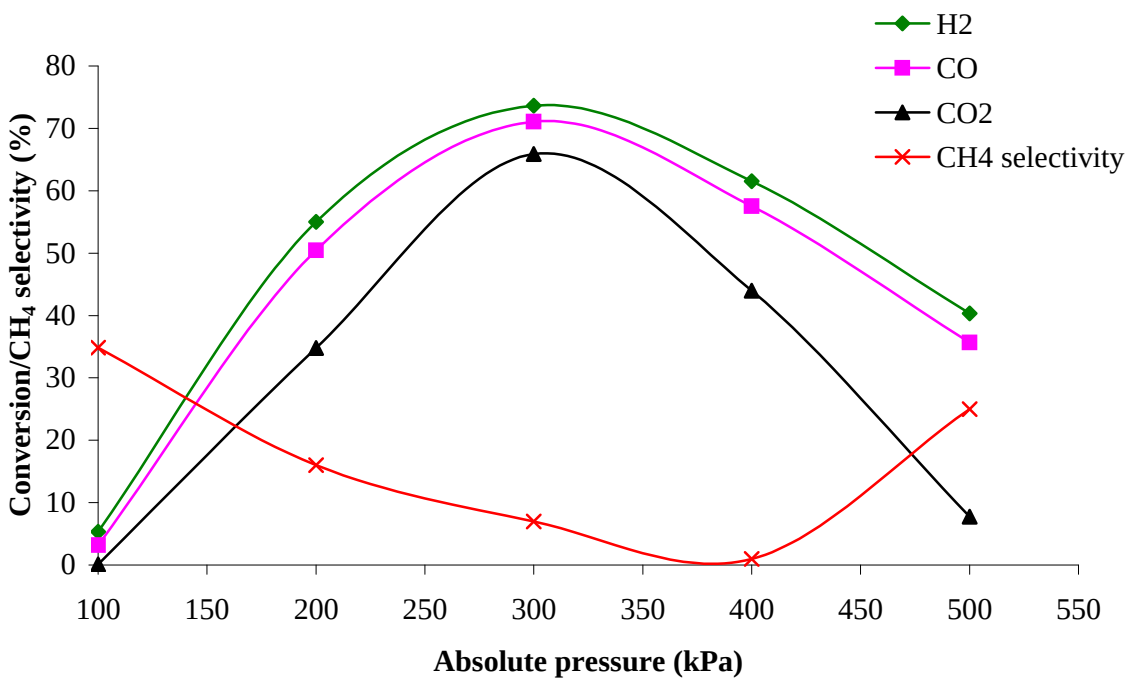

Figure 4.22: Effect of total pressure on conversion and methane selectivity of membrane BCo1 (T=220°C, GHSV=1642h^{-1})

Increase in pressure resulted in increase in density of the gas phase, which led to increase in conversion. However, with increasing pressure, multi-layer adsorption on active sites could have a slowing down effect on the conversion process. This trend as demonstrated in Figure 4.22 is totally in agreement with that observed by the originators of the process - Fischer and Pichler [1939] where they noticed that as the pressure was increased above atmospheric, the yield (and of course, conversion) increased and then decreased above 5 atmospheres. A similar observation was made in the review of synthetic liquid fuels from hydrogenation of carbon monoxide by Storch *et al*. [1948] for a cobalt-thoria-kieselguhr catalyst. They attributed the decrease to a noticeable formation of cobalt carbonyl and consequent loss of activity of the catalyst. Tien-Thao *et al*. [2007b] also reported that for the conversion of syngas to higher alcohols, a maximum conversion of syngas was

observed at about 500psi (3447.4kPa). Methane selectivity in the present work fell to zero at about 380kPa, offering a 100% selectivity to liquid products.

In Figure 4.23, there appears to be an intrinsic adjustment of the reacting system with increasing pressure to accommodate the higher rate of conversion. This is evidenced in the shift in the maximum conversion levels at different pressures and for different feed rates, although the conversion peaked at 78% and 75% for CO and CO_2 respectively, for a pressure of 300KPa at a space velocity of 2736 h^{-1}.

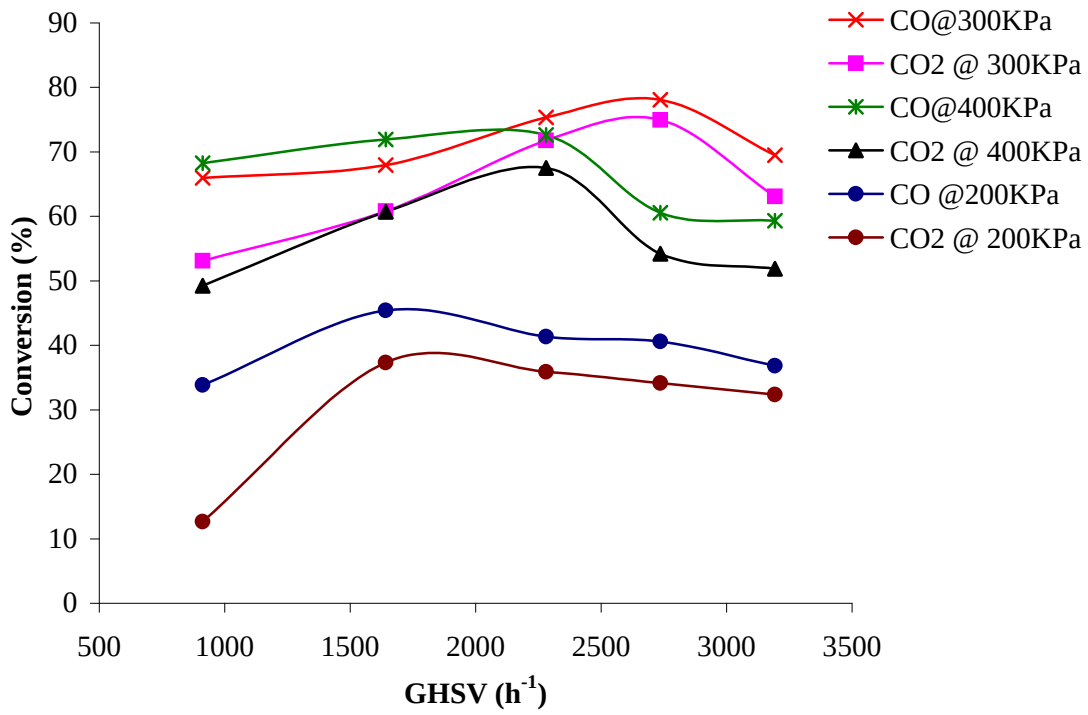

Figure 4.23: Variation of conversion with total pressure and GHSV on membrane BCo1 (T=220°C)

Effect of pressure on alcohol selectivity

As noted earlier, an increase in pressure increases the hydrodynamical residence times which apart from contributing to the observed higher conversions at increased pressures, also affect the formation of longer chain molecules. This effect is reflected in the selectivities of the different alcohols as shown in Figure 4.24.

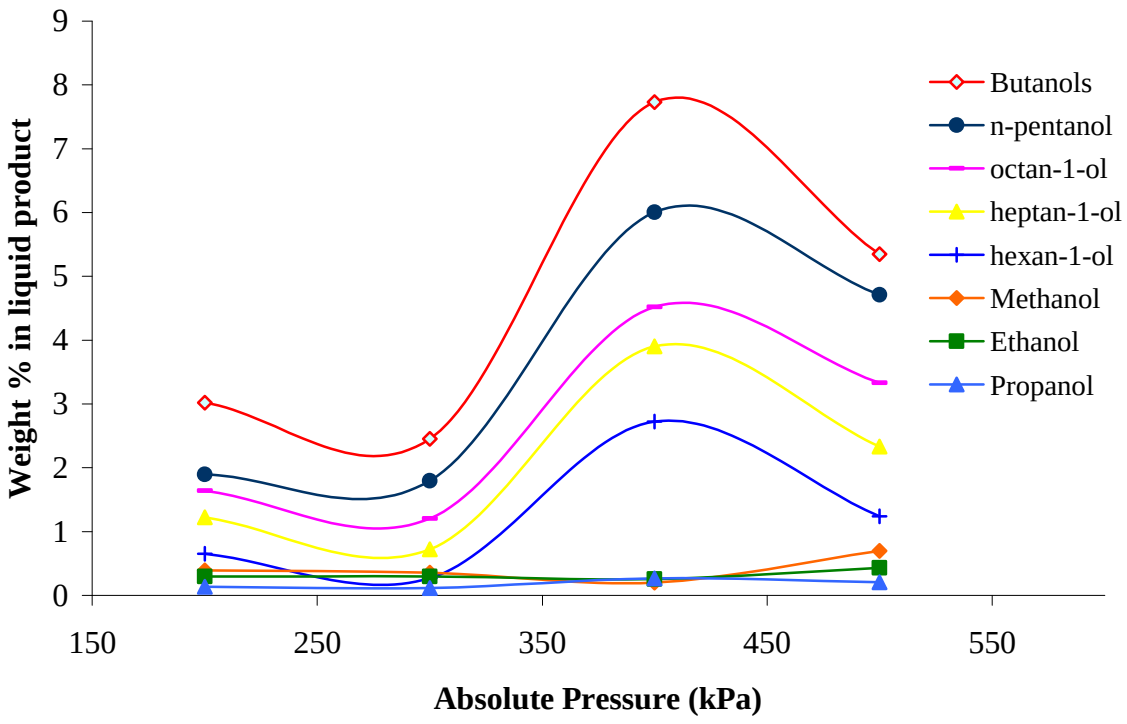

Figure 4.24: Variation of alcohol selectivity with total pressure over membrane BCo1 (T=210°C, GHSV=1642h^{-1})

According to Minahan *et al*. [2004], the thermodynamic equilibrium for methanol formation dictates that methanol concentration grows quadratically with total pressure while the concentration of higher alcohols exhibits a weaker dependence, resulting from kinetic considerations. Thus pressure does increase reaction rate, but is not an effective tool for boosting higher alcohol versus methanol production. However, hydrocarbon production is minimized at higher pressures, so that alcohol selectivity should rise.

A reaction will shift its equilibrium in the direction of volume contraction upon pressure increase. The extent of this shift will depend on the law of mass action based on the fugacity. The sum of stoichiometric coefficients amount to – 2 for the reaction to methanol, whereas this changes to – 4 for ethanol, – 6 for propanol, – 8 for butanol and – 10 for pentanol respectively [Qin *et al*, 2004]. Consequently, the equilibrium yield to

the higher alcohol is more influenced by a pressure change in comparison with the lower alcohol, as depicted by the anticlines above 400kPa in Figure 4.24.

Figure 4.25 shows the effect of pressure on alcohol-hydrocarbon production, and seems to suggest that although increase in pressure led to higher yields of both alcohols and hydrocarbons (especially at 400kPa), it had no net effect on the alcohol to hydrocarbon ratio.

Hu *et al*. [2007] however argued that for their Rh-Mn/SiO_2 catalysts operating at 300°C, alcohol selectivity was predominantly controlled by reaction temperature rather than pressure, and therefore changing reaction pressure did not cause any noticeable impact on product selectivity. Herman [2000] agreed that pressure had a positive effect on the synthesis of alcohols, but argued that the effect was only pronounced for methanol formation, noting that there was little effect on total hydrocarbon formation.

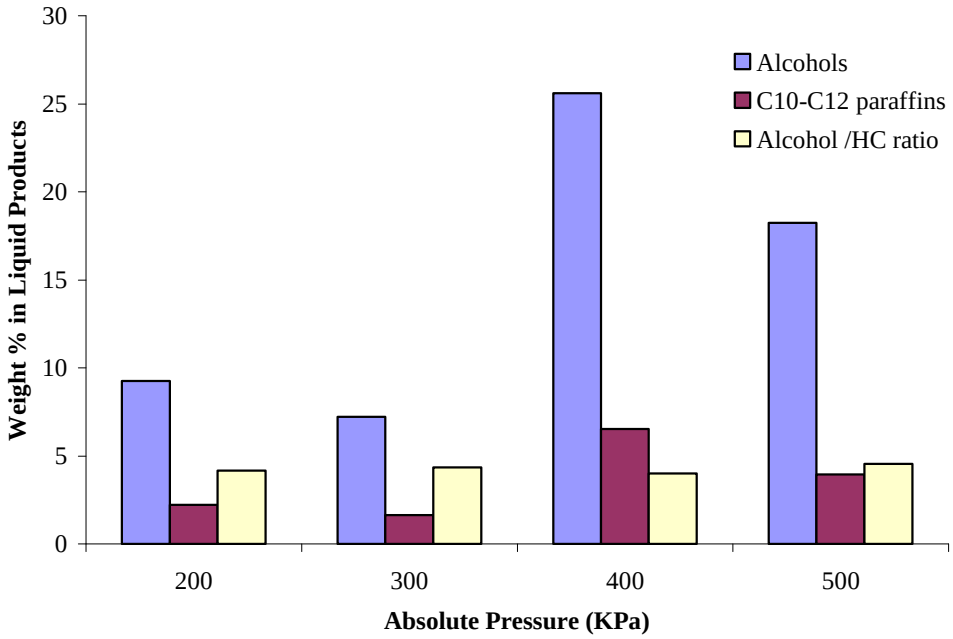

Figure 4.25: Effect of total pressure on hydrocarbon-to-alcohol ratio over membrane BCo1 (T=210°C)

Effect of total pressure on space-time yield (STY)

A study on ZrO_2/ZnO/MnO/K_2O/Pd catalyst by Vervek *et al*. [1999] showed that the application of higher pressures resulted in higher space-time yields for all products. In an attempt to develop sulphur tolerant catalysts for the synthesis of high quality transportation fuels, Koizumi *et al*. [2004] also observed that at atmospheric pressure, no alcohol was formed but at pressures of 1.1MPa and above, STY of alcohol increased with increasing pressures. These findings are in agreement with the observations made in this work, except that at atmospheric pressure, a space time yield of 14.6mg/g-cat/h was recorded, arising from a 3.16% conversion of CO at 220°C.

The plot of changes in space time yield with respect to increase in total pressure of the reaction is shown in Figure 4.26, where it observed that increase in pressure had minimal effect on STY between 200 and 400kPa. Beyond 400kPa, the increase became quite pronounced, although the selectivity to both alcohols and hydrocarbons dropped. It thus appeared that the major products at these conditions were water and methane.

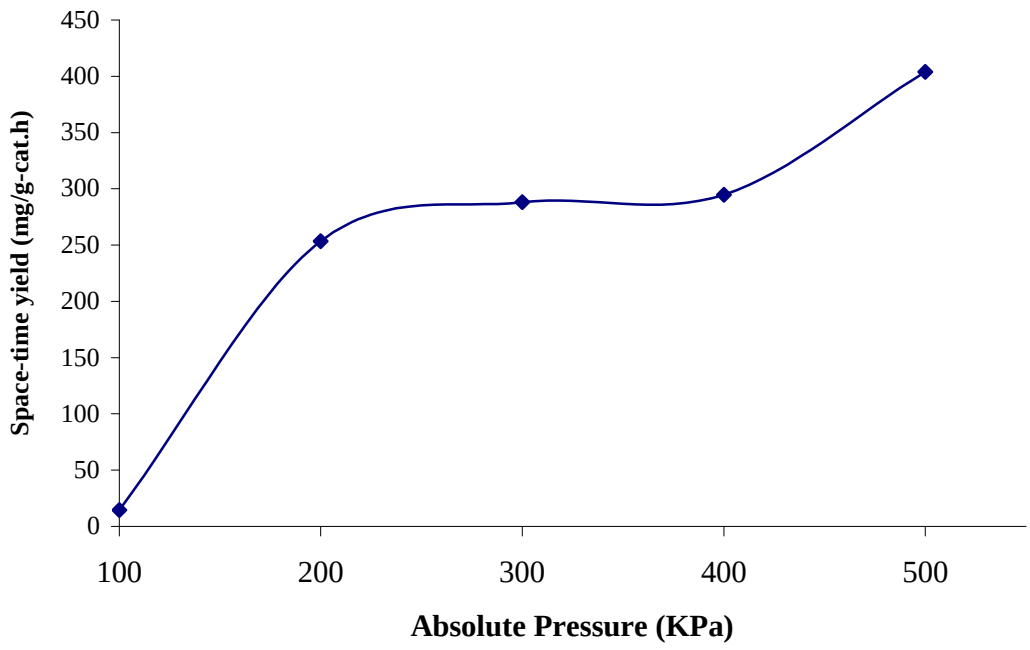

Figure 4.26: Effect of total pressure on space-time yield at 210°C over membrane BCo1. (P=200kPa).

4.3.1.6 Kinetic Analysis

The CMR was operated as a differential reactor, which implies that all reaction rates remained constant throughout the membrane thickness. In such a situation, the steady state composition of the gas phase and catalyst surface is homogeneous within the membrane. Although these conditions are normally obtained by operating a plug flow reactor at low conversions for every reactant, the small thickness of the catalyst bed (membrane), lack of both radial and axial gradients for the concentrations in the gas phase and on the surface, and the fact that all product formation reactions were irreversible as shown in the proposed mechanism, validate the assumption of differential conditions, even where the conversions were high. The rate could then be defined by equation 4.14.

The Fischer-Tropsch chemistry is often modelled by the simple power law equation:

$$-r_{CO} = kp_{H_2}^{m} p_{CO}^{n} \qquad (4.20)$$

where k is the rate constant and p_{CO} and p_{H_2} are partial pressures of CO and H_2 respectively, m is the reaction order with respect to hydrogen, and has been found to be positive (usually about 1.0) and n is the reaction order with respect to CO and usually has values between -0.1 and -0.35.

Using $m=1$, equation 4.20 could be simplified to give

$$-r_{CO} = k_o p_{CO}^n \tag{4.21}$$

where $k_o = kp_{H_2}$

Equation 4.16 can be linearized to give

$$\ln(-r_{CO}) = \ln k_o + n \ln p_{CO} \tag{4.22}$$

The reaction rate constant k_o is almost always strongly dependent on the temperature, and in some catalytic gas phase reactions on the catalyst and sometimes on the total pressure [Fogler, 2005].

A plot of the rate of consumption of CO against its partial pressure is shown in Figure 4.27. The order of the reaction obtained for CO is – *0.86* for membrane BCo1 and – 0.49 for BCo2. These reaction orders confirm the negative values proposed for cobalt catalysts by most authors [Outi *et al.*,1981; Yates & Satterfield, 1991; Zennaro *et al.*, 2000]. A better way of estimating rate constants is obtained from the analysis of the activation energy based on Arrhenius equation.

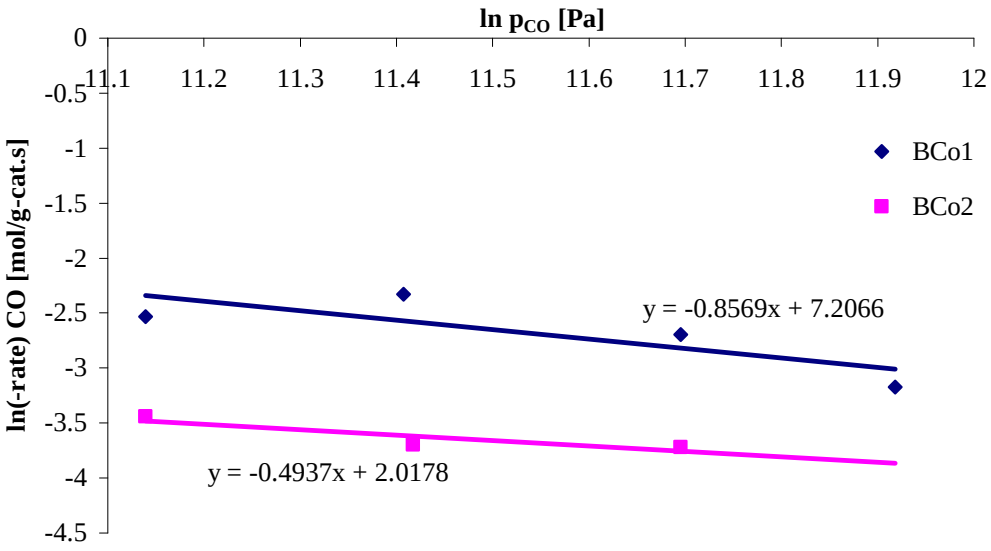

Figure 4.27: Plot of ln ($-r_{CO}$) vs ln p_{CO} (T= 489K, GHSV= 1642h^{-1})

Activation Energy

The temperature dependence of the specific reaction rate coefficient k_A of a reaction could be correlated by the Arrhenius equation, usually written as:

$$k_A = Ae^{-E_a/RT} \tag{4.22}$$

where A = pre-exponential or frequency factor

E_a = Activation energy, J/mol or cal/mol

R = Gas constant = 8.314J/mol.K (1.987cal/mol.K);

T = absolute temperature, K.

The Arrhenius equation gives the quantitative basis of the relationship between the activation energy and the rate at which a reaction proceeds. It shows that increasing the temperature or decreasing the activation energy (for example through the use of a catalyst) will result in an increase in reaction rate. It is mostly used empirically to show the

temperature behaviour of most reaction rate constants within experimental accuracy over fairly large temperature ranges.

By taking the natural logarithm, equation 4.22 becomes

$$\ln k_A = \ln A - \frac{E_a}{R}\left(\frac{1}{T}\right) \qquad (4.23)$$

So, when a reaction has a rate constant which obeys the Arrhenius equation, a plot of ln k versus 1/T gives a straight line whose slope and intercept can be used to determine E_a and the pre-exponential factor A.

A plot of the rate constant against the temperature for cobalt membrane at low conversions of CO is given in Figure 4.28.

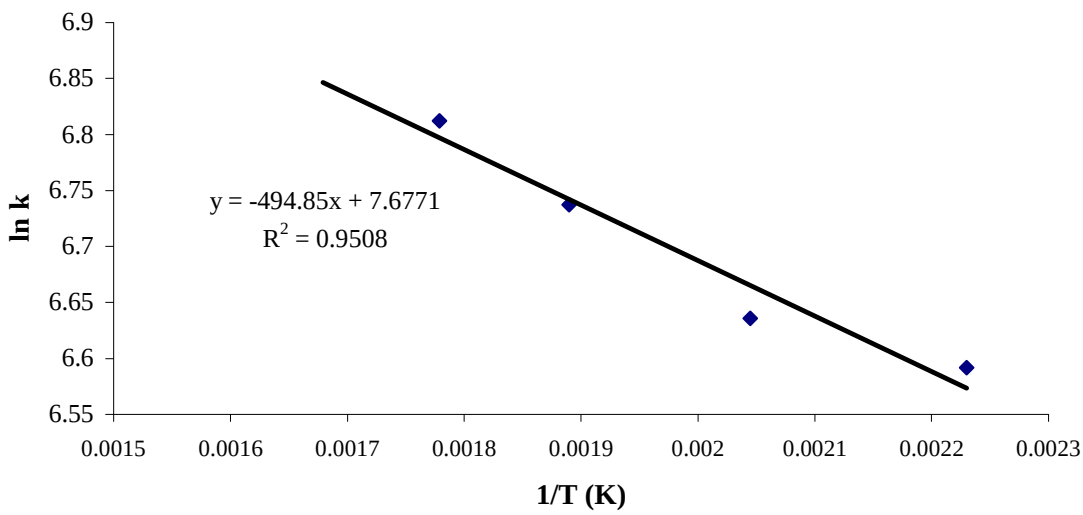

Figure 4.28: Arrhenius plot for Activation energy (P =200KPa; GHSV =1200h^{-1})

From the slope of Figure 4.28, the activation energy was evaluated as $E_a = 59.52 kJ/mol.K$; and the pre-exponential factor or frequency factor $A = 2158.35$. The value of E_a in literature is 93 – 95kJ.mol.K for cobalt catalyst [Yates & Satterfield, 1991] and

86.9kJ/mol.K for cobalt-ruthenium oxide catalyst [Irankhah *et al*., 2007]. Guettel & Turek (2009) reported that E_a could be as high as 170kJ in some reactors. It therefore implies that with the cobalt membrane used in this work the syngas conversion to products took place more readily, and the influence of temperature on the conversion was much less. This is in agreement with the observed conversion of over 45% CO at average temperatures below 180°C.

4.3.2 Cobalt-manganese/titania membranes

In these membranes, the need to increase the reaction rate per exposed metal site, (turnover frequency) created a demand for a textural promoter such as manganese. Lochner *et al*. [1986] believed that manganese oxide acts as an important structural modifier which distinctly influences the structure of a Fischer-Tropsch (FT) catalyst in bulk as well as on the crystal-lattice level. In recent times, several FT promoter elements (Pt, Re, Ru, and Mn) have been investigated. Pt and Re were reported to enhance the reducibility of the Co sites by means of H_2 spillover, and hence, to enhance the Co dispersion and led to increases in reaction rate [Vada *et al*., 1995; Jacobs *et al*., 2002]. Iglesia [1993] observed that Ru plays a role as a textural promoter for supported cobalt catalysts, increasing the activity per active site, and enhancing the regeneration of deactivated bimetallic Co-Ru catalysts. The use of Mn is reported to shift product distribution in FTS by increasing olefin and C_{5+} selectivity and decreasing the undesired production of methane [Morales *et al*., 2005; Morales *et al*., 2007]. In some other cases, manganese oxide is reported to act as a CO shift converter and catalyzes the water-gas shift reaction [Keyser *et al*., 1998; Riedel *et al*., 1999].

4.3.2.1 Performance of titania-supported cobalt-manganese membranes

The activity of the bimetallic Co-Mn is demonstrated by the results of CO and CO_2 hydrogenation shown by Membrane BCo5. Figure 4.29 shows the variation of conversion and methane selectivity with respect to syngas flow rate.

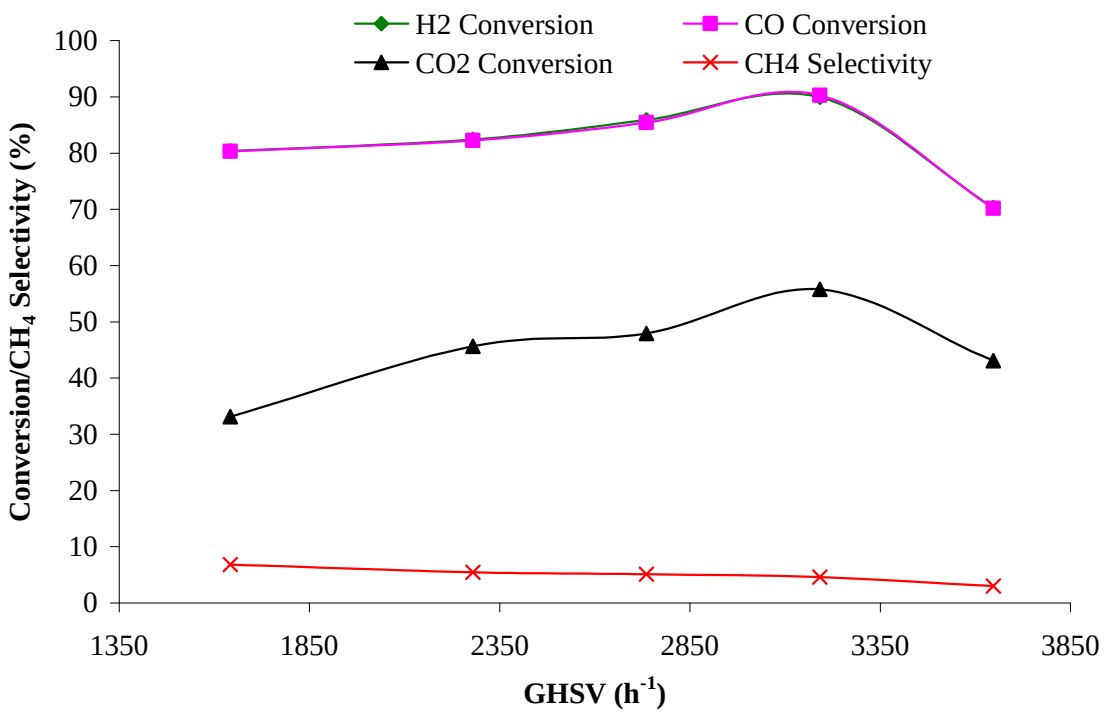

Figure 4.29: Variation of catalytic activity of Co-Mn membrane (BCo5) with syngas flow rate (T=490K; P=300KPa)

The result showed that the Co-Mn membrane exhibited the highest activity, giving a maximum of 90% conversion of CO, as compared to 78% CO conversion with the unpromoted cobalt membrane. However, there was a 25% drop in CO_2 conversion, an indication that the membrane might have shown WGS activity [Gottschalk *et al*., 1988; Keyser *et al*., 1998]. This is a very significant observation because an increase in WGS activity of cobalt would automatically make it a useful candidate for Fischer-Tropsch synthesis of low H_2:CO ratio syngas feedstock, such as those obtained from coal and

biomass gasification. Figure 4.29 also confirmed the role of MnO-promotion in suppressing methane formation, a behaviour Morales *et al* [2005] attributed to a reduction in hydrogenation activity of growing alkyl chains during FTS.

The space-time yields did not however show tremendous improvements over those of unpromoted Co-TiO2 membranes, as could be seen in Figure 4.30.

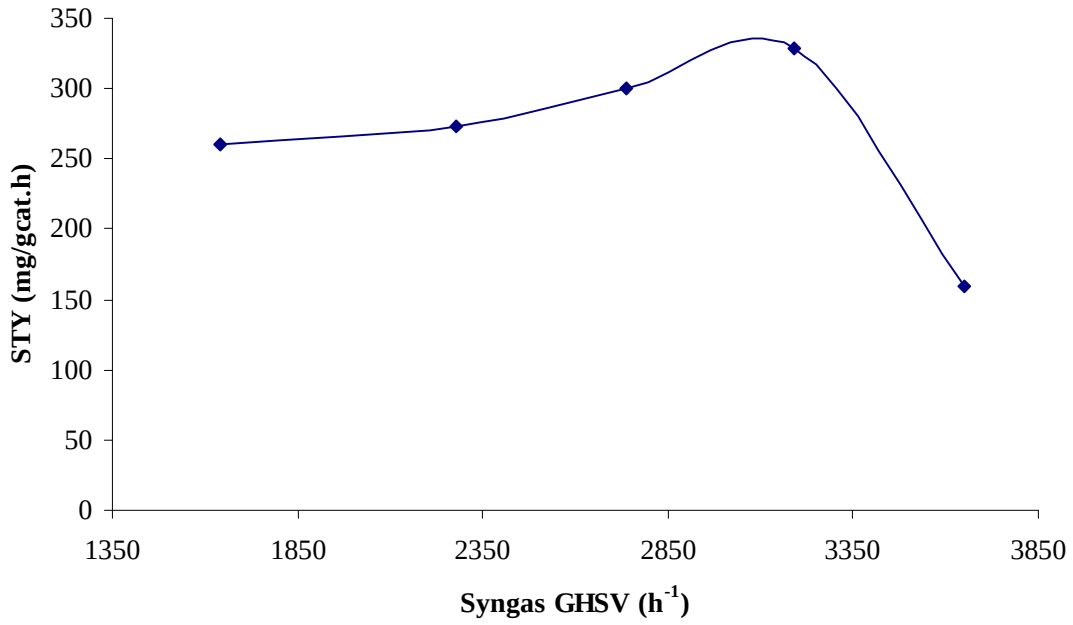

Figure 4.30: Change in space-time yield of liquid products with gas-hourly space velocity for Co-Mn membrane (T=490K; P=300KPa)

There was a steady increase in space-time yield of condensable products as GHSV increased, up to a maximum value of about 326mg/g-cat.h at a space velocity of 3192 h^{-1}. Beyond this limiting space velocity, there was a rapid drop in yield, an effect thought to be associated with the lack of adequate residence time for conversion to occur, and also the difference in the rate of adsorption of reacting species to that of desorption of products. This could be an obvious disadvantage with the forced pore-flow-through mode of operation that was utilized in this work. Therefore, it is necessary to operate the reactor at

optimal feed rate (GHSV=3192 h^{-1}) in order to maximize conversion and yield on a once-through basis.

4.3.2.2 Product selectivity of titania-supported Co-Mn membranes

Co-Mn membranes showed good improvement in terms of feed conversions, product yields and product selectivity, with a large selectivity to hydrocarbon products. It was very easy to separate the condensed products into two separate phases, namely the oil and the aqueous phases which were analysed separately on the GC-MS. This membrane showed unparalleled propensity for isomerization reaction, which could be a result of its ability to alkylate olefinic products, or its ability to promote hydroformylation reactions, and also hydrogenate the resulting aldehydes. The presence of isomers is very useful in gasoline formulations because it increases the octane number of the fuel. As is evident from Figure 4.31, the major products are within the naphtha range (C_7 – C_{13}). Thus, the catalytic membrane reactor operated in the forced pore-flow-through mode at low temperature and pressure using a titania-supported cobalt-manganese membrane was used to produce tailored fuel-grade gasoline, with linear primary alcohols as octane number enhancers.

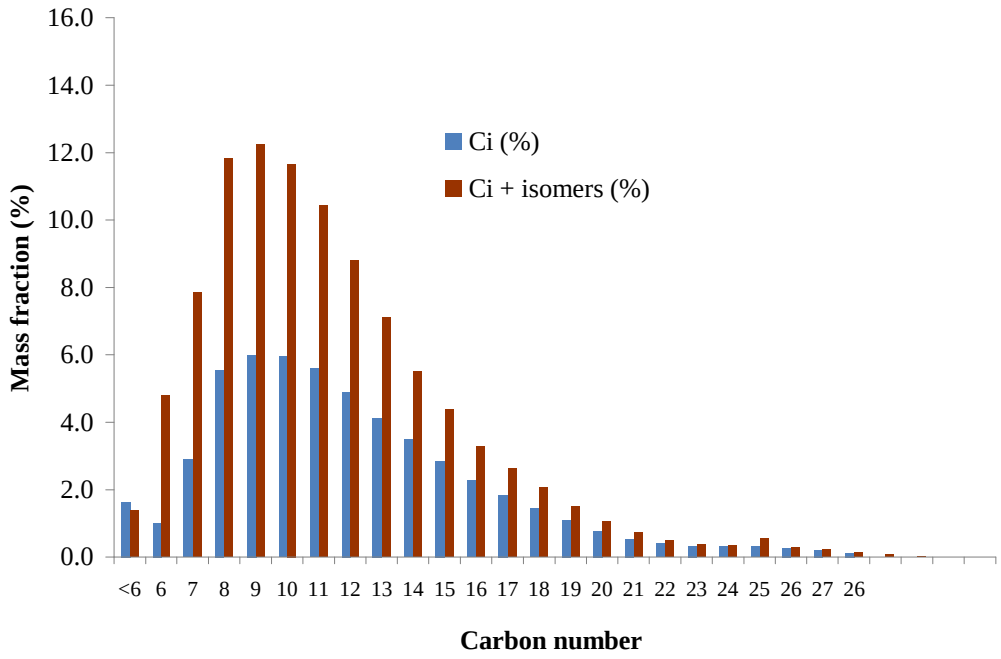

Figure 4.31: Distribution of paraffins in the oil products from Co-Mn membrane (T=220°C, P=300KPa, GHSV=3192h^{-1})

The selectivity to alcohols dropped, with some alcohols completely missing from the product spectra shown in Figure 4.32.

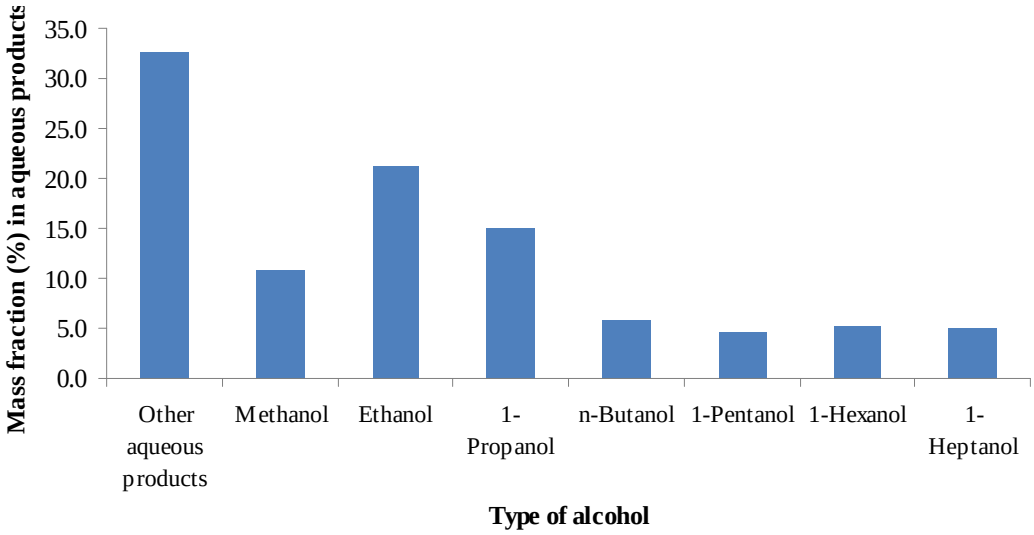

Figure 4.32: Alcohol products distribution for Co-Mn membrane (T=220°C, P=300KPa, GHSV=3192h^{-1})

4.3.3 Cobalt-copper membranes

Copper-promoted cobalt Fischer-Tropsch catalysts have been known to produce mixed alcohols, although the existing technology of higher alcohol synthesis is still on a small scale and the single-pass-conversion of the feed syngas and selectivity to C_{2+} alcohols are both relatively low [Dong *et al*., 2009]. Under the typical reaction conditions, most systems produce methanol (e.g., over alkali-promoted MoS_2 catalysts) or hydrocarbons (e.g., over modified Fischer-Tropsch catalysts) as the main products instead of higher alcohols [Kulawska & Skrzypek, 2001; Stiles *et al*., 1991]. Co-Cu membranes used for the hydrogenation of CO_2-containing syngas in this work gave the result presented in Figure 4.33

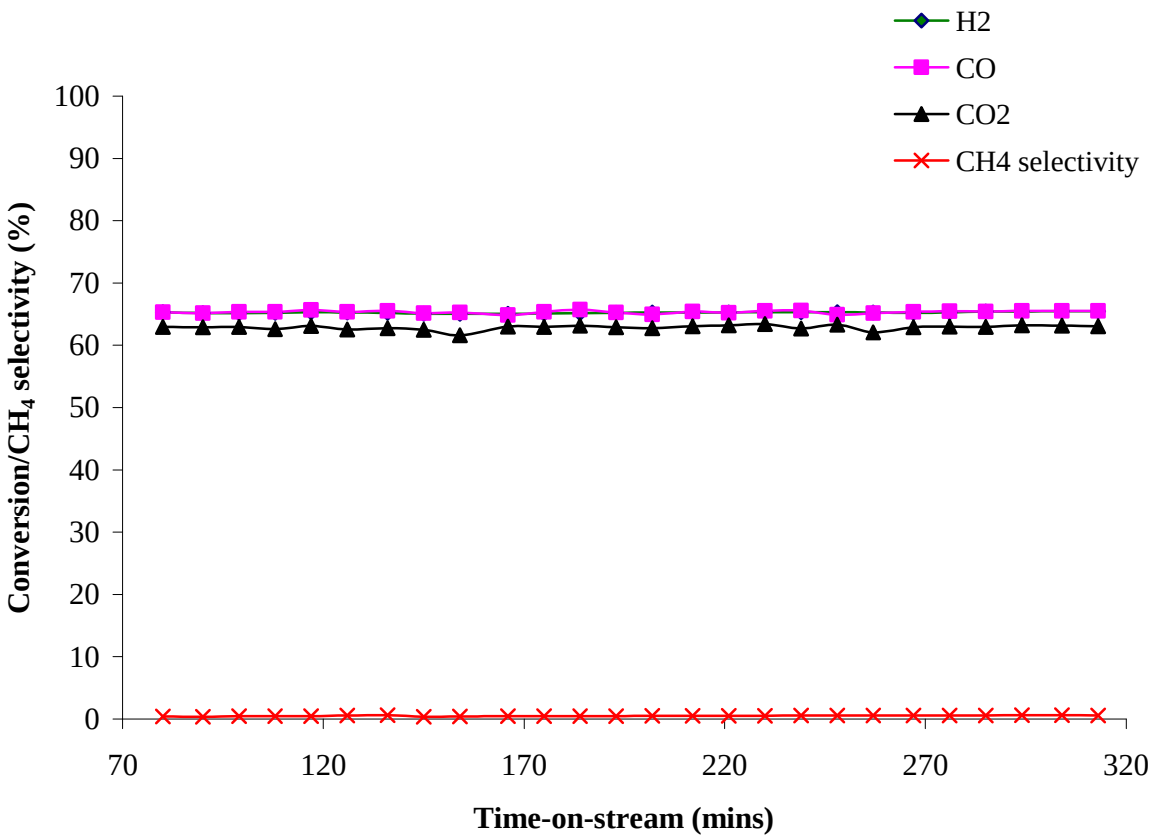

Figure 4.33: Real-time conversion and methane selectivity for Co-Cu membrane ($T=225^oC$, P=300KPa, GHSV= $1642h^{-1}$)

The membrane showed very good conversion of both CO with average value of 65.34% and CO_2 (62.87%) but the space-time yield of liquid products was found to be very low. (0.0552g/g-cat.h)

The temperature used for calcination of this membrane could have impacted negatively on the overall performance as copper is known to sinter rapidly above 300°C [Minahan et al, 2004]. Calcination and reduction of this membrane at 300°C could have permanently destroyed the alcohol synthesis activity of copper, allowing the cobalt in the vicinity of sintered copper particles to effect mostly methanation reactions.

Alkali-promotion has been used to activate hydrogen for the conversion of CO in a process developed by the *Institut Francais du Petrole* (IFP) and based on mixed-oxide formulation containing Cu and Co on an alumina support [Spath & Dayton, 2003]. Higher alcohols have been observed to proceed over mostly metal oxide catalysts and not the metallic forms. It was therefore considered that hydrogen reduction of the precursor oxide could have been an unnecessary superfluous step in the preparation of higher alcohol catalytic membranes. To this end, it was decided that activating the membrane in an inert gas atmosphere could be better than having to heat it with the reducing hydrogen gas. Membrane BCo4 (Co-Cu-K-TiO_2) was therefore produced with potassium doping, and was activated with helium after calcination at 350°C for 3 hours and at 450°C for 3 hours. Results from this membrane were however worse than those obtained using membrane BCo3 even when the total pressure was increased to 500KPa. This was probably caused by the high temperature used for the calcination, although it should be noted that alcohol synthesis using this modified Fischer-Tropsch catalyst at optimal conditions of 260-340°C and 6-20MPa was reported to show carbon conversion efficiency of CO and CO_2 of

between 5 and 30%, and produced a liquid product containing 30-50% higher alcohols with hydrocarbons being the primary by products [Xiaoding *et al*., 1987].

4.3.4 Iron-based membranes

Membrane BFe1 was produced from Fe, Mn, Cu, and K. Both H_2- and CO- temperature programmed reduction (TPR) profiles have confirmed that promotion of Fe with Cu reduces reduction temperature of the oxides, and increases oxygen removal rates [Zhang *et al*., 2006]. The use of copper in this membrane was aimed to increase the rate of FTS and to decrease the rate of WGS reaction. Copper promotion for iron FTS catalysts has been reported to also increase the average molecular weight of the products, though not as much as when potassium is used, while the use of MnO with Fe increases the selectivity of light olefins [Spath and Dayton, 2003]. Zhang *et al*. [2006] reported that their Fe-MnCuK/SiO2 catalyst reached steady-state FTS activity within a short time whereas that without Cu promotion showed a long induction period.

The performance of the Fe-based membrane in Fischer-Tropsch synthesis conducted at 500KPa pressure and 300°C for different syngas flow rates is shown in Figure 4.34

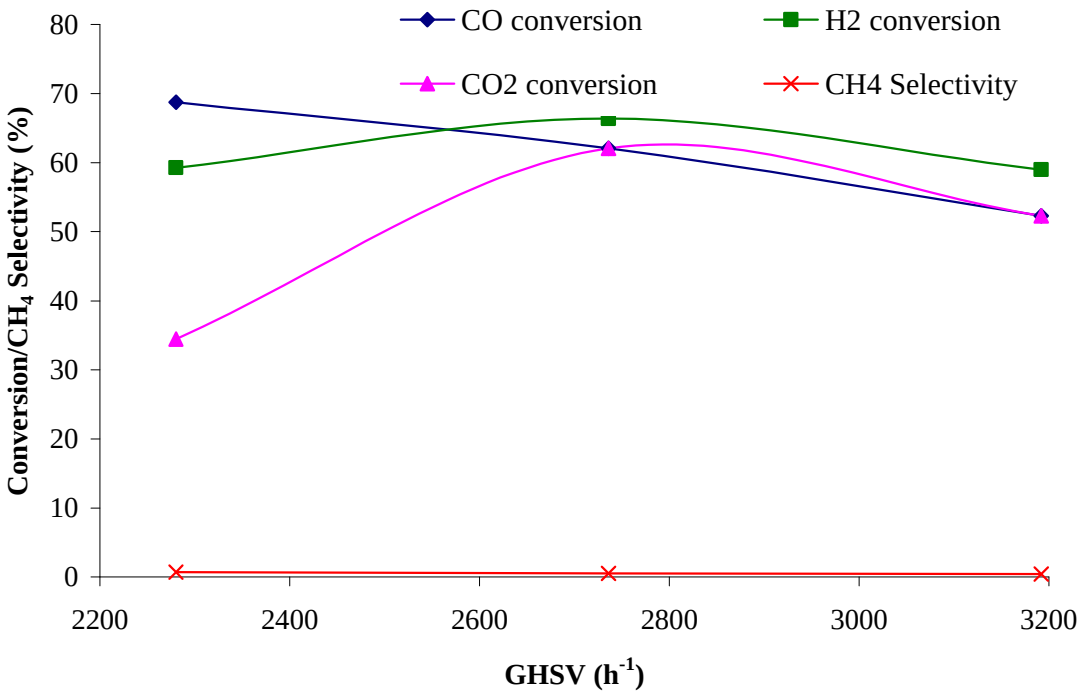

Figure 4.34: Catalytic performance of Fe-based membrane at 500KPa and 300°C

The FTS performance for iron-based membranes showed that CO conversion decreases linearly from about 70% with increasing syngas flow rate. CO_2 conversion on the other hand increased up to a maximum of over 62%, fuelling the suspicion that the competitive adsorption of these oxides on active iron centres could have been responsible for the consistent decrease in CO conversion. However, above gas hourly space velocities of 2736h^{-1}, all reacting species showed a decline in conversion, owing to a possible concentration polarization of the catalyst surface that hindered further adsorption of the reactants. Methane selectivity was observed to be very low, dropping from 0.7 to 0.4% over the feed flow rates studied. These results were better than those obtained from a fixed bed reactor [Herranz *et al*., 2006] and from a spinning basket reactor [Liu *et al*., 2007].

4.4 References

Ahón, V. R., Lage, P. L. C., de Souza, C. D. D., Mendes, F. M., Schmal, M. (2006). Kinetic Rates of the Fischer Tropsch Synthesis on a Co/Nb_2O_5 Catalyst. *Journal of Natural Gas Chemistry*, 15 (4), pp. 307-312

Akin, A. N., Ataman, M., Aksolyu, A. E., Onsan, Z. I. (2002). CO_2 fixation by hydrogenation over co-precipitated Co/Al_2O_3. *Reaction Kinetics and Catalysis Letters*, 76 (2), pp.265-270.

Anderson, R. B. (1984). *Fischer-Tropsch synthesis*. Orlando: Academic Press.

Bechara, R., Balloy, D., Vanhove, D. (2001). Catalytic properties of Co/Al_2O_3 system for hydrocarbon synthesis. *Applied Catalysis A: General*, 207, pp.343-353.

Blanchard, M., Derule, H., Canesson, P. (1989). Cobalt catalysts for the production of alcohols in the F. T. synthesis. *Catalysis Letters* 2, pp.319-322

Borodko, Y., Somorjai, G. A. (1999). Catalytic hydrogenation of carbon oxides – a 10-year perspective. *Applied Catalysis A: General*, 186 pp.355-362.

Calverly, E. M., Smith, K. J. (1992). Kinetic model for alcohol synthesis over a promoted $Cu/ZnO/Cr_2O_3$ catalyst. *Industrial & Engineering Chemistry Research* 31, pp.792-803.

Campos-Martin, J. M., Fierro, J. L. G., Guerrero-Ruiz, A., Herman, R. G., Klier, K. (1996). Promoter effect of caesium on C-C bond formation during alcohol synthesis from CO/H_2 over $Cu/ZnO/Cr_2O_3$ catalysts. *Journal of Catalysis*, 163, pp.418-428.

Cano, F. M., Gijzeman, O. L. J., de Groot, F. M. F., Weckhuysen, B. M. (2004). Manganese promotion in cobalt-based Fischer-Tropsch catalysis. *Studies in Surface Science Catalysis*, 147, p.271.

Chaumette, P., Courty, Ph., Kiennemann, A., Ernst, B. (1995). Higher alcohol and paraffin synthesis on cobalt-based catalysts: comparison of mechanistic aspects. *Topics in Catalysis*, 2 (1-4), pp.117-126.

Chu, W., Kieffer, R., Kiennemann, A., Hindermann, J. P. (1995). Conversion of syngas to C1-C6 alcohol mixtures on promoted $CuLa_2ZrO_7$ catalysts. *Applied Catalysis A: General*, 121, pp.95-111.

Clark, G. I., Walker, D. G. (2000). Multiple reactor system and method for Fischer-Tropsch synthesis. U. S. Patent 6,156,809 (assigned to Reema International Corporation).

Davis, B. H. (2009). Fischer-Tropsch synthesis: Reaction mechanisms for iron catalysts. *Catalysis Today*, 141, pp.25-33.

Davis, B. H. (2003). Fischer-Tropsch synthesis: relationship between iron catalyst composition and process variables. *Catalysis Today*, 84, pp.83-98.

Dong, X., Liang, X., Li, H., Lin, G., Zhang, P., Zhang, H. (2009). Preparation and characterization of carbon nanotube-promoted Co-Cu catalyst for higher alcohol synthesis from syngas. *Catalysis Today*, doi: 10.1016/j.cattod.2008.11.025

Dry, M. E. (1996). Practical and theoritical aspects of the catalytic Fischer-Tropsch process. *Applied Catalysis A: General*, 138, pp. 319-344.

Dulov, A. A., Abramova, L. A., Frankfurt, G. I., Golosman, E. Z., Lapidus, A. L., Sominskii, S. D., Yakerson, V. I. (1987). Phase analysis of the surface of supported copper-cobalt oxide catalysts by means of electrical conductivity thermal-vacuum curves. *Russian Chemical Bulletin*, 36 (8), pp.1594-1597.

Epling, W. S., Hoflund, G. B., Hart, W. M., Minahan, D. M. (1997). Reaction and Surface Characterization Study of Higher Alcohol Synthesis Catalysts. *Journal of Catalysis*, 169 (2), pp.438-446.

Fang, K., Li, D., Lin, M., Xiang, M., Wei, W., Sun, Y. (2009). A short review of heterogeneous process for mixed alcohols synthesis via syngas. *Catalysis Today*, doi:10.1016/j.cattod.2009.01.038

Farias, F. E. M., Silva, F. R. C., Cartaxo, S. J. M., Fernandes, F. A. N., Sales, F. G. (2007). Effect of operating conditions on Fischer-Tropsch liquid products. *Journal of Latin American Applied Research*, 37, pp.283-287.

Fischer, F., Pichler, H. (1939). The synthesis of paraffin from carbon monoxide and hydrogen upon cobalt catalyst (medium pressure synthesis). *Brennstoff-Chemie*, 20, pp.41-48.

Fogler, H. S. (2005). *Elements of Chemical Reaction Engineering*, 4th Edition. New York: Prentice Hall.

Gottschalk, F. M., Copperthwaite, R. G., van der Riet, M., Hutchings, G. J. (1988). Cobalt/Manganese oxide water gas shift catalysts I. competition between carbon monoxide hydrogenation and water gas shift activity. *Applied Catalysis*, 38, pp.103-108.

Govender, N. S., van Vuuren, M. J., Claeys, M., van Steen, E. (2006). Importance of the usage ratio in iron-based Fischer-Tropsch synthesis with recycle. *Industrial & Engineering Chemistry Research*, 45 (25), pp.8629-8633.

Hamada, H., Kuwahara, Y., Kintaichi, Y., Ito, T., Wakabayashi, K., Iijima, H., Sano, K. (1984). Selective synthesis of C_2-oxygenated compounds from synthesis gas over Ir-Ru bimetallic catalysts. *Chemistry Letters*, The Chemical Society of Japan, pp.1611-1612.

Herman, R. G. (2000). Advances in catalytic synthesis and utilization of higher alcohols. *Catalysis Today*, 55, pp.233-245.

Herranz, T., Rojas, S., Perez-Alonso, F. J., Ojeda, M., Terreros, P., Fierro, J. L. G. (2006). Hydrogenation of carbon oxides over promoted Fe-Mn catalysts prepare by the microemulsion methodology. *Applied Catalysis A: General*, 311, pp.66-75.

http://www.lmnoeng.com/Flow/GasViscosity.htm. [Accessed: 26 January, 2009]

Iglesia, E., Soled, S. L., Fiato, R. A., Via, G. H. (1993). Bimetallic synergy in cobalt ruthenium Fischer-Tropsch synthesis catalysts. *Journal of Catalysis*, 143(2), pp.345-368.

Irankhah, A., Haghtalab, A., Farahani, E. V., Sadaghiaizadeh, K. (2007). Fischer-Tropsch kinetics of cobalt catalyst in supercritical phase. *Journal of Natural Gas Chemistry*, 16 (2), pp.115-120.

Hu, J., Wang, Y., Cao, C., Elliott, D. G., Stevens, D. J., White, J. F. (2007). Conversion of biomass-derived syngas to alcohols and C_2 oxygenates using supported Rh catalysts in a microchannel reactor. *Catalysis Today*, 120, pp.90-95.

Jacobs, G., Patterson, P. M., Zhang, Y., Das, T., Li, J., Davis, B. H. (2002). Fischer-Tropsch synthesis: deactivation of noble metal-promoted Co/Al_2O_3 catalysts. *Applied Catalysis A: General*, 233, pp.215-226.

Jalama, K., Coville, N. J., Hilderbrandt, D., Glasser, D., Jewell, L. L. (2007). Fischer-Tropsch synthesis over Co/TiO_2: Effect of ethanol addition. *Fuel* 86, pp.73-80.

Jiang, T., Niu, Y., Zhong, B. (2001). Synthesis of higher alcohols from syngas over Zn-Cr-K catalyst in supercritical fluids. *Fuel Processing Technology*, 73, pp.175-183

Kapteijn, F., De Deugd, R. M., Moulijn, J. A. (2005). *Fischer-Tropsch synthesis using monolithic catalysts*. Proceedings of the International Conference on Structured Catalysts and Reactors No.2, Delft, October 2005.

Keyser, M. J., Everson, R. C., Espinoza, R. L. (1998). Fischer-Tropsch studies with cobalt-manganese oxide catalysts: synthesis, performance in a fixed bed reactor. *Applied Catalysis A: General*, 171, pp.99-107.

Kestel, U., Frohlich, G., Borgmann, D., Wedler, G. (1994). Hydrogenation of carbon dioxide on cobalt catalysts – activation, deactivation, influence of carbon monoxide. *Chemical Engineering & Technology*, 17 (6), pp.390-396.

Khodakov, A. Y., Griboval-Constant, A., Bechara, R., Zholobenko, V. L. (2002). Pore size effects in Fischer-Tropsch synthesis over cobalt-supported mesoporous silicas. *Journal of Catalysis* 206 (2), pp.230-241.

Kim, C. J. (1993). Water addition for increased CO/H_2 hydrocarbon synthesis activity over catalysts comprising cobalt, ruthenium and mixtures thereof which may include a promoter metal. U.S. patent # 5227407, assigned to Exxon Research and Engineering Company, N.J.

Koizumi, N., Kazuhito, M., Toshihiko, O., Yamada, M. (2004). Development of sulphur tolerant catalysts for the synthesis of high quality transportation fuels. *Catalysis Today* 89, pp.465-478

Kuipers, E. W., Scheper, C., Wilson, J. H., Vinkenburg, I. H., Oosterbeek, H. (1996). Non-ASF Product Distributions Due to Secondary Reactions during Fischer–Tropsch Synthesis. *Journal of Catalysis*, 158 (1), pp. 288-300.

Kulawska, M., Skrzypek, J. (2001). Kinetics of the synthesis of aliphatic alcohols from syngas over a modified methanol synthesis catalyst. *Chemical Engineering and Processing*, 40 (1), pp.33-40.

Kusama, H., Okabe, K., Sayama, K., Arakawa, H. (2000). Alcohol synthesis by catalytic hydrogenation of CO_2 over Rh-CO/SiO_2. *Applied Organometallic Chemistry*, 14 (12), pp.836-840.

Leite, L., Stonkus, V., Edolfa, K., Ilieva, L., Plyasova, L., Zaikovskii, V. (2006). Copper-promoted cobalt catalysts for 2.3-dihydrofuran synthesis. *Applied catalysis A: General*, 311, pp.86-93.

Li, D., Yang, C., Zhao, N., Qi, H., Li, W., Sun, Y., Zhong, B. (2007). The performances of higher alcohol synthesis over nickel modified K_2CO_3/MoS_2 catalyst. *Fuel Processing Technology*, 88, pp.125-127.

Li, K. (2007). *Ceramic membranes for separation and reaction*. Chichester: John Wiley.

Liu, Y., Teng, B., Guo, X., Li, Y., Chang, J., Tian, L., Hao, X., Wang, Y., Xiang, H., Xu, Y., Li, Y. (2007). Effect of reaction conditions on the catalytic performance of Fe-Mn catalyst for Fischer-Tropsch synthesis. *Journal of Molecular Catalysis A: Chemical*, 272, pp.182-190.

Lochner, U., Papp, H., Baerns, M. (1986). Iron/manganese oxide catalysts for Fischer-Tropsch synthesis Part III: Phase changes in iron manganese oxide Fischer-Tropsch catalysts during start-up and synthesis process. *Applied Catalysis*, 23(2), pp.339-354

Mahdavi, V., Peyrovi, M.H., Islamic, M., Mehr, J. Y. (2005). Synthesis of higher alcohols over Cu-Co_2O_3/ZnO, Al_2O_3 catalyst. *Applied Catalysis A: General*, 281, pp.259-265.

Matsuzaki, T., Hanaoka, T., Takeuchi, K., Arakawa, H., Sugi, Y., Wei, K., Dong, T., Reinikainen, M. (1997). Oxygenates from syngas over highly dispersed cobalt catalysts. *Catalysis Today*, 36, pp.311-324.

Matsuzaki, T., Takeuchi, K., Hanaoka, T., Arakawa, H., Sugi, Y. (1996). Highly dispersed cobalt catalysts derived from cobalt (II) acetate. *Catalysis Today*, 28 (3), pp.251-259.

Minahan, D. M., Hart, W. M., Epling, W. S., Hoflund, G. B. (2004). Synthesis of fuel alcohols and MBTE from syngas using spinel oxide based catalysts. http://www.anl.gov/PCS/acsfuel/preprints%20archive/File/42_2_SAN%20FRANCISCO_04-97_0715.pdf [Accessed: 23 February, 2009]

Morales, F., de Smit, E., de Groot, F. M. F., Visser, T., Weckhuysen, B. M. (2007). Effects of manganese oxide promoter on the CO and H_2 adsorption properties of titania-supported cobalt Fischer-Tropsch catalysts. *Journal of Catalysis*, 246, pp.91-99.

Morales, F., de Groot, F. M. F., Gijzeman, O. L. J., Mens, A., Stephan, O., Weckhuysen, B. M. (2005). Mn promotion in Co/TiO_2 Fischer-Tropsch catalysts as investigated by XPS and STEM-EELS. *Journal of Catalysis*, 230, pp.301-308.

Nunan, J. G., Bogdan, C. E., Klier, K., Smith, K. J., Young, C., Herman, R. G. (1989). Higher alcohol and oxygenate synthesis over caesium-doped Cu/ZnO catalysts. *Journal of Catalysis*, 116 (1), pp.195-221.

Olsen, S. K. (2003). Catalytic membrane reactors for synthesis gas production from natural gas via partial oxidation, PhD thesis, The Robert Gordon University, Aberdeen.

Park, T. Y., Nam, I., Kim, Y. G. (1997). Kinetic analysis of mixed alcohol synthesis from syngas over K/MoS. *Industrial Engineering Chemistry Research*, 36 (12), pp.5246-5257.

Qin, Z., Liu, J., Wang, J. (2004). Solvent effects on higher alcohol synthesis under supercritical conditions: a thermodynamic consideration. *Fuel Processing Technology*, 85, pp.1175-1192.

Raje, A., Inga, J. R., Davis, B. H. (1997). Fischer-Tropsch synthesis:considerations based on performance of iron-based catalysts. *Fuel*, 76, pp.273-280.

Reuel, R. C., Bartholomew, C. H. (1984). The stoichiometries of H_2 and CO adsorptions on cobalt: Effects of support and preparation. *Journal of Catalysis*, 85 (1), pp.63-77.

Richardson, J. F., Peacock, D. G. (Ed).(1994). *Coulson & Richardson's Chemical Engineering, Volume 3 (Chemical and Biochemical Reactors & Process Control)*, 3rd ed. Oxford: Elsevier Science Ltd.

Riedel, T., Claeys, M., Schulz, H., Schaub, G., Nam, S., Jun, K., Choi, M., Kishan, G., Lee, K. (1999). Comparative study of Fischer-Tropsch synthesis with H_2/CO and H_2/CO_2 syngas using Fe- and Co-based catalysts. *Applied Catalysis A: General*, 186, pp.201-213.

Roper, M. in Keim, W. (Ed.), (1983). *Catalysis in C1 Chemistry*. Dordrecht: D. Riedel Publishing Company.

Roque-Malherbe, R. M. A. (2007). *Adsorption and diffusion in nanoporous materials*. Florida: CRC Press.

Sakurai, H., Haruta, M. (1995). Carbon dioxide and carbon monoxide hydrogenation over gold supported on titanium, iron, and zinc oxides. *Applied Catalysis A: General*, 127, pp.93-105.

Silva, L., Plaza, A., Romero, J., Sanchez, J. Rios, G. M. (2008). Characterization of MFI zeolite membranes by means of permeability determination of near critical and supercritical CO_2. *Journal of Chilean Chemical Society*, 53 (1), pp.1415-1421.

Snel, R. (1988). Deviations of Fischer-Tropsch products from an Anderson-Schulz-Flory distribution. *Catalysis Letters*, 1 (10), pp.327-330.

Spath, P. L., Dayton, D. C. (2003). Preliminary Screening – Technical and economic assessment of synthesis gas to fuels and chemicals with emphasis on the potential for biomass-derived syngas. Prepared under Task No. BBB3.4210, NREL/TP-51034929, National Renewable Energy Laboratory, Colorado.

Stiles, A. B., Chen, F., Harrison, J. B., Hu, X., Storm, D. a., Yang, H. X. (1991). Catalytic conversion of synthesis gas to methanol and other oxygenated products. *Industrial Engineering Chemistry Research*, 30, pp.811-821.

Storch, H. H., Anderson, R. B., Hofer, J. E., Hawk, C. O., Anderson, H. C., Golumbic, N. (1948). *Synthetic liquid fuels from hydrogenation of carbon monoxide, Part 1 – Review of Literature*. Technical Paper 709, Bureau of Mines, U.S. Department of the Interior.

Subramani, V., Gangwal, S. K. (2008). A review of recent literature to search for an efficient catalytic process for the conversion of syngas to ethanol. *Energy and Fuels*, 22, pp.814-839.

Tien-Thao, N., Zahedi-Niaki, M. H., Alamdari, H., Kaliaguine, S. (2007a).Conversion of syngas to higher alcohols over nanosized $LaCo_{0.7}Cu_{0.3}O_3$ perovskite precursors. *Applied Catalysis A: General*, 326 (2), pp.152-163.

Tien-Thao, N., Zahedi-Niaki, M. H., Alamdari, H., Kaliaguine, S. (2007b). Effect of alkali additives over nanocrystalline Co-Cu-based perovskites as catalysts for higher-alcohol synthesis. *Journal of Catalysis*, 245, pp.348-357.

Toebes, M. L., van Dillen, J. A., de Jong, K. (2001). Synthesis of supported palladium catalysts. *Journal of Molecular Catalysis A: Chemical* 173, pp.75-98.

Uchytil, P., Schramm, O., Seidel-Morgenstern, A. (2000). Influence of the transport direction on gas permeation in two-layer ceramic membranes. *Journal of Membrane Science*, 170, pp.215-224.

Ugo, R. (1983). Hydroformylation and carbonylation reactions, *in* Keim, W. (Ed.). *Catalysis in C1 Chemistry*. Dordrecht: R. Reidel Publishing Company.

Vada, S., Hoff, A., Adnanes, E., Schanke, D., Holmen, A. (1995). Fischer-Tropsch synthesis on supported cobalt catalysts promoted by platinum and rhenium. *Topics in Catalysis*, 2, pp.155-162.

van de Loosdrecht, J., van der Haar, M., van der Kraan, A. M., van Dillen, A. J., Geus, J. W. (1997). Preparation and properties of supported cobalt catalysts for Fischer-Tropsch synthesis. *Applied Catalysis A: General*, 150, pp.365-376.

Voβ, M., Borgmann, D., Wedler, G. (2002). Characterization of alumina, silica, and titania supported cobalt catalysts. *Journal of Catalysis*, 212, pp.10-21.

Visconti, C. G., Lietti, L., Tronconi, E., Forzatti, P., Zennaro, R., Finocchio, E. (2009). Fischer-Tropsch synthesis on a Co/Al_2O_3 catalyst with CO_2 containing syngas, *Applied Catalysis A: General*, 355, pp.61-68.

Visconti, C. G., Tronconi, E., Lietti, L., Zennaro, R., Forzatti, P. (2007). Development of a complete kinetic model for the Fischer-Tropsch synthesis over Co/Al_2O_3 catalysts. *Chemical Engineering Science*, 62, pp.5338-5343.

Xiaoding, X., Doesburg, E. B. M., Scholten, J. J. F. (1987). Synthesis of higher alcohols from syngas – recently patented catalysts and tentative ideas on the mechanism. *Catalysis Today*, 2(1), pp.125-170.

Xiadong, X., Scholten, J. J. F., Mausbeck, D. (1982). Stability of copper/cobalt catalysts for the synthesis of higher alcohols. *Applied Catalysis A: General*, 82 (1), pp.91-109.

Yates, I. C., Satterfield, C. N. (1991). Intrinsic kinetics of the Fischer-Tropsch synthesis on a cobalt catalysts. *Energy and Fuels*, 5, pp.168-173.

Zennaro, R., Tagliabue, M., Bartholomew, C. H. (2000). Kinetics of Fischer-Tropsch synthesis on titania-supported cobalt. *Catalysis Today*, 58, pp.309-319.

Zhang, Y., Jacobs, G., Sparks, D. E., Dry, M. E., Davis, B. H. (2002). CO and CO_2 hydrogenation study on supported cobalt Fischer-Tropsch synthesis catalysts. *Catalysis Today*, 71, pp.411-418.

Chapter 5: - Conclusion and Recommendations

CHAPTER 5: Conclusion and Recommendations

5.1 Conclusion and significance of this work

The catalytic tests conducted demonstrate that the intrinsic properties of the membrane reactor are suitable for Fischer-Tropsch synthesis. A striking observation made from this study was the specificity and directivity of the catalytic membranes. For instance, whereas conventional Fischer-Tropsch synthesis normally results in a broad range of products that have to undergo further upgrading like hydroprocessing and refining into useable materials, this process gave rise to a distribution of hydrocarbons mostly within the gasoline range.

Most alcohols synthesis processes also normally produce methanol, and sometimes ethanol as the major primary product at pressures of up to 50 bars, but in this study, a mixed alcohol range suitable for direct blending with gasoline was obtained at as low a pressure as 2 bars. Besides, the Mn-promoted cobalt membrane showed high activity for isomerization reactions, producing iso-paraffins which are quite useful for improving the octane number of gasoline. This means that the only upgrading process required for the products of this innovation to be fit for direct utilization in internal combustion engines is simple dehydration, in order to remove co-produced water.

The catalytic membrane reactor technology is therefore presented to provide a novel method for converting synthesis gas to tailored clean fuels and chemicals, so that Fischer-Tropsch technology could be more cost-competitive with crude oil refining, and for the purpose of monetizing stranded natural gas, or for providing a useful alternative to liquefaction.

The following conclusions were arrived at:

- Catalyst dispersion on the surface and within the pores of the support was found to be high, and accounted for the high activity and productivity of the membranes.
- Gas permeation tests revealed that there was no separation of the feed gas mixture, because of the near absence of Knudsen diffusion.
- Synthesis gas conversion tests on cobalt-based membranes showed that CO conversion as well as the selectivity to methane increased linearly with temperature. CO_2 conversion however decreased with increase in temperature especially at low catalyst concentrations, eventually leading to the production rather than conversion of CO_2. Selectivity to higher alcohols was favored by increase in temperature, with the formation of hydrocarbons taking precedence over low molecular weight alcohols (C_1 – C_3). This suggested the possibility of homologation of alcohol products at high temperatures.
- Pressure and syngas flow rate produced almost similar effects on conversion, space-time yield (STY) and selectivity to alcohols and hydrocarbons, the performance of the membranes showing maximum values beyond which further increases in these operating parameters had negative effects, with the exception of STY.
- Kinetic analysis showed that ease of syngas conversion over cobalt is enhanced in a catalytic membrane reactor. This is because of the lower activation energy of 59.52 KJ/mol.K calculated for a CMR as against 86.9 – 95 KJ/mol.K obtained in other reactors.
- Increase in diffusion rates and accessibility of synthesis gas to the active catalytic centres eliminated mass transfer limitations usually associated with most FT

reactors, without introducing the problem of catalyst attrition which is the deficiency in fluidized bed reactors.

- Enhancement of adsorption of reacting species caused by the strong metal-support interaction (SMSI) between cobalt and titania, considered to be responsible for the high activity of the membranes.
- Absence of pressure losses. In conventional low temperature fixed bed FT reactors, there is limitation on the minimum particle size of the catalyst because small particles cause substantial pressure drop over the reactor while larger particles result in loss of activity due to increase in diffusion length. Even in the slurry phase reactor where no such constraints exist, there is the problem of back mixing of the gas phase bubbling through the slurry, which has been observed to cause significant decreases in conversion per pass and reactor productivity.
- Enhancement of heat removal from the reactor through the open channel morphology of the membrane support which eliminated both radial and axial temperature profiles (that usually exist in fixed bed reactors especially near reactor inlets) thus ensuring isothermal operations.
- The absence of high molecular weight products with low temperature cobalt-based catalysts coupled with the improved water-gas shift activity introduced by manganese promotion showed that promoted cobalt catalytic membranes can directly convert low hydrogen syngas (such as those obtained from coal and biomass gasification) into useful liquid products.
- The large pore diameter of the support was used to tinker with the particle size distribution of the catalyst metal crystal, and was observed to have a limiting effect on the chain length of paraffins formed.

- Waxy products were observed with Fe-based membranes operated at 300°C and 0.5MPa. This is in contrast to the mostly low molecular weight products obtainable from high temperature Fischer-Tropsch (HTFT) iron catalysts using the *Synthol* and *Sasol Advanced Synthol* (SAS) reactors. This creates a potential for producing FT diesel from high temperature catalytic reactors using the relatively cheaper iron-based membranes.
- High space-time yields were recorded, with usage factors of about 2 for a single pass even at 90% conversion of CO and 56% conversion of CO_2, implying that higher conversions and throughputs are achievable if the tail gas (which is mostly CO, CO_2 and H_2 with a small quantity of methane) is recycled without necessarily incurring high recompression cost since the process is operated at relatively low pressures.
- Low pressures used (maximum of 5 bars as against the conventional 10 to 25 bars for FTS) could lead to huge savings in operating cost, and lower CAPEX requirements, thus reducing the unit price of gasoline and enhancing the economics of the gas-to-liquid (GTL) process.
- The conversion of CO_2-rich syngas helped to eliminate the need for the CO_2-removal step of the gas-to-liquid (GTL), coal-to-liquid (CTL) or biomass-to-liquid (BTL) process and therefore enhanced the overall economies of scale.
- The membranes could be produced with ease, and there are no problems of separating the products from the catalysts, or the cumbersome and labour-intensive task of loading and removing the catalysts in conventional reactors.
- There is ease of construction and scale-up of the membrane reactors, which can be operated as an assembly of parallel reactors or as a cascade of reactors with

periodic operation. This way, it is possible to isolate any reactor for maintenance while continuous production is maintained, thus minimising downtime disturbances in the operation of the plant.

5.2 Recommendations for future work

The catalytic membrane reactor operated in the forced pore-flow-through mode offers a promising approach to improve synthesis gas access to the catalyst in all syngas conversion processes. This work could therefore be considered to have laid the basis for a number of related activities aimed at elucidating a better understanding of concepts observed herein, or at improving the performance of both the membrane and the reactor with respect to the chosen process.

The underlisted approaches which are hoped would advance the cause of this subject matter are therefore recommended:

- Fundamental studies on the catalyst preparation procedure are advocated because the efficiency of the impregnation process could be hampered by the inability to disentangle the effects of the individual preparation steps (impregnation, drying, calcinations and reduction).
- Kinetic and thermodynamic analyses should be carried out to determine system parameters such as enthalpies of adsorption of reacting species, free energies, activation energies, and equilibrium and reaction constants. The former would make for an understanding of the actual entitities and intermediates involved in the various reaction pathways while eliminating various possibilities, while the latter would help in the elucidation of accurate reaction rate expressions.

- Regression analysis should be used to obtain the best fit for the kinetic models proposed in order to generate both optimization and scale-up strategies based on the system's predictable response to changes in operating conditions.
- Long-term operation of the syngas conversion reactions using this CMR is required in order to obtain the deactivation profile for the catalytic membranes employed in this work using either the loss in surface area approach or the loss in activity based on turn-over frequency (TOF).
- Sensitivity analysis of both methane and carbon dioxide composition in the feed on membrane activity would be necessary in order to understand the effect of tail gas recycling on conversion and both selectivity and space-time yield of the products.
- Additional methods for membrane characterization which would complement and support each other should be explored since it is known that no single method is able to provide the whole scope of information necessary to describe the catalytic properties of the membranes.
- Iron-based catalytic membranes used in this work showed no tangible activity for the hydrogenation of either CO or CO_2 at 300KPa pressure and 210°C. However, when the pressure was increased to 500KPa and the temperature was raised to 300°C, methane and waxy products were obtained. This necessitated the use of both the hot trap (which was maintained at 150°C), and the cold trap. The primary product collected from the hot trap was completely waxy, and was suspected to be high molecular weight hydrocarbon products. These series of experiments require further investigation because of its huge potential for the conversion of CO_2, and the relative low price of iron as the primary catalyst. The actual effect of both

temperature and pressure on syngas conversion and product yield should be determined while the waxy products should be analyzed using toluene or any other appropriate organic solvent.

APPENDIX

APPENDIX A1: SYNTHESIS GAS CONVERSION PROCESSES [Spath & Dayton, 2003]

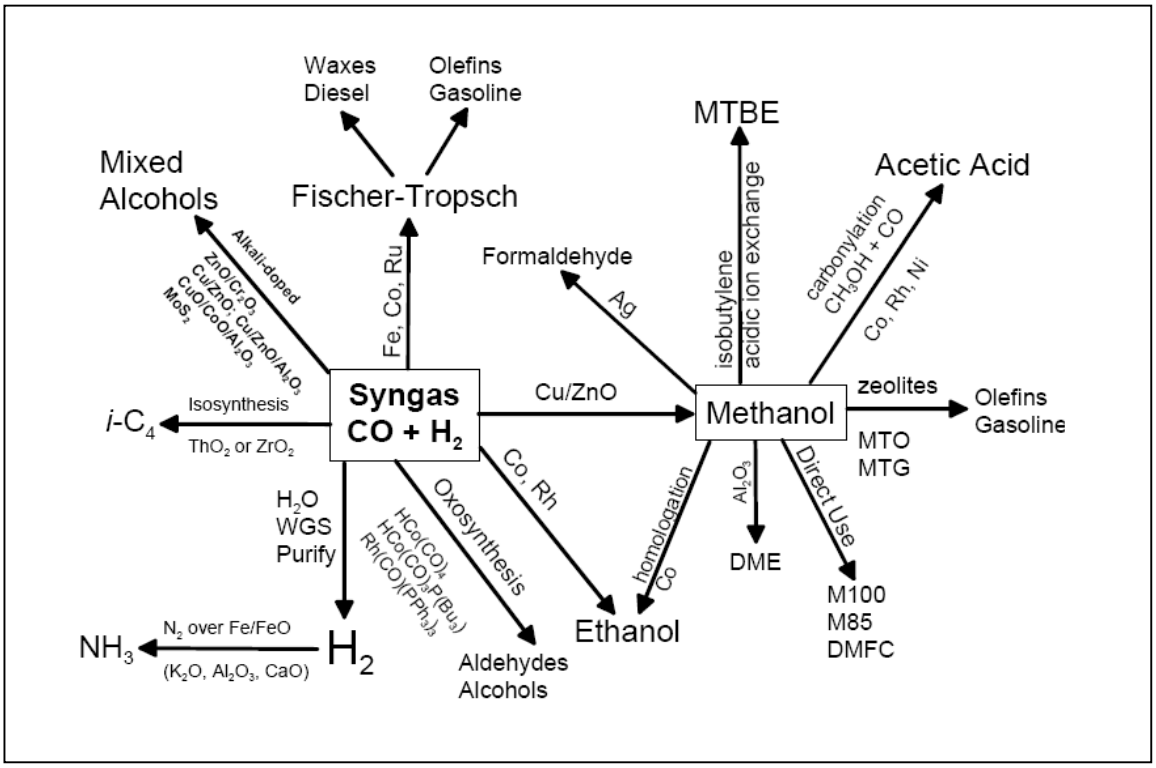

APPENDIX A2: SUMMARY OF SYNGAS CONVERSION PROCESSES AND CONDITIONS

Process	Catalyst	Process Conditions			% conv (CO basis)	Product	Selectivity
		T (°C)	P (bar)	H_2:CO			
Fischer-Tropsch Synthesis	Fe	300-350	10-40	1.7:1	50-90% with recycle	α-olefins gasoline	ASF -48% (max) 15-40% actual
	Co	200-240	7-12	2.15:1		Waxes diesel	ASF - 40% (max)
	Ru					Waxes	
Methanol Synthesis	ZnO/Cr_2O_3	350	250-350	3:1	99% (25% max/pass – 4-7% actual/pass)	Methanol	> 99% with recycle
	$Cu/ZnO/Al_2O_3$	220-275	50-100				
Ammonia	Fe/FeO + additives	430-480 (550 max)	100-500	2-3:1 H_2:N_2	10-35%/pass	Ammonia	> 99% with recycle
Higher Alcohols Synthesis	Alkali/ZnO/Cr_2O_3	300-425	125-300	1:1	5-20%	Branched primary alcohols	
	Alkali/Cu/ZnO(Al_2O_3)	275-310	50-100	2-3:1	20-30%	Primary alcohols	30-45% C_{2+} 17-25% CO_2
	Alkali/CuO/CoO	260-340	60-200	0.5-4:1	5-30%	Linear primary alcohols	ASF
	Alkali/MoS_2	260-350	30-175	1:1	10%	Linear alcohols	75-90% C_{2+} in liquid product
Oxosynthesis	Co carbonyl	110-200	200-300	1:1 + olefin			
	Co – P modified	160-200	50-100	1:1 + olefin		C_{11}-C_{14} alcohols	
	Rh – P modified	60-120	7-25	1:1 + propylene		C_4 aldehydes	> 90%
Isosynthesis	ThO_2	400-450	100-1000 (300)	0.85:1	40-50%	*i*-C_4	
	ZrO_2	300-425	350	1:1	30%		15
Steam Methane Reforming	Ni	850	15-30	na	100% CH_4 conversion	Syngas/ hydrogen	

APPENDIX B: ALCOHOL SYNTHESIS

The synthesis of alcohols obtained from hydrogenation of carbon oxides over transition metals, is an alternative for the production of chemical commodities and less-polluting renewable fuels. The catalytic conversion of syngas to a mixture of linear alcohols is recognized as an important route for providing clean fuels and petrochemicals. It is known that the presence of ethanol in gasoline improves simultaneously the volatility of the mixture, the water tolerance, and the solubility of hydrocarbons [de Aquino & Cobo, 2001]. Therefore, the most promising application of the mixed higher alcohols is as a blending stock for automotive fuel to meet the octane requirement resulting from legislative regulation of lead-free gasoline and to replace MTBE in order to reduce environmental pollution.

Methanol Synthesis

Methanol (methyl alcohol, CH_3OH) like Fischer-Tropsch liquids is produced from synthesis gas as crude methanol and later upgraded to fuel or chemical grade. Complete proprietary processes for methanol synthesis are currently available under license from many companies including ICI, Haldor Topsoe, Lurgi, MW Kellog, Mitsubishi Gas Chemicals and Krupp Udhe.

World demand for methanol totalled 30.789 million tonnes in 2003 and is expected to grow at about 3% per annum [Metcall LLC, 2006]. It is largely used as a feedstock for a wide variety of intermediate chemical compounds and the fuel oxygenate methyl-tertiary-butyl-ether (MTBE), although prevention of MTBE as octane number enhancer in US gasoline has affected this market. Less than 4% of total methanol consumption is directly for fuel, although it serves as a component in the transesterification of triglycerides to biodiesel and is also used in direct methanol fuel cells (DMFC). When blended with gasoline (M85) as an oxygenated additive in internal combustion engines it delivers more power than pure gasoline because of its high octane rating (100), and also reduces exhaust emissions. Methanol is also easily dehydrated to dimethyl ether (DME), which is an effective fuel particularly in diesel engines due to its high cetane number and favourable properties [Olah *et al*., 2006]

World installed production capacity for methanol currently stands at 35 million tonnes and 'Methanex' remains the dominant producer and seller.

The methanol to gasoline (MTG) process was developed by Mobil and an industrial facility was built in Motunui, New Zealand in the 1980s. In the TIGAS process developed by Haldor Topsoe AS for the manufacture of gasoline, the methanol synthesis and the MTG reactions are integrated- without the separation of methanol as an intermediate product.

Methanol synthesis is usually carried out at high pressures (50-350 bars) and low temperatures over a variety of catalysts mostly based on zinc and chromium oxides (ZnO –Cr_2O_3).

The main reactions for the formation of methanol from synthesis gas are [Moulijn *et al*., 2001]:

$$CO + 2H_2 \rightleftharpoons CH_3OH \qquad \Delta H^\circ_{298K} = -90.8\text{kJ/mol} \qquad \text{(B1)}$$

$$CO_2 + 3H_2 \rightleftharpoons CH_3OH + H_2O \qquad \Delta H^\circ_{298K} = -49.6\text{kJ/mol} \qquad \text{(B2)}$$

These methanol-forming reactions are coupled with the water-gas shift reaction,

$$CO + H_2O \rightleftharpoons CO_2 + H_2 \qquad \Delta H^\circ_{298K} = -41\text{kJ/mol} \qquad \text{(B3)}$$

The methanol thus formed may be converted to gasoline by the Mobil process. First methanol is dehydrated to give dimethyl ether:

$$2\ CH_3OH \longrightarrow CH_3OCH_3 + H_2O \qquad \text{(B4)}$$

This is then further dehydrated over a zeolite catalyst, ZSM-5, to give gasoline with 80% (by weight based on the organics in the product stream) C_{5+} hydrocarbon products.

Higher Alcohols Synthesis

The oil embargos of the 1970's spurred interest in the use of syngas to produce alcohols (methanol, ethanol, butanol, etc.) for blending with gasoline. Currently, methanol is commercially produced from syngas, but higher alcohols (ethanol, butanol, etc.) are not.

Higher alcohols, or mixtures of higher alcohols with methanol, have better fuel properties than pure methanol. The technical advantages of using mixed alcohols (C_1-C_6) for blending with gasoline over pure methanol are:

- higher octane ratings (greater resistance to uncontrolled ignition in internal combustion engines),
- improved control of volatility,
- lower tendency toward phase separation in the presence of water,
- improved hydrocarbon solubility,
- better compatibility with certain engine components,
- lower vapour pressure, and
- higher overall heating value.

And, when used as a diesel substitute at levels of 20-30% weight, the calorific value, lubrication properties, and ignition properties are improved compared to pure methanol.

Historically, several processes have been developed to make mixed alcohols from syngas, however, commercial production has been hampered by poor selectivity and low product yields (typically around 10 percent of the syngas is converted to alcohol with methanol the most prevalent component). Currently there are no commercial plants that produce mixed alcohols in the C_2 to C_6 range, largely due to poor selectivity and low product yields caused by the lack of appropriate catalysts [Spath & Dayton, 2008].

The mechanism for higher alcohol synthesis involves numerous reactions each with multiple pathways leading to a variety of products. The three major process routes are: reductive carbonylation, methanol homologation and direct synthesis of ethanol from syngas. The first two mechanisms involve the synthesis of methanol followed by the stepwise carbonylation of the proceeding alcohol molecule to sequentially produce ethanol, propanol, butanol, etc. The only difference is that in reductive carbonylation, the preceding alcohol is first converted to the corresponding acid before subsequent hydrogenation of the acid to the next higher alcohol. Branched higher alcohols like isopropyl alcohol (IPA) and isobutanol can also be produced. The system of reactions for mixed alcohol synthesis is shown in Table B1.

Table B1: System of homologation reactions for mixed alcohol synthesis

Reaction	Chemical equation
Methanol	$CO + 2H_2 \longrightarrow CH_3OH$
Ethanol	$CO + 2H_2 + CH_3OH \longrightarrow C_2H_5OH + H_2O$
Propanol	$CO + 2H_2 + C_2H_5OH \longrightarrow C_3H_7OH + H_2O$
n-Butanol	$CO + 2H_2 + C_3H_7OH \longrightarrow C_4H_9OH + H_2O$
1-Pentanol	$CO + 2H_2 + C_4H_9OH \longrightarrow C_5H_{11}OH + H_2O$
1-Hexanol	$CO + 2H_2 + C_5H_{11}OH \longrightarrow C_6H_{13}OH + H_2O$
1-Heptanol	$CO + 2H_2 + C_6H_{13}OH \longrightarrow C_7H_{15}OH + H_2O$
1-Octanol	$CO + 2H_2 + C_7H_{15}OH \longrightarrow C_8H_{17}OH + H_2O$

The overall stoichiometric reaction can be summarized as:

$$2nH_2 + nCO \longrightarrow C_nH_{2n+1}OH + (n-1)H_2O \quad \Delta H^{\circ}_{298K} = -256\text{kJ/mol} \qquad \text{(B5)}$$

The types of reactions that occur are affected by the operating conditions and the types of catalysts used. Higher alcohol production is favoured at high pressures, higher temperatures, and a syngas H_2/CO ratio close to 1 [Gerber *et al*., 2007]. It has been observed that thermodynamic constraints limit the theoretical yields of higher alcohols, and the heat generated during the chemical reactions must be removed to maintain control of process temperatures [Vervek *et al*., 1999]. Compared to methanol, production of higher alcohols generates more heat. Water and carbon dioxide are produced as by-products of higher alcohol production and secondary reactions can result in the production of other products including aldehydes, ketones, and paraffins especially methane [Roberts *et al*., 1992].

All syngas conversion reactions require that catalysts play a pivotal role. The basic concept of a catalytic reaction is that chemical compounds adsorb onto the catalyst surface, rearrange, and combine into products followed by desorption from the catalyst surface. A number of different types of catalysts can be used to produce higher alcohols [Herman, 1991].

Modified high pressure methanol synthesis catalysts operate at temperatures ranging from 300-425°C and at pressures ranging from 125 to 300 bar. They are used to produce branched primary alcohols and are composed of ZnO/Cr_2O_3 with an alkali added. Modified low pressure methanol synthesis catalysts are used at temperatures ranging from

275-310°C and at pressures ranging from 50 to 100 bar. They consist of Cu/ZnO or Cu/ZnO/Al_2O_3 with alkali added and used to produce primary alcohols [Caraballo, 2005]. Many of the early processes used these catalysts and methanol is the most abundant (about 80%) alcohol produced [Spath & Dayton, 2003].

Modified Fischer-Tropsch catalysts, CuO/CoO/Al_2O_3/alkali operate at temperatures between 260-340°C and pressures of 60 to 200 bar and catalyze the production of linear primary alcohols. This development (based on copper, cobalt and nickel) was mostly floated by Institut Francais du Petrole (IFP). Courty and co-workers found that at optimal conditions, syngas is converted to a liquid product containing 30-50% higher alcohols [Courty *et al*., 1982; Courty *et al*., 1984]. Mahdavi and his group [Mahdavi *et al*., 2005] also reported total alcohol selectivity of 80% with selectivity to heavier alcohols of 50%. However, the lack of long-term stability and low activity of these catalysts hinders their commercial application.

Modified sulphide catalysts (mainly MoS_2-based) are used at temperatures between 260-350°C and pressures between 30 and 175 bar and produce linear alcohols. Alkali metals such as Caesium (Cs) or potassium (K) are often added as promoters to provide a basic site to catalyse the aldol condensation reaction by activating surface adsorbed CO and enhancing the formate intermediate. At H_2/CO ratio of 1, these catalysts selectively give 10% CO conversion with a selectivity of 75-90% to higher alcohols [Herman, 1991]. Some advantages of these catalysts include resistance to sulphur poisoning, less severe coke deposition even with syngas having a low H_2/CO ratio, and less sensitivity to CO_2 in the syngas stream compared to other alcohol synthesis catalysts. Sulphide catalysts are extremely resistant to sulphur poisoning, and in fact, require 50-100 parts per million (ppm) of sulphur in the syngas to maintain the catalyst [Courty *et al*., 1998]. However, the presence of carbon dioxide in the syngas can shift the reaction toward the production of methanol rather than higher alcohols [Herman, 1991]. Activity of the sulphide catalyst can also depend on the support material [Iranmahboob & Hill, 2002]. By manipulating the composition of the catalyst and the reaction operating conditions it is possible to vary the ratio of methanol to C_{2+} alcohols.

A major hurdle to the commercial production of higher alcohols from syngas is the need to improve the selectivity and productivity of catalysts.

Another technology is to produce alcohols by a catalytic method in which the catalyst is in the form of unsupported nano-sized particles or supported on a high surface area support such as carbon, alumina, or silica [Mahajan & Jackson, 2004]. In either arrangement, the nano-sized catalyst is suspended in an inert solvent such as high molecular weight hydrocarbon solvent to form slurry. The synthesis gas is then passed through the catalyst slurry to produce alcohols in the product stream. The operating temperature is 200 to 300°C and the pressure ranges from 35 to 207 bar.

Production of higher alcohols occurs in reactors similar to those used in methanol and Fischer-Tropsch processes, and like those processes, removal of the large amount of excess heat generated during reactions is essential to maintaining control of the process temperature, to maximizing yields, and to minimizing deactivation of the catalysts. New designs of reactors are also being examined. Currently higher and mixed alcohols are not commercially produced from syngas, but a number of companies are conducting research including Dow, IFP, Snamprogetti, Lurgi, Hoechst, etc. Some of their major findings are reported in Table B2.

Although not commercialized, a few HAS processes have advanced to the pilot-scale stage, and conceptual processes, based on patented catalytic technologies, have been developed [Subramani & Gangwal, 2008]. Some examples are listed in Table B3.

A number of studies have examined the cost of producing higher alcohols using natural gas as the feedstock [Courty *et al*., 1984; Betchel, 1998]. Generally, about 50 percent of the costs of producing alcohols from syngas as for FTS are for the capital costs associated with syngas production, with 29% of the costs attributed to alcohol synthesis, 17% for CO_2 removal, and 4% for alcohol fractionation. Some patents relevant to higher alcohols synthesis are given in Table B4

Company	Country	Catalyst type	Temp. (^oC)	Pressure (psi)	H_2/CO ratio	Products	Conversion and selectivity information
Lurgi	Germany	Modified methanol	250 – 420	725 –1450	1 – 1.2	53.5 wt% methanol 41.9 wt% C_2-C_6	CO conversion = 20 – 60%
Union Carbide	U. S.	Rhodium	300 – 350	1000-2500	not found	not found	CO selectivity to Ethanol (EtOH) = 60%
Sagami Research Centre	Japan	Rhodium	200 – 300	735	1.4	Mainly methanol, ethanol & CH_4	CO conversion = 14% Selectivity to EtOH up to 61% Selectivity to alcohols = 90%
IFP	France	Modified methanol	260 – 320	850-1450	1 – 2	30-50 wt% C2-C4	CO conversion = 12-18% Selectivity to alcohols = 70-75%
Hoechst	Germany	Rhodium	275	1455	not found	not found	CO selectivity to EtOH = 74.5%
Snamprogetti	Italy	Modified methanol	260 – 420	2610-3822	0.5 – 5	20-40 wt% C2-C4	CO conversion = 17% Selectivity to alcohols = 71%
Texaco (Liquid phase system)	U. S.	Modified FT	220 – 240	6615	not found	12-39 wt% non-alcohol oxygenates	Syngas conversion = 40% Selectivity to products = 75%
Dow	U.S.	Modified FT	229 – 310	1500-2000	1.1 – 1.2	30-70 wt% MeOH	CO conversion = 10-40% Selectivity to alcohols = 85%

Table B2: Companies and information regarding Mixed Alcohols Research [Spath & Dayton, 2003]

Table B3: Current Status of selected Catalytic and combined catalytic and fermentation processes for the synthesis of Mixed Alcohols [Subramani & Gangwal, 2008]

	Overall process scheme	Stage of development	Scale	Comments
IFP-Idemitsu	Reform natural gas to syngas; Cu-Co-based modified FTS catalyst; methanol distillation; extractive distillation with DEG; DEG recovery	Pilot plant	7000 bbl/y	Produced C_1-C_7 linear alcohols; higher alcohols between 20-70%
SEHT (Snamprogetti, Enichem, Haldor-Topsoe)	Partial oxidation of natural gas to syngas; Cu-Zn-based modified MeOH synthesis catalyst; high pressure fixed bed process; distillation of MeOH and EtOH; water distillation; azeotropic distillation for C_{3+} alcohols	Pilot plant	400 ton/d	Crude alcohol mixture contained 20% H_2O; final H_2O content <0.1%; blended (at 5%) to make premium gasoline
Lurgi-Octamix	Steam and autothermal natural gas reforming; Cu-Zn-based modified MeOH synthesis catalyst; low temperature, low pressure conversion of to mixed alcohols; stabilizer column	Pilot plant	2 ton/d	Process produced mixed alcohols containing 1-2% water
Dow Chemical	MoS2 –based catalyst	Bench scale		
Ecalene	Syngas with sulphur converted to higher alcohols with nanosized improved MoS2-based catalyst; 200-300°C; 500-3000 psig	Bench scale	Planned scale up to 500 gallon/d	Higher alcohol yield of >0.4g/ (g catalyst h)
MixAlco	Fermentation of municipal solid waste into chemicals such as acids, esters, ketones, etc. followed by catalytic hydrogenation of acids; H2 for hydrogenation is produced by gasification of undigested biomass component	Pilot scale	100 lb/d	Process produces 2-propanol as major alcohol component; planning to expand to production scale

Table B4: Some relevant Alcohols synthesis patents

Inventors	Assignee	Patent Title	Patent no./ Application no	Year
Sugier, A., Freund, E.	IFP, France	Process for manufacturing alcohols, particularly linear saturated primary alcohols from synthesis gas	U. S. Patent 4122110	1978
Greene, M. I.. Gelbein, A. P.	Chem Systems Inc., N.Y. (US)	Process for the synthesis of aliphatic alcohol-containing mixtures	U. S. Patent 4477594	1984
Lin, F., Pennella, F.	Phillips Petroleum Company, Okla. (US)	Alcohol synthesis	U. S. Patent 4537909	1985
Shibata, M., Uchiyama, S., Aoki, Y.	Research Association for Petroleum Alternatives Development, Tokyo (JP)	Process for the production of mixed alcohols	U. S. Patent 4564643	1986
Nay, B., Stewart, D. G.	BP, London (GB)	Catalyst composition for the production of alcohols from synthesis gas	U. S. Patent 4567160	1986
Courty, P., Chaumette, P., Verdon, C.	IFP, France	Process for manufacturing a mixture of primary alcohols from synthesis gas, in the presence of a catalyst containing copper, cobalt, zinc and at least one alkali and/or alkaline earth metal	U. S. Patent 4780481	1988
Stevens, R. R., Conway, M. M.	The Dow Chemical Company, MI (US)	Mixed alcohols production from syngas	U. S. Patent 4831060	1989

Miller, J. T., Radlowski, C. A.	Amoco Corporation, Chicago (US)	Catalytic process for producing olefins or higher alcohols from synthesis gas	U. S. Patent 5109027	1992
Underwood, R. P., Toseland., B. A., Thomas,	Air Products and Chemicals, Inc., PA (US)	Process for the synthesis of a C2+ aliphatic alcohol in a slurry reactor comprising an in-situ catalyst impregnation step	U. S. Patent 5530168	1996
Sofianos, A., Scurrel M. S.	Patlico International BV, Rotterdam (NL)	Synthesis of higher alcohols	U. S. Patent 5627295	1997
Jackson, G. R., Mahajan, D.	PowerEnerCat. Inc., CO (US)	Method for production of mixed alcohols from synthesis gas	U. S. Patent 6248796	2001
Atkins, M., Bolton, L., Gracey, B. P., Sunley, J. G.	BP Chemicals Ltd., Middlesex (GB)	Process for conversion of synthesis gas to oxygenates	WO/2006/123158	2006
Bolton, L. W. Gracey, B. P.	BP Chemicals Ltd., Middlesex (GB)	Process for conversion of synthesis gas to oxygenates	WO/2007/138303	2007
Hu, J., Wang, Y., Dagle, R., Cao, C., Elliot, D., Stevens, D. J., White, J. F., Holladay, J. D.	Battelle Memorial Institute, WA (US)	Alcohol synthesis from CO or CO_2	WO/2007/075428	2007
Lucero, A. J., Sethi, V. K., Tuminello, W. H.	University of Wyoming Research Corporation, WY (US)	Process and catalyst for production of mixed alcohols from synthesis gas	WO/2007/127429	2007

Tirtowidjojo, M. Fish, B., Pelt, H. Jewell, D., Bearden, M.	The Dow Chemical Company, MI (US)	Mixed alcohol synthesis with enhanced carbon value use	PCT/US2007/ 006967	2007
Wang, K. Cook, R. A.	ExxonMobil Chemical Patents, Inc. TX (US)	Production of alcohols from synthesis gas	U. S. Patent 7449425	2008

Oxo-alcohols synthesis (Hydroformylation)

Olefins produced during the Fischer-Tropsch synthesis can be hydroformylated to oxygenate fuels in the presence of synthesis gas. This observation was made by Otto Roelen in 1938 while investigating the origin of oxygenated products (aldehydes, alcohols, ethers and ketones) occurring in cobalt-catalyzed Fischer-Tropsch reactions [Cornils *et al*., 1994]. In hydroformylation reaction, the elements of formaldehyde (H and CHO) are added across an olefinic double bond to give both linear and branched aldehydes. These can then be reduced to oxo-alcohols depending on the catalyst and reaction conditions. The basic chemistry is represented by the following equations:

$$R_1CH = CHR_2 + CO/H_2 \xrightarrow{\text{catalyst}} R_3 - \overset{H}{\overset{|}{C}} = O \;+\; R_4 - \underset{H}{\underset{|}{\overset{R_5}{\overset{|}{C}}}} - \underset{H}{\underset{|}{C}} = O \qquad \text{(B6)}$$

(α- or internal olefin) (syngas) (linear aldehyde) (branched aldehyde)

$$R_3\overset{H}{\overset{|}{C}} = O + R_4 - \underset{H}{\underset{|}{\overset{R_5}{\overset{|}{C}}}} - \underset{H}{\underset{|}{C}} = O \xrightarrow{H_2} R_3 - C\,H_2OH \;+\; R_4 - \underset{H}{\underset{|}{\overset{R_5}{\overset{|}{C}}}} - C\,H_2OH \qquad \text{(B7)}$$

(aldehyde mixture) (linear alcohol) (branched alcohol)

Hydroformylation of alkenes is usually carried out using homogeneous catalysts composed of rhodium, cobalt, and transition metal complexes [Frohning & Kohlpainter, 1996, Lenarda *et al*., 1996]. In order to avoid the drawbacks of homogeneous catalysis,

such as, very high pressure, problem of separating catalyst from products and expensive metal losses, a lot of efforts have been made to develop heterogeneous catalysts for hydroformylation [Qiu *et al*., 2001]. Cobalt is extensively used in homogeneous process due to its high activity and relatively low cost, but most of the studies on heterogeneous systems have been carried out on supported rhodium catalyst. Homogeneous alkene hydroformylation is believed to proceed via the formation of a carbonyl intermediate such as $Co_2(CO)_8$, which has been found to show high reaction rate and activity both in *n*-octane and methanol solvents [Li *et al*., 2003]. Kainulainen *et al*. [1998] applied Co/SiO_2 catalyst in the gas-phase hydroformylation of ethylene at 173°C and 5 bar pressure and observed that Co/SiO_2 catalyst was very active and stable in flow conditions. Li *et al*. [2003] used activated carbon as cobalt support to suppress olefin hydrogenation and reported good activity and selectivity for olefin hydroformylation at low pressure.

Ethylene hydroformylation and CO hydrogenation to form methanol and C_2 oxygenates share several features, namely, CO insertion and metal-carbon (acyl or alkyl) bond hydrogenation. However, these processes look different just because CO hydrogenation requires an initial CO dissociation before catalysis can proceed, as shown in Figure 2.5. Due to the similarity of several key steps, a comparison of ethylene hydroformylation and CO hydrogenation could help define the key mechanistic steps, elucidate the critical step in Fischer-Tropsch synthesis and potentially lead to improvements in both processes [Hanaoka *et al*., 2000]. These similarities could also lend credence to the argument that both processes are considered to be occurring together in this present invention. The oxo-reaction as applied to the synthesis of detergent-range alcohols is currently employed commercially in a variety of modifications. The major differences among the processes involve the type of olefin, catalysts and co-catalysts, stoichiometry, process conditions (including catalyst recovery), handling of intermediates, product composition and by-product formation. Leading companies involved in oxo-synthesis include Shell Chemical Company, BASF Corporation, Exxon Chemical, Noroxo (formerly CdF Chimie Specialities), CONDEA Vista (US) and CONDEA Chemie GmbH in Germany, Nippon Shokubai Co., Ltd, Japan and Henkel KGaA in Germany.

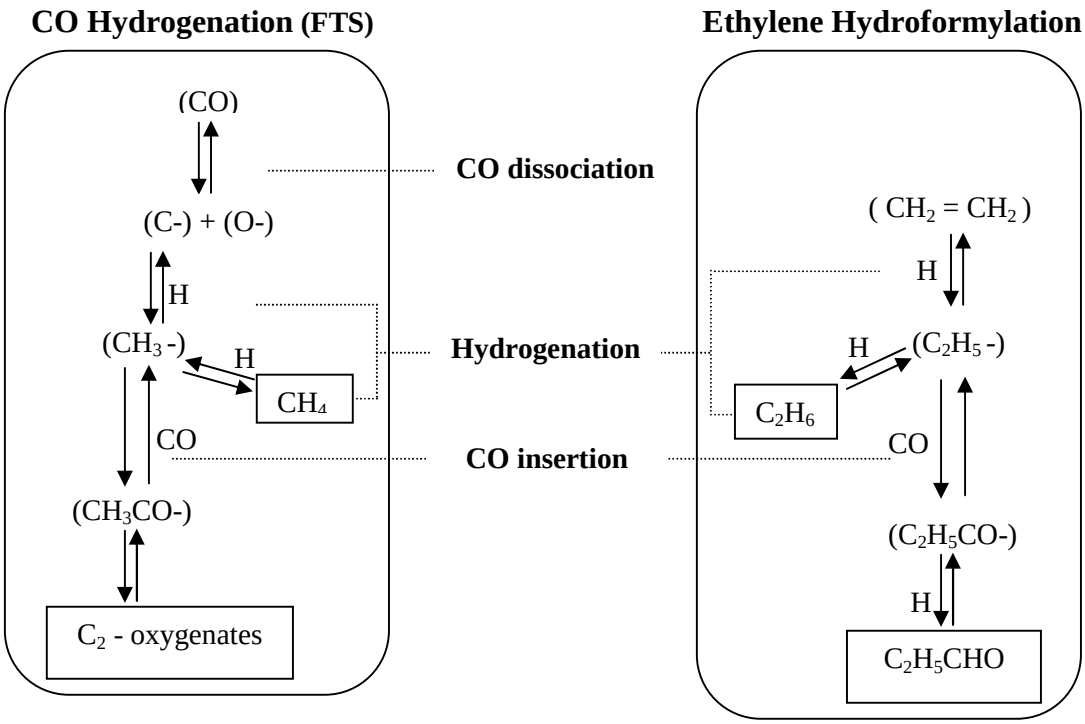

Figure 2.5: Similarities in mechanisms of CO hydrogenation to oxygenates and Ethylene hydroformylation [Adapted from Hanaoka *et al*., 2000].

References

Betchel Corporation. (1998). Task 4.2 Commercial Applications – Economics of MTBE via mixed alcohol. *Subcontract No. PT5781-B*, Prepared for Air Products and Chemicals.

Caraballo, J. (2005). Ethanol synthesis. Ist European summer school on renewable motor fuels, Berkenfeld, Germany, 29-31 August

Cornils, B., Herrmann, W. A., Rasch, M. (1994). Otto Roelen, pioneer in industrial homogeneous catalysis. *Angewandte Chemie International Edition in English*, 33 (21), pp.2144-2163

Courty, P., Durand, D., Freund, E., Sugier, A. (1982). C1-C6 alcohols from synthesis gas on copper-cobalt catalysts. *Journal of Molecular Catalysis*, 17 (2-3), 1982, pp.241-254

Courty, P., Arlie, J. P., Convers, A., Mikitenko, P., Sugier, A. (1984). C_1-C_6 alcohols from syngas. *Hydrocarbon Processing*, 63 (11), pp.105-108.

Courty, P., Chaumette, P., Durrand, D., Verdon, C. (1998). Process for manufacturing a mixture of primary alcohols from a synthesis gas , in the presence of a catalyst containing copper, cobalt, zinc and at least one alkali and/alkaline earth metal. U.S. Patent 4,780,481.

de Aquino, A., Cobo, A. J. G. (2001). Synthesis of higher alcohols with cobalt and copper based model catalysts: effects of the alkaline metals. *Catalysis Today* 65, p.209

Frohning, C. D., Kohlpainter, C. W. (1996) in: Cornils, B., Herrmann, W. A. (Eds.), *Applied Homogeneous Catalysis with Organometallic compounds*, Weinheim: VCH, p.29

Gerber, M. A., White, J. F., Gray, M. J., Stevens, D. J. (2007). Mixed alcohol synthesis catalyst screening. 2007 Progress Report prepared for the U. S. Department of Energy under contract DE-AC05-76RL01830 by Pacific Northwest National Laboratory, Richland, Washington.

Hanaoka, T., Arakawa, H., Matsuzaki, T., Sugi, Y., Kanno, K., Abe, Y. (2000). Ethylene hydroformylation and carbon monoxide hydrogenation over modified and unmodified silica supported rhodium catalysts. *Catalysis Today*, 58, pp.271-280.

Herman, R. G. (1991). Classical and non-classical routes for alcohol synthesis, in: Guczi, L. (Ed.), *New Trends in CO Activation*. New York: Elsevier.

Iranmahboob, J., Hill, D. O. (2002). Alcohol synthesis from syngas over K_2CO_3/Co-MoS_2 on activated carbon. *Catalysis Letters*, 78 (1-4), pp.49-55.

Kainulainen, T. A., Niemela, M. K., Krause, A. O. I. (1998). Ethene hydroformylation on Co/SiO_2 catalysts, *Catalysis Letters*, 53, pp.97-101

Lenarda, M., Storaro, L., Ganzerla, R. (1996). Hydroformylation of simple olefins catalyzed by metals and clusters supported on unfunctionalized organic carriers, *Journal of Molecular Catalysis A*, 111, pp.203-237.

Li, B., Li, X., Asami, K., Fujimoto, K. (2003). Hydroformylation of 1-Hexene over cobalt-based solid catalysts at low pressure, *Journal of Chemical Engineering of Japan*, 36 (8), pp.932-939.

Mahajan, D., Jackson, G. R. (2004). Method for the production of mixed alcohols from synthesis gas. United States Patent number 6753353, June 22.

Mahdavi, V., Peyrovi, M. H., Islami, M., Mehr, J. Y. (2005). Synthesis of higher alcohols from syngas over Cu-Co_2O_3/ZnO, Al_2O_3 catalyst. *Applied Catalysis A: General*, 281, pp. 259-265.

Metcall LLC (2006). Product Info: Methanol. http://www.jordantek.com/web/metcall/methanol.html. [Accessed: 29 December, 2008]

Moulijn, J. A., Makkee, M., van Diepen, A. (2001). *Chemical Process Technology*. Chichester: John Wiley.

Olah, G. A., Goeppert, A., Prakash, G. K. S. (2006).Beyond oil and gas: Thew methanol economy. Weinheim: WILEY-VCH.

Qiu, X., Tsubaki, N., Fujimoto, K. (2001). Hydroformylation of 1-Hexene over Co/SiO_2 catalysts: Influence of pore size of support, *Journal of Chemical Engineering of Japan*, 34 (11), pp.1366-1372.

Roberts, G. W., Lim, P. K., McCuthen, M. S., Mawson, S. (1992). The thermodynamics of higher alcohol synthesis. *Preprints – American Chemical Society, Division of Petroleum Chemistry*, 37 (1), pp.225-233.

Spath, P., Dayton, D. (2003). Technical Report on "Preliminary Screening – Technical and economic assessment of synthesis gas to fuels and chemicals with emphasis on the potential for biomass-derived syngas". NREL/TP-510-34929.

Spath, P. & Dayton, D. (2008). *Products from Syngas - Mixed Higher Alcohols (Metal Catalyst).* [Accessed: 11 November, 2008]. http://bioweb.sungrant.org/General/Bioproducts/Bioproducts+from+Syngas/Mixer+Higher+Alcohols/Default.htm

Subramani, V., Gangwal, S. K. (2008). A review of recent literature to search for an efficient catalytic process for the conversion of syngas to ethanol. *Energy and Fuels*, 22, pp.814-839.

Vervek, K.A.N., Jaeger, B., Finkeldei, C., Wilhelm, K. (1999). Recent developments in isobutanol synthesis from synthesis gas. *Applied catalysis A: General*, 186, pp.407-431

APPENDIX C1: TYPICAL CHROMATOGRAM – GAS ANALYSIS

```
Title        :
Run File     : C:\star\data\08-05-07btf3.2012.run
Method File  : C:\star\BENGAS.mth
Sample ID    : 08-05-07btf3.2

Injection Date: 5/7/2008 1:34 PM    Calculation Date: 5/7/2008 1:43 PM

Operator    : UMOH                  Detector Type: 3800 (10 Volts)
Workstation: RG02701                Bus Address  : 44
Instrument : Varian Star #1         Sample Rate  : 10.00 Hz
Channel     : Front = TCD           Run Time     : 8.493 min

** GC Workstation Multi Instrument Version 6.41 ** 01141-2588-C69-24B5 **

Chart Speed =    2.29 cm/min   Attenuation = 350          Zero Offset = 2%
Start Time  =   0.000   min     End Time    = 8.493   min   Min / Tick  = 1.00
```

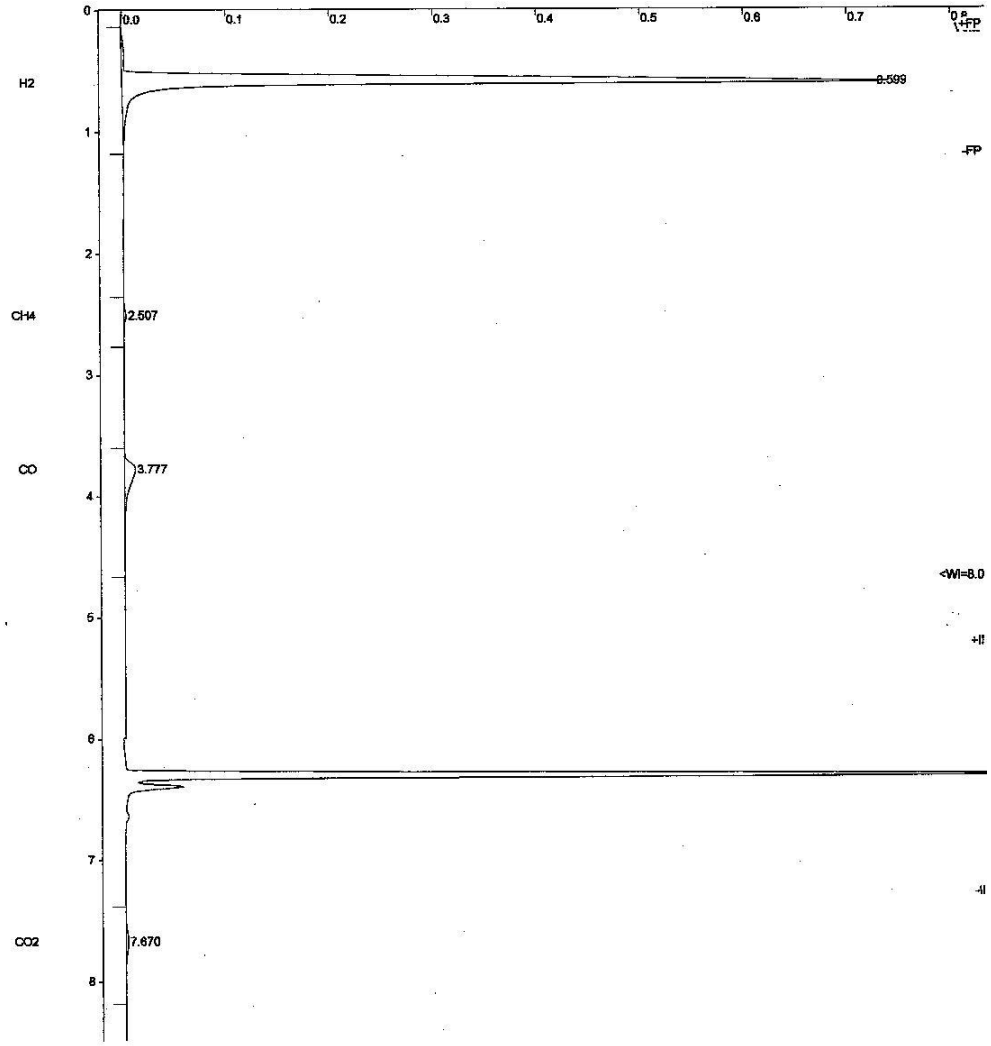

APPENDIX C2: GC METHOD FOR GAS ANALYSIS

```
*************************************************************************

GC Workstation Multi Instrument - Method Listing   Wed May 06 13:57:55 2009

Method: BENGAS

*************************************************************************

*************************************************************************

**********************
    3800 GC
**********************
Module Address: 44

Valve Table
-----------
     Valve 1: Gas Sampling Valve
              Initial: Fill
             0.01 min: Fill
             6.00 min: Inject

     Valve 2: Gas Sampling Valve
              Initial: Fill
             0.01 min: Inject
             6.00 min: Inject


 Front Injector Type 1041
-------------------------
      Oven Power: On
     Temperature: 150 C

Middle Injector Type 1041
-------------------------
      Oven Power: On
     Temperature: 150 C

 Front Injector EFC Type 4
-------------------------
 Pressure     Rate       Hold      Total
    (psi) (psi/min)    (min)      (min)
 -------------------------------------
     14.5     0.00       3.50       3.50

      Time     Total Flow
      (min)     (ml/min)
      ------------------
    Initial         40

Middle Injector EFC Type 4
--------------------------
 Pressure     Rate       Hold      Total
    (psi) (psi/min)    (min)      (min)
 -------------------------------------
     32.0     0.00       3.00       3.00

      Time     Total Flow
      (min)     (ml/min)
      ------------------
    Initial         40

Column Oven
-----------
                Coolant: On
     Enable Coolant at: 50 C
       Coolant Timeout: 10.00 min
    Stabilization Time: 0.50 min

     Temp     Rate       Hold      Total
      (C)    (C/min)    (min)      (min)
     ---------------------------------
       27      0.0       8.50       8.50

 Front TCD Detector
-------------------
      Oven Power: On
     Temperature: 125 C
     Electronics: On
   Filament Temp: 150 C
   Time Constant: Slow
      Temp Limit: 390 C
     Carrier Gas: N2-Ar

      Time     Range  Autozero  Polarity
      (min)
```

```
      ----------------------------------
    Initial     0.05      yes     positive
       6.00     0.05      yes     negative

Middle FID Detector
-------------------
      Oven Power: Off
     Temperature: 50 C
     Electronics: Off
   Time Constant: Slow

      Time     Range  Autozero
      (min)
      ------------------------
    Initial      9      yes

Output Port A
-------------
      Time     Signal    Attenuation
      (min)    Source
      ----------------------------
    Initial    Middle           1

Output Port B
-------------
      Time     Signal    Attenuation
      (min)    Source
      ----------------------------
    Initial     Front           1

Output Port C
-------------
      Time     Signal    Attenuation
      (min)    Source
      ----------------------------
    Initial     Front           1

Data Acquisition
----------------
      Detector Bunch Rate : 4 points (10.0 Hz)
           Monitor Length : 64 bunched points (6.4 sec)
       Front FID/TSD Scale: 10 Volts
      Middle FID/TSD Scale: 10 Volts
        Rear FID/TSD Scale: 10 Volts


Integration Parameters  Address 44  Channel Front
-------------------------------------------------
Subtract Blank Baseline      : No
Initial S/N Ratio            : 5
Initial Peak Width           : 4 sec
Initial Tangent Height %     : 10%
Monitor Noise                : Before every run
Measurement Type             : Peak Area
Initial Peak Reject Value    : 1000     counts
Report Unidentified Peaks    : Yes
Report Missing Peaks         : No
Normalize Results            : No


Calibration Setup        Address 44  Channel Front
-------------------------------------------------
Calculation Type             : External Standard
Number of Calibration Levels: 1
Curve Origin                 : Force
Curve Fit                    : Linear
Weighted Regression          : (None)
Replicate Treatment          : Keep Replicates Separate
Replicate Tolerance          : Always add new replicates
    Out-of-Tolerance Action : No Action
Calibration Range Tolerance :       10.0%
    Out-of-Tolerance Action : No Action


Verification Setup       Address 44  Channel Front
-------------------------------------------------
Deviation Tolerance          : 100.0%
    Out-of-Tolerance Action : No Action


Peak Table  Address 44  Channel Front
```

```
-----------------------------------
Reference Peaks Time Windows:Width:  0.10 min.  Retention Time 2.0%
Other Peaks Time Windows    :Width:  0.05 min.  Retention Time 8.9%

Peak Name       : H2
Attributes      : Ref:N  Std:N  RRT:N  Lock:N  Group:0  Time:   0.599 min
Uses Standard   :
Level  1 Amount: 50
Coefficients    : +0.0000e+000x^3 +0.0000e+000x^2 +5.6760e+004x +0.0000e+000

Peak Name       : N2
Attributes      : Ref:N  Std:N  RRT:N  Lock:N  Group:0  Time:   1.498 min
Uses Standard   :
Level  1 Amount: 4
Coefficients    : +0.0000e+000x^3 +0.0000e+000x^2 +5.6195e+003x +0.0000e+000

Peak Name       : CH4
Attributes      : Ref:N  Std:N  RRT:N  Lock:N  Group:0  Time:   2.420 min
Uses Standard   :
Level  1 Amount: 8
Coefficients    : +0.0000e+000x^3 +0.0000e+000x^2 +1.3728e+004x +0.0000e+000

Peak Name       : CO
Attributes      : Ref:N  Std:N  RRT:N  Lock:N  Group:0  Time:   3.666 min
Uses Standard   :
Level  1 Amount: 28
Coefficients    : +0.0000e+000x^3 +0.0000e+000x^2 +5.4201e+003x +0.0000e+000

Peak Name       : CO2
Attributes      : Ref:N  Std:N  RRT:N  Lock:N  Group:0  Time:   7.651 min
Uses Standard   :
Level  1 Amount: 10
Coefficients    : +0.0000e+000x^3 +0.0000e+000x^2 +3.3969e+003x +0.0000e+000


Time Events Table   Address 44  Channel Front
-------------------------------------------
Force Peak          :     0.1801  until      1.1790
Force Peak          :     3.3968  until      4.6358
Inhibit Integrate   :     5.2065  until      7.2708

Report Format: Module 3800 Address 44 Channel Front
---------------------------------------------------
Title                       :
Print Chromatogram          :  No


Print Results               :  No
Convert Results to ASCII?:  Off


Calibration Block Reports
Print Report                :  No
Convert Report to ASCII?  :  Off

Print Copies                :  1


**********************
    3800 GC
**********************
Module Address: 45

Column Oven
-----------
                Coolant: Off
     Enable Coolant at: 50 C
       Coolant Timeout: 20.00 min
    Stabilization Time: 2.00 min

     Temp     Rate       Hold      Total
      (C)    (C/min)    (min)      (min)
     -------------------------------------
       50      0.0      20.00      20.00

Data Acquisition
----------------
      Detector Bunch Rate : 4 points (10.0 Hz)
           Monitor Length : 64 bunched points (6.4 sec)
       Front FID/TSD Scale: 1 Volts
      Middle FID/TSD Scale: 1 Volts
        Rear FID/TSD Scale: 1 Volts
```

APPENDIX C3: TYPICAL CHROMATOGRAM FOR LIQUID ANALYSIS (Micro GC *Varian 3900*)

```
Title        :  APPENDIX C3
Run File     : C:\star\data\08-05-05btf1002.run
Method File  : c:\star\zebron.mth
Sample ID    : 08-05-05BTF1

Injection Date: 5/21/2008 2:26 PM    Calculation Date: 5/21/2008 2:44 PM

Operator    : UMOH                   Detector Type: 39XL (1 Volt)
Workstation: RG02695                 Bus Address  : 44
Instrument : Varian Star #1          Sample Rate  : 20.00 Hz
Channel     : Front = FID            Run Time     : 13.666 min

** GC Workstation Multi Instrument Version 6.41 ** 01141-2588-C69-24B5 **

Chart Speed =    1.42 cm/min   Attenuation = 2452          Zero Offset = 2%
Start Time  =   0.000   min     End Time    = 13.666  min   Min / Tick  = 1.00
```

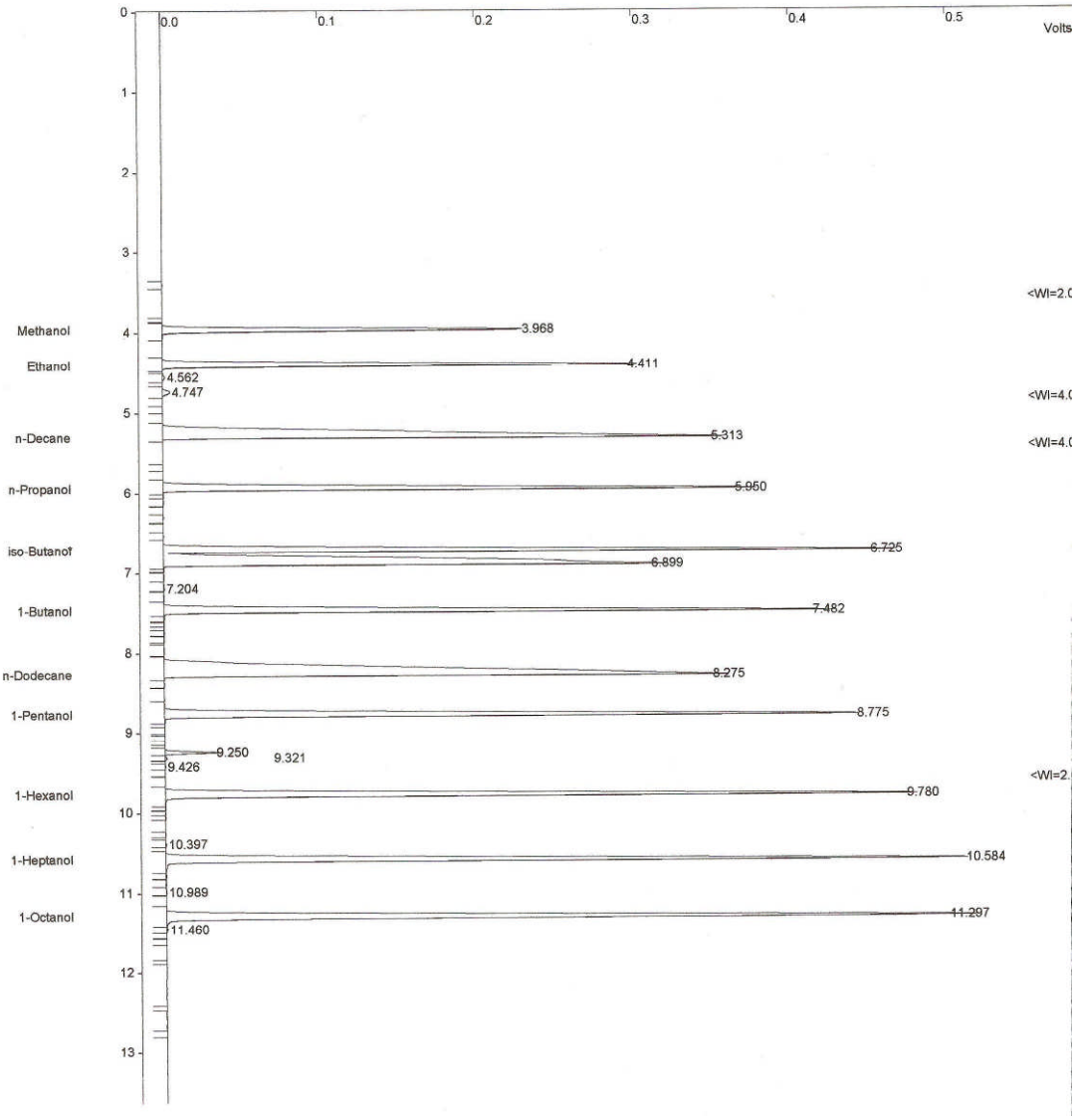

APPENDIX C4: GC METHOD FOR LIQUID ANALYSIS

```
*************************************************************************

GC Workstation Multi Instrument - Method Listing   Fri May 22 16:20:50 2009

Method: BenHAS

*************************************************************************

*************************************************************************

**********************
    39XL GC
**********************
Module Address: 44

Injector Type 1177
------------------
      Oven Power: On
     Temperature: 250 C

      Time     Split    Split
      (min)    State    Ratio
      ----------------------
    Initial      On        80

Injector EFC Type 1
-------------------
 Pressure     Rate      Hold      Total
    (psi) (psi/min)    (min)      (min)
 -------------------------------------
      10.0     0.00     11.50      11.50

Column Oven
-----------
                Coolant: Off
     Enable Coolant at:   50 C
       Coolant Timeout: 0.20 min
    Stabilization Time: 0.50 min

     Temp     Rate      Hold      Total
      (C)   (C/min)    (min)      (min)
     --------------------------------
       60      0.0      3.00       3.00
      130     15.0      4.33      12.00

FID Detector
-------------------
      Oven Power: On
     Temperature: 250.00 C
     Electronics: On
   Time Constant: Fast

      Time     Range  Autozero
      (min)
      ----------------------
    Initial     12      yes

Type 11 Detector EFC
----------------------------
      Make up Flow:  25 ml/min
           H2 Flow:  30 ml/min
          Air Flow: 300 ml/min

Valve Table
-----------
     Valve 1: Event 1 Valve
             Initial: Off

     Valve 2: Event 2 Valve
             Initial: Off


Data Acquisition
----------------
      Detector Bunch Rate : 4 points (20.0 Hz)
           Monitor Length : 64 bunched points (3.2 sec)
       FID Scale: 1 Volts


Integration Parameters  Address 44  Channel Front
---------------------------------------------
Subtract Blank Baseline      : No
Initial S/N Ratio            : 6
Initial Peak Width           : 4 sec
Initial Tangent Height %     : 10%
```

```
Monitor Noise                  : Before every run
Measurement Type               : Peak Area
Initial Peak Reject Value      : 1000    counts
Report Unidentified Peaks      : Yes
Report Missing Peaks           : No
Normalize Results              : No


Calibration Setup        Address 44  Channel Front
---------------------------------------------
Calculation Type               : External Standard
Number of Calibration Levels: 1
Curve Origin                   : Force
Curve Fit                      : Linear
Weighted Regression            : (None)
Replicate Treatment            : Keep Replicates Separate
Replicate Tolerance            : Always add new replicates
    Out-of-Tolerance Action : No Action
Calibration Range Tolerance :       10.0%
    Out-of-Tolerance Action : No Action


Verification Setup       Address 44  Channel Front
---------------------------------------------
Deviation Tolerance            : 100.0%
    Out-of-Tolerance Action : No Action


Peak Table  Address 44  Channel Front
-----------------------------------
Reference Peaks Time Windows:Width:  0.10 min.  Retention Time 2.0%
Other Peaks Time Windows    :Width:  0.10 min.  Retention Time 0.8%

Peak Name       : Methanol
Attributes      : Ref:N  Std:N  RRT:N  Lock:N  Group:0  Time:   3.097 min
Uses Standard   :
Level  1 Amount: 7.7
Coefficients    : +0.0000e+000x^3 +0.0000e+000x^2 +2.8392e+004x +0.0000e+000

Peak Name       : Ethanol
Attributes      : Ref:N  Std:N  RRT:N  Lock:N  Group:0  Time:   3.288 min
Uses Standard   :
Level  1 Amount: 7.7
Coefficients    : +0.0000e+000x^3 +0.0000e+000x^2 +4.3201e+004x +0.0000e+000

Peak Name       : n-Decane
Attributes      : Ref:N  Std:N  RRT:N  Lock:N  Group:0  Time:   3.644 min
Uses Standard   :
Level  1 Amount: 7.7
Coefficients    : +0.0000e+000x^3 +0.0000e+000x^2 +1.4404e+005x +0.0000e+000

Peak Name       : 1-Propanol
Attributes      : Ref:N  Std:N  RRT:N  Lock:N  Group:0  Time:   4.050 min
Uses Standard   :
Level  1 Amount: 7.7
Coefficients    : +0.0000e+000x^3 +0.0000e+000x^2 +7.3859e+004x +0.0000e+000

Peak Name       : n-undecane
Attributes      : Ref:N  Std:N  RRT:N  Lock:N  Group:0  Time:   4.624 min
Uses Standard   :
Level  1 Amount: 7.7
Coefficients    : +0.0000e+000x^3 +0.0000e+000x^2 +2.8690e+005x +0.0000e+000

Peak Name       : iso-butanol
Attributes      : Ref:N  Std:N  RRT:N  Lock:N  Group:0  Time:   5.191 min
Uses Standard   :
Level  1 Amount: 7.7
Coefficients    : +0.0000e+000x^3 +0.0000e+000x^2 +8.9788e+004x +0.0000e+000

Peak Name       : 1-Butanol
Attributes      : Ref:N  Std:N  RRT:N  Lock:N  Group:0  Time:   5.855 min
Uses Standard   :
Level  1 Amount: 7.7
Coefficients    : +0.0000e+000x^3 +0.0000e+000x^2 +2.4433e+005x +0.0000e+000

Peak Name       : n-Dodecane
Attributes      : Ref:N  Std:N  RRT:N  Lock:N  Group:0  Time:   6.466 min
Uses Standard   :
Level  1 Amount: 7.7
Coefficients    : +0.0000e+000x^3 +0.0000e+000x^2 +1.1282e+005x +0.0000e+000

Peak Name       : 1-Pentanol
```

```
Attributes      : Ref:N  Std:N  RRT:N  Lock:N  Group:0  Time:   7.327 min
Uses Standard   :
Level  1 Amount: 7.7
Coefficients    : +0.0000e+000x^3 +0.0000e+000x^2 +5.0963e+003x +0.0000e+000

Peak Name       : 1-Hexanol
Attributes      : Ref:N  Std:N  RRT:N  Lock:N  Group:0  Time:   7.659 min
Uses Standard   :
Level  1 Amount: 7.7
Coefficients    : +0.0000e+000x^3 +0.0000e+000x^2 +1.3856e+005x +0.0000e+000

Peak Name       : 1-Heptanol
Attributes      : Ref:N  Std:N  RRT:N  Lock:N  Group:0  Time:   9.051 min
Uses Standard   :
Level  1 Amount: 7.7
Coefficients    : +0.0000e+000x^3 +0.0000e+000x^2 +1.8170e+005x +0.0000e+000

Peak Name       : 1-Octanol
Attributes      : Ref:N  Std:N  RRT:N  Lock:N  Group:0  Time:  10.749 min
Uses Standard   :
Level  1 Amount: 7.7
Coefficients    : +0.0000e+000x^3 +0.0000e+000x^2 +2.1203e+005x +0.0000e+000


Time Events Table   Address 44  Channel Front
-----------------------------------------
            Time Events Table Empty

Report Format: Module 39XL Address 44 Channel Front
-----------------------------------------------------
Title                      :
Print Chromatogram         :  Yes
   Chromatogram Options:
Start Retention Time       :  0.00 minutes
End Retention Time         :  1440.00 minutes
Length in Pages            :  1
Initial Chart Speed        :  0.0 cm/min
Minutes per Tick           :  1.0
Autoscale                  :  On
Time Events                :  On
Chromatogram Events        :  On
Retention Times            :  On
Peak Names                 :  On
Baseline                   :  On


Print Results              :  Yes
   Results Options:
Units                      :
Number of Decimal Digits   :  4
Show Peak Group Totals     :  Yes
Run Log                    :  Off
Error Log                  :  Off
Calibration Report         :  Off
Revision Log               :  On
Notes                      :  Off
Method Notes               :  Off
Convert Results to ASCII?: Off


Calibration Block Reports
Print Report               :  No
Convert Report to ASCII?   :  Off

Print Copies               :  1
```